frontiers | Research Topics

Experimental and computational methods in the development of diagnostics and therapeutics for colon cancer

Edited by
Muhammad Suleman, Farooq Rashid, Shahid Ali and Faez Iqbal Khan

Published in
Frontiers in Molecular Biosciences

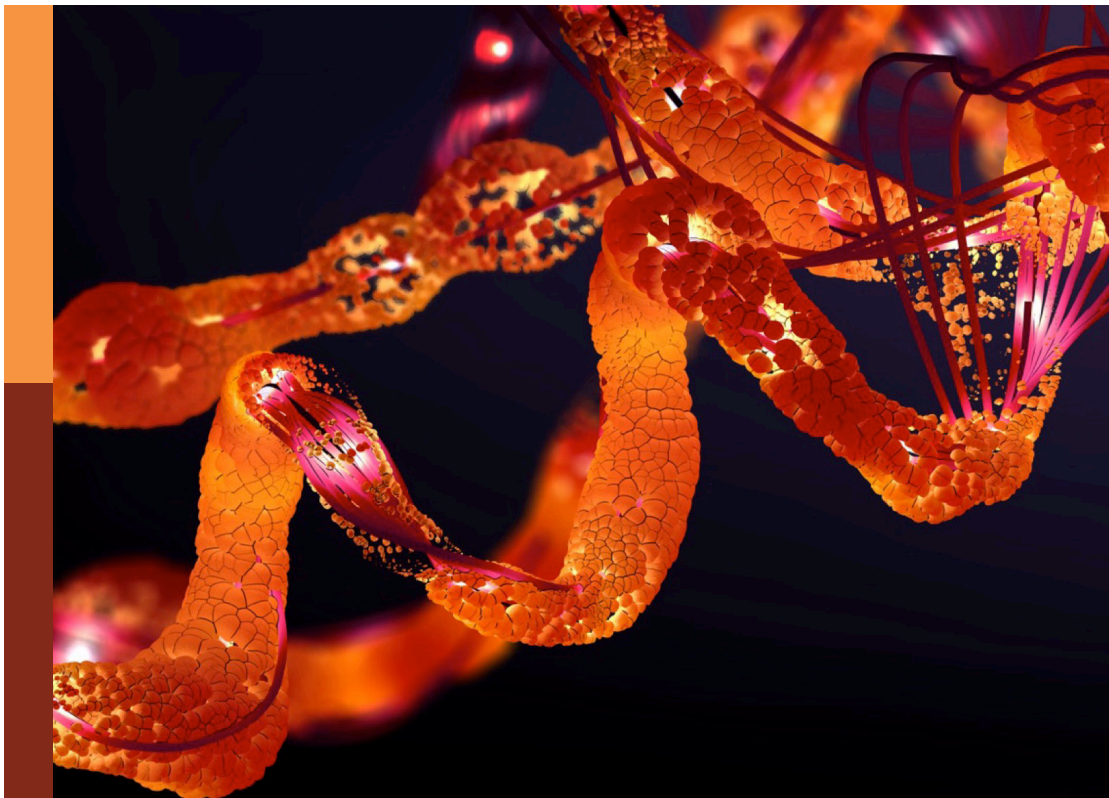

ISSN 1664-8714
ISBN 978-2-8325-6065-5
DOI 10.3389/978-2-8325-6065-5

About Frontiers

Frontiers is more than just an open access publisher of scholarly articles: it is a pioneering approach to the world of academia, radically improving the way scholarly research is managed. The grand vision of Frontiers is a world where all people have an equal opportunity to seek, share and generate knowledge. Frontiers provides immediate and permanent online open access to all its publications, but this alone is not enough to realize our grand goals.

Frontiers journal series

The Frontiers journal series is a multi-tier and interdisciplinary set of open-access, online journals, promising a paradigm shift from the current review, selection and dissemination processes in academic publishing. All Frontiers journals are driven by researchers for researchers; therefore, they constitute a service to the scholarly community. At the same time, the *Frontiers journal series* operates on a revolutionary invention, the tiered publishing system, initially addressing specific communities of scholars, and gradually climbing up to broader public understanding, thus serving the interests of the lay society, too.

Dedication to quality

Each Frontiers article is a landmark of the highest quality, thanks to genuinely collaborative interactions between authors and review editors, who include some of the world's best academicians. Research must be certified by peers before entering a stream of knowledge that may eventually reach the public - and shape society; therefore, Frontiers only applies the most rigorous and unbiased reviews. Frontiers revolutionizes research publishing by freely delivering the most outstanding research, evaluated with no bias from both the academic and social point of view. By applying the most advanced information technologies, Frontiers is catapulting scholarly publishing into a new generation.

What are Frontiers Research Topics?

Frontiers Research Topics are very popular trademarks of the *Frontiers journals series*: they are collections of at least ten articles, all centered on a particular subject. With their unique mix of varied contributions from Original Research to Review Articles, Frontiers Research Topics unify the most influential researchers, the latest key findings and historical advances in a hot research area.

Find out more on how to host your own Frontiers Research Topic or contribute to one as an author by contacting the Frontiers editorial office: frontiersin.org/about/contact

Experimental and computational methods in the development of diagnostics and therapeutics for colon cancer

Topic editors

Muhammad Suleman — University of Swat, Pakistan

Farooq Rashid — Department of Biotechnology, Guangxi Veterinary Research Institute, China

Shahid Ali — University of Swat, Pakistan

Faez Iqbal Khan — Xi'an Jiaotong-Liverpool University, China

Citation

Suleman, M., Rashid, F., Ali, S., Khan, F. I., eds. (2025). *Experimental and computational methods in the development of diagnostics and therapeutics for colon cancer*. Lausanne: Frontiers Media SA. doi: 10.3389/978-2-8325-6065-5

Table of contents

frontiers | Frontiers in Molecular Biosciences

TYPE Editorial
PUBLISHED 19 February 2025
DOI 10.3389/fmolb.2025.1568721

OPEN ACCESS

EDITED AND REVIEWED BY
Matteo Becatti,
University of Firenze, Italy

*CORRESPONDENCE
Muhammad Suleman,
suleman@uswat.edu.pk
Faez Iqbal Khan,
khanfaeziqbal@gmail.com,
Faez.Khan@xjtlu.edu.cn

RECEIVED 30 January 2025
ACCEPTED 12 February 2025
PUBLISHED 19 February 2025

CITATION
Suleman M, Ali S, Rashid F and Khan FI (2025) Editorial: Experimental and computational methods in the development of diagnostics and therapeutics for colon cancer.
Front. Mol. Biosci. 12:1568721.
doi: 10.3389/fmolb.2025.1568721

Editorial: Experimental and computational methods in the development of diagnostics and therapeutics for colon cancer

Muhammad Suleman[1,2]*, Shahid Ali[1], Farooq Rashid[3] and Faez Iqbal Khan[4]*

[1]Centre for Biotechnology and Microbiology, University of Swat, Mingora, Pakistan, [2]Laboratory of Animal Research Center (LARC), QU Health, Qatar University, Doha, Qatar, [3]Department of Biotechnology, Guangxi Veterinary Research Institute, Nanning, China, [4]Department of Biosciences and Bioinformatics, School of Science, Xi'an Jiaotong-Liverpool University, Suzhou, China

KEYWORDS

colon cancer, diagnostics, therapeutics, machine-learning, computational, experimental

Editorial on the Research Topic
Experimental and computational methods in the development of diagnostics and therapeutics for colon cancer

Cancer continues to be one of the major causes of illness and death worldwide. It is growing an alarming rate, and affects every geographic region of the world. Therefore, the goal is to investigate novel biomarkers both experimentally and computationally in the development of colon cancer and drug resistance. Computational methods play a crucial role in modern cancer research, facilitating drug discovery and improving therapeutic strategies (Ahmad et al., 2024; Shaikh et al., 2023). In this Research Topic, we aim to provide an overview of recent technologies in experimental and computational areas, such as artificial intelligence and machine learning approaches, relevant to the identification of novel biomarkers and drug testing in cancer diagnosis, management, and treatment. Recent studies highlight three key areas: biomarker discovery, therapeutic developments, and computational modeling in cancer research. Grouping the studies under these themes provides a cohesive narrative, highlighting key trends and challenges in the field.

The identification of novel biomarkers is crucial for early detection and targeted therapy in cancer treatment. Sorokin et al. compared gene fusion detection in colorectal cancer patients, identifying 93 new fusion genes, with 11 appearing in multiple patients. Notably, a novel LRRFIP2-ALK fusion was identified, with potential implications for ALK inhibitor therapies. Cao et al. developed a prognostic model using three cellular senescence-related lncRNAs (CSRLs), demonstrating its predictive power for overall survival and immune response in colon cancer patients. Tambaro et al. analyzed circulating miRNAs in gastrointestinal (GI) cancer patients, finding specific miRNAs associated with adiposity levels and cachexia, suggesting their potential as diagnostic biomarkers. Wang et al. explored the prognostic and immunogenic characteristics of disease regulators in colon cancer. Their analysis revealed that age, tumor stage, and ferroptosis score were significantly correlated with prognosis.

Understanding drug resistance and optimizing therapeutic strategies are crucial for effective cancer treatment. Burov et al. investigated the effects of multikinase inhibitors (MKIs) on proteasome expression in colorectal cancer cells, revealing increased expression of non-constitutive proteasomes in BRAF-mutant tumors. MKI treatment induced oxidative stress and proteasome redistribution, shedding light on potential therapeutic targets. Yang et al. developed a necroptosis-related prognostic model using key genes (CALB1, CHST13, and SLC4A4), effectively predicting patient survival and immune response. Bukhari et al. discussed the clinical implications of long noncoding RNA LINC-PINT, emphasizing its role as a potential therapeutic target in cancer treatment. Zhang et al. reviewed the impact of immunosenescence on solid gastrointestinal tumors, highlighting how senescence-related mechanisms diminish immunotherapy effectiveness and proposing senotherapy strategies to counteract these effects.

Computational models enhance predictive accuracy and statistical analyses in cancer research. Su et al. compared competing-risk analysis and Cox regression models to assess prognostic factors in adenocarcinoma of the transverse colon (ATC), finding that traditional Cox regression underestimated cancer stage-related risks. Prior studies on AI-driven drug discovery, such as sphingosine kinase 1 inhibitors and FDA-approved PIM-1 kinase inhibitors, demonstrate the potential of virtual screening and molecular dynamics simulations in identifying promising therapeutic compounds (Khan et al., 2020; Rathi et al., 2024). Wang et al. investigated the PD-1/PD-L1 interaction mechanism using computational approaches, reinforcing the role of immune checkpoint inhibitors like pembrolizumab in cancer treatment (Wang and Khan, 2023). Insights from previous studies on human peroxiredoxin 6 further underscore the intricate roles of molecular targets in cancer, demonstrating its dual role in cancer progression and inhibition, highlighting its potential as a therapeutic target (Qausain et al., 2023).

This Research Topic underscores the significant advancements in biomarker discovery, therapeutic development, and computational modeling in cancer research. The integration of AI and ML continues to enhance predictive accuracy, streamline drug discovery, and improve patient outcomes. Despite these advancements, challenges remain in overcoming drug resistance and improving the efficacy of immunotherapies. Future research should refine computational models, explore novel therapeutic targets, and bridge experimental and computational methodologies to optimize cancer diagnosis and treatment.

Author contributions

MS: Writing–review and editing. SA: Writing–review and editing. FR: Writing–review and editing. FK: Writing–original draft, Writing–review and editing.

Funding

The author(s) declare that financial support was received for the research, authorship, and/or publication of this article. The author, FK, would like to thank the XJTLU Research Development Fund (RDF-22-02-090) for its support.

Conflict of interest

The authors declare that the research was conducted in the absence of any commercial or financial relationships that could be construed as a potential conflict of interest.

Generative AI statement

The author(s) declare that no Generative AI was used in the creation of this manuscript.

Publisher's note

References

Ahmad, K., Shaikh, S., Khan, F. I., and Khan, M. E. (2024). Editorial: computational drug discovery of medicinal compounds for cancer management, volume II. *Front. Chem.* 12, 1446510. doi:10.3389/fchem.2024.1446510

Khan, F. I., Lai, D., Anwer, R., Azim, I., and Khan, M. K. A. (2020). Identifying novel sphingosine kinase 1 inhibitors as therapeutics against breast cancer. *J. Enzyme Inhib. Med. Chem.* 35(1), 172–186. doi:10.1080/14756366.2019.1692828

Qausain, S., Khan, F. I., and Khan, M. K. A. (2023). Conserved acidic second shell residue modulates the structure, stability and activity of non-seleno human peroxiredoxin 6. *Int. J. Biol. Macromol.* 242(Pt 3), 124796. doi:10.1016/j.ijbiomac.2023.124796

Rathi, A., Noor, S., Sulaimani, M. N., Ahmed, S., Taiyab, A., AlAjmi, M. F., et al. (2024). FDA-approved drugs as PIM-1 kinase inhibitors: a drug repurposed approach for cancer therapy. *Int. J. Biol. Macromol.* 292, 139107. doi:10.1016/j.ijbiomac.2024.139107

Shaikh, S., Ahmad, K., Khan, M. E., and Khan, F. I. (2023). Editorial: computational drug discovery of medicinal compounds for cancer management. *Front. Chem.* 11, 1343183. doi:10.3389/fchem.2023.1343183

Wang, S., and Khan, F. I. (2023). Investigation of molecular interactions mechanism of pembrolizumab and PD-1. *Int. J. Mol. Sci.* 24(13). doi:10.3390/ijms241310684

frontiers | Frontiers in Immunology

TYPE Original Research
PUBLISHED 22 December 2022
DOI 10.3389/fimmu.2022.1085038

OPEN ACCESS

EDITED BY
Muhammad Suleman,
University of Swat, Pakistan

REVIEWED BY
Farman Ullah,
University of Swat, Pakistan
Susanna Ulahannan,
University of Oklahoma, United States
Murad Ali Rahat,
University of Swat, Pakistan

*CORRESPONDENCE
Xiaobing Chen
zlyychenxb0807@zzu.edu.cn

†These authors have contributed equally to this work

SPECIALTY SECTION
This article was submitted to Cancer Immunity and Immunotherapy, a section of the journal Frontiers in Immunology

RECEIVED 31 October 2022
ACCEPTED 08 December 2022
PUBLISHED 22 December 2022

CITATION
Yang W, Lu S, Peng L, Zhang Z, Zhang Y, Guo D, Ma F, Hua Y and Chen X (2022) Integrated analysis of necroptosis-related genes for evaluating immune infiltration and colon cancer prognosis. *Front. Immunol.* 13:1085038. doi: 10.3389/fimmu.2022.1085038

Integrated analysis of necroptosis-related genes for evaluating immune infiltration and colon cancer prognosis

Wei Yang[1†], Shuaibing Lu[1†], Liangqun Peng[1†], Zhandong Zhang[1], Yonglei Zhang[1], Dandan Guo[2], Fei Ma[1], Yawei Hua[1] and Xiaobing Chen[3,4*]

[1]Department of General Surgery, The Affiliated Cancer Hospital of Zhengzhou University, Henan Cancer Hospital, Zhengzhou, China, [2]Department of Radiology, The Third Affiliated Hospital of Zhengzhou University, Zhengzhou, China, [3]Department of Medical Oncology, The Affiliated Cancer Hospital of Zhengzhou University, Henan Cancer Hospital, Zhengzhou, China, [4]Zhengzhou Key Laboratory for Precision Therapy of Gastrointestinal Cancer, Zhengzhou, China

Background: Colon cancer (CC) is the second most common gastrointestinal malignancy. About one in five patients have already developed distant metastases at the time of initial diagnosis, and up to half of patients develop distant metastases from initial local disease, which leads to a poor prognosis for CC patients. Necroptosis plays a key role in promoting tumor growth in different tumors. The purpose of this study was to construct a prognostic model composed of necroptosis-related genes (NRGs) in CC.

Methods: The Cancer Genome Atlas was used to obtain information on clinical features and gene expression. Gene expression differential analysis, weighted gene co-expression network analysis, univariate Cox regression analysis and the least absolute shrinkage and selection operator regression algorithm were utilized to identify prognostic NRGs. Thereafter, a risk scoring model was established based on the NRGs. Biological processes and pathways were identified by gene ontology and gene set enrichment analysis (GSEA). Further, protein-protein interaction and ceRNA networks were constructed based on mRNA-miRNA-lncRNA. Finally, the effect of necroptosis related risk score on different degrees of immune cell infiltration was evaluated.

Results: CALB1, CHST13, and SLC4A4 were identified as NRGs of prognostic significance and were used to establish a risk scoring model. The time-dependent receiver operating characteristic curve analysis revealed that the model could well predict the 1-, 3-, and 5-year overall survival (OS). Further, GSEA suggested that the NRGs may participate in biological processes, such as the WNT pathway and JAK-Stat pathway. Eight key hub genes were identified, and a ceRNA regulatory network, which comprised 1 lncRNA, 5 miRNAs and 3 mRNAs, was constructed. Immune infiltration analysis revealed that the low-risk group had significantly higher immune-related scores than the high-risk group. A nomogram of the model was constructed based on the risk score, necroptosis, and the clinicopathological features (age and TNM stage). The

calibration curves implied that the model was effective at predicting the 1-, 3-, and 5-year OS of CC.

Conclusion: Our NRG-based prognostic model can assist in the evaluation of CC prognosis and the identification of therapeutic targets for CC.

KEYWORDS

weighted gene co-expression network analysis (WGCNA), tumor microenvironment, tumor immune infiltrating cells, copy number variation (CNV), nomogram, calibration curves, ceRNA networks

1 Introduction

Colon cancer (CC) is a deadly tumor that affects individuals worldwide. The incidence of CC is increasing, especially in cities and regions with rapid economic development in the United States (1). With the popularization of cancer screening and advancements in treatment-related medical technology, patient outcomes have improved significantly. But as the onset of CC is insidious, there's still a lot patients diagnosed in the advanced stage, where the condition is severe and difficult to treat, and palliative care is the only available treatment option (2, 3). Only few biomarkers are available for the diagnosis and therapy of CC. Circulating tumor DNA (ctDNA) is a subset of circulating free DNA (cfDNA) from tumor cells. In many studies, ctDNA has been found to be of great value in the early diagnosis, efficacy evaluation, drug resistance monitoring and prognosis prediction of tumors. Among them, targeted drug therapy guided by ctDNA is the most important clinical application at present (4, 5). At present, ctDNA as biological markers have been found to be associated with the prognosis of colon cancer, but they have not been widely applied in clinic (6–8). Therefore, exploring potential biomarkers of CC remains the focus of CC-related research.

Necroptosis is a lytic manner of programmed cell death that prevents the self-destruction of activated cells that are blocked by apoptosis. In some degenerative or inflammatory diseases, necrotizing apoptosis plays a role in destroying infected cells or damaged cells (9). Unlike apoptosis, the activation of necroptosis does not depend on caspase kinase activation. Under caspase inhibition, the binding of death receptor and ligand can trigger necrotizing apoptosis (10). Necrotizing apoptosis plays a dual role in tumorigenesis and development, which can not only enhance cellular immunity (11) and play an anti-tumor role, but also stimulate the tumor to form an immunosuppressive microenvironment and promote tumor progression (12). According to previous studies (13) and owing to the activity of intracellular RIP-1 and MLKL, the combination of 5-FU and ZVAD (caspase inhibitor) can promote necroptosis of colorectal cancer (CRC) cells, highlighting the important value of necroptosis in the study of tumor drug resistance. However, a prognostic scoring system for CC based on the tags of genes associated with necroptosis has not been established.

Recently, high-throughput sequencing and the gene chip technology have been widely used in the field of life science (14, 15). Bioinformatics is an important tool for analyzing large volumes of existing biological data. By analyzing the potentially important core genes or prognostic factors within the data (16, 17), potential tumor markers or therapeutic targets can be explored (18). Several previous studies focused on single genes as diagnostic and prognostic indicators (19, 20). However, these biomarkers, especially individual gene expression levels that may be influenced by multiple factors, are insufficient to accurately and independently predict patient outcomes. As a result, these markers cannot be used as reliable and independent prognostic indicators. Therefore, in this study, statistical models composed of multiple prognostic necroptosis-related markers were employed to improve the predictive power of CC.

In recent years, the ceRNA hypothesis has attracted attention and has become one of the hot spots in the study of RNA interaction. The regulatory mechanisms among mRNA, miRNA, lncRNA, or circRNA are extremely complex and have important biological significance. LncRNA or circRNA can compete with mRNA to bind to miRNA, thereby forming a complex lncRNA-miRNA-mRNA network or circRNA-miRNA-mRNA network. However, an imbalance in the ceRNA regulatory network can lead to the initiation and progression of tumors (21). To date, the function of most mRNAs as ceRNAs in the progression and prognosis of CC has not been thoroughly defined.

In this study, the prognostic risk model of necroptosis-related genes (NRGs) was established, and the diagnostic and

predictive significance of the model was evaluated. Thereafter, a ceRNA network was constructed based on mRNA-miRNA-lncRNA, and the effects of necroptosis-related risk score on different degrees of immune cell infiltration were evaluated. Overall, the findings of this study provide a theoretical foundation for further assessments of the diagnosis, treatment, and molecular mechanism of CC.

2 Materials and methods

2.1 Data download

The Cancer Genome Atlas (TCGA) Genomic Data Commons (GDC) website (https://portal.gdc.cancer.gov/) was used to obtain the expression spectrum data for colon cancer (colon adenocarcinoma, COAD) patients (n = 514), such as the count, and FPKM and TPM values; and patient clinical data (n=430), such as gender, age, TMN stage, and survival prognosis. "Masked somatic mutation" was selected as the somatic mutation data (n=420) and downloaded. The somatic mutations were visualized using maftools package (22) in R to obtain tumor mutation burden (TMB) for per patient. Additionally, the MSI data in the TCGA-COAD patients' dataset was obtain the tumor mutation burden (TMB) per patient. Additionally, the MSI data in TCGA-COAD patient dataset were obtained from the cBioPortal database (https://www.cbioportal.org). The baseline information of TCGA-COAD patients is provided in Table 1.

Gene expression data and the clinical characteristics of patients of GSE17536 (23) and GSE39582 (24) were downloaded from the GEO database. The data samples were obtained from *Homo Sapiens*. The chip platforms were grounded in the GPL570 [HG-U133_plus_2] Affymetrix Human Genome U133 Plus 2.0 Array. After deleting patients lacking clinical information, 177 COAD tissue samples were included in GSE17536, all of which were used in the analysis. GSE39582 included 585 COAD tissue samples. As survival information was not available for 5 samples, 580 were included in the analysis. R's limma package (25) was used to standardize the two data sets separately. Table S1 shows the information from GEO.

TABLE 1 Baseline data table of patients in TCGA-COAD dataset.

Characteristic	levels	Overall
n		363
status, n (%)	Alive	279 (80.9%)
	death	66 (19.1%)
Age, n (%)	<60	96 (26.4%)
	≥60	267 (73.6%)
Gender, n (%)	female	177 (48.8%)
	male	186 (51.2%)
Stage, n (%)	stage I	62 (17.4%)
	stage II	145 (40.7%)
	stage III	103 (28.9%)
	stage IV	46 (12.9%)

2.2 Calculation of the necroptosis score based on gene expression matrix

For all samples in the combined dataset and based on 36 necrotizing apoptosis-related genes from previously published literature (26), the necroptosis score (NPs) of every sample in the TCGA-COAD dataset was determined using the R package, GSVA (27), and the ssGSEA method according to the gene expression matrix of the respective sample.

2.3 Screening of differentially expressed genes (DEGs)

Using the above method, the NPs of each sample was obtained, and the optimal cut-off value was selected in combination with the patient's survival data. Based on the NPs score, the NPs group was separated into high and low NPs. To identify genes associated with NPs, the DEGs between high NPs and low NPs in TCGA-COAD samples were identified using the R package, limma (25). The screening threshold of the DEGs was set to $|\log2 \text{ fold change (FC)}|>1$ and adjusted $P < 0.05$. The results of the difference analysis are presented as a heatmap and a volcano plot.

2.4 Weighted gene co-expression network analysis (WGCNA)

WGCNA was implemented using the R package, WGCNA (28). First, the weighted values of the calculated correlation coefficients between any two genes were used to generate connections between genes in the network to assemble a scale-free network. A hierarchical clustering tree was then established according to the correlation coefficients. The branches of the cluster tree highlighted various genetic modules, and various colors signified different modules. The module saliency was then calculated. All mRNAs of the sample were input into WGCNA to measure the associations between the two NPs groups and different modules. All genes were recorded in their respective modules. The genes in the respective modules were considered as modular characteristic genes (MEs). The correlation between the NPs values and genes was determined based on the significance of genes. Module membership was determined

according to the relevance between module genes and DEG expression profile. The modules of interest were selected using the MS score, and all genes in these modules were recognized to have a high correlation with NPs.

2.5 Subtype analysis of patients with CC based on necroptotic genes

Based on the necroptosis characteristic genes and TCGA-COAD expression data, the k-means method in "ConsensusClusterPlus" R package (29) was used to perform unsupervised cluster analysis to identify the necroptosis subtypes. The concordant clustering algorithm was used to discern the cluster number. The analysis was repeated 1000 times to ensure stability of the category. Principal component analysis (PCA) was conducted for patients with grouped subtypes to determine the differences between samples. Survival analysis was implemented after grouping to determine the influence of various subtypes on prognosis.

2.6 Establishment and testing of the prognostic risk models based on NPs characteristic genes

The results of differential expression analysis combined with WGCNA analysis were used to acquire the NPs-related characteristic genes. The significantly differentially expressed NPs-related characteristic genes were involved in the model, and the prognostic genes were screened using univariate Cox regression analysis, with a cut-off P value of 0.1. Subsequently, the selected genes were regularized and dimensionally reduced using the least absolute shrinkage and selection operator regression (LASSO) algorithm to further identify prognostic-related genes. Thereafter, the weighted normalized gene expression value of the penalty coefficient acquired by multivariate Cox analysis (STEP method) was used to establish a risk score formula. Using the median risk score, patients were divided into high-risk and low-risk groups.

$$\text{risk}Score = \sum_i Coefficient\ (hub\ gene_i) * mRNA\ Expression\ (hub\ gene_i)$$

The above dataset based on TCGA-COAD served as a training set, and the internal test was conducted using the bootstrap method with 1000 re-sampling. Thereafter, the coefficient based on model variables was used to calculate the risk score for each sample in test sets, GSE17536 and GSE39582, using the predict function in the "survival" R package (https://CRAN.R-project.org/package=survival>). Finally, a time-dependent receiver operating characteristic (ROC) curve was plotted. The area under the curve (AUC) was used to reflect the performance of the model.

2.7 Analysis of DEGs in the NPs-related metabolic model

To acquire genes relevant to the NPs model, DEGs between the high-risk group and low-risk group of TCGA-COAD patients were analyzed using the R limma package. The screening threshold of the significantly different DEGs was defined as $|\text{LogFC}| > 1$ and adj. P value < 0.05. The DEGs were visualized using volcano maps and heat maps.

2.8 Functional enrichment analysis

GO (30) analysis is an approach adopted for massive functional enrichment research, including biological processes (BP), molecular functions (MF), and cellular components (CC). Kyoto Encyclopedia of Genes and Genomes (KEGG) (31) is an extensively used database that stores data regarding genomes, biological pathways, diseases, and drugs. The ClusterProfiler package of R (32) was used for GO and KEGG analyses of significant DEGs. The critical value of FDR less than 0.05 indicated significant difference.

To explore the discrepancies in biological processes among different subgroups, GSEA was performed according to the gene expression profiling dataset of COAD patients. The gene set "c2.cp.v7.2.Symbols. gmt" obtained from the MSigDB (33) database was used for GSEA. An FDR < 0.25 indicated statistical significance.

2.9 Identification and correlation analysis of the tumor immune infiltrating cells

To quantitatively analyze the relative tumor infiltration degree of various immunocytes in COAD, the ssGSEA algorithm was employed to differentiate between highly sensitive and specific phenotypes of various human immune cells in the tumor microenvironment (TME). The algorithm revealed 28 gene sets for labeling various tumor-infiltrating immunocyte types based on a study by Bindea et al. (34). The gene sets comprised various human immunocyte subtypes, such as macrophages, mast cells, etc. Enrichment scores obtained using ssGSEA in R's GSVA package indicated the degree of infiltration of various immune cell types in every sample. Meanwhile, R's ESTIMATE package (35) was employed to evaluate the immunological activity of the tumor. ESTIMATE quantitatively analyzes the immune activity of a tumor sample according to its gene expression profile to obtain an immune score per tumor sample. Herein, the discrepancies in immune infiltration features between the two groups of patients with COAD were compared.

2.10 Analysis of copy number variation (CNV)

To compare the copy number differences between the two groups of TCGA-COAD patients, the TCGAbiolinks package (36) of R was used to obtain the Masked Copy Number Segment information. The downloaded CNV fragments were subjected to GISTIC 2.0 analysis by GenePattern (https://cloud.genepattern.org); default parameters were used for the analysis.

2.11 Establishment of the prognostic model according to the NPs risk score

The predictive power of the NPs risk score in combination with clinicopathological characteristics on OS based on univariate and multivariate Cox analysis was used to demonstrate that the NPs risk score in combination with clinicopathological features can be used to estimate patient prognosis. The risk scoring model was then combined with clinicopathological features to establish a nomogram, and the accuracy of the model was reflected by the AUC values under the time-ROC curve. The performance of the rosette was assessed using a calibration curve that compared the predicted values of the rosette with the observed actual values. Testing of the model was carried out using the bootstrap method, and internal re-sampling was performed 1000 times.

2.12 Establishment of the PPI network and screening of hub-genes

The STRING (37) online tool was applied to establish the PPI network. Genes with scores > 0.7, which indicates high credibility, were selected from the STRING database to construct the network model visualized using Cytoscape (version3.7.2) (38). The Maximal Clique Centrality (MCC) of each node was calculated using the cytoHubba plug-in (39) in Cytoscape software.

2.13 Establishment of the ceRNA network according to mRNA-miRNA-lncRNA

Information on the miRNA-mRNA interactions was collected from the miRTarBase database (40). The core mRNAs acquired from the PPI analysis were used to predict the miRNAs that might be regulated. The relevant lncRNAs were further predicted based on evidence from the luciferase reporter gene assay. The results of ceRNA analysis were visualized using Cytoscape software. The P values of all hypothetical tests were two-sided, and a p value of less than 0.05 was considered to indicate statistical significance.

2.14 Statistical analysis

Data analysis was performed using R software. version 4.0.2. Independent Student's t test and Mann–Whitney U test (namely Wilcoxon rank-sum test) were used to estimate the differences between two groups of normally distributed and two groups of non-normally distributed continuous variables, respectively. The $\chi 2$ test or Fisher exact test was carried out to determine the difference between the two groups of categorical variables. Survival analysis was carried out using R's survival package. The Kaplan–Meier survival curve was applied to display survival differences, and log-rank test was performed to compare the differences in survival. Univariate and multivariate Cox analyses were based on the R survival package. LASSO analysis was carried out using the glmnet R package (41).

3 Results

3.1 Expression and mutation of necroptotic genes in CC patients

The whole research design was illustrated in Figure 1. First, 36 necroptotic genes were extracted from the RNA-seq data of TCGA-COAD and their expression differences were compared between the normal group and tumor group. A total of 30 necroptotic genes were found to be differentially expressed, and only 6 genes were not differentially expressed. Such results suggest that necroptosis may play crucial role in COAD (Figures 2A, B). According to the somatic mutation data of TCGA-COAD samples, mutation information was obtained for the 36 necroptotic genes using the maftools package. The necroptotic genes were not found to mutate significantly in COAD patients, except TP53, in which the mutation frequency of TNF, CASP6, and TNFSF10 was less than 1% (Figure 2C). In addition, the prognostic status of the 36 genes was analyzed. Only TRAF2, RIPK3, and IPMK genes were found to have significant prognostic differences, and may thus serve as potential prognostic markers (Figure S1).

3.2 Calculation of the necroptosis score and screening of characteristic genes

Based on the above differential necroptosis genes, the NPs of each COAD patient was obtained using the ssGSEA algorithm to represent the necroptosis level of the patient. The optimal cut-off value was determined using prognostic analysis based on the necroptosis score. Thereafter, TCGA-COAD samples were

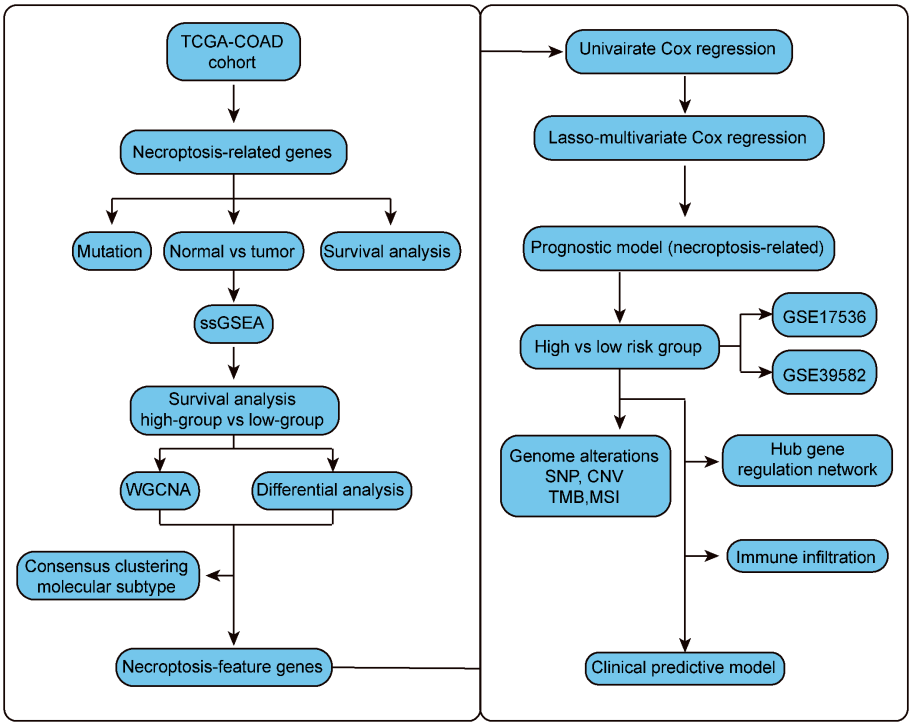

FIGURE 1
The flow chart.

divided into groups with high NPs and low NPs. Survival analysis revealed that patients with low necrosis apoptosis scores had worse prognosis than patients with high necroptosis score (log-rank $P < 0.024$; Figure 3A). Subsequently, 766 DEGs were acquired through rigorous analysis, including 380 significantly upregulated and 386 downregulated genes, respectively (Figures 3B, C). A gene co-expression network was also established to identify biologically significant gene modules through WGCNA and further identify genes closely related to COAD necroptosis. In this study, 4 modules (except grey module) were obtained for subsequent analysis (Figures 3D, E). As shown in Figure 3F, we integrated the difference analysis results with the MEturquoise, MEblue, and MEbrown modules to obtain a total of 209 necrotizing apoptotic characteristic genes.

3.3 Identification of necroptotic subtypes

Based on the above genes with necroptosis characteristics, consistent clustering was employed to cluster LIHC samples. Here, K=2 was selected and two subgroups, subgroup 1 and subgroup 2, were obtained (Figure S2A). Dimension reduction analysis was conducted *via* PCA and the PCA results of the two groups were plotted. Based on the results, the degree of differentiation between the two groups was not obvious, which may be due to the insignificant clustering gene characteristics, resulting in insignificant grouping differences (Figure S2B). The prognostic characteristics of subgroup 1 and subgroup 2 was subsequently analyzed using the KM curve; however, no distinct difference in prognosis was found between the two groups, suggesting that clustering subtypes based on all necroptotic characteristic genes could not distinguish differences in the prognosis of patients (Figure S2C). However, when the expression distributions of characteristic genes of type 1 and type 2 were compared, necroptotic characteristic genes were found to be significantly differentiated in the two subtypes, suggesting that the classification is of guiding significance for assessing the mechanism of necroptosis, but not suitable for identifying clinical prognostic markers (Figure S2D).

3.4 Construction and evaluation of risk models related to necroptosis

Based on the necroptosis characteristic genes, a necroptosis-related risk score system was constructed to quantitatively evaluate the prognostic information of each COAD patient by

10.3389/fimmu.2022.1085038

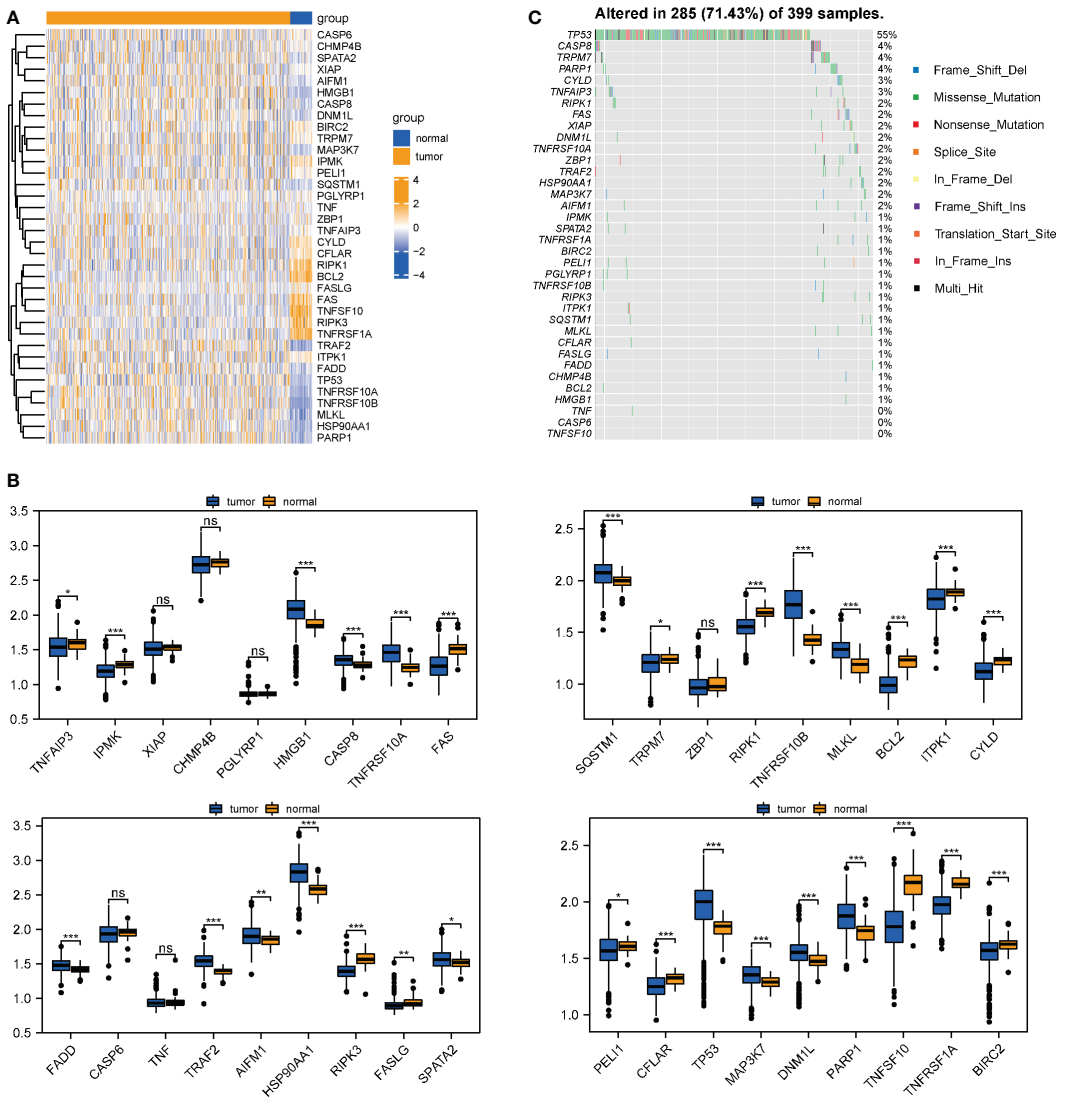

FIGURE 2
Differential expression and mutation information of necroptotic genes in TCGA-COAD datasets. **(A, B)** Necroptotic genes were compared between the normal and tumor groups in TCGA-COAD dataset using the Wilcoxon test. *P < 0.05, **P < 0.01, ***P < 0.001. **(C)** Mutation information of the necroptotic genes in TCGA-COAD. "ns" represents "no significance".

risk score. First, univariate Cox regression analysis revealed that 23 genes met the screening criteria ($P < 0.05$). Dimension reduction was analyzed using LASSO (Figure 4A). When 5 variables were present, the most stable model was obtained. Multivariate Cox regression analysis revealed that Calbindin 1 (CALB1), Carbohydrate sulfotransferases (CHST13), and solute carrier family 4 member 4 (SLC4A4) were independent prognostic factors (Figure 4B). Multivariate Cox analysis was also carried out to obtain the model coefficients of important characteristic genes. Thereafter, the gene expression was multiplied and summed with its coefficients to construct a risk score. The final risk score (necroptosis risk score related to prognosis) was calculated for each sample. In terms of the risk score and gene expression values of patients, a heat map of the risk factors was plotted to show the distribution of the risk score (Figure 4C). The time-dependent ROC curve analysis revealed AUC values of 0.684, 0.657, and 0.710 for the 1-, 3-, and 5-year OS, respectively, which indicated that risk score was an ideal predictor of OS in COAD patients (Figure 4D). For the external dataset test, the GSE39582 and GSE17536 datasets were

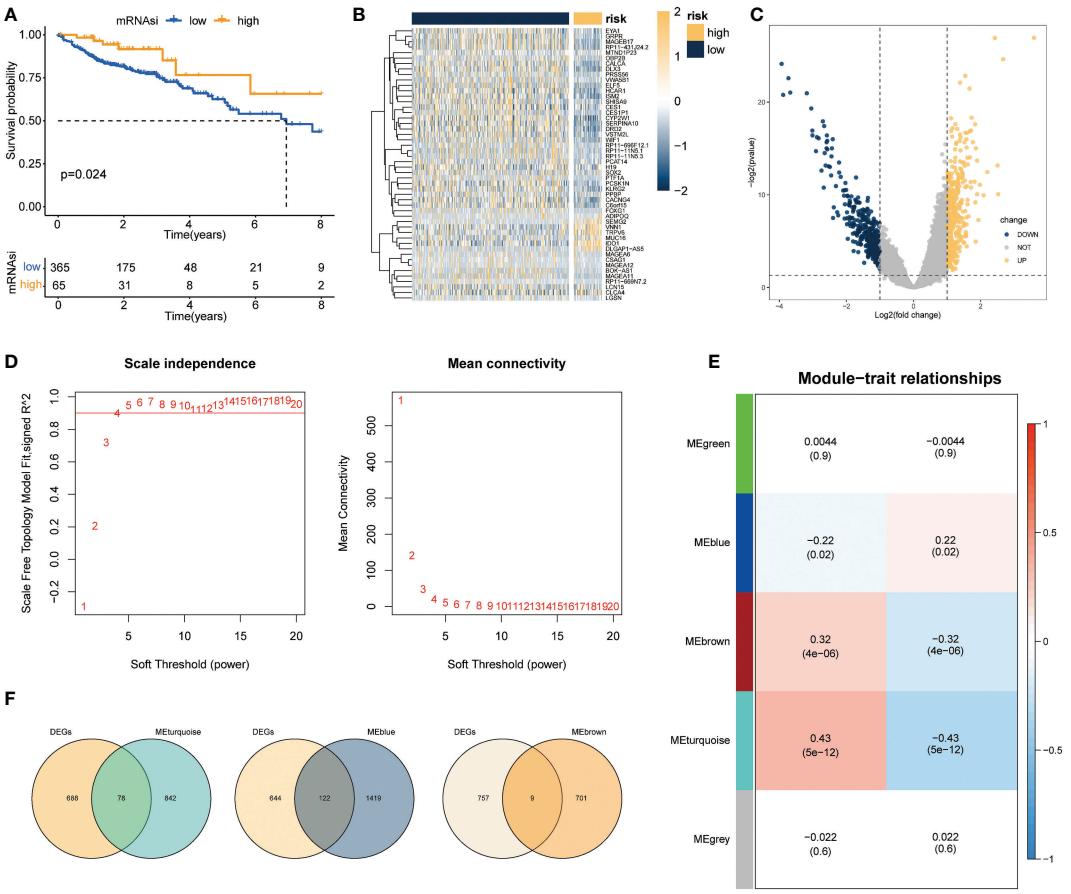

FIGURE 3
Screening of genes associated with necroptosis. **(A)** Survival analysis results revealed marked difference in survival status between groups with high and low necrotizing apoptosis scores (log-rank *P* =0.024); **(B, C)** Volcano maps and heat maps revealing DEG expression among COAD samples in the groups with high and low necrotizing apoptosis. **(D)** Quality control result selected by WGCNA softpower as 4. **(E)** Set of genes associated with the necroptosis phenotype analyzed and screened using WGCNA. The heat map demonstrated the correlation and significant difference between different gene modules and necroptosis score, where the P values are shown in parentheses. **(F)** Intersection of DEGs and genes in the significant module of WGCNA.

employed. After data normalization, the model was tested. For GSE39582, the ROC curve revealed AUC values of 0.682, 0.623, and 0.708 for the 1-, 3-, and 5-year OS, respectively. For GSE17536, the AUC values were 0.665, 0.712, and 0.758 for the 1-, 3-, and 5-year OS, respectively, indicating that the model had been well tested in external datasets (Figure S3).

3.5 Analysis of DEGs and functional enrichment in patients with high- and low-risk necroptosis score

To determine the role of the necroptosis-related risk model on the evolution of COAD samples, TCGA-COAD patients were divided into high-risk group and low-risk group based on the expression median value of the COAD patient risk model score in TCGA dataset. Subsequently, the DEGs in the two groups of patients were identified. Overall, 317 genes were significantly differentially expressed in COAD patients, among which 185 and 132 genes were significantly upregulated and downregulated, respectively (Figures 5A, B).

Functional enrichment analysis was performed using 317 genes identified as significantly DEGs. The GO analysis results revealed that the significant DEGs were related to GO:0044421 extracellular region part, GO:0005576 extracellular region, GO:0042588 zymogen granule, GO:0071752 secretory dimeric IgA immunoglobulin complex, and other functions (Figure 5C). KEGG functional analysis suggested that significant DEGs mainly had an impact on nitrogen metabolism, bile secretion, and rheumatoid arthritis, and other pathways (Figure 4D). Many pathways were found to be related to immunity, such as the chemokine signaling pathway, WNT signaling pathway, etc.

10.3389/fimmu.2022.1085038

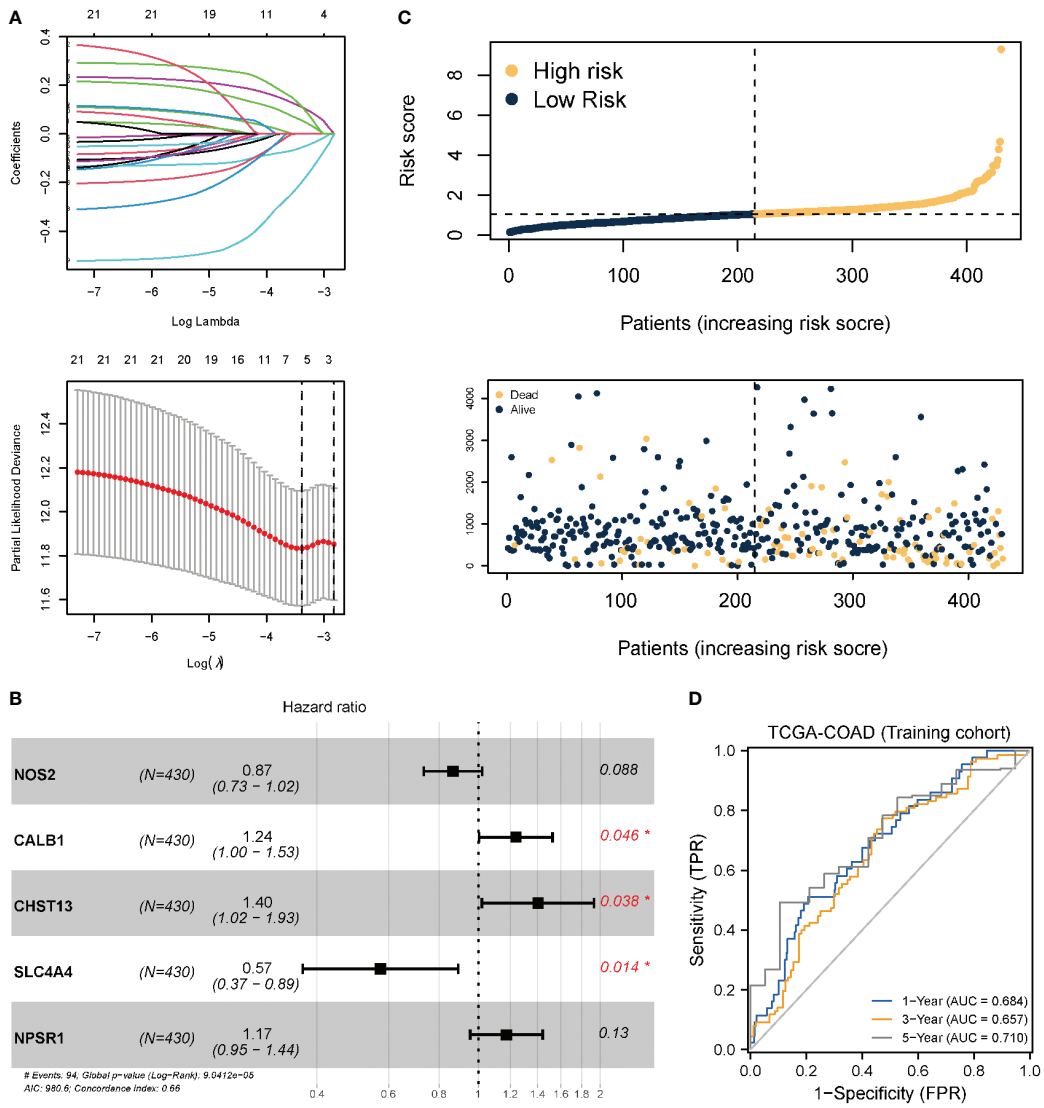

FIGURE 4
Prognostic model and model test based on necroptotic characteristic genes. **(A)** LASSO regression analysis; the number of variables corresponding to the optimal λ value is 5. **(B)** Three genes identified as independent prognostic factors through multivariate Cox stepwise regression analysis. *P < 0.05. **(C)** Risk score distribution and survival status of COAD patients; **(D)** TimeROC curve of TCGA-COAD (training set). Internal validation was performed using the Bootstrap method, with 1000 iterations.

Detailed GO and KEGG results are presented in Tables S2 and S3.

Based on the results of expression analysis, we continued GSEA and summarized the related results of the pathway database based on C2. KEGG pathway results and GSEA results revealed distinct differences in the activity of the JAK-STAT signaling pathway, WNT signaling pathway, fructose and mannose metabolism, primary immunodeficiency, and nitrogen metabolism (Figure 5). The detailed results of GSEA and the metabolism-related pathways are provided in Table S4. These findings coincide with those obtained from the KEGG database, and suggest the activation and inhibition characteristics of the high- and low-risk groups.

3.6 Protein interaction and regulatory network analysis

In terms of the DEGs in the high- and low- risk groups, we aimed to identify the hub gene that played a key role, and its

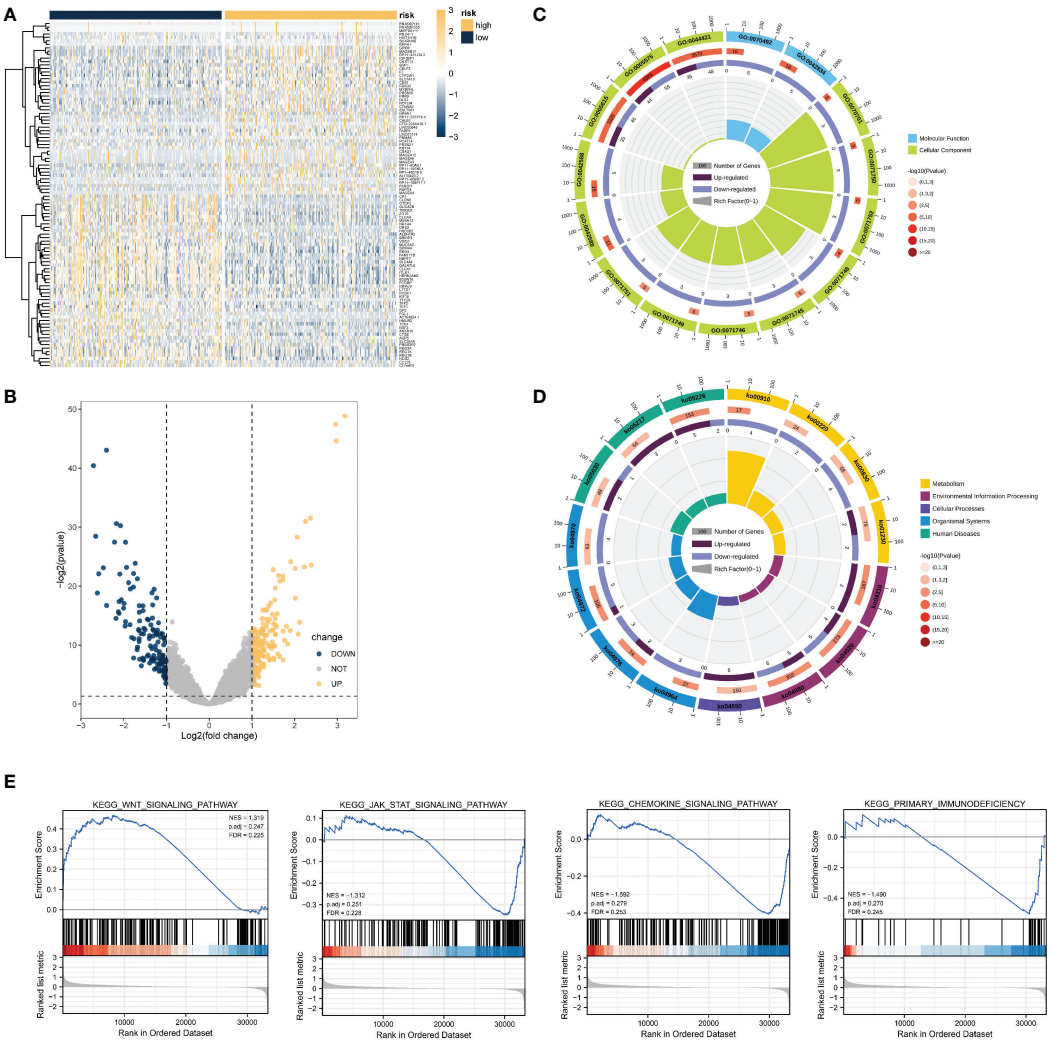

FIGURE 5
DEG analysis and functional enrichment analysis based on the necroptosis-related risk model. **(A, B)** Volcano map and heat map revealing DEG expression between the high- and low- risk groups in TCGA-COAD dataset. **(C)** GO analysis revealed that the differential genes were correlated with GO:0044421 extracellular region part, GO:0005576 extracellular region, GO:0042588 zymogen granule, GO:0071752 secretory dimeric IgA immunoglobulin complex, and other functions. **(D)** KEGG results revealed that these DEGs participated in nitrogen metabolism, bile secretion, rheumatoid arthritis, and other pathways. **(E)** GSEA results suggested that the KEGG results were similar to those of differential gene enrichment, and the main enrichment pathways were the WNT pathway, JAK-STAT pathway, immune-related pathway, etc.

potential molecular interaction mechanism. First, the STRING database was used to analyze the protein interaction mechanism. As shown in Figure 6A, after screening with a confidence of 0.700, the number of PPI nodes (protein) was 233. Further, 81 edges were identified, with an average connection degree of 0.695 for each node. The enrichment statistic P value of the whole PPI network was less than 1.0e-16.

The interacting proteins were further identified as hub genes using the cytoHubba plugin in Cytoscape. After the calculations, MUC5AC, MUC5B, WNT16, WIF1, and other interacting proteins that had the top 8 scores were found (Figure 6B). Subsequently, miRNA molecules and lncRNAs that potentially regulate these hub genes were analyzed using miRTarBase database. Finally, a ceRNA regulatory network was established using Cytoscape (Figure 6C).

3.7 Differential expression analysis of immunocyte infiltration

The influence of necroptosis-associated risk scores in patients with TCGA-COAD on their holistic immune

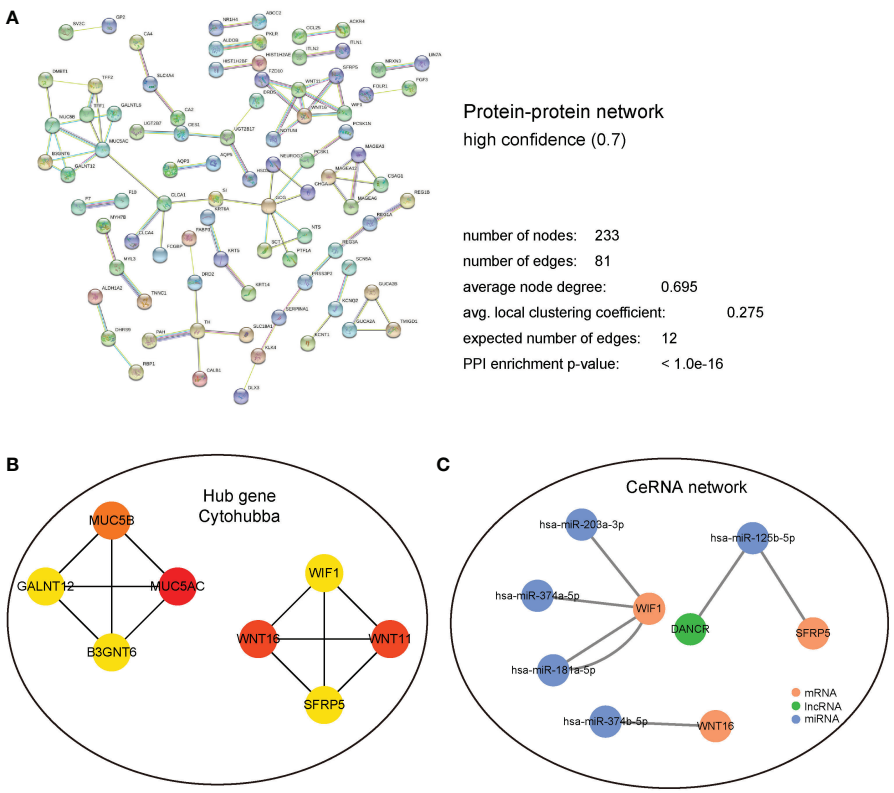

FIGURE 6
PPI and regulatory network analysis. **(A)** PPI regulation network, detailed display of the network node information, connection line information, and the composition of the different sub-network information. **(B)** Hub gene regulation network based on cytoHubba calculation. **(C)** CeRNA regulatory network predicted using the miRTarBase database. Blue represents miRNA; green represents LncRNA; and Brown represents mRNA.

characteristics and varying degrees of immunocyte infiltration was analyzed. Patients in the high-risk group were found to have significantly lower immune-related scores ($P < 0.001$); however, no distinct difference was found in the matrix score (Figures 7A, B). ssGSEA was used to appraise the changes and effects of immunological characteristics of COAD tissues during pathogenesis. Through ssGSEA, the relative enrichment scores of 28 different subtypes of immunocytes in the high- and low-risk groups of COAD patients was obtained. Heat maps were generated to illustrate their expression in different patients (Figure 7C). Based on the results, the expression abundance of immunocytes in the low-risk group was lower than that in the high-risk group. The correlation analysis results revealed that most immune cell infiltration levels were positively correlated (Figure 7D). Differential analysis also revealed distinctions in the infiltration levels of various immune cells between COAD samples in the high and low necrotizing apoptosis-related risk groups. Only effector memory CD8+ T cells, immature dendritic (iDC) cells, and other cells were not found to significantly differ between the groups (Figure 7E). A distinct difference was found between the HLA family expression levels and the various immunological targets of the high- and low-risk groups. Further, the immunoactive genes were almost all elevated in the low-risk group (Figures 7F, G).

3.8 Effects of the necroptosis-related risk score on genomic changes in COAD samples

The influence of the necroptosis-related risk score on changes in genetic variation levels, including single nucleotide polymorphism and CNV, in COAD patients was evaluated. The analysis of single-nucleotide mutations in common tumor-driven genes revealed that the high mutation levels were similar or close between patients with high and low scores in the necroptosis-related model (Figure 8A). Based on assessments of the frequency of CNV changes, CNV was found to be widely present in high- and low-risk samples. However, no distinct discrepancy in CNV was found between the two groups

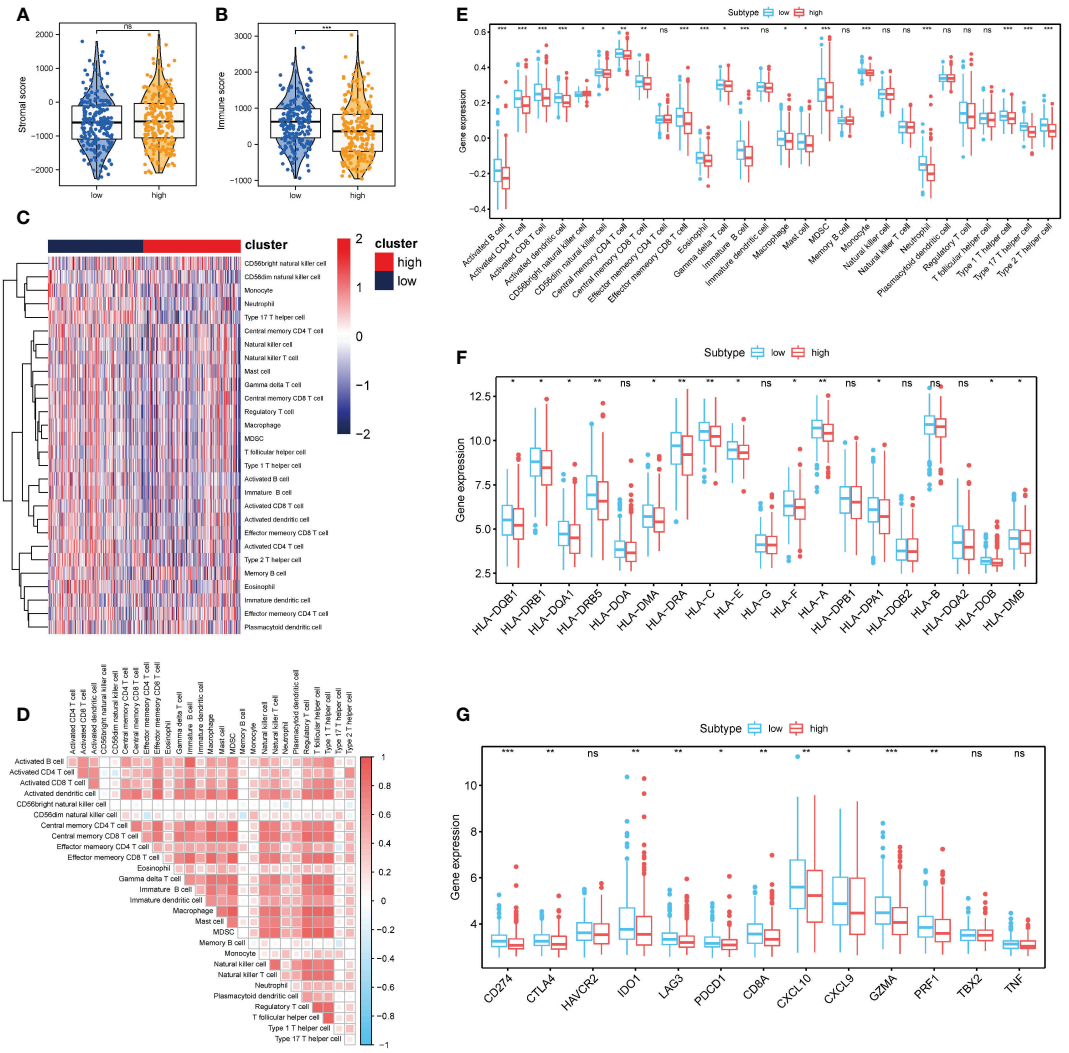

FIGURE 7
Correlation between necrosis risk scores and the infiltrates of different immunocytes **(A, B)** Immune score and stromal score between the low- and high- risk groups; **(C)** Heat map showing the invasion degrees of 28 different immune cells in TCGA and GEO database; **(D)** Association heat map showing the association between various levels of immunocyte infiltration. **(E)** Differential analysis of 28 different immunocyte infiltration levels between the two groups; **(F)** Analysis of differences in the expression of multiple members of the HLA family between the high- and low-risk related subgroups; **(G)** Differential expression analysis of multiple immunotherapy-related targets between the high- and low-risk related groups. *$P < 0.05$, **$P < 0.01$, ***$P < 0.001$. "ns" represents "no significance".

(Figures 8B, C). When TMB and MSI were compared between the two patient groups, no distinct discrepancy in TMB and MSI was found between the high and low risk groups. This result suggests that changes at the genomic level were not significant in the two groups (Figures 8D, E).

Based on the significant role of immunotherapy in tumors, the TIDE algorithm was employed to calculate the sensitivity of patients in the high- and low-risk groups to immunotherapy. The TIDE score in the low-risk group was higher than that in the high-risk group, suggesting that the immunotherapy response of the high-risk group might be better than that of the low-risk group (Figure 8F).

3.9 Establishment of a prognostic model according to the necroptosis-related risk score

To further probe the clinical value of necroptosis-related risk score, the clinical characteristics related to the high-risk and low-risk groups, such as the discrepancy in age and TNM stage, were analyzed. Notably, no distinct discrepancy was found in the age of patients in the high-risk group (Figure 9A). For gender, the proportion of women in the high-risk group increased (Figure 9B). In terms of stage, a significantly higher proportion of advanced patients was identified in the high-risk

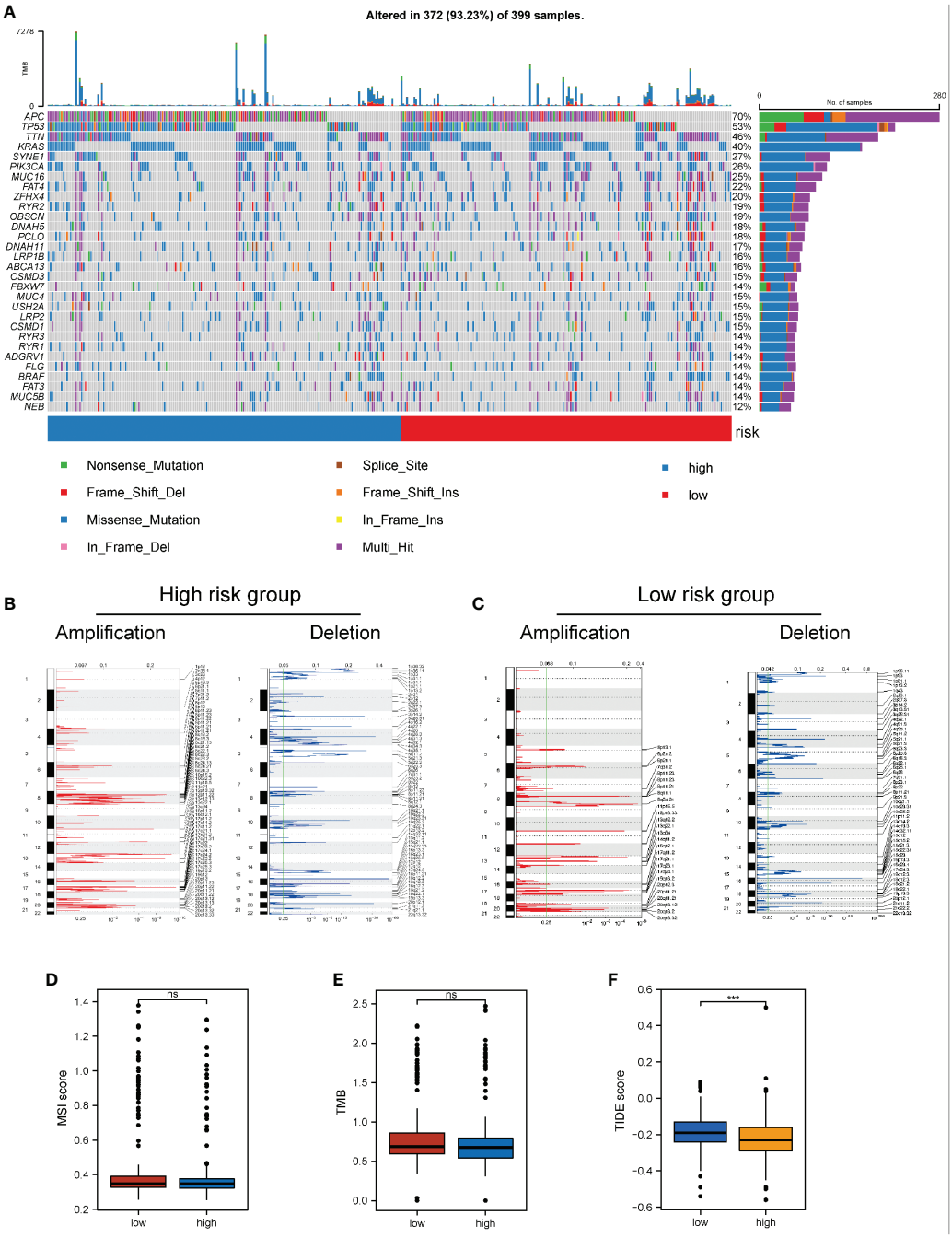

FIGURE 8
Impact of necroptosis-related risk grouping on genetic variation and immunotherapy in COAD samples. **(A)** Mutation map of common tumorigenic driver genes in patients in the high- and low-risk groups. Mutation information per gene per sample is presented as a waterfall plot, and different colors represent different types of mutation. The subsection above the legend shows the sudden change load; **(B, C)** Changes in the copy number levels of different genes in the high-risk and low-risk groups, where genes with significant copy number increase in red and genes with significant copy number deletions in blue; **(D, E)** Comparison of the difference in MSI level and TMB level between patients in the high- and low-risk groups, respectively; **(F)** Discrepancy between the high-risk and low-risk groups based on the tide score calculated from the tide database. ***$P < 0.001$. "ns" represents "no significance".

group (Figure 9C). Subsequently, based on the risk scores associated with necroptosis and clinicopathologic features (age and TNM stage), we established a prognostic model for COAD patients (Figure 9D) and analyzed the model *via* 1000 resampling using the bootstrap method. Based on timeROC, the AUC values were 0.798, 0.772, and 0.741 for 1-, 3-, and 5-years, respectively (Figure 9E). Calibration curves were generated to present the consistency of the model. A good consistency was found between the model's estimated 1-, 3-, and 5-year OS and the actual observed OS of patients (Figure 9F).

4 Discussion

In recent years, the incidence of CC among young people has gradually increased (42). Necroptosis has different functions in diverse tumors, including promoting tumor progression in lung cancer, pancreatic cancer, and glioblastoma (43–45), or inhibiting tumor growth in gastric cancer (GC), head and neck squamous cell carcinoma, melanoma and CRC (46–49). Necroptosis also has a two-way effect of promoting cancer and suppressing cancer in breast cancer (50, 51). As a result, we cannot appraise the prognosis of CC according to the expression

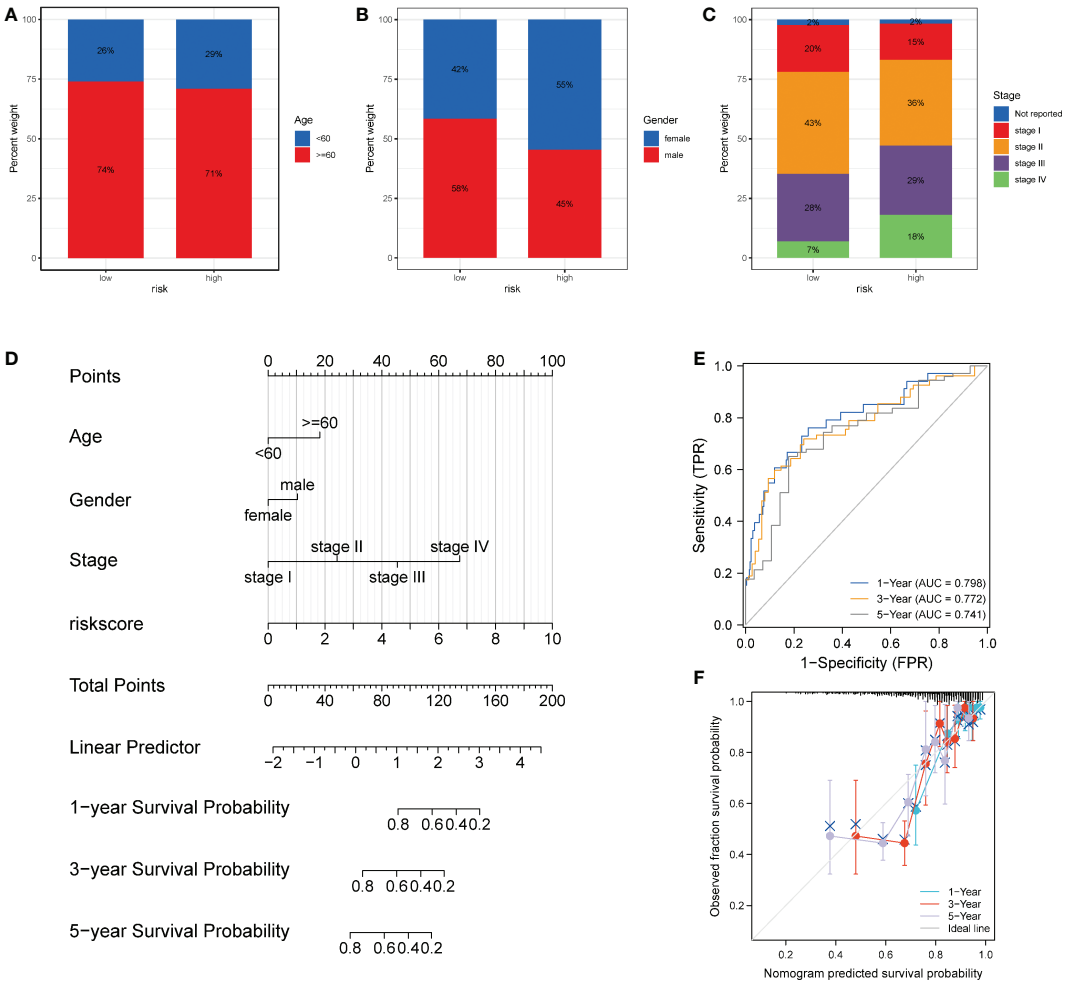

FIGURE 9
Performance of the necroptosis risk scores in the prediction of prognosis for patients with COAD. **(A-C)** Superimposed histogram showing the proportion of age, sex, and stage in patients in the high- and low-risk groups. The effect of age was similar in both groups, with an increased proportion of women in the high-risk group and significantly more advanced patients in the high-risk group. **(D)** Nomogram of the model. **(E)** Time-dependent ROC curve of the clinical prediction model based on risk score. **(F)** For the calibration curve of the nomogram, the bootstrap method was adopted, and resampling was performed 1000 times. The abscissa is the survival predicted by the nomogram, and the ordinate is the actual observed survival. The calibration plot revealed that the bias-corrected line for 1-, 3-, and 5- years OS was close to the ideal line, indicating good consistency between the predicted value and the actual value.

of individual necrosis regulators alone. Targeting NRGs is regarded as one of the effective methods for reducing tumor chemotherapy resistance, opening up a new approach for cancer treatment (52). A prior study revealed the construction of a prognostic model of lncRNA associated with GC necroptosis to differentiate hot and cold tumors of gastric carcinoma, to ultimately predict prognosis and the effectiveness of immunotherapy (53). Nevertheless, the theory of necroptosis in CC remains indistinct. In this study, prognostic risk models based on NPs characteristic genes was constructed to predict prognosis and immunotherapy, and systematically analyze the correlation between immune cell infiltration, immune checkpoints, and CC.

A total of 30 necroptotic genes were found to be differentially expressed. Thereafter, an analysis of DEGs revealed 766 DEGs in the high NPs group and low NPs group. A gene co-expression network was also established to identify biologically significant gene modules through WGCNA. Finally, a total of 209 necrotizing apoptotic characteristic genes were identified. The results of univariate Cox regression analysis, LASSO, and multivariate Cox regression analysis revealed that CALB1, CHST13, and SLC4A4 are independent prognostic marks. The final risk score was then calculated for each sample.

CALB1 is a vitamin D-dependent calcium-binding protein with six EF hands on the long arm of chromosome 8 at position 21.3 (54). CALB1, a component of Calbindin, has been confirmed to restrain tumor cell apoptosis. A prior study suggested that CALB1 may exert carcinogenic effects in ovarian cancer by inhibiting the p53 pathway (55). CALB1 is overexpressed in nonsmall cell lung cancer (NSCLC) tissues, and has a significant connection with lymph node metastasis and prediction of worse survival (56). In osteosarcoma, the downregulation of CALB1 gene expression resulted in reduced cell proliferation and cell clonal formation (57). In this study, CALB1 was verified to be an independent risk factor for prognosis. Further, its expression was found to increase, indicating poor prognosis of patients. Previous studies did not directly explain the relationship between CALB1 and CC. However, this study provides ideas for future diagnosis and treatment using *CALB1* as an oncogene.

Chondroitin sulfate (CS) is a glycosaminoglycans (GAGs) that participates in multiple biological processes and exerts crucial function in the interaction among stromal tumor cells (58). CHST13 gene is located on chromosome 3q21.3. A prior study suggested that CHST13 may serve as a negative regulator of HCC cell invasion and chemotherapy sensitivity by modulating Mitogen-Activated Protein Kinase (MAPK) activity (59). The mRNA expression of CHST13 was found to be significantly higher in in ovarian cancer specimens than in non-malignant tumor specimens (60). The results of this study indicate that CALB1 is an independent prognostic marker that plays the role of an oncogenic gene in the occurrence and development of CC. Thus, CALB1 could serve as an original biomarker for the diagnosis and prognosis evaluation of CC. However, no prior study has revealed that CHST13 can serve as a high-risk independent prognostic factor for OS. Accordingly, the present study is an important supplement to this field.

Homo sapiens solute vector family Member 4 (SLC4A4) is a member of the solute vector family which encodes an electrogenic Na+/HCO3− cotransporter (61). A previous study showed that SLC4A4 is increasingly expressed in prostate cancer tissues and cell lines. Further, the SLC4A4 expression level in cancer tissues was significantly associated with the degree of disease progression. SLC4A4 promotes prostate cancer progression through the Akt-mediated signaling pathway (62). Mir-222-3p expression was increased in PTC, while that of SLC4A4 was low. SLC4A4 could reverse the promoting function of Mir-222-3p on the proliferation, invasion, and migration of PTC cells (63). SLC4A4 had a lower expression in CRC than normal tissue, indicating that SLC4A4 was associated with poor prognosis (64). This study revealed that SLC4A4 may be an individual prognostic factor for CC patients and may exert a protective function in the tumorigenesis and progression of CC, which aligned well with the proposals from existing studies.

TCGA-COAD samples were divided into high- and low-risk groups based on the median expression value of the COAD patient risk model score in TCGA dataset. DEG analysis and functional enrichment analysis were then performed. The main enrichment pathways included the WNT pathway, JAK-STAT pathway, primary immunodeficiency pathway, chemokine pathway, fructose and mannose metabolism, nitrogen metabolism, etc.

The abnormal WNT signaling pathway is highly relevant to tumorigenesis and progression of multiple tumors, including CC (65–67). A previous study confirmed that activation of Wnt/β-catenin signaling contributes to the aberrant expression of several oncogenes that regulate the dedifferentiation phenotype and EMT in CC cells (68). Another study demonstrated that RBBP4 activates the Wnt/β-catenin pathway to accelerate the progression of CC (69). Based on this analysis, the WNT signaling pathway was identified to be significantly differentially enriched in the high-risk group phenotype.

The JAK/STAT pathway plays an increasingly vital role in regulating immune function, cell proliferation, differentiation, and death (70–72). Fibroblast growth factor receptor was reported to mediate PD-L1 expression in CC by activating the JAK2/STAT3 signaling pathway (73). Notably, activation of the JAKs structure promotes phosphorylation of the STAT family (74). The STAT3 signaling pathway is in close contact with the construction of a tumorigenic inflammatory microenvironment (75). The proliferation and viability of macrophages were reported to be enhanced by STAT3 activation, the immune tolerance of CC cells, and inhibition of extracellular matrix remodeling, thereby playing tumor-promoting roles (76). Based on this analysis, the JAK/STAT signaling pathway was

identified to be significantly differentially enriched in the low-risk group phenotype. Consistent with the results of this study, necroptosis may promote tumor progression by inhibiting the JAK/STAT pathway.

A systematic review of all cases of clinically diagnosed primary immunodeficiency and early-onset gastrointestinal (GI) cancer in three publicly available databases (MEDLINE, SCOPUS, and EMBASE) was previously conducted. Based on the results, primary immunodeficiency may be linked with potential risk factors for GI tumor. Adenocarcinomas of the stomach and colon were identified as the most common GI tumor (77). A previous literature revealed the involvement of chemokine (CC theme) ligand 7 (CCL7) in the progression of CRC (78). Another literature revealed the ectopic expression of the novel chemokine, CXCL17, in primary CC. The expression of CXCL17 might inform the prognosis of CC patients as CXCL17 enhances angiogenesis and attracts immune cells (79).

Based on the differential genes in the high and low risk groups, we opted to identify the key hub genes and their underlying molecular interaction mechanisms. These hub genes were *MUC5AC*, *MUC5B*, *WNT16*, *WNT11*, *WIF1*, *SFRP5*, *B3GNT6*, and *GALNT12*.

Mucin is a type of high molecular weight glycoprotein that is mainly involved in protecting epithelial cells of different organs from physical, chemical, and pathogenic damage (80). Mucin has abnormal expression in many malignant tumors, which is correlated with the proliferation, migration, invasion, adhesion and metastasis of tumor cells (81, 82). Changes in mucin expression have been reported to have a high correlation with the occurrence of CRC (81). Normally, expression of the secreted mucin, MUC5AC, is restricted to the stomach, lung, ear, conjunctiva, nasopharynx, and gallbladder. Several studies revealed that secreted MUC5AC is overexpressed in pancreatic cancer, lung cancer, and breast cancer (83–85). In fact, the secreted mucin, MUC5AC, was not identified in normal colonic mucosa, but was present in benign and malignant colon (80, 86). Prior literature confirmed that MUC5AC across the membrane protein, CD44, mediated the initiation and progression of CC, and provided resistance to chemotherapy in CRC through the β-catenin/p53/p21 signaling pathways (87). Secreted MUC5B mucin is generally not expressed in normal adult gastrointestinal mucosa, but has been proven to be differentially overexpressed in some subtypes of GC and CRC (88–90).

Numerous studies proved that over-activation of the Wnt signaling pathway is the main culprit in the onset of most human malignant tumors (91, 92). The Wnt signaling pathway plays a crucial role in multiple biological processes, such as embryogenesis and tissue homeostasis, exerting significant functions in the tumorigenesis and progression of CRC (93). A previous study found one or more mutations downstream in the Wnt signaling pathway, especially adenomatous polyposis coli (APC), in more than 90% of patients with CRC (94). WNT16 is one of the most impressive members of the WNT pathway (95, 96). The Wnt signaling pathway consists of canonical signals and noncanonical signals. Transmembrane proteins and their receptors mediate canonical Wnt signaling. Atypical Wnt signaling involves two pathways: the Wnt/Ca2+ pathway and the Wnt/c-jun N-terminal kinase (JNK)(planar cell polarity) pathway (97, 98). Wnt11 exerts its role *via* the noncanonical WNT pathway (97). Studies have confirmed that Wnt11 has a vital effect in the regulation of CRC cell proliferation, migration, and invasion (99, 100).

Wnt inhibitory factor 1 (WIF1) can interact with the Wnt protein to inhibit the canonical and non-canonical Wnt pathways to exert tumor inhibitory effect. WIF1 silenced by methylation has been found to participate in CC progression (101).

Secreted frizzled-related protein 5 (SFRP5) is a new type of adipocytokine, belonging to the SFRP family. Plasma SFRP5 levels were found to be distinctly decreased in obese patients and patients with diabetes, coronary artery disease, and other related diseases (102, 103). SFRP5 is underexpressed in moderate tumor tissues including lung cancer, ovarian cancer, GC, and breast cancer tissues, and is associated with poor prognosis (104–107). GALNT12 has been revealed to be a strong candidate for CRC susceptibility (108).

The B3GNT protein family is differentially expressed in multiple cancers, such as GI cancer, pancreatic carcinoma, and prostate cancer (109–111). The expression of B3GNT was found to be significantly decreased in GC and CRC (112). Although the 8 hub genes are relevant to tumorigenesis and progression, relevant studies on CRC are insufficient.

Based on increasing evidence, the ceRNA regulatory network plays a key role in the progression of various common cancers (113, 114). Shang et al. (115) found that the tumor-derived exosome, circPACRGL, acts as a sponge molecule of miR-142-3p/miR-506-3p, promoting the propagation, diversion, invasion, and adhesion of CC cells and N1 to N2 neutrophil differentiation. Wu et al. (116) showed that the LNC473-MIR574/miR15B-APAF1 IRES signaling axis could manipulate the propagation and apoptosis of CRC cells to influence the initiation and progression of CRC. In this study, a ceRNA regulatory network was constructed with 1 lncRNA, 5 miRNAs, and 3 mRNAs, revealing the potential regulatory mechanism of lncRNA-miRNA-mRNA in CC, and indicating the direction for further exploration of the pathogenesis of CC.

The immune microenvironment of CC and immunotherapy for CC patients should be explored. Immune cells in the TME perform vital functions in tumor progression (117). Based on prior studies, immune checkpoint inhibitors (ICIs) have great potential in immunotherapy of CC (118).

Immunocheckpoint inhibitor therapy of CC is in the "MSI era" because microsatellite instability (MSI) or mismatch repair gene status (MMR) is the best predictor of efficacy. Based on MSI

status, CC patients can be divided into two groups according to the efficacy of immunotherapy: "advantaged population" – MSI-H/dMMR type (MSI-H type for short); "Invalid population" – MSS/pMMR type cancer (MSS type cancer for short) (119). However, only about 5% of metastatic colorectal cancer (mCRC) is MSI-H, and about 95% is MSS type (120). How to turn "cold tumor" into "hot tumor" effective for immunotherapy has been a hot research direction. EYNOTE 016 Phase II clinical trial results showed that the objective response rate (ORR) of MSI-H mCRC patients was 40%, while the ORR of MSS mCRC patients was 0 (121). Immunotherapy has enriched the treatment modalities of multiple malignancies, including cytotoxic T lymphocyte-associated protein 4 (CTLA-4) and inhibitor of programmed death-1 (P D-1)/programmed cell death ligand 1(PD-L1). In patients with MSS mCRC, single-agent immunotherapy has failed, and multiple clinical trials of immunotherapy in combination with other therapies are being actively explored, including combination immunotherapy and immunotherapy combined with targeted therapy, radiotherapy, oncolytic virus, bisspecific antibodies, etc. Pd-1/PD-L1 inhibitors in combination with other immunotherapies may play a synergistic role in enhancing the antitumor effect. In a Phase II trial, durvalumab, a PD-L 1 inhibitor, combined with CTLA-4 inhibitor tremelimumab in refractory mCRC patients (92% pMMR/MSS) showed significant benefits in overall survival (OS) (122). In addition, in 2019, 24 patients with pMMR/MSS colon cancer who had failed standard treatment were included in the REGONIVO study. The ORR reached 33.3% after treatment with regorafenib combined with navulizumab, which significantly improved progression free survival (PFS) and OS (123).

In this study, the low-risk group was found to have higher levels of infiltration of multiple immunocytes, several HLA family members, and multiple immunotherapy targets. In addition, based on the significant role of immunotherapy in tumors, the TIDE algorithm was used to assess the sensitivity of both groups to immunotherapy. The TIDE score was lower in the high-risk group than the low-risk group, suggesting that the immunotherapy response of the high-risk group might be better than that of the low-risk group.

To further enhance the prediction accuracy of the model, a nomogram model based on the risk score prognostic model and clinical indicators (including age and pathological stage), which markedly improved the precision of the model, was established. The time-dependent ROC curve suggested that the risk score had favorable predictive performance for the OS of COAD patients. Calibration curves revealed a good consistency between the model's estimated 1-, 3-, and 5-year OS and the actual observed OS of patients.

This study had some limitations. First, clinical information and basic experimental verification are lacking. Further, the reliability of the results is dependent on the accuracy of TCGA dataset. In the future, the results of this study should first be verified through clinical trials and basic experiments. Prospective studies are also needed as retrospective studies may be subject to bias. Finally, clinical follow-up data are lacking to prove the accuracy of our prognostic model.

In this study, a prognostic risk model based on NRGs was established, and the diagnostic and predictive significance of the risk model was evaluated. The results of this study will help to reveal the pathogenesis of CRC, enabling the development of new diagnostic ideas, and facilitate the search for new therapeutic targets and prognostic molecular markers.

Data availability statement

The datasets for this study can be found in the Cancer Genome Atlas (TCGA) Genomic Data Commons (GDC) website (https://portal.gdc.cancer.gov/). The original contributions presented in the study are included in the article/Supplementary Material, further inquiries can be directed to the corresponding author.

Author contributions

WY designed the ideas for this paper. WY, DG, and FM contributed to the writing of the manuscript. SL, LP, ZZ, and YZ contributed to data collation and data analysis. WY, SL, YH, and XC analyzed and interpreted the data. All authors contributed to the article and approved the submitted version.

Funding

This study was supported by Henan Province Medical Science and Technology Tackling Program Joint Co-construction Project (No. LHGJ20200188).

Acknowledgments

We appreciate all participants and the staff of Fusheng Ge, SL, LP, ZZ, YH, and XC, and Affiliated Tumor Hospital of Zhengzhou University.

Conflict of interest

The authors declare that the research was conducted in the absence of any commercial or financial relationships that could be construed as a potential conflict of interest.

Publisher's note

All claims expressed in this article are solely those of the authors and do not necessarily represent those of their affiliated organizations, or those of the publisher, the editors and the reviewers. Any product that may be evaluated in this article, or claim that may be made by its manufacturer, is not guaranteed or endorsed by the publisher.

Supplementary material

The Supplementary Material for this article can be found online at: https://www.frontiersin.org/articles/10.3389/fimmu.2022.1085038/full#supplementary-material

References

1. Siegel RL, Miller KD, Fuchs HE, Jemal A. Cancer statistics, 2022. *CA: Cancer J Clin* (2022) 72(1):7–33. doi: 10.3322/caac.21708

2. Biller LH, Schrag D. Diagnosis and treatment of metastatic colorectal cancer: A review. *Jama* (2021) 325(7):669–85. doi: 10.1001/jama.2021.0106

3. Dekker E, Tanis PJ, Vleugels JLA, Kasi PM, Wallace MB. Colorectal cancer. *Lancet (London England)* (2019) 394(10207):1467–80. doi: 10.1016/S0140-6736(19)32319-0

4. Cohen JD, Li L, Wang Y, Thoburn C, Afsari B, Danilova L, et al. Detection and localization of surgically resectable cancers with a multi-analyte blood test. *Sci (New York NY)* (2018) 359(6378):926–30. doi: 10.1126/science.aar3247

5. Jiang T, Li X, Wang J, Su C, Han W, Zhao C, et al. Mutational landscape of cfDNA identifies distinct molecular features associated with therapeutic response to first-line platinum-based doublet chemotherapy in patients with advanced NSCLC. *Theranostics* (2017) 7(19):4753–62. doi: 10.7150/thno.21687

6. Osumi H, Shinozaki E, Yamaguchi K, Zembutsu H. Clinical utility of circulating tumor DNA for colorectal cancer. *Cancer Science* (2019) 110(4):1148–55. doi: 10.1111/cas.13972

7. Osumi H, Shinozaki E, Takeda Y, Wakatsuki T, Ichimura T, Saiura A, et al. Clinical relevance of circulating tumor DNA assessed through deep sequencing in patients with metastatic colorectal cancer. *Cancer Med* (2019) 8(1):408–17. doi: 10.1002/cam4.1913

8. Holm M, Andersson E, Osterlund E, Ovissi A, Soveri LM, Anttonen AK, et al. Detection of KRAS mutations in liquid biopsies from metastatic colorectal cancer patients using droplet digital PCR, idylla, and next generation sequencing. *PLoS One* (2020) 15(11):e0239819. doi: 10.1371/journal.pone.0239819

9. Snyder AG, Oberst A. The antisocial network: Cross talk between cell death programs in host defense. *Annu Rev Immunol* (2021) 39:77–101. doi: 10.1146/annurev-immunol-112019-072301

10. Newton K, Wickliffe KE, Dugger DL, Maltzman A, Roose-Girma M, Dohse M, et al. Cleavage of RIPK1 by caspase-8 is crucial for limiting apoptosis and necroptosis. *Nature* (2019) 574(7778):428–31. doi: 10.1038/s41586-019-1548-x

11. Yatim N, Jusforgues-Saklani H, Orozco S, Schulz O, Barreira da Silva R, Reis e Sousa C, et al. RIPK1 and NF-κB signaling in dying cells determines cross-priming of $CD8_+$ T cells. *Sci (New York NY)* (2015) 350(6258):328–34. doi: 10.1126/science.aad0395

12. Wang W, Marinis JM, Beal AM, Savadkar S, Wu Y, Khan M, et al. RIP1 kinase drives macrophage-mediated adaptive immune tolerance in pancreatic cancer. *Cancer Cell* (2020) 38(4):585–90. doi: 10.1016/j.ccell.2020.09.020

13. Oliver Metzig M, Fuchs D, Tagscherer KE, Gröne HJ, Schirmacher P, Roth W. Inhibition of caspases primes colon cancer cells for 5-fluorouracil-induced TNF-α-dependent necroptosis driven by RIP1 kinase and NF-κB. *Oncogene* (2016) 35(26):3399–409. doi: 10.1038/onc.2015.398

14. Angelescu R, Dobrescu R. MIDGET:Detecting differential gene expression on microarray data. *Comput Methods Programs Biomed* (2021) 211:106418. doi: 10.1016/j.cmpb.2021.106418

15. Wang Y, Zhao Y, Bollas A, Wang Y, Au KF. Nanopore sequencing technology, bioinformatics and applications. *Nat Biotechnol* (2021) 39(11):1348–65. doi: 10.1038/s41587-021-01108-x

16. Czech L, Huerta-Cepas J, Stamatakis A. A critical review on the use of support values in tree viewers and bioinformatics toolkits. *Mol Biol Evol* (2017) 34(6):1535–42. doi: 10.1093/molbev/msx055

17. Ma J, Chen X, Lin M, Wang Z, Wu Y, Li J. Bioinformatics analysis combined with experiments predicts CENPK as a potential prognostic factor for lung adenocarcinoma. *Cancer Cell Int* (2021) 21(1):65. doi: 10.1186/s12935-021-01760-y

18. Wang YC, Tian ZB, Tang XQ. Bioinformatics screening of biomarkers related to liver cancer. *BMC Bioinf* (2021) 22(Suppl 3):521. doi: 10.1186/s12859-021-04411-1

19. Long X, Deng Z, Li G, Wang Z. Identification of critical genes to predict recurrence and death in colon cancer: Integrating gene expression and bioinformatics analysis. *Cancer Cell Int* (2018) 18:139. doi: 10.1186/s12935-018-0640-x

20. Jia W, He YF, Qian XJ, Chen J. TPMT mRNA expression: A novel prognostic biomarker for patients with colon cancer by bioinformatics analysis. *Int J Gen Med* (2022) 15:151–60. doi: 10.2147/IJGM.S338575

21. van Eijck MM, Schoonman GG, van der Naalt J, de Vries J, Roks G. Diffuse axonal injury after traumatic brain injury is a prognostic factor for functional outcome: A systematic review and meta-analysis. *Brain Injury* (2018) 32(4):395–402. doi: 10.1080/02699052.2018.1429018

22. Mayakonda A, Koeffler HP. Maftools: Efficient analysis, visualization and summarization of MAF files from large-scale cohort based cancer studies. (2016). doi: 10.1101/052662

23. Smith JJ, Deane NG, Wu F, Merchant NB, Zhang B, Jiang A, et al. Experimentally derived metastasis gene expression profile predicts recurrence and death in patients with colon cancer. *Gastroenterology* (2010) 138(3):958–68. doi: 10.1053/j.gastro.2009.11.005

24. Marisa L, de Reyniès A, Duval A, Selves J, Gaub MP, Vescovo L, et al. Gene expression classification of colon cancer into molecular subtypes: characterization, validation, and prognostic value. *PLoS Med* (2013) 10(5):e1001453. doi: 10.1371/journal.pmed.1001453

25. Ritchie ME, Phipson B, Wu D, Hu Y, Law CW, Shi W, et al. Limma powers differential expression analyses for RNA-sequencing and microarray studies. *Nucleic Acids Res* (2015) 43(7):e47–e. doi: 10.1093/nar/gkv007

26. Qi L, Xu R, Ren X, Zhang W, Yang Z, Tu C, et al. Comprehensive profiling reveals prognostic and immunogenic characteristics of necroptosis in soft tissue sarcomas. *Front Immunol* (2022) 13:877815. doi: 10.3389/fimmu.2022.877815

27. Hänzelmann S, Castelo R, Guinney JJBb. GSVA. Gene set variation analysis for microarray and RNA-seq data. *BMC Bioinformatics* (2013) 14(1):1–15. doi: 10.1186/1471-2105-14-7

28. Langfelder P, Horvath S. WGCNA: An R package for weighted correlation network analysis. *BMC Bioinf* (2008) 9:559. doi: 10.1186/1471-2105-9-559

29. Wilkerson MD, Hayes DN. ConsensusClusterPlus: a class discovery tool with confidence assessments and item tracking. *Bioinf (Oxford England)* (2010) 26(12):1572–3. doi: 10.1093/bioinformatics/btq170

30. Ashburner M, Ball CA, Blake JA, Botstein D, Cherry JMJNG. Gene ontology: Tool for the unification of biology. *Gene Ontol Consortium* (2000) 25(1):25–9. doi: 10.1038/75556

31. Ogata H, Goto S, Sato K, Fujibuchi W, Kanehisa MJNAR. KEGG: kyoto encyclopedia of genes and genomes. *Nucleic Acids Res* (1999) 27(1):29–34. doi: 10.1093/nar/27.1.29

32. Yu G, Wang L-G, Han Y, He Q-Y. JOajoib. clusterProfiler: an r package for comparing biological themes among gene clusters. *OMICS* (2012) 16(5):284–7. doi: 10.1089/omi.2011.0118

33. Liberzon A, Birger C, Thorvaldsdóttir H, Ghandi M, Mesirov JP, Tamayo P. The molecular signatures database (MSigDB) hallmark gene set collection. *Cell Systems* (2015) 1(6):417–25. doi: 10.1016/j.cels.2015.12.004

34. Bindea G, Mlecnik B, Tosolini M, Kirilovsky A, Waldner M, Obenauf AC, et al. Spatiotemporal dynamics of intratumoral immune cells reveal the immune landscape in human cancer. *Immunity* (2013) 39(4):782–95. doi: 10.1016/j.immuni.2013.10.003

35. Yoshihara K, Shahmoradgoli M, Martínez E, Vegesna R, Kim H, Torres-Garcia W, et al. Inferring tumour purity and stromal and immune cell admixture from expression data. *Nat Commun* (2013) 4(1):1–11. doi: 10.1038/ncomms3612

36. Colaprico A, Silva TC, Olsen C, Garofano L, Cava C, Garolini D, et al. TCGAbiolinks: An R/Bioconductor package for integrative analysis of TCGA data. *Nucleic Acids Res* (2016) 44(8):e71. doi: 10.1093/nar/gkv1507

37. Mering CV, Huynen M, Jaeggi D, Schmidt S, Bork P, Snel B. STRING: a database of predicted functional associations between proteins. *Nucleic Acids Res* (2003) 31(1):258–61. doi: 10.1093/nar/gkg034

38. Shannon P, Markiel A, Ozier O, Baliga NS, Wang JT, Ramage D, et al. Cytoscape: A software environment for integrated models of biomolecular interaction networks. *Genome Res* (2003) 13(11):2498–504. doi: 10.1101/gr.1239303

39. Chin CH, Chen SH, Wu HH, Ho CW, Ko MT, Lin CY. cytoHubba: Identifying hub objects and sub-networks from complex interactome. *BMC Syst Biol* (2014) 8 Suppl 4(Suppl 4):S11. doi: 10.1186/1752-0509-8-S4-S11

40. Huang HY, Lin YC, Li J, Huang KY, Shrestha S, Hong HC, et al. miRTarBase 2020: Updates to the experimentally validated microRNA-target interaction database. *Nucleic Acids Res* (2020) 48(D1):D148–d54. doi: 10.1093/nar/gkz896

41. Simon N, Friedman J, Hastie T, Tibshirani RJ. Regularization paths for cox's proportional hazards model *via* coordinate descent. *J Stat Softw* (2011) 39(5):1. doi: 10.18637/jss.v039.i05

42. Islami F, Ward EM, Sung H, Cronin KA, Tangka FKL, Sherman RL, et al. Annual report to the nation on the status of cancer, part 1: National cancer statistics. *J Natl Cancer Institute* (2021) 113(12):1648–69. doi: 10.1093/jnci/djab131

43. Wang Q, Chen W, Xu X, Li B, He W, Padilla MT, et al. RIP1 potentiates BPDE-induced transformation in human bronchial epithelial cells through catalase-mediated suppression of excessive reactive oxygen species. *Carcinogenesis* (2013) 34(9):2119–28. doi: 10.1093/carcin/bgt143

44. Seifert L, Werba G, Tiwari S, Giao Ly NN, Alothman S, Alqunaibit D, et al. The necrosome promotes pancreatic oncogenesis *via* CXCL1 and mincle-induced immune suppression. *Nature* (2016) 532(7598):245–9. doi: 10.1038/nature17403

45. Park S, Hatanpaa KJ, Xie Y, Mickey BE, Madden CJ, Raisanen JM, et al. The receptor interacting protein 1 inhibits p53 induction through NF-kappaB activation and confers a worse prognosis in glioblastoma. *Cancer Res* (2009) 69(7):2809–16. doi: 10.1158/0008-5472.CAN-08-4079

46. Ke H, Augustine CK, Gandham VD, Jin JY, Tyler DS, Akiyama SK, et al. CYLD inhibits melanoma growth and progression through suppression of the JNK/AP-1 and β1-integrin signaling pathways. *J Invest Dermatol* (2013) 133(1):221–9. doi: 10.1038/jid.2012.253

47. Feng X, Song Q, Yu A, Tang H, Peng Z, Wang X. Receptor-interacting protein kinase 3 is a predictor of survival and plays a tumor suppressive role in colorectal cancer. *Neoplasma* (2015) 62(4):592–601. doi: 10.4149/neo_2015_071

48. McCormick KD, Ghosh A, Trivedi S, Wang L, Coyne CB, Ferris RL, et al. Innate immune signaling through differential RIPK1 expression promote tumor progression in head and neck squamous cell carcinoma. *Carcinogenesis* (2016) 37(5):522–9. doi: 10.1093/carcin/bgw032

49. Ertao Z, Jianhui C, Kang W, Zhijun Y, Hui W, Chuangqi C, et al. Prognostic value of mixed lineage kinase domain-like protein expression in the survival of patients with gastric caner. *Tumour Biol J Int Soc Oncodevelopmental Biol Med* (2016) 37(10):13679–85. doi: 10.1007/s13277-016-5229-1

50. Koo GB, Morgan MJ, Lee DG, Kim WJ, Yoon JH, Koo JS, et al. Methylation-dependent loss of RIP3 expression in cancer represses programmed necrosis in response to chemotherapeutics. *Cell Res* (2015) 25(6):707–25. doi: 10.1038/cr.2015.56

51. Liu X, Zhou M, Mei L, Ruan J, Hu Q, Peng J, et al. Key roles of necroptotic factors in promoting tumor growth. *Oncotarget* (2016) 7(16):22219–33. doi: 10.18632/oncotarget.7924

52. Wu Y, Dong G, Sheng C. Targeting necroptosis in anticancer therapy: mechanisms and modulators. *Acta Pharm Sin B* (2020) 10(9):1601–18. doi: 10.1016/j.apsb.2020.01.007

53. Zhao Z, Liu H, Zhou X, Fang D, Ou X, Ye J, et al. Necroptosis-related lncRNAs: Predicting prognosis and the distinction between the cold and hot tumors in gastric cancer. *J Oncol* (2021) 2021:6718443. doi: 10.1155/2021/6718443

54. Kang CM, Lee JH, Jeon M, Song JS, Kim SO. The effect of MMP-13, MMP-12, and AMBN on gingival enlargement and root deformation in a new type of gingival fibromatosis. *J Clin Pediatr Dentistry* (2018) 42(1):50–4. doi: 10.17796/1053-4628-42.1.9

55. Cao LQ, Wang YN, Liang M, Pan MZ. CALB1 enhances the interaction between p53 and MDM2, and inhibits the senescence of ovarian cancer cells. *Mol Med Rep* (2019) 19(6):5097–104. doi: 10.3892/mmr.2019.10212

56. Jin C, Lin T, Shan L. Downregulation of calbindin 1 by miR-454-3p suppresses cell proliferation in nonsmall cell lung cancer in vitro. *Cancer Biother Radiopharm* (2019) 34(2):119–27. doi: 10.1089/cbr.2018.2598

57. Huang Z, Fan G, Wang D. Downregulation of calbindin 1, a calcium-binding protein, reduces the proliferation of osteosarcoma cells. *Oncol Lett* (2017) 13(5):3727–33. doi: 10.3892/ol.2017.5931

58. Sugahara K, Kitagawa H. Recent advances in the study of the biosynthesis and functions of sulfated glycosaminoglycans. *Curr Opin Struct Biol* (2000) 10(5):518–27. doi: 10.1016/S0959-440X(00)00125-1

59. Zhou H, Li Y, Song X, Zhao Y, Cheng L, Zhao L, et al. CHST11/13 regulate the metastasis and chemosensitivity of human hepatocellular carcinoma cells *Via* mitogen-activated protein kinase pathway. *Digest Dis Sci* (2016) 61(7):1972–85. doi: 10.1007/s10620-016-4114-5

60. Oliveira-Ferrer L, Heßling A, Trillsch F, Mahner S, Milde-Langosch K. Prognostic impact of chondroitin-4-sulfotransferase CHST11 in ovarian cancer. *Tumour Biol J Int Soc Oncodevelopmental Biol Med* (2015) 36(11):9023–30. doi: 10.1007/s13277-015-3652-3

61. Huynh KW, Jiang J, Abuladze N, Tsirulnikov K, Kao L, Shao X, et al. CryoEM structure of the human SLC4A4 sodium-coupled acid-base transporter NBCe1. *Nat Commun* (2018) 9(1):900. doi: 10.1038/s41467-018-03271-3

62. Liu Z, Wang Q, Zhai G, Ke S, Yu X, Guo J. SLC4A4 promotes prostate cancer progression *in vivo* and *in vitro via* AKT-mediated signalling pathway. *Cancer Cell Int* (2022) 22(1):127. doi: 10.1186/s12935-022-02546-6

63. Zhang C, Chang Q, Hu Y, Chang W, Guo X, Fu L, et al. MiR-222-3p promotes the proliferation, migration and invasion of papillary thyroid carcinoma cells through targeting SLC4A4. *Histol Histopathol* (2021) 36(11):1199–207. doi: 10.14670/HH-18-387

64. Chen X, Chen J, Feng Y, Guan W. Prognostic value of SLC4A4 and its correlation with immune infiltration in colon adenocarcinoma. *Med Sci Monit Int Med J Exp Clin Res* (2020) 26:e925016. doi: 10.12659/MSM.925016

65. Carreira-Barbosa F, Nunes SC. Wnt signaling: Paths for cancer progression. *Adv Exp Med Biol* (2020) 1219:189–202. doi: 10.1007/978-3-030-34025-4_10

66. Bienz M. The subcellular destinations of APC proteins. *Nat Rev Mol Cell Biol* (2002) 3(5):328–38. doi: 10.1038/nrm806

67. Dietinger V, García de Durango CR, Wiechmann S, Boos SL, Michl M, Neumann J, et al. Wnt-driven LARGE2 mediates laminin-adhesive O-glycosylation in human colonic epithelial cells and colorectal cancer. *Cell Communication Signaling CCS* (2020) 18(1):102. doi: 10.1186/s12964-020-00561-6

68. Cheng R, Sun B, Liu Z, Zhao X, Qi L, Li Y, et al. Wnt5a suppresses colon cancer by inhibiting cell proliferation and epithelial-mesenchymal transition. *J Cell Physiol* (2014) 229(12):1908–17. doi: 10.1002/jcp.24566

69. Li YD, Lv Z, Zhu WF. RBBP4 promotes colon cancer malignant progression *via* regulating wnt/β-catenin pathway. *World J Gastroenterol* (2020) 26(35):5328–42. doi: 10.3748/wjg.v26.i35.5328

70. Salas A, Hernandez-Rocha C, Duijvestein M, Faubion W, McGovern D, Vermeire S, et al. JAK-STAT pathway targeting for the treatment of inflammatory bowel disease. *Nat Rev Gastroenterol Hepatol* (2020) 17(6):323–37. doi: 10.1038/s41575-020-0273-0

71. Villarino AV, Kanno Y, O'Shea JJ. Mechanisms and consequences of jak-STAT signaling in the immune system. *Nat Immunol* (2017) 18(4):374–84. doi: 10.1038/ni.3691

72. Yu H, Lee H, Herrmann A, Buettner R, Jove R. Revisiting STAT3 signalling in cancer: new and unexpected biological functions. *Nat Rev Cancer* (2014) 14(11):736–46. doi: 10.1038/nrc3818

73. Li P, Huang T, Zou Q, Liu D, Wang Y, Tan X, et al. FGFR2 promotes expression of PD-L1 in colorectal cancer *via* the JAK/STAT3 signaling pathway. *J Immunol (Baltimore Md 1950)* (2019) 202(10):3065–75. doi: 10.4049/jimmunol.1801199

74. Zhao H, Wu L, Yan G, Chen Y, Zhou M, Wu Y, et al. Inflammation and tumor progression: Signaling pathways and targeted intervention. *Signal Transduct Target Ther* (2021) 6(1):263. doi: 10.1038/s41392-021-00658-5

75. Wu J, Liu W, Williams JP, Ratner N. EGFR-Stat3 signalling in nerve glial cells modifies neurofibroma initiation. *Oncogene* (2017) 36(12):1669–77. doi: 10.1038/onc.2016.386

76. Yu H, Pardoll D, Jove R. STATs in cancer inflammation and immunity: A leading role for STAT3. *Nat Rev Cancer* (2009) 9(11):798–809. doi: 10.1038/nrc2734

77. Zheng B, Artin MG, Chung H, Chen B, Sun S, May BL, et al. Immunogenetics of gastrointestinal cancers: A systematic review and retrospective survey of inborn errors of immunity in humans. *J Gastroenterol Hepatol* (2022) 37(6):973–82. doi: 10.1111/jgh.15848

78. Kurzejamska E, Sacharczuk M, Landázuri N, Kovtonyuk O, Lazarczyk M, Ananthaseshan S, et al. Effect of chemokine (C-c motif) ligand 7 (CCL7) and its receptor (CCR2) expression on colorectal cancer behaviors. *Int J Mol Sci* (2019) 20 (3):686. doi: 10.3390/ijms20030686

79. Ohlsson L, Hammarström ML, Lindmark G, Hammarström S, Sitohy B. Ectopic expression of the chemokine CXCL17 in colon cancer cells. *Br J Cancer* (2016) 114(6):697–703. doi: 10.1038/bjc.2016.4

80. Niv Y, Rokkas T. Mucin expression in colorectal cancer (CRC): Systematic review and meta-analysis. *J Clin Gastroenterol* (2019) 53(6):434–40. doi: 10.1097/MCG.0000000000001050

81. Krishn SR, Kaur S, Smith LM, Johansson SL, Jain M, Patel A, et al. Mucins and associated glycan signatures in colon adenoma-carcinoma sequence: Prospective pathological implication(s) for early diagnosis of colon cancer. *Cancer Lett* (2016) 374(2):304–14. doi: 10.1016/j.canlet.2016.02.016

82. Reynolds IS, Fichtner M, McNamara DA, Kay EW, Prehn JHM, Burke JP. Mucin glycoproteins block apoptosis; promote invasion, proliferation, and migration; and cause chemoresistance through diverse pathways in epithelial cancers. *Cancer Metastasis Rev* (2019) 38(1-2):237–57. doi: 10.1007/s10555-019-09781-w

83. Kaur S, Smith LM, Patel A, Menning M, Watley DC, Malik SS, et al. A combination of MUC5AC and CA19-9 improves the diagnosis of pancreatic cancer: A multicenter study. *Am J Gastroenterol* (2017) 112(1):172–83. doi: 10.1038/ajg.2016.482

84. Lakshmanan I, Rachagani S, Hauke R, Krishn SR, Paknikar S, Seshacharyulu P, et al. MUC5AC interactions with integrin β4 enhances the migration of lung cancer cells through FAK signaling. *Oncogene* (2016) 35(31):4112–21. doi: 10.1038/onc.2015.478

85. Pereira MB, Dias AJ, Reis CA, Schmitt FC. Immunohistochemical study of the expression of MUC5AC and MUC6 in breast carcinomas and adjacent breast tissues. *J Clin Pathol* (2001) 54(3):210–3. doi: 10.1136/jcp.54.3.210

86. Krishn SR, Ganguly K, Kaur S, Batra SK. Ramifications of secreted mucin MUC5AC in malignant journey: A holistic view. *Carcinogenesis* (2018) 39(5):633–51. doi: 10.1093/carcin/bgy019

87. Pothuraju R, Rachagani S, Krishn SR, Chaudhary S, Nimmakayala RK, Siddiqui JA, et al. Molecular implications of MUC5AC-CD44 axis in colorectal cancer progression and chemoresistance. *Mol Cancer* (2020) 19(1):37. doi: 10.1186/s12943-020-01156-y

88. Perrais M, Rousseaux C, Ducourouble MP, Courcol R, Vincent P, Jonckheere N, et al. Helicobacter pylori urease and flagellin alter mucin gene expression in human gastric cancer cells. *Gastric Cancer* (2014) 17(2):235–46. doi: 10.1007/s10120-013-0267-5

89. Pinto-de-Sousa J, Reis CA, David L, Pimenta A, Cardoso-de-Oliveira M. MUC5B expression in gastric carcinoma: Relationship with clinico-pathological parameters and with expression of mucins MUC1, MUC2, MUC5AC and MUC6. *Virchows Archiv an Int J Pathol* (2004) 444(3):224–30. doi: 10.1007/s00428-003-0968-y

90. Mino-Kenudson M, Tomita S, Lauwers GY. Mucin expression in reactive gastropathy: An immunohistochemical analysis. *Arch Pathol Lab Med* (2007) 131 (1):86–90. doi: 10.5858/2007-131-86-MEIRGA

91. van Neerven SM, Vermeulen L. The interplay between intrinsic and extrinsic Wnt signaling in controlling intestinal transformation. *Differentiation; Res Biol Diversity* (2019) 108:17–23. doi: 10.1016/j.diff.2019.02.002

92. Nie X, Liu Y, Chen WD, Wang YD. Interplay of miRNAs and canonical wnt signaling pathway in hepatocellular carcinoma. *Front Pharmacol* (2018) 9:657. doi: 10.3389/fphar.2018.00657

93. Pandurangan AK, Divya T, Kumar K, Dineshbabu V, Velavan B, Sudhandiran G. Colorectal carcinogenesis: Insights into the cell death and signal transduction pathways: A review. *World J Gastrointest Oncol* (2018) 10(9):244–59. 10.4251/wjgo.v10.i9.244

94. Cancer Genome Atlas Network. Comprehensive molecular characterization of human colon and rectal cancer. *Nature* (2012) 487(7407):330–7. doi: 10.1038/nature11252

95. Ara H, Takagishi M, Enomoto A, Asai M, Ushida K, Asai N, et al. Role for daple in non-canonical wnt signaling during gastric cancer invasion and metastasis. *Cancer Science* (2016) 107(2):133–9. doi: 10.1111/cas.12848

96. Mao J, Fan S, Ma W, Fan P, Wang B, Zhang J, et al. Roles of wnt/β-catenin signaling in the gastric cancer stem cells proliferation and salinomycin treatment. *Cell Death Dis* (2014) 5(1):e1039. doi: 10.1038/cddis.2013.515

97. Cohen ED, Tian Y, Morrisey EE. Wnt signaling: an essential regulator of cardiovascular differentiation, morphogenesis and progenitor self-renewal. *Dev (Cambridge England)* (2008) 135(5):789–98. doi: 10.1242/dev.016865

98. Veeman MT, Axelrod JD, Moon RT. A second canon. functions and mechanisms of beta-catenin-independent wnt signaling. *Dev Cell* (2003) 5 (3):367–77. doi: 10.1016/S1534-5807(03)00266-1

99. Nishioka M, Ueno K, Hazama S, Okada T, Sakai K, Suehiro Y, et al. Possible involvement of Wnt11 in colorectal cancer progression. *Mol Carcinog* (2013) 52 (3):207–17. doi: 10.1002/mc.21845

100. He D, Yue Z, Liu L, Fang X, Chen L, Han H. Long noncoding RNA ABHD11-AS1 promote cells proliferation and invasion of colorectal cancer *via* regulating the miR-1254-WNT11 pathway. *J Cell Physiol* (2019) 234(7):12070–9. doi: 10.1002/jcp.27877

101. Sánchez-Vega F, Gotea V, Chen YC, Elnitski L. CpG island methylator phenotype in adenocarcinomas from the digestive tract: Methods, conclusions, and controversies. *World J Gastrointest Oncol* (2017) 9(3):105–20. doi: 10.4251/wjgo.v9.i3.105

102. Hu Z, Deng H, Qu H. Plasma SFRP5 levels are decreased in Chinese subjects with obesity and type 2 diabetes and negatively correlated with parameters of insulin resistance. *Diabetes Res Clin Pract* (2013) 99(3):391–5. doi: 10.1016/j.diabres.2012.11.026

103. Miyoshi T, Doi M, Usui S, Iwamoto M, Kajiya M, Takeda K, et al. Low serum level of secreted frizzled-related protein 5, an anti-inflammatory adipokine, is associated with coronary artery disease. *Atherosclerosis* (2014) 233(2):454–9. doi: 10.1016/j.atherosclerosis.2014.01.019

104. Veeck J, Geisler C, Noetzel E, Alkaya S, Hartmann A, Knüchel R, et al. Epigenetic inactivation of the secreted frizzled-related protein-5 (SFRP5) gene in human breast cancer is associated with unfavorable prognosis. *Carcinogenesis* (2008) 29(5):991–8. doi: 10.1093/carcin/bgn076

105. Su HY, Lai HC, Lin YW, Liu CY, Chen CK, Chou YC, et al. Epigenetic silencing of SFRP5 is related to malignant phenotype and chemoresistance of ovarian cancer through wnt signaling pathway. *Int J Cancer* (2010) 127(3):555–67. doi: 10.1002/ijc.25083

106. Zhao C, Bu X, Zhang N, Wang W. Downregulation of SFRP5 expression and its inverse correlation with those of MMP-7 and MT1-MMP in gastric cancer. *BMC Cancer* (2009) 9:224. doi: 10.1186/1471-2407-9-224

107. Zhou W, Ye C, Li L, Liu L, Wang F, Yu L, et al. Adipocyte-derived SFRP5 inhibits breast cancer cells migration and invasion through wnt and epithelial-mesenchymal transition signaling pathways. *Chin J Cancer Res = Chung-kuo yen cheng yen chiu* (2020) 32(3):347–60. doi: 10.21147/j.issn.1000-9604.2020.03.06

108. Evans DR, Venkitachalam S, Revoredo L, Dohey AT, Clarke E, Pennell JJ, et al. Evidence for GALNT12 as a moderate penetrance gene for colorectal cancer. *Hum Mutation* (2018) 39(8):1092–101. doi: 10.1002/humu.23549

109. Lee SH, Hatakeyama S, Yu SY, Bao X, Ohyama C, Khoo KH, et al. Core3 O-glycan synthase suppresses tumor formation and metastasis of prostate carcinoma PC3 and LNCaP cells through down-regulation of alpha2beta1 integrin complex. *J Biol Chem* (2009) 284(25):17157–69. doi: 10.1074/jbc.M109.010934

110. Iwai T, Kudo T, Kawamoto R, Kubota T, Togayachi A, Hiruma T, et al. Core 3 synthase is down-regulated in colon carcinoma and profoundly suppresses the metastatic potential of carcinoma cells. *Proc Natl Acad Sci U States A* (2005) 102(12):4572–7. doi: 10.1073/pnas.0407983102

111. Cao P, Wu Y, Sun D, Zhang W, Qiu J, Tang Z, et al. IGF2BP2 promotes pancreatic carcinoma progression by enhancing the stability of B3GNT6 mRNA *via* m6A methylation. *Cancer Med* (2022). doi: 10.1002/cam4.5096

112. Xiao S, Yang C, Zhang Y, Lai C. Downregulation of B3GNT6 is a predictor of poor outcomes in patients with colorectal cancer. *World J Surg Oncol* (2022) 20 (1):110. doi: 10.1186/s12957-022-02561-x

113. Qi X, Zhang DH, Wu N, Xiao JH, Wang X, Ma W. ceRNA in cancer: possible functions and clinical implications. *J Med Genet* (2015) 52(10):710–8. doi: 10.1136/jmedgenet-2015-103334

114. Sun C, Li S, Zhang F, Xi Y, Wang L, Bi Y, et al. Long non-coding RNA NEAT1 promotes non-small cell lung cancer progression through regulation of miR-377-3p-E2F3 pathway. *Oncotarget* (2016) 7(32):51784–814. doi: 10.18632/oncotarget.10108

115. Shang A, Gu C, Wang W, Wang X, Sun J, Zeng B, et al. Exosomal circPACRGL promotes progression of colorectal cancer *via* the miR-142-3p/miR-506-3p- TGF-β1 axis. *Mol Cancer* (2020) 19(1):117. doi: 10.1186/s12943-020-01235-0

116. Wu H, Hu X, Li Y, Chen Q, Sun T, Qiao Y, et al. LNC473 regulating APAF1 IRES-dependent translation *via* competitive sponging miR574 and miR15b: Implications in colorectal cancer. *Mol Ther Nucleic Acids* (2020) 21:764–79. doi: 10.1016/j.omtn.2020.07.009

117. Lei X, Lei Y, Li JK, Du WX, Li RG, Yang J, et al. Immune cells within the tumor microenvironment: Biological functions and roles in cancer immunotherapy. *Cancer Lett* (2020) 470:126–33. doi: 10.1016/j.canlet.2019.11.009

118. Wang Y, Bhave MS, Yagita H, Cardell SL. Natural killer T-cell agonist α-galactosylceramide and PD-1 blockade synergize to reduce tumor development in a preclinical model of colon cancer. *Front Immunol* (2020) 11:581301. doi: 10.3389/fimmu.2020.581301

119. Wang M, Wang S, Desai J, Trapani JA, Neeson PJ. Therapeutic strategies to remodel immunologically cold tumors. *Clin Trans Immunol* (2020) 9(12):e1226. doi: 10.1002/cti2.1226

120. Overman MJ, McDermott R, Leach JL, Lonardi S, Lenz HJ, Morse MA, et al. Nivolumab in patients with metastatic DNA mismatch repair-deficient or microsatellite instability-high colorectal cancer (CheckMate 142): An open-label, multicentre, phase 2 study. *Lancet Oncol* (2017) 18(9):1182–91. doi: 10.1016/S1470-2045(17)30422-9

121. Le DT, Uram JN, Wang H, Bartlett BR, Kemberling H, Eyring AD, et al. PD-1 blockade in tumors with mismatch-repair deficiency. *New Engl J Med* (2015) 372(26):2509–20. doi: 10.1056/NEJMoa1500596

122. Chen EX, Jonker DJ, Loree JM, Kennecke HF, Berry SR, Couture F, et al. Effect of combined immune checkpoint inhibition vs best supportive care alone in patients with advanced colorectal cancer: The Canadian cancer trials group CO.26 study. *JAMA Oncol* (2020) 6(6):831–8. doi: 10.1001/jamaoncol.2020.0910

123. Yukami H, Kawazoe A, Lin YT, Koyama S, Fukuoka S, Hara H, et al. Updated efficacy outcomes of anti-PD-1 antibodies plus multikinase inhibitors for patients with advanced gastric cancer with or without liver metastases in clinical trials. *Clin Cancer Res an Off J Am Assoc Cancer Res* (2022) 28(16):3480–8. doi: 10.1158/1078-0432.CCR-22-0630

frontiers | Frontiers in Molecular Biosciences

TYPE Perspective
PUBLISHED 17 March 2023
DOI 10.3389/fmolb.2023.1097694

OPEN ACCESS

EDITED BY
William C. Cho,
QEH, Hong Kong SAR, China

REVIEWED BY
Sajad Najafi,
Shahid Beheshti University of Medical Sciences, Iran
Niaz Muhammad,
Minhaj University Lahore, Pakistan
Abdullah Shah,
Shaheed Benazir Bhutto University, Pakistan

*CORRESPONDENCE
Pengyuan Zheng,
pyzheng@zzu.edu.cn
Yang Mi,
yangmi198@zzu.edu.cn
Rick Francis Thorne,
rickfthorne@gmail.com

SPECIALTY SECTION
This article was submitted to Molecular Diagnostics and Therapeutics, a section of the journal Frontiers in Molecular Biosciences

RECEIVED 14 November 2022
ACCEPTED 24 February 2023
PUBLISHED 17 March 2023

CITATION
Bukhari I, Khan MR, Li F, Swiatczak B, Thorne RF, Zheng P and Mi Y (2023), Clinical implications of lncRNA LINC-PINT in cancer.
Front. Mol. Biosci. 10:1097694.
doi: 10.3389/fmolb.2023.1097694

Clinical implications of lncRNA LINC-PINT in cancer

Ihtisham Bukhari[1], Muhammad Riaz Khan[2], Fazhan Li[1], Bartlomiej Swiatczak[3], Rick Francis Thorne[4]*, Pengyuan Zheng[1]* and Yang Mi[1]*

[1]Henan Key Laboratory of Helicobacter pylori, Microbiota and Gastrointestinal Cancer, Marshall Medical Research Center, Fifth Affiliated Hospital of Zhengzhou University, Zhengzhou, China, [2]Research Center on Aging, Centre Intégré Universitaire de Santé et Services Sociaux de l'Estrie-Centre Hospitalier Universitaire de Sherbrooke, Sherbrooke, QC, Canada, [3]Department of History of Science and Scientific Archeology, University of Science and Technology of China, Hefei, China, [4]School of Environmental and Life Sciences, The University of Newcastle, Callaghan, NSW, Australia

Long noncoding RNAs (lncRNAs) possess the potential for therapeutic targeting to treat many disorders, including cancers. Several RNA-based therapeutics (ASOs and small interfering RNAs) have gained FDA approval over the past decade. And with their potent effects, lncRNA-based therapeutics are of emerging significance. One important lncRNA target is LINC-PINT, with its universalized functions and relationship with the famous tumor suppressor gene *TP53*. Establishing clinical relevance, much like p53, the tumor suppressor activity of LINC-PINT is implicated in cancer progression. Moreover, several molecular targets of LINC-PINT are directly or indirectly used in routine clinical practice. We further associate LINC-PINT with immune responses in colon adenocarcinoma, proposing the potential utility of LINC-PINT as a novel biomarker of immune checkpoint inhibitors. Collectively, current evidence suggests LINC-PINT can be considered for use as a diagnostic/prognostic marker for cancer and several other diseases.

KEYWORDS

PINTology, LncRNA, LINC-PINT, Colon adenocarcinoma (CAC), Cancer biomarkers, Cancer therapy, Immune checkpoint inhibitors

Introduction

Sequencing of the human genome has revealed that ~20,000 traditional genes encode protein molecules, occupying just 2% of the total genetic landscape (Salzberg, 2018; Viggiano, 2022). The remaining genome consists of non-protein-coding regions, including numerous 'RNA only' genes, among which there is a large but diverse group called long non-coding RNAs or lncRNAs for short (Elkon and Agami, 2017; Dietlein et al., 2022; Paloviita and Vuoristo, 2022). Subsequent analyses have shown that lncRNAs fulfill various regulatory roles in healthy and cancerous tissues (Geng et al., 2018; Bi et al., 2019; Farzaneh et al., 2022a; Farzaneh et al., 2022b; Farzaneh et al., 2022c; Nasrolahi et al., 2022). As such, their expression and function are often altered in disease states (Kleinbrink et al., 2021; Yang et al., 2021; Anderson and Anderson, 2022; Dietlein et al., 2022; Erdogan et al., 2022) with selected examples now being used as diagnostic markers for various diseases including cancers (Li et al., 2019; Deng and Zou, 2022; Najafi et al., 2022; Zhang et al., 2022). Among these, one particular lncRNA called LINC-PINT (**P**53 **I**nduced **l**ong **N**on-coding **T**ranscript) appears exceptional because of its universalized functions and relationship to the famous tumor suppressor gene P53 (He

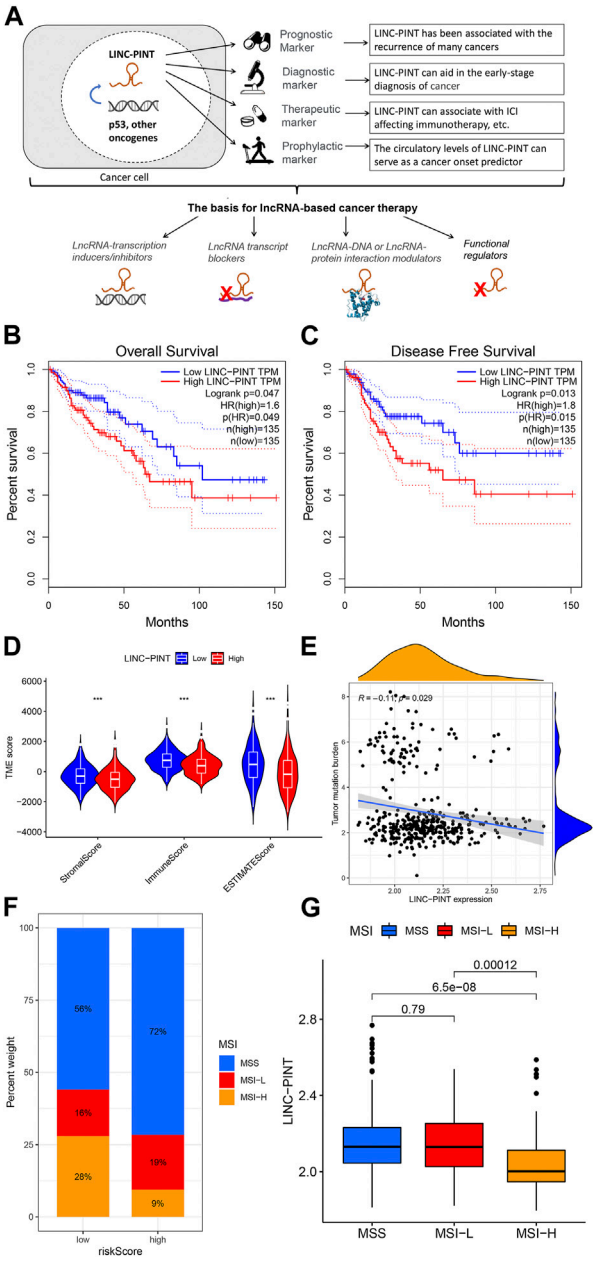

FIGURE 1
Clinical potentials of LINC-PINT. **(A)** Overview of the clinical applications of LINC-PINT. In short, it can be used as a prognostic marker to ascertain the course of cancer progression based on its expression level. It can also be used as a diagnostic marker to aid the early detection of ontological transformation. The third type of application, already in pre-clinical testing, predicts response to cancer therapy. Finally, less explored but equally important is the potential of LINC-PINT-based studies to determine the susceptibility of healthy subjects to cancer. These applications can be used, in turn, to tailor and administer suitable lncRNA-based cancer therapies. Correlation of LINC-PINT expression with **(B)** Overall survival and **(C)** Disease-free survival in Colon Adenocarcinoma **(D)** Association of LINC-PINT expression with immune scores, including stromal, immune, and ESTIMATE scores, **(E)** Tumor Mutation Burden, and **(F–G)** microsatellite instability in colon adenocarcinoma patients.

et al., 2021; Bukhari et al., 2022). Indeed, like P53, LINC-PINT was first proposed as an oncogene but later revealed as a tumor suppressor in human cancers.

LINC-PINT contributes to a variety of biological processes impacting cancer cell growth and metastasis, with involvement in processes ranging from DNA damage responses to cell senescence and apoptosis (Simchovitz et al., 2020; He et al., 2021; Wang et al., 2021; Xiang et al., 2021; Zhang et al., 2021; Bukhari et al., 2022). It has also been shown to be an essential regulator of many other diseases, including autoimmune diseases (Wang and Zhao, 2020; Salviano-Silva et al., 2021). These functions arise through interactions affecting epigenetic regulation or direct interactions with other biomolecules, including proteins and other lncRNAs (Xu et al., 2019; Bukhari et al., 2022). Some alternatively spliced variants of LINC-PINT also act as host transcripts for circular RNA (circRNA) generation, and these can serve as sources for the translation of short functional peptides (Xiang et al., 2021). More than 100 alternatively spliced variants of LINC-PINT have been identified (Bukhari et al., 2022). Still, to date, only a few of these have been thoroughly studied—a feature earning the name PINTology to describe the current and future studies involving LINC-PINT.

Therapeutic importance of lncRNA LINC-PINT

Cancer cells exhibit variability formally termed tumor heterogeneity, and this is a well-known explanation behind the failure of cancer therapy where resistant cells selectively survive repeated drug treatments (Brutovsky, 2022; Mahinfar et al., 2022). Contributing to this problem is also the lack of suitable diagnostic, therapeutic and prognostic biomarkers (Najafi, 2022). Hence, optimizing treatment outcomes for any disease is only possible with full knowledge of the underlying mechanisms. In this regard, recent studies involving lncRNAs have substantially contributed to understanding the cancer (Li et al., 2022b; Singh et al., 2022; Zhong et al., 2022). However, exploiting the potential of lncRNAs as biomarkers and therapeutic targets is just the beginning (Mirzaei et al., 2022). For example, lncRNAs associated with immune checkpoints (Li et al., 2022a; Jiang et al., 2022; Wen et al., 2022) have been used as disease biomarkers in the new wave of cancer immunotherapy that is currently revolutionizing oncology practice (Figure 1A). Nevertheless, small successes in the clinical setting are expected to help build confidence in lncRNAs as biomarkers and produce the momentum needed for their broader applications.

Although the tumor-suppressive function and downregulation of LINC-PINT in different cancers have been thoroughly established (He et al., 2021; Bukhari et al., 2022), its clinical use remains extremely limited. It is interesting to note that many of the vital protein targets of LINC-PINT involved in cell cycle regulation are already widely used in the diagnostic setting (Caputo et al., 2014; Xu et al., 2019). Furthermore, some of these are cancer treatments with inhibitors of LINC-PINT's targets now being used in treating melanoma (George et al., 2019). As a starting point, the most appropriate clinical application of LINC-PINT would be as a diagnostic or predictive marker for specific cancers such as esophageal cancer, where LINC-PINT has been associated with cancer recurrence (Zhang et al., 2019; Rong et al., 2021). Indeed, the abnormal expression of LINC-PINT reflects many vital predictors of cancer outcomes such as lymph node metastasis, tumor size, and differentiation status (Figure 1A). Notably, the

levels of LINC-PINT released by tumor cells into the blood could also be used to measure therapeutic responses, as specific anti-cancer drugs induce the re-expression of LINC-PINT. Other positive associations with neuropathy along with pemphigus foliaceous, diabetes, and arthritis may also be exploited, suggesting LINC-PINT as a multifaceted target for cancers and other diseases.

Data collection

The complete gene expression profiles and clinical information of 473 colon cancer patients were downloaded from the TCGA online database (https://portal.gdc.cancer.gov/). The R software package "maftools" was used to calculate each sample's tumor mutation burden (TMB). The microsatellite instability (MSI) score and groupings of the "TCGA-COAD" samples were downloaded using "TCGAbiolinks," including: "MSI -H," "MSI-L," and "MSS."

Survival and immune function analyses

We analyzed the overall survival and disease-free survival of LINC-PINT in COAD within the online database GEPIA (http://gepia.cancer-pku.cn/). The Estimation of Stromal and Immune Cells in Malignant Tumors using the Expression Data (ESTIMATE) algorithm was used to determine the unique properties of the transcriptional profiles to infer the tumor cellularity as the tumor purity. The relationship of LINC-PINT expression, Stromal Score, and Immune Score with ESTIMATEScore was plotted as a violin plot using the "violin" package in the R program. Furthermore, we analyzed the correlations between different LINC-PINT expression groups, TMB and MSI with data presented as boxplots and scatterplots using "ggplot2".

Relationship between LINC-PINT and immune responses in colon adenocarcinoma (COAD)

We assessed the survival of patients and immune function associated with LINC-PINT expression in COAD tissues from the TCGA resource. Notably, patients whose tumors expressed low levels of LINC-PINT showed better overall and disease-free survival (Figure 1B, C). Subsequently, LINC-PINT showed a strong association with immune indicators, Tumor Mutation Burden (TMB), and Microsatellite Instability (MSI) in the COAD tumor microenvironment. COAD cases exhibiting higher expression of LINC-PINT had significantly lower immune scores, including stromal, immune, and ESTIMATE scores (Figure 1D), meaning that patients with low expression of LINC-PINT have a better immune response. Additionally, TMB and MSI have been used as prognostic markers for many cancers, especially for those receiving immunotherapy (Rizzo et al., 2021); thus, these can be used as predictive biomarkers for the efficacy of immunotherapy. Patients with low expression of LINC-PINT showed significantly higher TMB and MSI scores (Figures 1E–G), reflecting that LINC-PINT may be used as a novel biomarker of immune checkpoint inhibitors (ICIs).

Clinical features of LINC-PINT in COAD

Additionally, we took advantage of the clinical characteristics and other clinical information of the 388 COAD cases available within the TCGA database. We stratified patients based on LINC-PINT expression in their primary tumors, dividing the samples into high-expression and low-expression groups. The relationship between LINC-PINT and the clinical features of COAD was then studied using the Wilcoxon rank sum test using $p < 0.05$ to denote statistical significance. Table 1 compares the differences between the high and low-expression LINC-PINT groups wherein high LINC-PINT expression showed a significantly higher proportion of tumor metastasis index (M1) cases compared to the low-expression group ($p = 0.0357$). Similarly, the boxplot analysis showed that the expression level of LINC-PINT was higher in patients with metastases (Figure 2A) ($p = 0.003$).

Furthermore, we validated the immune efficacy of LINC-PINT expression *via* the TCIA database. The IPS values were calculated based on immunogenicity from the TCIA database and then analyzed against LINC-PINT expression, finding higher effectiveness of immunotherapy in the low-risk group ($p < 0.001$) (Figures 2B, C). Moreover, Tumor Immune Dysfunction and Exclusion (TIDE) algorithm predicts ICB response and evaluates immune escape ability (http://tide.dfci.harvard.edu/). Therefore, we used the TIDE database to verify the relationship between risk scores and immune checkpoint inhibitors (ICIs) and found that the high LINC-PINT expression group has lower TIDE scores (Figure 2D). Together, this suggests that patients with high LINC-PINT expression have a lower possibility of immune escape than patients with low LINC-PINT expression, so they are more suitable for Immune Checkpoint Inhibitors (ICI) treatment.

The relationship between LINC-PINT and anticancer therapies

In addition, we also analyzed the relationship between the expression of LINC-PINT and tumor sensitivity to immunotherapy and chemotherapy drugs. IPS-PD1/PD-L1 blocker and IPS-CTLA4 blocker data on COAD from the TCGA were obtained and analyzed using The Cancer Immunome Atlas database (TCIA, https://tcia.at/home) to predict the patients' response to ICI as high- and low-risk groups. To explore the efficacy of chemotherapeutic drugs and their relationship with PINT, we used the pRRophetic package. Using the Wilcoxon test, we screened the chemotherapeutic drugs significantly different in the LINC-PINT expression group and displayed the IC^{50} distribution of different drugs in the two groups of samples through a boxplot (pFilter = 0.0001). We chose the top 10 chemotherapy drugs having highly significant differences in different risk groups and displayed the IC^{50} distribution of different drugs in the two groups of samples by boxplot (pFilter = 0.0001) (Figure 2E–N). The results showed that COAD patients with different expressions of LINC-PINT have apparent differences in sensitivity to various chemotherapeutic drugs, particularly patients whose tumors exhibit low LINC-PINT expression are more sensitive to chemotherapy.

TABLE 1 Clinical features of the LINC-PINT in COAD. Out of the total of 473 COAD samples, we filtered out the complete clinical information of 388 cases from TCGA, and based on the LINC-PINT expression, the patients were divided into high and low-expression groups. Furthermore, patients were categorized based on their clinical characteristics (age, gender, T, N, M, stage, etc.) and compared the distribution of LINC-PINT high and low-expression samples in different groups. The proportion of M0 and M1 in the high-expression group was 80.2% and 19.8%, whereas in the low-expression group M0 and M1 proportion was observed as 88.48% and 11.52%, respectively. The distributions of metastasis-related clinical features were also significantly different than the control.

Covariates	Type	Total	High_LINC-PINT	Low_LINC-PINT	*p*-value
Age	≤65	152 (39.18%)	68 (34.52%)	84 (43.98%)	0.0711
Age	>65	236 (60.82%)	129 (65.48%)	107 (56.02%)	
Gender	FEMALE	184 (47.42%)	87 (44.16%)	97 (50.79%)	0.2284
Gender	MALE	204 (52.58%)	110 (55.84%)	94 (49.21%)	
Stge	Stge I-II	225 (57.99%)	111 (56.35%)	114 (59.69%)	0.573
Stge	Stge III-IV	163 (42.01%)	86 (43.65%)	77 (40.31%)	
T	T1-2	73 (18.81%)	31 (15.74%)	42 (21.99%)	0.1482
T	T3-4	315 (81.19%)	166 (84.26%)	149 (78.01%)	
M	M0	327 (84.28%)	158 (80.2%)	169 (88.48%)	0.0357
M	M1	61 (15.72%)	39 (19.8%)	22 (11.52%)	
N	N0	233 (60.05%)	116 (58.88%)	117 (61.26%)	0.8924
N	N1	88 (22.68%)	46 (23.35%)	42 (21.99%)	
N	N2	67 (17.27%)	35 (17.77%)	32 (16.75%)	

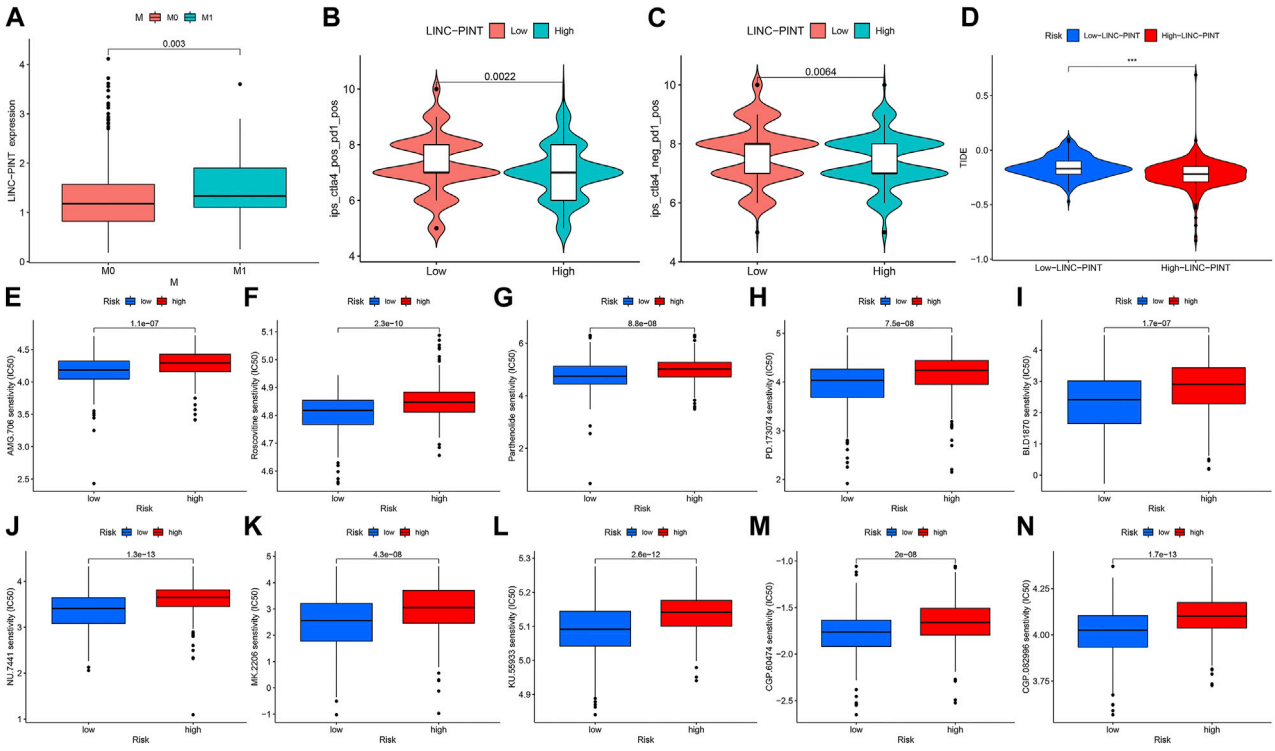

FIGURE 2
Relationship between LINC-PINT and clinical characteristics of patients with COAD. **(A)** Boxplot of differences in LINC-PINT expression levels between metastatic and non-metastatic groups of COAD patients. M0: non-metastasis; M1: tumor metastasis. **(B, C)** The immunophenotype scores in the low-LINC-PINT group and high-LINC-PINT group. **(D)** The TIDE score distribution between high- and low- LINC-PINT groups. **(E–N)** Drug sensitivity analysis of multiple chemotherapeutic drugs in the high LINC-PINT expression group and the low LINC-PINT expression group, respectively.

The future of lncRNA LINC-PINT

Compared to most lncRNAs, extensive literature exists for LINC-PINT, but a key question is whether this truly reflects most or, if not all, the underlying molecular mechanisms involved. In particular, the relationship between the functions of LINC-PINT in cancers *versus* non-malignant diseases needs to be better explored. For example, in viral hepatitis leading to liver cancer development, LINC-PINT foremost contributes to inflammation during viral infection and then later, to the pathogenic properties of the cancer cells (Khatun et al., 2021a; Khatun et al., 2021b), but whether the underlying processes involved are the same in both disease stages is not clear. Consequently, more intensive patient-based clinical studies are required to dissect these points. Furthermore, the large number of splice variants complicates this task, and it will be necessary to identify which variants share functions *versus* those that contribute to different functions. It is worth mentioning that at least one LINC-PINT variant produces small peptides, but this phenomenon's frequency needs to be clarified. As functional products, these peptides may themselves serve as diagnostic molecules or treatment targets. It would be similarly valuable to ascertain more knowledge of the natural activators or inhibitors of LINC-PINT, which could be used to open potential new doors in cancer therapeutics. And to end on a sobering note, the number of lncRNA genes may rival or exceed the number of coding genes with LINC-PINT just one amongst thousands. However, there is the expectation that the pioneering studies involving LINC-PINT will provide important precedents for the clinical applications of lncRNAs.

Discussion

LncRNAs are crucial regulators of various cellular pathways specifically cancer-associated pathways and use different mediators to function (Peng et al., 2017; Kopp and Mendell, 2018; Ali and Grote, 2020), while the majority of lncRNAs are functionally uncharacterized (Li et al., 2017; Lorenzi et al., 2021). Specifically, the regulation of lncRNAs occurs during specific occasions, such as development and cell growth (Sun et al., 2018). Mechanistically, lncRNAs bind with DNA, RNA, and proteins for transcriptional, post-transcriptional, and post-translational regulations (Schmitt et al., 2016; Hull et al., 2021; Yue et al., 2021). LncRNAs play vital roles in cancer initiation and progression or inhibition by affecting various pathways and expression of genes (Zhuo and Kang, 2017; Statello et al., 2021), showing that lncRNAs are either onco-suppressor or onco-promoter.

Similarly, LINC-PINT is a crucial lncRNA that mainly acts as an onco-suppressor in various cancers, but its clinical use is almost neglected. However, studies have suggested it as a potential biomarker for cancer prognosis (Ghafouri-Fard et al., 2021; He et al., 2021; Ghafouri-Fard et al., 2022). Through analysis of colon cancer data from the TCGA data, we determined an enticing relationship between LINC-PINT expression, prognosis and patients' survival. Interestingly, patients with low expression of LINC-PINT showed better survival and significantly higher TMB and MSI scores together with better responses to chemotherapy, thus supporting the clinical importance of LINC-PINT, especially its use as a biomarker for monitoring responses to immunotherapy and chemotherapy.

Conclusion

It is now commonly known that lncRNAs are key players in cancer regulation, a feature that promotes their application as target-based therapies in cancer and other relevant diseases. Interestingly, this promise has now been realized with several RNA-based therapeutics being recently approved by the FDA although their integration into the healthcare system still requires extensive clinical trials. It is well known that LINC-PINT has universalized tumor suppressor functions and a relationship to the tumor suppressor gene TP53 and several LINC-PINT targets are commonly used in clinical practice (directly or indirectly). Based on these facets, LINC-PINT emerges as a priority target for studying the clinical potential of lncRNAs (PINTology), especially for cancer therapeutics. However, the direct application of LINC-PINT is still limited due to the lack of clinical trials and clinicians' confidence. Nevertheless, the current evidence proposes applications as a diagnostic marker for cancer and several other diseases with alterations in LINC-PINT circulatory levels providing a readily accessible platform to develop appropriate tests.

Author contributions

IB, PZ, and YM conceptualized the study, IB and MK collected data and analyzed it, IB wrote the first draft, RFT thoroughly revised the manuscript and analyzed data. FL and BS performed bioinformatics analyses and prepared figures, PZ and YM supervised the overall work and reviewed the manuscript. All authors have read the final version of the manuscript and approved it for publication.

Funding

This work was supported by Zhengzhou Major Collaborative Innovation Project (No.18XTZX12003); Key projects of discipline construction in Zhengzhou University (No. XKZDJC202001); National Key Research and development program in China (No.2020YFC2006100); Medical service capacity improvement project of Henan Province in China (grant number Yu Wei Medicine [2017] No.66).

Acknowledgments

We gratefully acknowledge the role of our host institutes in this study, and we also thank our colleagues who are listed as authors of this manuscript for their support and encouragement.

Conflict of interest

The authors declare that the research was conducted in the absence of any commercial or financial relationships that could be construed as a potential conflict of interest.

Publisher's note

References

Ali, T., and Grote, P. (2020). Beyond the RNA-dependent function of LncRNA genes. *Elife* 9, e60583. doi:10.7554/eLife.60583

Anderson, K. M., and Anderson, D. M. (2022). LncRNAs at the heart of development and disease. *Mamm. Genome* 33, 354–365. doi:10.1007/s00335-021-09937-6

Bi, X., Guo, X. H., Mo, B. Y., Wang, M. L., Luo, X. Q., Chen, Y. X., et al. (2019). LncRNA PICSAR promotes cell proliferation, migration and invasion of fibroblast-like synoviocytes by sponging miRNA-4701-5p in rheumatoid arthritis. *EBioMedicine* 50, 408–420. doi:10.1016/j.ebiom.2019.11.024

Brutovsky, B. (2022). Scales of cancer evolution: Selfish genome or cooperating cells? *Cancers (Basel)* 14, 3253. doi:10.3390/cancers14133253

Bukhari, I., Khan, M. R., Hussain, M. A., Thorne, R. F., Yu, Y., Zhang, B., et al. (2022). PINTology: A short history of the lncRNA LINC-PINT in different diseases. *Wiley Interdiscip. Rev. RNA* 13, e1705. doi:10.1002/wrna.1705

Caputo, E., Miceli, R., Motti, M. L., Tate, R., Fratangelo, F., Botti, G., et al. (2014). AurkA inhibitors enhance the effects of B-RAF and MEK inhibitors in melanoma treatment. *J. Transl. Med.* 12, 216. doi:10.1186/s12967-014-0216-z

Deng, M., and Zou, W. (2022). Noncoding RNAs: Novel targets for opioid tolerance. *Curr. Neuropharmacol.* 21. doi:10.2174/1570159X21666221129122932

Dietlein, F., Wang, A. B., Fagre, C., Tang, A., Besselink, N. J. M., Cuppen, E., et al. (2022). Genome-wide analysis of somatic noncoding mutation patterns in cancer. *Science* 376, eabg5601. doi:10.1126/science.abg5601

Elkon, R., and Agami, R. (2017). Characterization of noncoding regulatory DNA in the human genome. *Nat. Biotechnol.* 35, 732–746. doi:10.1038/nbt.3863

Erdogan, I., Sweef, O., and Akgul, B. (2022). Long noncoding RNAs in human cancer and apoptosis. *Curr. Pharm. Biotechnol*. doi:10.2174/1389201023666220624094950

Farzaneh, M., Ghasemian, M., Ghaedrahmati, F., Poodineh, J., Najafi, S., Masoodi, T., et al. (2022a). Functional roles of lncRNA-TUG1 in hepatocellular carcinoma. *Life Sci.* 308, 120974. doi:10.1016/j.lfs.2022.120974

Farzaneh, M., Najafi, S., Dari, M. A. G., Sheykhi-Sabzehpoush, M., Dayer, D., Cheraghzadeh, M., et al. (2022b). Functional roles of long noncoding RNA MALAT1 in gynecologic cancers. *Clin. Transl. Oncol.* 25, 48–65. doi:10.1007/s12094-022-02914-8

Farzaneh, M., Najafi, S., Sheykhi-Sabzehpoush, M., Nezhad Dehbashi, F., Anbiyaee, O., Nasrolahi, A., et al. (2022c). The stem cell-specific long non-coding RNAs in leukemia. *Clin. Transl. Oncol.* 25, 345–351. doi:10.1007/s12094-022-02952-2

Geng, H., Bu, H. F., Liu, F., Wu, L., Pfeifer, K., Chou, P. M., et al. (2018). In inflamed intestinal tissues and epithelial cells, interleukin 22 signaling increases expression of H19 long noncoding RNA, which promotes mucosal regeneration. *Gastroenterology* 155, 144–155. doi:10.1053/j.gastro.2018.03.058

George, J., Nihal, M., Singh, C. K., and Ahmad, N. (2019). 4'-Bromo-resveratrol, a dual Sirtuin-1 and Sirtuin-3 inhibitor, inhibits melanoma cell growth through mitochondrial metabolic reprogramming. *Mol. Carcinog.* 58, 1876–1885. doi:10.1002/mc.23080

Ghafouri-Fard, S., Khoshbakht, T., Hussen, B. M., Taheri, M., and Samsami, M. (2022). Emerging role of non-coding RNAs in the regulation of Sonic Hedgehog signaling pathway. *Cancer Cell Int.* 22, 282. doi:10.1186/s12935-022-02702-y

Ghafouri-Fard, S., Shirvani-Farsani, Z., Hussen, B. M., and Taheri, M. (2021). The critical roles of lncRNAs in the development of osteosarcoma. *Biomed. Pharmacother.* 135, 111217. doi:10.1016/j.biopha.2021.111217

He, T., Yuan, C., and Zhao, C. (2021). Long intragenic non-coding RNA p53-induced transcript (LINC-PINT) as a novel prognosis indicator and therapeutic target in cancer. *Biomed. Pharmacother.* 143, 112127. doi:10.1016/j.biopha.2021.112127

Hull, R., Mbita, Z., and Dlamini, Z. (2021). Long non-coding RNAs (LncRNAs), viral oncogenomics, and aberrant splicing events: Therapeutics implications. *Am. J. Cancer Res.* 11, 866–883.

Jiang, H., Sun, J., Liu, F., Wu, X., and Wen, Z. (2022). An immune-related long noncoding RNA pair as a new biomarker to predict the prognosis of patients in breast cancer. *Front. Genet.* 13, 895200. doi:10.3389/fgene.2022.895200

Khatun, M., Sur, S., Steele, R., Ray, R., and Ray, R. B. (2021a). Inhibition of long noncoding RNA linc-pint by hepatitis C virus in infected hepatocytes enhances lipogenesis. *Hepatology* 74, 41–54. doi:10.1002/hep.31656

Khatun, M., Zhang, J., Ray, R., and Ray, R. B. (2021b). Hepatitis C virus evades interferon signaling by suppressing long noncoding RNA linc-pint involving C/EBP-β. *J. Virol.* 95, e0095221. doi:10.1128/JVI.00952-21

Kleinbrink, E. L., Gomez-Lopez, N., Ju, D., Done, B., Goustin, A. S., Tarca, A. L., et al. (2021). Gestational age dependence of the maternal circulating long non-coding RNA transcriptome during normal pregnancy highlights antisense and pseudogene transcripts. *Front. Genet.* 12, 760849. doi:10.3389/fgene.2021.760849

Kopp, F., and Mendell, J. T. (2018). Functional classification and experimental dissection of long noncoding RNAs. *Cell* 172, 393–407. doi:10.1016/j.cell.2018.01.011

Li, F., Wen, H., Bukhari, I., Liu, B., Guo, C., Ren, F., et al. (2022a). Relationship between CNVs and immune cells infiltration in gastric tumor microenvironment. *Front. Genet.* 13, 869967. doi:10.3389/fgene.2022.869967

Li, S., Xie, X., Peng, F., Du, J., and Peng, C. (2022b). Regulation of temozolomide resistance via lncRNAs: Clinical and biological properties of lncRNAs in gliomas (Review). *Int. J. Oncol.* 61, 101. doi:10.3892/ijo.2022.5391

Li, Y., Xu, J., Shao, T., Zhang, Y., Chen, H., and Li, X. (2017). RNA function prediction. *Methods Mol. Biol.* 1654, 17–28. doi:10.1007/978-1-4939-7231-9_2

Li, Y., Zhao, J., Yu, S., Wang, Z., He, X., Su, Y., et al. (2019). Extracellular vesicles long RNA sequencing reveals abundant mRNA, circRNA, and lncRNA in human blood as potential biomarkers for cancer diagnosis. *Clin. Chem.* 65, 798–808. doi:10.1373/clinchem.2018.301291

Lorenzi, L., Chiu, H. S., Avila Cobos, F., Gross, S., Volders, P. J., Cannoodt, R., et al. (2021). The RNA Atlas expands the catalog of human non-coding RNAs. *Nat. Biotechnol.* 39, 1453–1465. doi:10.1038/s41587-021-00936-1

Mahinfar, P., Mansoori, B., Rostamzadeh, D., Baradaran, B., Cho, W. C., and Mansoori, B. (2022). The role of microRNAs in multidrug resistance of glioblastoma. *Cancers (Basel)* 14, 3217. doi:10.3390/cancers14133217

Mirzaei, S., Paskeh, M. D. A., Okina, E., Gholami, M. H., Hushmandi, K., Hashemi, M., et al. (2022). Molecular landscape of LncRNAs in prostate cancer: A focus on pathways and therapeutic targets for intervention. *J. Exp. Clin. Cancer Res.* 41, 214. doi:10.1186/s13046-022-02406-1

Najafi, S. (2022). Circular RNAs as emerging players in cervical cancer tumorigenesis; A review to roles and biomarker potentials. *Int. J. Biol. Macromol.* 206, 939–953. doi:10.1016/j.ijbiomac.2022.03.103

Najafi, S., Khatami, S. H., Khorsand, M., Jamali, Z., Shabaninejad, Z., Moazamfard, M., et al. (2022). Long non-coding RNAs (lncRNAs); roles in tumorigenesis and potentials as biomarkers in cancer diagnosis. *Exp. Cell Res.* 418, 113294. doi:10.1016/j.yexcr.2022.113294

Nasrolahi, A., Azizidoost, S., Radoszkiewicz, K., Najafi, S., Ghaedrahmati, F., Sheykhi-Sabzehpoush, M., et al. (2022). Long non-coding RNAs involved in retinoblastoma. *J. Cancer Res. Clin. Oncol.* 149, 401–421. doi:10.1007/s00432-022-04398-z

Paloviita, P., and Vuoristo, S. (2022). The non-coding genome in early human development - recent advancements. *Semin. Cell Dev. Biol.* 131, 4–13. doi:10.1016/j.semcdb.2022.02.010

Peng, W. X., Koirala, P., and Mo, Y. Y. (2017). LncRNA-mediated regulation of cell signaling in cancer. *Oncogene* 36, 5661–5667. doi:10.1038/onc.2017.184

Rizzo, A., Ricci, A. D., and Brandi, G. (2021). PD-L1, TMB, MSI, and other predictors of response to immune checkpoint inhibitors in biliary tract cancer. *Cancers* 13, 558. doi:10.3390/cancers13030558

Rong, H., Chen, B., Ma, K., Wei, X., Peng, J., and Zhu, J. (2021). Downregulation of lncRNA LINC-PINT participates in the recurrence of esophageal squamous cell carcinoma possibly by interacting miRNA-21. *Cancer Biother Radiopharm.* 36, 273–279. doi:10.1089/cbr.2019.3167

Salviano-Silva, A., Farias, T. D. J., Bumiller-Bini, V., Castro, M. S., Lobo-Alves, S. C., Busch, H., et al. (2021). Genetic variability of immune-related lncRNAs: Polymorphisms in LINC-PINT and LY86-AS1 are associated with pemphigus foliaceus susceptibility. *Exp. Dermatol* 30, 831–840. doi:10.1111/exd.14275

Salzberg, S. L. (2018). Open questions: How many genes do we have? *BMC Biol.* 16, 94. doi:10.1186/s12915-018-0564-x

Schmitt, A. M., Garcia, J. T., Hung, T., Flynn, R. A., Shen, Y., Qu, K., et al. (2016). An inducible long noncoding RNA amplifies DNA damage signaling. *Nat. Genet.* 48, 1370–1376. doi:10.1038/ng.3673

Simchovitz, A., Hanan, M., Yayon, N., Lee, S., Bennett, E. R., Greenberg, D. S., et al. (2020). A lncRNA survey finds increases in neuroprotective LINC-PINT in Parkinson's disease substantia nigra. *Aging Cell* 19, e13115. doi:10.1111/acel.13115

Singh, D., Assaraf, Y. G., and Gacche, R. N. (2022). Long non-coding RNA mediated drug resistance in breast cancer. *Drug Resist Updat* 63, 100851. doi:10.1016/j.drup.2022.100851

Statello, L., Guo, C. J., Chen, L. L., and Huarte, M. (2021). Gene regulation by long non-coding RNAs and its biological functions. *Nat. Rev. Mol. Cell Biol.* 22, 96–118. doi:10.1038/s41580-020-00315-9

Sun, Q., Tripathi, V., Yoon, J. H., Singh, D. K., Hao, Q., Min, K. W., et al. (2018). MIR100 host gene-encoded lncRNAs regulate cell cycle by modulating the interaction between HuR and its target mRNAs. *Nucleic Acids Res.* 46, 10405–10416. doi:10.1093/nar/gky696

Viggiano, E. (2022). Molecular research in medical genetics. *Int. J. Mol. Sci.* 23, 6625. doi:10.3390/ijms23126625

Wang, J., and Zhao, Q. (2020). LncRNA LINC-PINT increases SOCS1 expression by sponging miR-155-5p to inhibit the activation of ERK signaling pathway in rheumatoid arthritis synovial fibroblasts induced by TNF-α. *Int. Immunopharmacol.* 84, 106497. doi:10.1016/j.intimp.2020.106497

Wang, Y. H., Guo, Z., An, L., Zhou, Y., Xu, H., Xiong, J., et al. (2021). LINC-PINT impedes DNA repair and enhances radiotherapeutic response by targeting DNA-PKcs in nasopharyngeal cancer. *Cell Death Dis.* 12, 454. doi:10.1038/s41419-021-03728-2

Wen, H., Li, F., Bukhari, I., Mi, Y., Guo, C., Liu, B., et al. (2022). Comprehensive analysis of colorectal cancer immunity and identification of immune-related prognostic targets. *Dis. Markers* 2022, 7932655. doi:10.1155/2022/7932655

Xiang, X., Fu, Y., Zhao, K., Miao, R., Zhang, X., Ma, X., et al. (2021). Cellular senescence in hepatocellular carcinoma induced by a long non-coding RNA-encoded peptide PINT87aa by blocking FOXM1-mediated PHB2. *Theranostics* 11, 4929–4944. doi:10.7150/thno.55672

Xu, Y., Wang, H., Li, F., Heindl, L. M., He, X., Yu, J., et al. (2019). Long non-coding RNA LINC-PINT suppresses cell proliferation and migration of melanoma via recruiting EZH2. *Front. Cell Dev. Biol.* 7, 350. doi:10.3389/fcell.2019.00350

Yang, W., Zhao, P., Liu, Y., Cao, P., Ji, X., Gao, Y., et al. (2021). Transcriptome analysis of lncRNA expression patterns in human congenital lung malformations. *BMC Genomics* 22, 861. doi:10.1186/s12864-021-08204-x

Yue, J., Wu, Y., Qiu, L., Zhao, R., Jiang, M., and Zhang, H. (2021). LncRNAs link cancer stemness to therapy resistance. *Am. J. Cancer Res.* 11, 1051–1068.

Zhang, C., Gong, C., Li, J., and Tang, J. (2021). Downregulation of long non-coding RNA LINC-PINT serves as a diagnostic and prognostic biomarker in patients with non-small cell lung cancer. *Oncol. Lett.* 21, 210. doi:10.3892/ol.2021.12471

Zhang, D., Xue, J., and Peng, F. (2022). The regulatory activities of MALAT1 in the development of bone and cartilage diseases. *Front. Endocrinol. (Lausanne)* 13, 1054827. doi:10.3389/fendo.2022.1054827

Zhang, L., Chen, J., Wang, L., Chen, L., Du, Z., Zhu, L., et al. (2019). Linc-PINT acted as a tumor suppressor by sponging miR-543 and miR-576-5p in esophageal cancer. *J. Cell Biochem.* 120, 19345–19357. doi:10.1002/jcb.28699

Zhong, C., Xie, Z., Zeng, L. H., Yuan, C., and Duan, S. (2022). MIR4435-2HG is a potential pan-cancer biomarker for diagnosis and prognosis. *Front. Immunol.* 13, 855078. doi:10.3389/fimmu.2022.855078

Zhuo, W., and Kang, Y. (2017). Lnc-ing ROR1-HER3 and Hippo signalling in metastasis. *Nat. Cell Biol.* 19, 81–83. doi:10.1038/ncb3467

frontiers | Frontiers in Immunology

TYPE Original Research
PUBLISHED 25 May 2023
DOI 10.3389/fimmu.2023.1100725

OPEN ACCESS

EDITED BY
Muhammad Suleman,
University of Swat, Pakistan

REVIEWED BY
Mikhail Danilov,
A.S.Loginov Moscow Clinical Scientific Centre, Russia
Fakhrul Hassan,
Riphah International University, Pakistan

*CORRESPONDENCE
Xueyang Wang
wangxy198812@163.com
Dekang Zhang
1660482257@qq.com

†These authors contributed equally to this work

RECEIVED 17 November 2022
ACCEPTED 02 May 2023
PUBLISHED 25 May 2023

CITATION
Wang X, Meng Q, Chen Y, Zhang Y, Huang X, Xiang L, Kong H, Wang C, Wang X and Zhang D (2023) Prognostic immunogenic characteristics of iron pendant disease modifiers in colon cancer. *Front. Immunol.* 14:1100725. doi: 10.3389/fimmu.2023.1100725

Prognostic immunogenic characteristics of iron pendant disease modifiers in colon cancer

Xian Wang[2†], Qingyu Meng[1†], Yawen Chen[1,4], Yanjun Zhang[1], Xiaohui Huang[1,2], Longquan Xiang[5], Haiyang Kong[6], Chunxi Wang[1,2], Xueyang Wang[7*] and Dekang Zhang[1,3*]

[1]Department of General Surgery, the First Medical Center, Chinese PLA General Hospital, Beijing, China, [2]Department of Health Management, The Second Medical Center and National Clinical Research Center for Geriatric Diseases, Chinese PLA General Hospital, Beijing, China, [3]Department of Radiology, the First Medical Center, Chinese PLA General Hospital, Beijing, China, [4]Department of Graduate ,Medical School of Chinese PLA, Beijing, China, [5]Department of Pathology, Jining NO.1 People's Hospital, Shandong Jining, China, [6]Department of General Surgery, Qufu Hospital of Traditional Chinese Medicine, Qufu, China, [7]Department of Radiology, Yancheng Traditional Chinese Medicine Hospital Affiliated to Nanjing University of Chinese Medicine, Yancheng, China

Background: We explored the prognostic and immunogenic characteristics of iron pendant disease regulators in colon cancer to provide a scientific basis for the prediction of tumor prognosis-related markers and potential immunotherapeutic drug targets.

Methods: RNA sequencing and matched complete clinical information of colon cancer (COAD) were retrieved from the UCSC Xena database, and genomic and transcriptomic data of colon cancer from the TCGA database were downloaded. Then univariate and multifactorial Cox regression were used to process these data. The prognostic factors were analyzed by single-factor and multi-factor Cox regression, followed by Kaplan-Meier survival curves with the aid of R software "survival" package. Then we use FireBrowse online analysis tool to analyze the expression variation of all cancer genes, and draw a histogram according to the influencing factors to predict the 1, 3, and 5 year survival rates of patients.

Results: The results show that age, tumor stage and iron death score were significantly correlated with prognosis ($p<0.05$). Further multivariate cox regression analysis confirmed that age, tumor stage and iron death score were still significantly correlated with prognosis ($p<0.05$); The calibration curve results show that the deviation between the predicted values of 1 year, 3 years and 5 years and the diagonal of the figure is very small; the ROC curve results show that the AUC values of the 1-year and 5-year ROC curves of the bar graph are high; the DCA curve results show that the net yield of the bar graph is the largest; The scores of T cells and B cells in the high iron death score group were significantly lower than those in the low iron death score group, and the activities of immune related pathways were significantly reduced. There was a significant difference in the iron death score between the iron death molecular subtype and the gene cluster subtype.

Conclusions: The model showed a superior response to immunotherapy in the high-risk group, revealing a potential relationship between iron death and tumor immunotherapy, which will provide new ideas for the treatment and prognostic assessment of colon cancer patients.

KEYWORDS

colon cancer, iron pendant disease modifier, prognosis, immunogenic characteristics, prognostic risk model

1 Introduction

Since the 21st century, the incidence of colorectal cancer in China has remained high (1). 2018 Chinese cancer statistics show that the incidence and mortality rate of colorectal cancer in China occupy two of the top five positions among all malignant tumors, which is a high incidence cancer, and the incidence of colorectal cancer is still on the rise, and the incidence of colorectal cancer in urban population is much higher than the incidence of colorectal cancer in rural population (2, 3). The disease can lead to abdominal pain, abdominal lumps and other symptoms, and in serious cases, metastasis may occur, leading to death, which poses a threat to patients' physical and psychological health and life safety (4–6). At the same time, colon cancer has the characteristics of high incidence and insidious development, so that in most cases, patients only seek medical treatment when they have symptoms in the middle and late stages. The complexity of the regulatory mechanism of colon cancer can be reflected in the fact that the process of colon cancer development can be regulated in many aspects and levels through multiple signaling pathways (7–10). In addition, colon cancer is influenced by the external environment, which cannot be ignored. It has been found that factors such as alcohol consumption, smoking, genetics, immune deficiency and high fat may be related to the occurrence of colon cancer. Although surgical procedures, radiotherapy, chemotherapy and other treatments have been actively developed, the insidious onset of colorectal cancer leads to the fact that most patients are already in the middle and late stages of the tumor when they are diagnosed. So most of them lose the opportunity of standard treatment, and the prognosis of colorectal cancer patients is poor (11–14), which includes late detection of the disease. Therefore, the existing treatment methods are no longer able to maximize the effect on patients' prognosis and survival quality. With the development of oncology, immunology, molecular biology and other related disciplines and interdisciplinary cross cutting content, and the continuous optimization of technical means, researchers have been able to further study and understand the impact of tumor microenvironment and gene level on tumors, which has led to the rapid development of tumor immunotherapy research (15, 16). More and more tumor immunotherapy targets have been discovered by researchers one after another. In the context of the development of big data era, immunotherapy has gradually become a new research hotspot and research focus in tumor treatment, and a new direction for colorectal cancer treatment (17). The research and development of immunotherapy have improved the prognosis of some colorectal cancer patients to a certain extent. Research has found that there are multiple prognostic genes in various human cancers. Prognostic gene identification based on genome database is helpful to determine the prognostic impact of cancer and understand the progress of cancer (18). Therefore, it is possible to benefit more patients from scientific research by conducting research related to immunotherapy by starting from colon cancer-specific genes, such as immune-related genes, and thus proceeding along the research path of further improving the treatment methods for colorectal cancer patients. Currently, some progress has been made in the screening of prognostic genes for colon cancer, and previous studies have shown that iron death may be a potential rake point for tumor growth inhibition and immunotherapy (19–22). Based on this, this study combined bioinformatics approach with real-world clinical data, using bioinformatics analysis of gene microarrays and high-throughput sequencing data published in major public databases such as TCGA and GEO, and mining gene expression profile data and transcriptome data published in databases for differential gene analysis between tumor and normal paired samples, so as to provide prediction of tumor prognosis-related markers and potential immunotherapeutic drug targets.

2 Methods

2.1 Data acquisition and processing

RNA sequencing and matched complete clinical information (age, sex, survival status, tumor stage) for colon cancer (COAD) were retrieved from the UCSC Xena database, and genomic and transcriptomic data for colon cancer from the TCGA database were downloaded. After filtering samples without survival status and survival time, samples with both genomic, transcriptomic and clinical data were retained, resulting in a total of 426 Count values were normalized to the number of transcripts per kilobase million (TPMs).

Combining the literature data and the iron death database, the intersection of related gene sets was taken to obtain a total of 69 iron death suppressor regulators, and 68 of which were present in TCGA-COAD. The analysis was performed by ConsensusClusterPlus

package, and principal component analysis (PCA) was used to examine the discrimination between subtypes after clustering. Similarly, consistency clustering based on differential genes among iron death subtypes was performed using the same method for clustering and discriminant testing. We collected the original expression profile data and clinical survival data of the COAD tumor samples GSE39582 and GSE17536 from the GEO database, and used the affy package to process the CONSENSUS clustering data of the TCGA-COAD dataset based on 69 iron death inhibitors. Then use the CONSENSUSClusterPlus package for analysis. After clustering, principal component analysis (PCA) was used to check the differences between subtypes. Similarly, consistency clustering based on differential genes among iron death subtypes was performed using the same method for clustering and discrimination test. Based on the mRNA expression profiles of 68 FRGs in COAD samples from the TCGA database, COAD patients were classified into three molecular patterns (C1:n=81; C2:n=226; C3:n=119) by unsupervised cluster analysis to assess the correlation between these patterns and the characteristics of the tumor immune microenvironment, as well as the biological behavior among the three iron death molecular patterns. The iron death score of each COAD sample was calculated according to the principal component analysis (PCA), and then all patients were divided into high iron death score group and low iron death score group, and their correlation with the prognosis of colorectal cancer was analyzed. At the same time, the age and clinical stage information of patients were collected, and their impact on the prognosis was analyzed using univariate and multivariate Cox regression, respectively. Then the Kaplan Meier survival curve was drawn using R software, FireBrowse online analysis tool was used to analyze the difference of gene expression in different cancer species, and a line graph was constructed based on influencing factors to predict the survival rate of patients in 1, 3 and 5 years. The GSE39582 and GSE17536 datasets were used as validation datasets to validate this prognostic risk model. Finally, PCA and Tsne clustering results were analyzed. Tumor samples were screened for high and low risk as a new grouping basis, and differential gene reanalysis was performed on the training set (TCGA) and validation set (GEO) data.

2.2 Statistical analysis

R4.0.3 software and Graphad Prism 9.0 software were used for statistical analysis and graphing. Wilcoxon rank sum test and Kruskal-Wallis test were used for comparison between groups. Kaplan-Meier survival curves were used to analyze the survival of patients with colon cancer. The data obtained in R language were labeled using the mean ± standard deviation (SD). When the obtained data conformed to a normal distribution with a statistically significant two-by-two comparison, the obtained data were subjected to t-test for correlation analysis, and ANOVA test was used for analysis when multiple groups were compared. For data that did not conform to a normal distribution, the Wilcoxon test was used for correlation analysis. The correlation of the clinical data of the patients was argued by the statistical X2 test. The Kaplan-Meier survival curves were then plotted using the R software "survival" package, and the FireBrowse online analysis tool was used to analyze the differences in gene expression across cancer species. Column plots were constructed to predict patient survival at 1, 3, and 5 years, with overall survival defined as the time from the day the patient underwent tumor resection to the day the patient died. The GSE39582 and GSE17536 datasets were used as validation datasets to validate this prognostic risk model, and finally PCA and Tsne clustering results were analyzed. Subject work characteristic (ROC) curves were used to evaluate the efficacy of the prognostic risk model in predicting 1, 3, and 5 year survival of colon cancer patients. The test level α for this study was 0.05, and all data were further analyzed using SPSS 22.0 as well as GraphPad Prism 9.0.2.

3 Results

A total of 69 FRGs were included in this study, 68 of which were present in TCGA-COAD. Figure 1A shows the copy number variation (CNV) locations of these FRGs on the chromosomes. Based on the mRNA expression profiles of 68 FRGs in COAD samples from The Cancer Genome Atlas (TCGA) database, COAD patients were classified into three molecular patterns (C1:n=81; C2: n=226; C3:n=119) by unsupervised clustering analysis. Principal component analysis (PCA) confirmed that these three subtypes were fully distinguishable (Figure 1B). Figure 1C shows the three patterns of COAD patients with different clinicopathological features. In addition, we assessed the correlation between these patterns and the immune microenvironmental characteristics of the tumors. Our data showed variability in the degree of immune cell infiltration in different samples (Figures 1D, E), significant differences in FEG expression values between almost all three molecular patterns, and regular differences in the expression of iron death inhibitory regulator genes in the three molecular patterns, such as GCLC, CD44, and other genes with the lowest expression in pattern I and the highest expression in pattern III (Figure 2A); and SRC, MTOR. There were also significant differences in immune cell infiltration (Figures 2B, C) and immune function (Figure 2D), especially for B cells and T cells, etc. (*: p<0.05; **:p<0.01; ***:p<0.001; ****:p<0.00001.)

3.1 TME characteristics in three ferroptosis gene clusters for COAD

We further explored the biological behavior among the three molecular patterns of iron death. Differential expression analysis was performed on these three patterns, and the concatenation of the three differentially expressed genes (DEGs) totaling 7425 (Figure 3A) was taken for univariate cox regression analysis to screen genes associated with prognosis, resulting in 255 genes. Based on these 255 genes, unsupervised clustering was performed and the TCGA-COAD cohort was divided into 2 gene clusters (Figure 3B) as gene cluster A and gene cluster B (Figure 3C), respectively. There were significant differences in immune cell infiltration (Figure 3D, E) and immune function (Figure 3F)

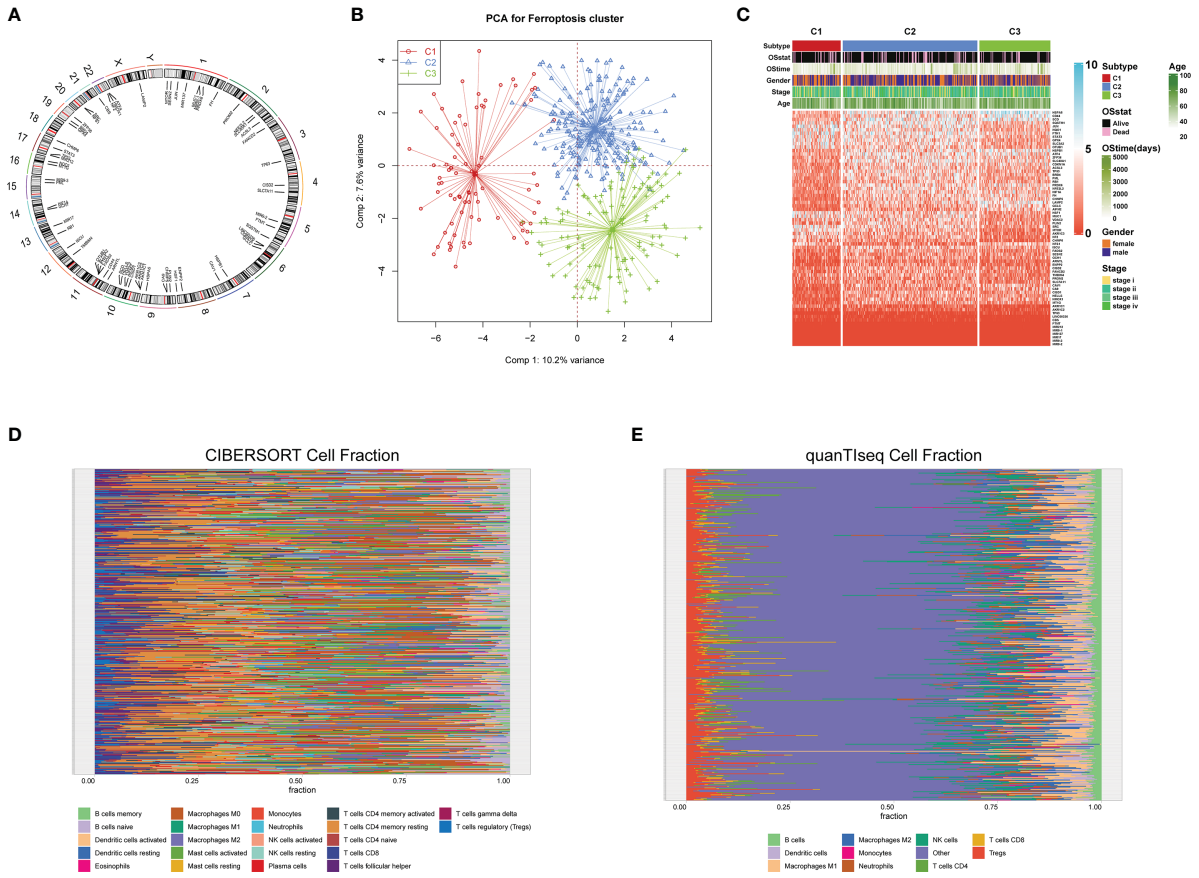

FIGURE 1
Copy number variation (CNV) locations of these FRGs on the chromosomes**(A)**;Principal component analysis **(B)**;Three patterns of COAD patients with different clinicopathological features**(C)**; The correlation between these patterns and the immune microenvironmental characteristics of the tumors **(D, E)**.

between the two gene clusters, especially for B cells and T cells. The 255 genes were classified into gene features A and B using Pearson's correlation coefficient, where gene feature A represents its positive correlation with gene cluster (r>0), and gene feature B represents its negative correlation with gene cluster (r<0), and they were downscaled using Boruta's algorithm to obtain 115 gene features A and 31 gene features B.

3.2 Development of the ferroptosis scoring system for COAD

Iron death scores were calculated for each COAD sample based on principal component analysis (PCA). All patients were then divided into a high iron death score group and a low iron death score group. Figure 4A shows the relationship between the high and low iron death score groups of TCGA-COAD samples and prognostic survival. The overall survival was higher in the high iron death score group samples compared to the low iron death score group. Meanwhile, in the two external COAD validation sets, GSE39582 (Figure 4B) and GSE175362 (Figure 4C), the survival difference between the high and low iron death score groups remained significant ($p< 0.05$), and both the survival rates of the high score group were greater than those of the low score group, indicating that our iron death score system constructed in TCGA-COAD has good generalizability and strong robustness.

3.3 Ferroptosis score as an independent prognostic factor for COAD

To perform an in-depth analysis of the prognostic value of the iron death score, we performed prognostic analysis of iron death score with other clinical characteristics in the TCGA-COAD cohort, and the results of one-way cox regression analysis showed (Figure 5A) that age, tumor stage, and iron death score were significantly associated with prognosis ($p< 0.05$). Further multifactorial cox regression analysis confirmed (Figure 5B) that age, tumor stage, and iron death score were still significantly associated with prognosis ($p< 0.05$). Therefore, we constructed column line plots (Figure 5C) to predict patient survival at 1, 3 and 5 years based on these three clinical characteristics, and validated the accuracy of column line plots to predict prognosis by calibration curves, ROC curves, and DCA curves. The calibration curve results showed (Figure 5C) that the predicted values at 1, 3 and 5 years deviated very little from the diagonal of the graph. The

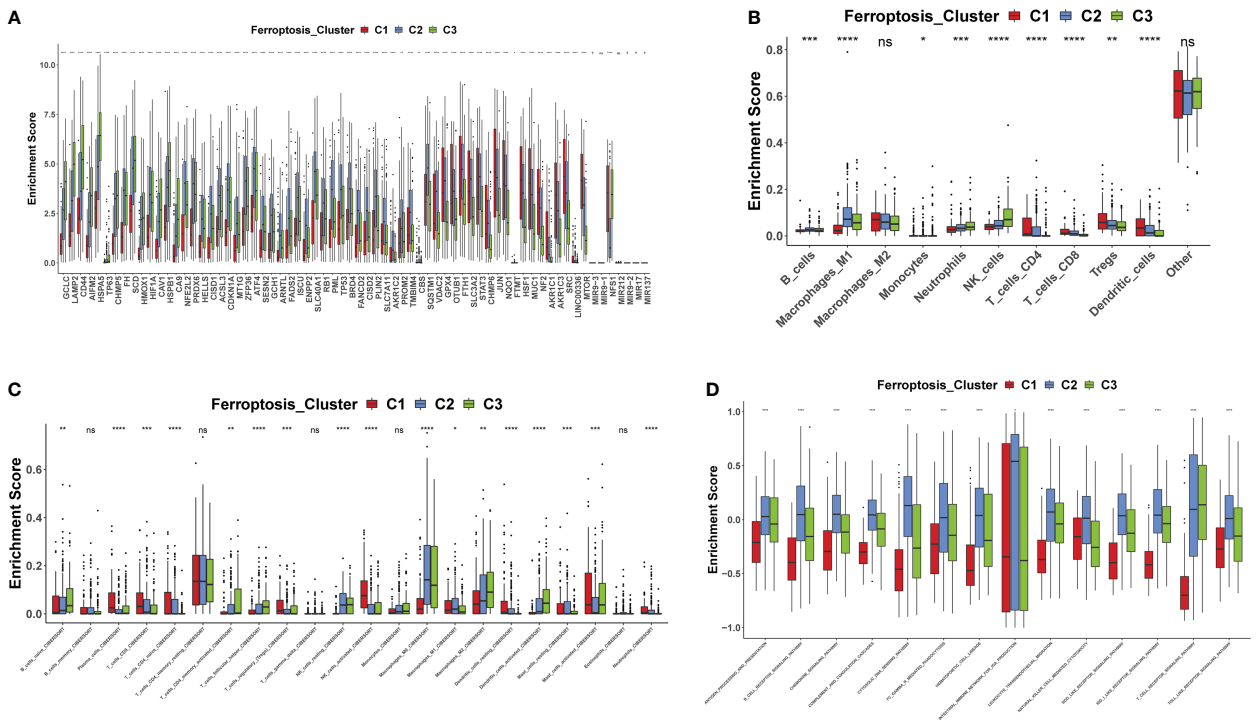

FIGURE 2
FEGs differences between the three molecular patterns **(A–D)**. *: p<0.05; **:p<0.01; ***: p<0.001; ****:p<0.00001; ns, no significance.

ROC curve results showed (Figure 5E–G) that the AUC values of the 1, 3 and 5 year ROC curves of the column line graph were high (greater than 0.7), and the DCA curve results found that (Figures 5H–J) the net benefit of the column line graph was the largest (compared with other individual clinical features). All three of the above methods all indicate that the column line graph has good accuracy in predicting patient prognosis.

3.4 Ferroptosis score is associated with TME features of COAD

This study further explored the correlation between iron death scores and TME characteristics. The data showed that the high iron death score group had significantly lower scores of T cells and B cells (Figures 6A, B, D) and lower activity in immune-related pathways (Figure 6C) compared to the low iron death score group. Also, the iron death scores differed significantly between iron death molecular subtypes and gene cluster subtypes (Figure 6E, F). Taken together, iron death scores were closely associated with TME in COAD.

3.5 Characteristics in groups with high or low ferroptosis score

We compared the differences in estimated half-maximal inhibitory concentration (IC50) levels of six chemotherapeutic agents, including erlotinib (Figure 7A), gemcitabine (Figure 7B), cytarabine (Figure 7C), gefitinib (Figure 7D), the Akt1/2/3 inhibitor MK.2206 (Figure 7E), and the PPM1D (WIP1) inhibitor CCT007093 (Figure 7F). Our data showed that the high iron death score group was more sensitive to erlotinib, gefitinib, and PPM1D (WIP1) inhibitor CCT007093 compared to the low iron death score group. In contrast, the low-iron death scoring group was more sensitive to gemcitabine, cytarabine and Akt1/2/3 inhibitor MK.2206. In addition to this, the immunotherapy response in the high and low scoring groups was further investigated based on the GSE78220 and IMvigor210 datasets, and we found that survival in the high and low scoring groups had opposite results in GSE78220 (Figure 8A) and IMvigor210 (Figure 8B), however, this did not affect the relationship between sample survival and immunotherapy response (Figure 8C, D), i.e., the higher the survival rate of the samples, the worse their response to immunotherapy. Finally, we performed differential analysis between high and low iron death groups (low vs. high) to obtain 748 DEGs (upregulated = 40, downregulated = 708) (Figure 9A, B), and the results of GO (Figure 9C) and KEGG (Figure 9D) enrichment analysis showed that these genes were mainly enriched in GO pathways such as RNA splicing, chromosomal regions and protein activation as well as NOD-like receptor signaling pathways, endoplasmic reticulum KEGG pathway such as protein processing.

4 Discussion

Colon cancer is one of the most common but preventable malignant tumors of the gastrointestinal tract, mainly caused by

10.3389/fimmu.2023.1100725

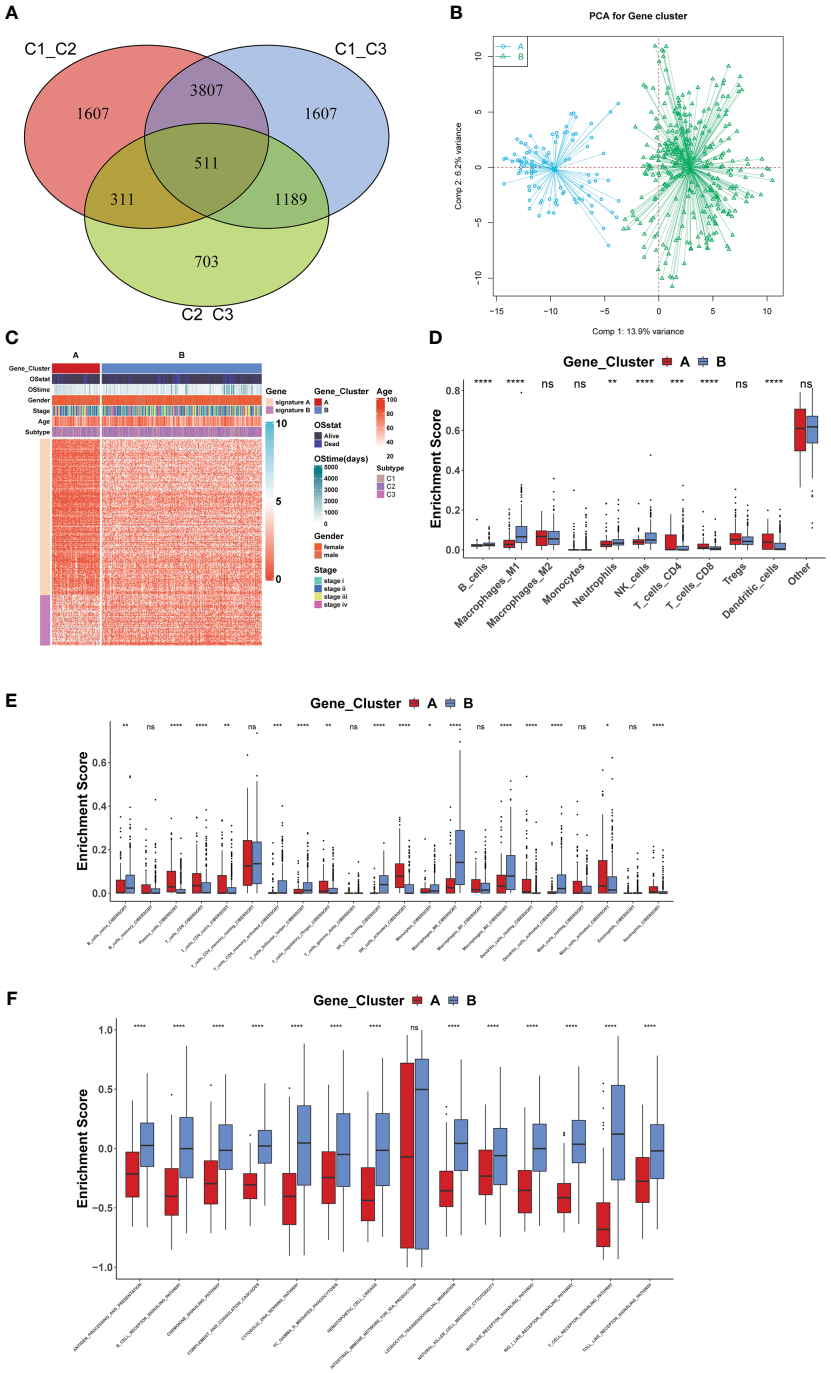

FIGURE 3
Biological behavior among the three molecular patterns of iron death **(A–F)**. *: p<0.05; **: p<0.01; ***: p<0.001; ****: p<0.00001; ns, no significance.

the deterioration of benign lesions of the colonic mucosal epithelium, and its incidence is only after malignant tumors of the stomach and esophagus (8, 23). It is the third most common cancer in the world and the second most common malignant tumor in China and the second most common cause of cancer death. Every year, the number of patients dying from colon cancer is increasing. Colon cancer is characterized by high incidence, susceptibility to poor prognosis, genetic and environmental factors (24). The main cause of death of colon cancer patients is due to its insidious onset, slow progression, lack of characteristic clinical manifestations, metastasis in the early stages of tumor lymph nodes and poor prognosis, which is also the reason why the clinical diagnosis is easily confused with diseases such as intestinal inflammatory diseases and functional disorders of the intestine. Studies have found that colon cancer is related to alcohol consumption, smoking, genetics, immunodeficiency, high fat and other factors. With the increasing per capita standard of living in China, changes in eating habits and diet structure, as well as the lack of exercise and excessive mental stress among urban workers, coupled with the increased intake of meat and protein, in addition, the amount of

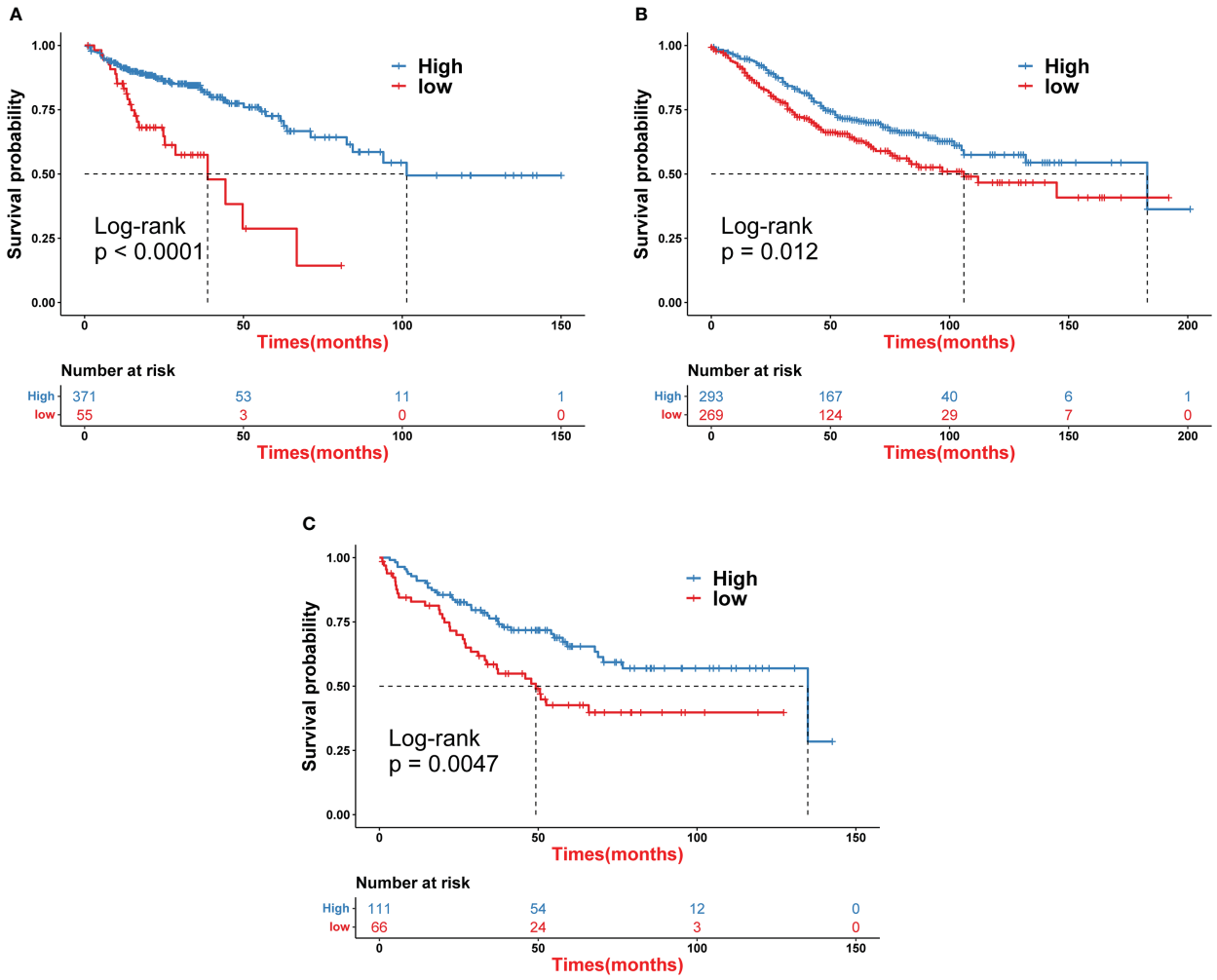

FIGURE 4
Iron death scores were calculated for each COAD sample based on principal component analysis **(A–C)**.

alcohol consumption in life has increased, which makes the average age of onset of patients suffering from colon cancer faster than in Europe and the United States, and the age has gradually become younger (25). The 2014 World Health Cancer Report shows that due to Environmental pollution tends to change heavily from day to day, which may directly or indirectly lead to an increase in the prevalence of malignant tumors and an increase in the number of patients dying from cancer. Environmental pollution in China has been worsening day by day in the past decade, and environmental pollution in cities is worse than in rural areas, which may be part of the reasons for the increased incidence of colon cancer in China, the younger and urbanized incidence of colon cancer, and the lower incidence in rural areas compared to urban areas. Therefore, there are many factors influencing the prognostic risk of colon cancer patients in the clinical setting, including the patient's age, daily habits, site of tumor occurrence, biological characteristics and tumor stage. The incidence of colon cancer in our country has tended to increase rapidly in the last few years (26–29). Due to the poor compliance of colonoscopy, many patients do not receive physical examination and other preventions before the appearance of typical symptoms, so that the best time for surgery and treatment is lost, thus leading to poor prognosis of colon cancer patients after clear diagnosis. Although the present surgery, radiotherapy and targeted therapy have a certain degree of relationship to prolong the survival time of colon cancer patients, and the multiple treatments carried out at the same time can prolong the survival time of advanced patients, the tumor has a high probability of local recurrence and metastasis after the tumor is diagnosed and treated, the 5-year survival rate of colon cancer patients after surgery is 50%, and 5-20% of colon cancer patients recur after treatment (30–33). Recurrence and metastasis are the leading causes of death from colorectal cancer and a major obstacle for improving the overall survival of colon cancer patients. However, there is no clear standard for the pathogenesis of colon cancer, therefore, early screening is particularly important for clinical diagnosis and treatment assessment of colon cancer and prognosis (34). In order to further improve the clinical treatment of colon cancer patients, it is necessary to continuously research and explore more convenient and rapid screening indicators that are readily accepted by patients, which are important in improving the survival rate after surgery, as well as in assessing the immediate and long-term survival of colon cancer patients (35).

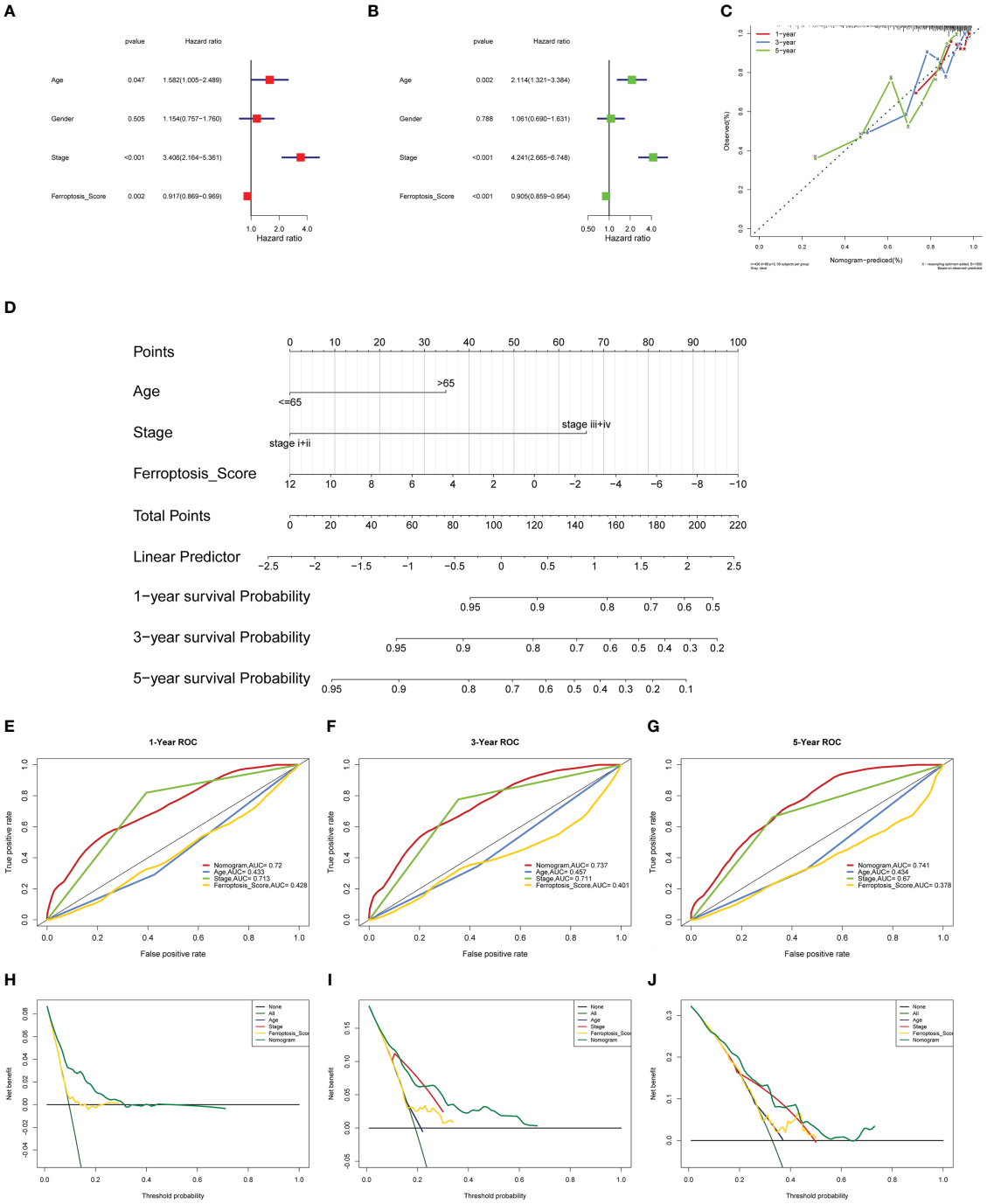

FIGURE 5
To perform an in-depth analysis of the prognostic value of the iron death score **(A–J)**.

Iron death is a newly discovered mode of programmed tumor cell death in 2012, which can lead to multiple death pathways (e.g., apoptosis, autophagy, scorch death, etc.) and can cause significant differences in the morphology, genetics, and mechanisms of action of cancer cells from other cell death processes, representing a new regulatory pathway for antitumor therapy (36). With the increasing understanding and awareness of iron death in recent years, the complex biological and clinical features of iron death have been analyzed and studied. For example, the pattern of cell death due to iron death is morphologically very different from other cell death pathways, and the morphological features of cells can be characterized by a decrease in intracellular mitochondrial volume, a decrease or disappearance of mitochondrial folds, and an increase in bilayer density following the massive accumulation of iron ions in iron death and its action on tumor cells (37, 38). Iron death has been reported to be genetically regulated by a variety of genes, mainly involving genetic changes in cells and disturbances in human iron homeostasis and lipid metabolism [z In terms of the biochemical reactions and mechanisms occurring within cells, iron death is also very different from other programmed modes of death, mainly:

10.3389/fimmu.2023.1100725

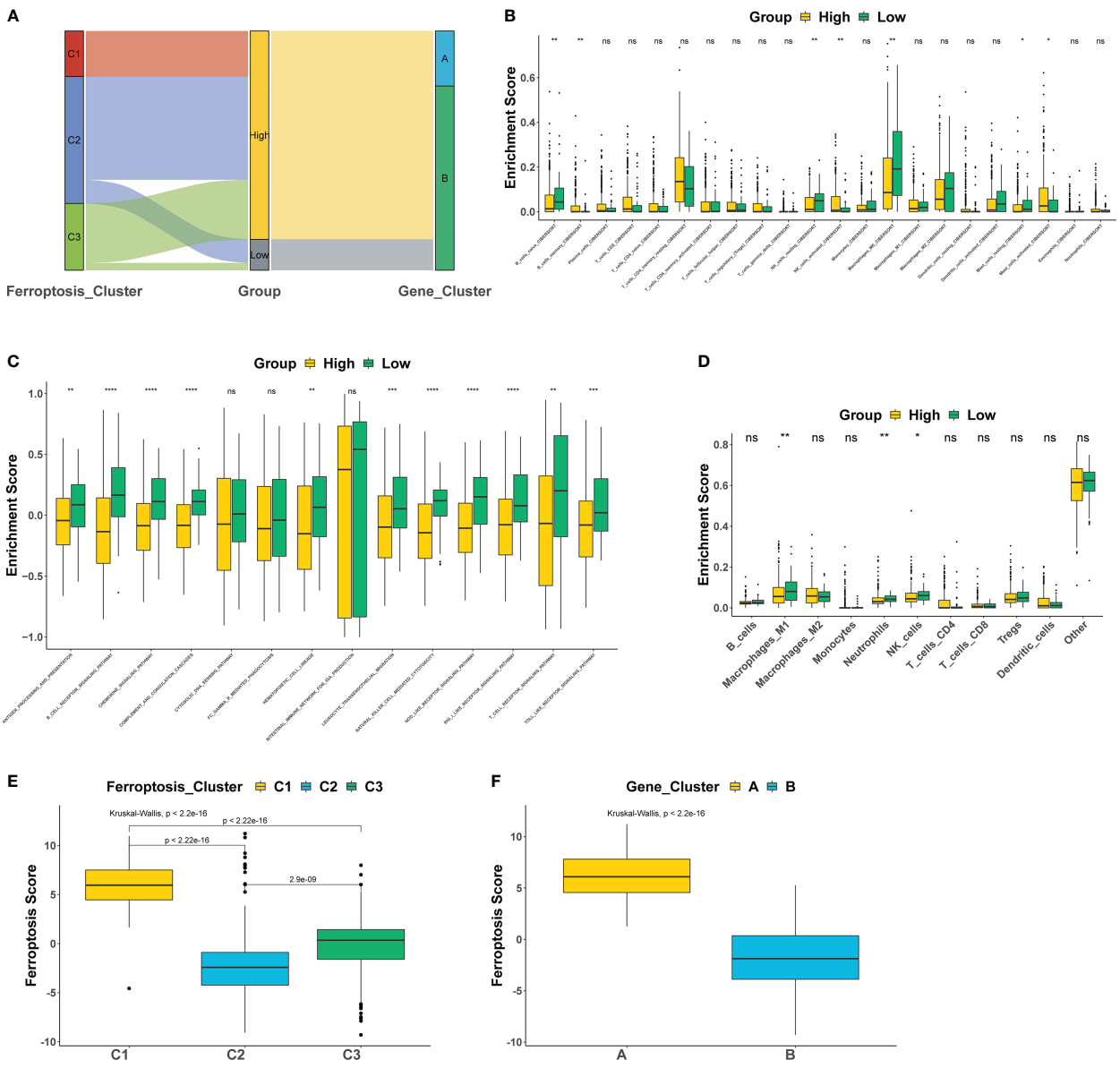

FIGURE 6
The correlation between iron death scores and TME characteristics **(A–F)**. *: p<0.05; **: p<0.01; ***: p<0.001; ****: p<0.00001; ns, no significance.

reduced activity of glutathione peroxidase 4 (GPX4), causing a decrease in intracellular glutathione (GSH) and even depletion of This leads to the inability of lipid oxidation to activate the glutathione redox reaction catalyzed by GPX4, which eventually disrupts the redox reaction metabolism while generating large amounts of reactive oxides (ROS) through the Fenton reaction (Fenton), and finally leads to cell death (17, 39, 40). Iron death has excellent antitumor efficacy and great potential in precision medicine. However, the specific key mechanisms of increased iron ions in tumorigenesis, progression, invasion, and metastasis have not been elucidated.

Immunotherapy against tumors is one of the major emerging therapeutic modalities in recent years, and it has been found that immune escape of tumor cells is involved in the processes related to the occurrence, development, metastasis, recurrence, and drug resistance in the treatment of tumor tissues in the human body. The immune escape of tumor cells is one of the main reasons for the low efficacy or even failure of comprehensive immunotherapy (41, 42). Therefore, restoring or reversing the ability of immune cells to recognize and kill tumor cells is the main research problem of tumor immunotherapy. In existing studies and clinical trials, immunotherapy has been shown to have good response effects and long-lasting responses in various solid tumors, such as melanoma, non-small cell lung cancer, and kidney cancer, and immunotherapy for tumors can significantly inhibit tumor progression at different stages and improve the long-term prognosis of patients. In tumor immunotherapy, iron death, a novel cell-regulated death modality, has shown great potential to induce not only tumor-specific immune responses but also to repolarize macrophages from an immunosuppressive M2 phenotype to an anti-tumor M1 phenotype (43). In tumor cells, T cells alter the tumor microenvironment and cause reduced or even depleted levels of cystine and cysteine, key fuels for tumor cells, causing impaired metabolism and ultimately cell death, which can be inhibited or even reversed by inhibiting iron death-

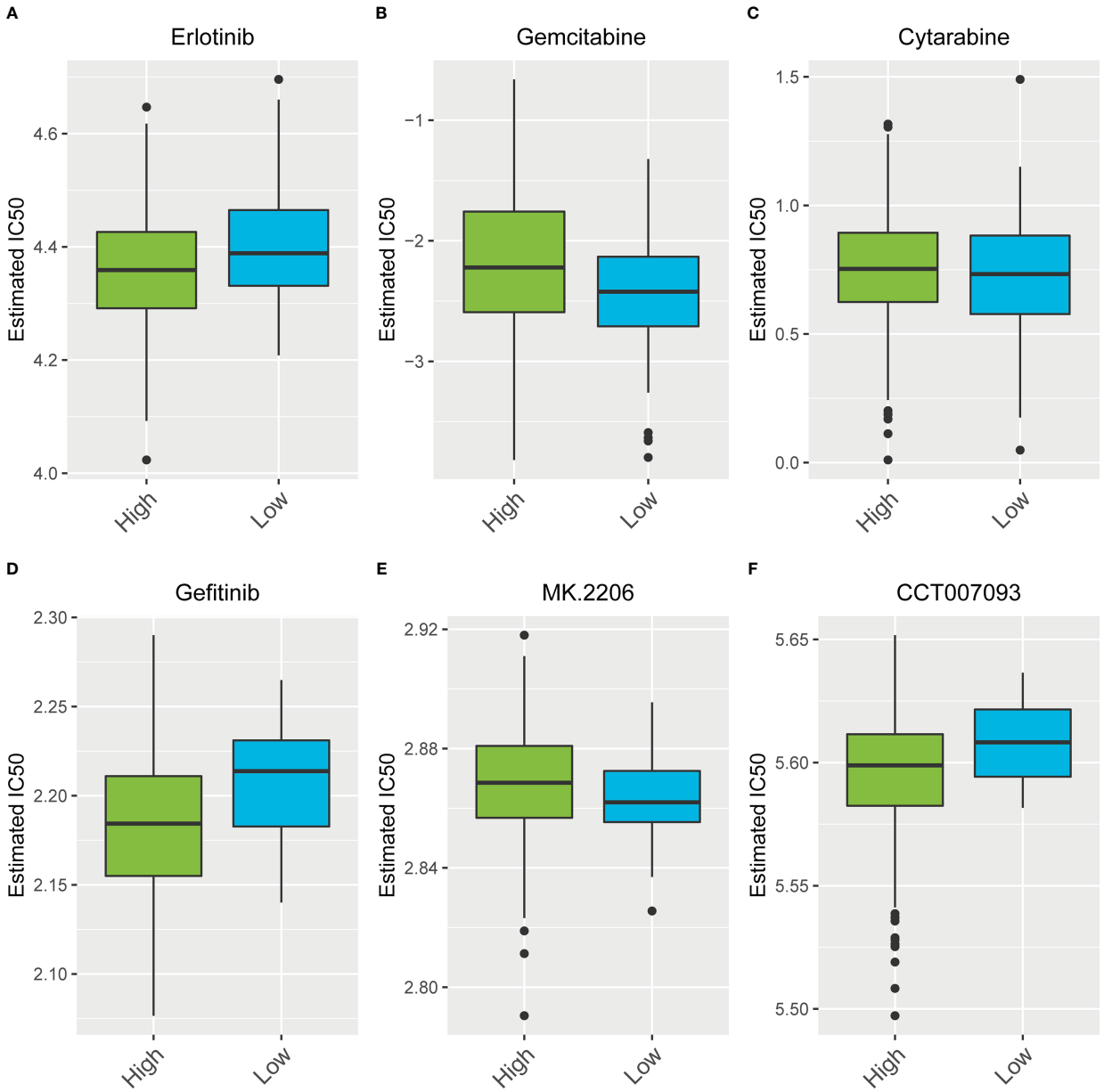

FIGURE 7
The differences in estimated half-maximal inhibitory concentration (IC50) levels of six chemotherapeutic agents **(A–F)**.

related pathways, i.e., when immunotherapy is combined with iron death sensitizer treatment, the effect on tumor progression is significantly better than with iron death alone immunotherapy or iron death sensitizers alone. The anti-tumor mechanism of cytotoxic T cells, i.e., CD8+ T cells, is mainly through the release of perforin and granzyme to specifically identify and kill human tumor cells, while some studies have shown that CD8+ T cells can act on tumor cells through the Fas-fasL pathway to cause apoptosis without harming normal tissue cells. Recent research has shown that the nitric oxide pathway inhibits the role of macrophages in iron death, providing a new opportunity to use tumor cell iron death to modulate intrinsic immunity in human tumors. In nanobased cancer vaccine immunotherapy, iron death can be involved in suppressing the primary tumor and its distant metastasis and improving the efficiency of drug delivery. Although immunotherapy has achieved great success in precision cancer therapy, and tumor progression can be significantly inhibited and even down-staged in immune-responsive patients, only about 30% of tumor patients currently respond to immunotherapy, which leads to this effective therapeutic approach not achieving its goal. However, only about 30% of tumor patients currently respond to immunotherapy, which results in this effective treatment method not achieving its desired effect (44, 45).A linear risk-prognosis model of iron death-related genes will be constructed by bioinformatics analysis and combined with public databases, and the model will be validated by using the data set in the GEO database. Finally, a risk-prognosis model consisting of 6 iron death-related genes will be derived, and the relationship between the iron death risk-prognosis model on tumor immune infiltration, immune transport pathway, and immune efficacy will be analyzed, aiming to The aim of this study is to screen high-risk tumor patients and treat them with

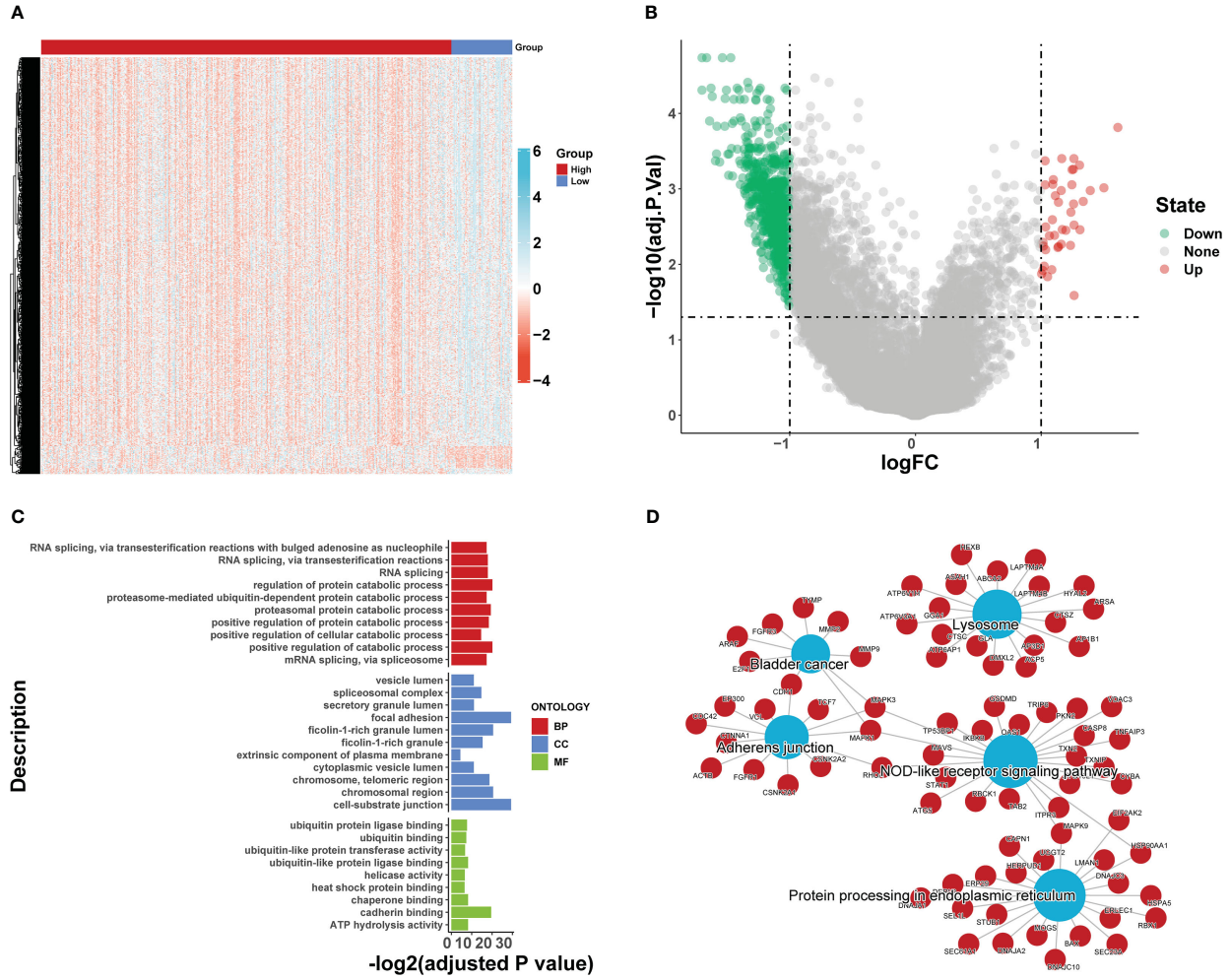

FIGURE 8
The immunotherapy response in the high and low scoring groups was further investigated based on the GSE78220 and IMvigor210 datasets **(A–D)**.

effective and precise immunotherapy to maximize the efficacy of immunotherapy.

The results of this study showed that 69 FRGs were included in this study, 68 of which were present in TCGA-COAD. Based on the mRNA expression profiles of 68 FRGs in COAD samples from The Cancer Genome Atlas (TCGA) database, COAD patients were classified into three molecular patterns by unsupervised cluster analysis (C1: n = 81; C2: n = 226; C3:n = 119), and PCA confirmed that the three subtypes were completely distinguishable; there was variability in the degree of immune cell infiltration in different samples, and the expression values of FEG were almost all significantly different among the three molecular patterns; there were regular differences in the expression of iron death inhibitory regulator genes in the three molecular patterns, such as GCLC, CD44, and other genes were least expressed in pattern I and most expressed in pattern III; while SRC and MTOR were the opposite. There were also significant differences in immune cell infiltration and immune function, especially for B cells and T cells; one-way cox regression analysis was performed to screen genes associated with prognosis, and 255 genes were finally obtained. Based on these 255 genes, unsupervised clustering was performed, and the TCGA-COAD cohort was divided into 2 gene clusters, named Gene Cluster A and Gene Cluster B. Immune cell infiltration and immune function were significantly different between the two gene clusters, especially for B cells and T cells. The 255 genes were classified into gene features A and B using Pearson's correlation coefficient, where gene feature A represents its positive correlation with gene cluster (r> 0), and gene feature B represents its negative correlation with gene cluster (r 0), and downscaled using the Boruta algorithm to obtain 115 gene features A and 31 gene features B. The high-iron death scoring group samples had higher overall survival rates compared with the low-iron death scoring group, while the survival differences between the high and low iron death scoring groups remained significant in the two external COAD validation sets GSE39582 and GSE175362 (p< 0.05) and were both greater in the high scoring group than in the low scoring group, indicating that the iron death scoring system we constructed in TCGA-COAD has good The results of one-way cox regression analysis showed that age, tumor stage, and iron death score were all significantly associated with prognosis (p< 0.05). Further multifactorial cox regression analysis confirmed that age, tumor stage and iron death score were still significantly associated

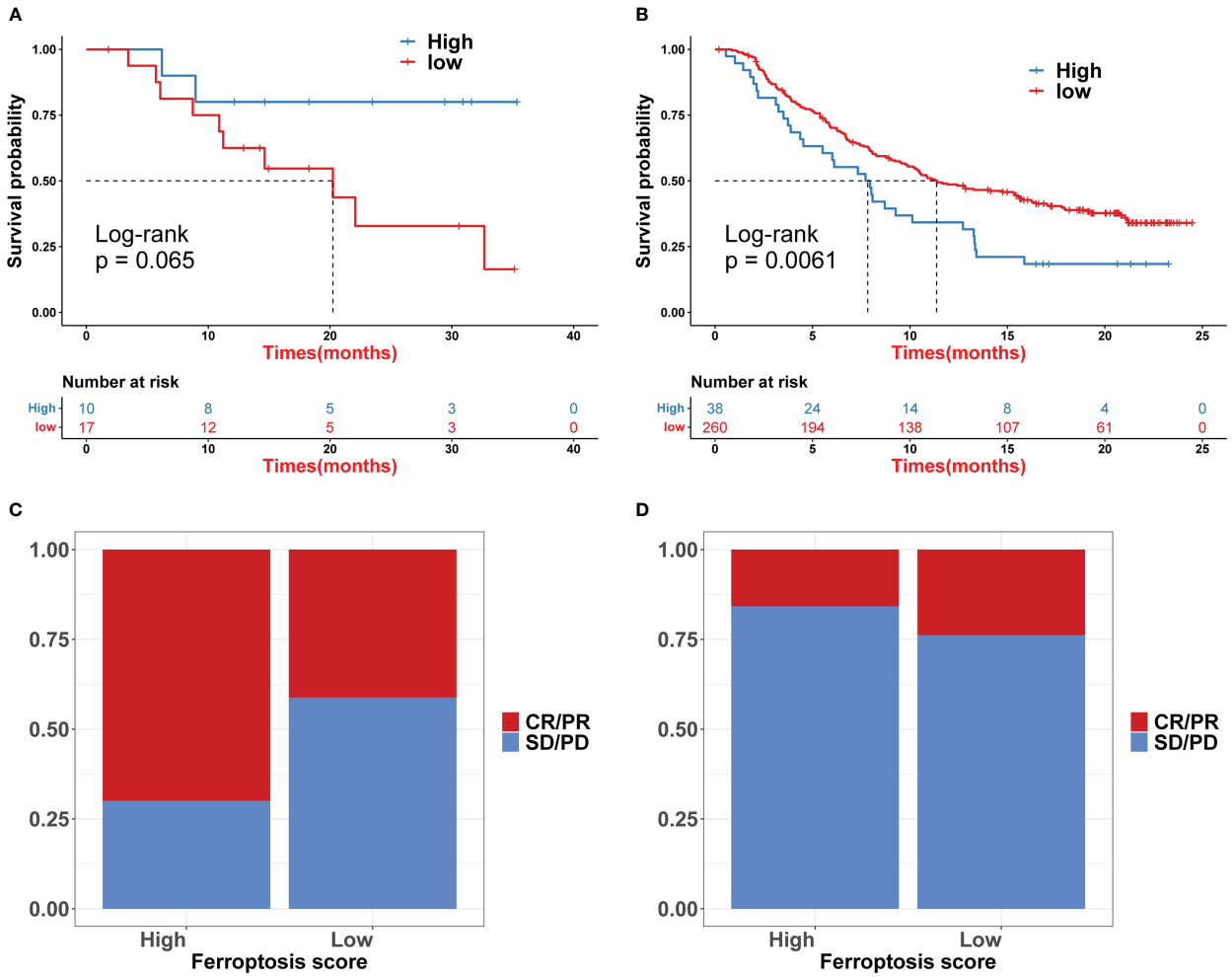

FIGURE 9
Differential analysis between high and low iron death groups (low vs. high) **(A, B)**, and the results of GO **(C)** and KEGG **(D)** enrichment analysis.

with prognosis ($p< 0.05$); the calibration curve results showed (Figure 5C) that the predicted values at 1, 3 and 5 years deviated little from the diagonal line in the figure; and the ROC curve results indicated that the AUC values of the ROC curves at 1, 3 and 5 years were higher (> 0.7) for the column line plots. The DCA curve results found that the net yield of the column line graph was the largest (compared to other individual clinical features), and all three tests above indicated that the column line graph had better accuracy in predicting patient prognosis; the high iron death score group had significantly lower scores for T cells and B cells (Figure 6B, D) and lower activity in immune-related pathways (Figure 6C) compared to the low iron death score group, while the iron death scores differed significantly between iron death molecular subtypes and gene cluster subtypes, and the above results can indicate that iron death scores are closely related to TME in colon cancer. Compared with the low iron death score group, the high iron death score group was more sensitive to erlotinib, gefitinib, and PPM1D (WIP1) inhibitor CCT007093. In contrast, the low-iron death scoring group was more sensitive to gemcitabine, cytarabine, and Akt1/2/3 inhibitor MK.2206. In addition to this, the immunotherapy response of high and low-scoring groups was further investigated based on the GSE78220 and IMvigor210 datasets, and we found that the survival of high and low-scoring groups had opposite results in GSE78220 and IMvigor210. However, this did not affect the relationship between sample survival and immunotherapy response, i.e., the higher the survival of the sample, the worse their response to immunotherapy. Finally, we performed differential analysis between high and low iron death groups to obtain 748 DEGs (upregulated = 40, downregulated = 708), and the results of GO and KEGG enrichment analysis showed that these genes were mainly enriched in GO pathways such as RNA splicing, chromosomal regions, and protein activation, and KEGG pathways such as NOD-like receptor signaling pathway and protein processing of endoplasmic reticulum.

After reviewing the relevant literature, Wang Yuqing et al. (46) successfully constructed a prognostic risk model for colon cancer based on iron death-related lncRNAs and established a column line graph that could be used to determine the overall survival rate of colon cancer patients. ITGB1-DT may promote the development of colon cancer, and Zhang Tao et al. (47) showed that iron death-related lncRNAs may play an important role in the tumor immunity of colon cancer patients, which could be used for prognostic analysis of colon cancer patients. All the above findings are close to the present study. P53RRA increased the concentration of

intracellular iron and lipid reactive oxygen species while enhancing the growth inhibition induced by Erastin, an iron-induced cell death activator, a mechanism closely associated with iron death in tumors (48–51). In addition, the lncRNA APCDC1L-AS can induce resistance to erktinib (EGFR-tyrosine kinase inhibitor) in lung adenocarcinoma by inhibiting autophagic degradation of epithelial growth factor receptor (EGFR) (52, 53).

This study is innovative because there are few studies on iron death in colon cancer, and even fewer studies combining immune cell infiltration and immune pathways. In this experiment, we used bioinformatics to analyze the expression of iron death differential genes in colon cancer, constructed a linear risk prediction model, and used the model to detect and verify the relationship between iron death-related genes in colon cancer and immune infiltration, as well as to classify patients into high and low risk based on the model, and to investigate the response of each group of patients to immunotherapy, which is somewhat novel and necessary.

This study is innovative because there are few studies on iron death in colon cancer, and even fewer studies combining immune cell infiltration and immune pathways. In this experiment, we used bioinformatics to analyze the expression of iron death differential genes in colon cancer, constructed a linear risk prediction model, and used the model to detect and verify the relationship between iron death-related genes in colon cancer and immune infiltration, as well as to classify patients into high and low risk based on the model, and to investigate the response of each group of patients to immunotherapy, which is somewhat novel and necessary.

Data availability statement

The datasets presented in this study can be found in online repositories. GSE39582 and GSE17536 from the GEO database.

Author contributions

(I) Conception and design: XiW and YWC. (II) Administrative support: CXW QYM and DKZ. (III) Provision of study materials or patients:YJZ, XiW and YWC. (IV) Collection and assembly of data: XYW, YWC XHH and QYM. (V) Data analysis and interpretation: XiW, LQX and HYK.(VI) All authors contributed to the article and approved thesubmitted version.

Acknowledgments

We thank the editor and reviewers for their time and effort, and for their insightful comments and valuable improvements to the paper.

Conflict of interest

The authors declare that the research was conducted in the absence of any commercial or financial relationships that could be construed as a potential conflict of interest.

Publisher's note

Supplementary material

The Supplementary Material for this article can be found online at: https://www.frontiersin.org/articles/10.3389/fimmu.2023.1100725/full#supplementary-material

References

1. Siena S, Di Bartolomeo M, Raghav K, Masuishi T, Loupakis F, Kawakami H, et al. DESTINY-CRC01 investigators. trastuzumab deruxtecan (DS-8201) in patients with HER2-expressing metastatic colorectal cancer (DESTINY-CRC01): a multicentre, open-label, phase 2 trial. *Lancet Oncol* (2021) 22(6):779–89. doi: 10.1016/S1470-2045(21)00086-3

2. Lenz HJ, Van Cutsem E, Luisa Limon M, Wong KYM, Hendlisz A, Aglietta M, et al. First-line nivolumab plus low-dose ipilimumab for microsatellite instability-High/Mismatch repair- deficient metastatic colorectal cancer: the phase II CheckMate 142 Study. *J Clin Oncol* (2022) 40(2):161–70. doi: 10.1200/JCO.21.01015

3. Nakamura Y, Okamoto W, Kato T, Esaki T, Kato K, Komatsu Y, et al. Circulating tumor DNA-guided treatment with pertuzumab plus trastuzumab for HER2-amplified metastatic colorectal cancer: a phase 2 trial. *Nat Med* (2021) 27(11):1899–903. doi: 10.1038/s41591-021-01553-w

4. Meyerhardt JA, Shi Q, Fuchs CS, Meyer J, Niedzwiecki D, Zemla T, et al. Effect of celecoxib vs placebo added to standard adjuvant therapy on disease-free survival among patients with stage III colon cancer: the CALGB/SWOG 80702 (Alliance) randomized clinical Trial. *JAMA* (2021) 325(13):1277–86. doi: 10.1001/jama.2021.2454

5. Gao C, Kong N, Zhang F, Tang T, Li J, Ding H, et al. Risk stratification of lung adenocarcinoma using a nomogram combined with ferroptosis-related LncRNAs and subgroup analysis with immune and N6-methyladenosine modification. *BMC Med Genomics* (2022) 15(1):15. doi: 10.1186/s12920-022-01164-5

6. Watanabe J, Sasaki S, Kusumoto T, Sakamoto Y, Yoshida K, Tomita N, et al. S-1 and oxaliplatin versus tegafur-uracil and leucovorin as post-operative adjuvant chemotherapy in patients with high-risk stage III colon cancer: updated 5-year survival of the phase III ACTS-CC 02 trial. *ESMO Open* (2021) 6(2):100077. doi: 10.1016/j.esmoop.2021.100077

7. Lee S, Ma C, Zhang S, Ou FS, Bainter TM, Niedzwiecki D, et al. Marital status, living arrangement, and cancer recurrence and survival in patients with stage III colon cancer: findings from CALGB 89803 (Alliance). *Oncologist* (2022) 27(6):e494–505. doi: 10.1093/oncolo/oyab070

8. Yuyan Z, Xuejun C. Bioinformatics analysis of CXCL2 and THBS2 in the diagnosis, prognosis and immune infiltration of colon cancer. *J Pract Cancer* (2022) 37(02):154–62. doi: 10.13267/j.cnki.syzlzz.2022.025

9. Dan X, Bin H. Clinical efficacy of oxaliplatin combined with capecitabine in the treatment of advanced colon cancer and its impact on immune function. *J Clin Rational Drug Use* (2022) 15(09):99–101. doi: 10.15887/j.cnki.13-1389/r.2022.09.029

10. Yanchun Z, Guowen Y, Xinan L, Jingjing Z, Caixia Y, Qing Y, et al. Effect of entropy index combined with protective pulmonary ventilation on neural function, cognitive function and immune function of elderly patients undergoing laparoscopic radical colon cancer surgery. *Hebei Med J* (2022) 44(05):687–90. doi: 10.3969/j.issn.1002-7386.2022.15.008

11. Xiaoli Q, Chao Y, Pengbo Z. Study on the improvement of perioperative immune function of laparoscopic colon cancer patients by intravenous infusion of dexmedetomidine. *Cancer Prog* (2021) 19(23):2432–5. doi: 10.3969/j.issn.1002-7386.2020.22.008

12. Zhilin L, Jiping X, Hao W. Analysis of the effect of fuzheng xiaoji decoction combined with chemotherapy on the short-term efficacy and immune function of patients with advanced colon cancer. *J Chronic Dis* (2021) 22(11):1701–1702+1705. doi: 10.3969/j.issn.1673-7202.2015.02.015

13. Yantong Z, Chunxiao L, Jinsong W, Fangzho S, Dongkui X, Haiyan Z, et al. Single cell transcriptome sequencing analysis of the relationship between immune cell subsets in the microenvironment of colon cancer and cancer progression. *J PLA Med* (2021) 46(07):692–701. doi: 10.11855/j.issn.0577-7402.2021.07.09

14. Yamazaki K, Yamanaka T, Shiozawa M, Manaka D, Kotaka M, Gamoh M, et al. Oxaliplatin-based adjuvant chemotherapy duration (3 versus 6 months) for high-risk stage II colon cancer : the randomized phase III ACHIEVE-2 trial. *Ann Oncol* (2021) 32 (1):77–84. doi: 10.1016/j.annonc.2020.10.480

15. Sadahiro S, Sakamoto K, Tsuchiya T, Takahashi T, Ohge H, Sato T, et al. Prospective observational study of the efficacy of oral uracil and tegafur plus leucovorin for stage II colon cancer with risk factors for recurrence using propensity score matching (JFMC46-1201). *BMC Cancer* (2022) 22(1):170. doi: 10.1186/s12885-022-09267-z

16. Munechika T, Kajitani R, Matsumoto Y, Nagano H, Komono A, Aisu N, et al. Safety and effectiveness of high ligation of the inferior mesenteric artery for cancer of the descending colon under indocyanine green fluorescence imaging: a pilot study. *Surg Endosc* (2021) 35(4):1696–702. doi: 10.1007/s00464-020-07556-x

17. Zexin Z, Siqi L, Zifeng L, Wenfeng W, Ziyi H, Weiqi C, et al. Identification of molecular target and construction of prognosis model of dahuang mudan decoction for colon cancer based on network pharmacology and bioinformatics. *China Modern Appl Pharm* (2022) 39(15):1925–37. doi: 10.13748/j.cnki.issn1007-7693.2022.15.002

18. Xiaohu W, Chaozhuang S, Chenggang X, Yusong W, Xingwen W, Haitang X, et al. Bioinformatics based screening of key genes of colon cancer and active components of traditional Chinese medicine. *Chin J Med Clin Sci* (2022) 22(07):614–617+673-674. doi: 10.11655/zgywylc2022.07.007

19. Zhiwen G, Yinteng W, Cun L, Ma H, Zhang S, Zhang X, et al. Analysis of prognosis related genes of colon cancer and their correlation with immune cells based on bioinformatics. *Colorectal Anal Surg* (2022) 28(03):255–260+265. doi: 10.19668/j.cnki.issn1674-0491.2022.03.013

20. Guo C, Limin T, Xiaoping L. Screening of genes related to the prognosis of patients with stage III colon cancer based on bioinformatics. *J Ningxia Med Univ* (2022) 44(05):493–498+504. doi: 10.16050/j.cnki.issn1674-6309.2022.05.010

21. Qian L, Guoping Q, Huayi Y, Yuyang D, Wenbin L, Jianhua J, et al. Bioinformatics analysis of screening core genes and independent prognostic factors in colon cancer. *J Jilin Univ (Medical Edition)* (2022) 48(03):755–65. doi: 10.13481/j.1671-587X.20220325

22. Zhongze C, Shuang H, Lizhen L, Shuhua W. Screening key genes of colon cancer based on bioinformatics analysis. *Med Inf* (2022) 35(10):1–7. doi: 10.3969/j.issn.1006-1959.2022.10.001

23. Chenglu W, Yujie N, Runsang P, Lan Z, Shuanhui C, Hui C, et al. Screening of pivotal genes related to colon cancer progression based on bioinformatics methods. *Shandong Med* (2022) 62(01):15–9. doi: 10.3969/j.issn.1002-266X.2022.01.004

24. Mingchao H, Baosong Z. Bioinformatics analysis of the diagnostic and prognostic value of NDC1 gene in colon cancer: a study based on TCGA database. *Lingnan Modern Clin Surg* (2021) 21(06):598–602. doi: 10.3969/j.issn.1009•976X.2021.06.002

25. Siyu W, Yanyan L, Qian A. Mining of key genes for the diagnosis and prognosis of colon cancer based on WGCNA and differential expression analysis, [C]. *Professional Committee on Tumor Markers of Chinese Anti-Cancer Association. Proceedings of the 2021 China Cancer Markers Academic Conference and the 15th Cancer Markers Young Scientists Forum*. (2021) 2021:202–203. doi: 10.26914/c.cnkihy.2021.046139

26. Zhengchun K, Feihu Y, Zhen W, Ziye Z, Enda N, JJunjie X, et al. Bioinformatics analysis of the effect of chromatin open state on colon cancer related functional pathways. *J Second Military Med Univ* (2021) 42(07):762–9. doi: 10.16781/j.0258-879x.2021.07.0762

27. Mingjing P, Lei S, Jie C. Bioinformatics analysis of PARPBP gene expression and function in colon cancer. *Cancer Pharm* (2021) 11(03):305–308+319. doi: 10.3969/j.issn.2095-1264.2021.03.10

28. Cheng Z, Guoping Q, Ying S, Wenbin L, Jianzhong D, Qian L, et al. Screening and verification of colon cancer core genes based on bioinformatics. *J Jiangsu Univ (Medical Edition)* (2021) 31(04):296–302. doi: 10.13312/j.issn.1671-7783.y210046

29. Zhixiang D, Bingwei S, Yongfang W, Xian G, Qian L. Screening and verification of potential pivotal genes of colon cancer based on bioinformatics. *Chin J Immunol* (2021) 37 (02):201–5. doi: 10.3969/j.issn.1000-484X.2021.02.014

30. Weiqiang L, Guangwen C, Yiang Y, Xiangyuan Z, Haibo W, Minting L, et al. Expression of iron death related protein GPX4 in colon cancer and its correlation with prognosis. *J Clin Exp Pathol* (2022) 38(09):1035–41. doi: 10.13315/j.cnki.cjcep.2022.09.003

31. Shaukat A, Shyne M, Mandel JS, Snover D., Church. Colonoscopy with polypectomy reduces long-term incidence of colorectal cancer in both men and women: extended results from the Minnesota colon cancer control Study. *Gastroenterology* (2021) 160(4):1397–1399.e3. doi: 10.1053/j.gastro.2020.11.014

32. Yinan Z. Resveratrol regulates the mechanism of iron death in the treatment of colon cancer by downregulating miR-31 [D]. *Shanxi Med Univ* (2022).

33. Zhuan J, Rui Z, Angang Y, Huilong Y. Mutant p53 promotes iron death of human colon cancer and lung cancer cells by down regulating the expression of glutathione peroxidase 4 (GPX4) and increasing the production of lipid reactive oxygen species. *J Cell Mol Immunol* (2022) 38(06):522–7.

34. Huixia L, Weibo Y, Li C, Jianping W. The role of glutathione peroxidase 4 in triptolide induced iron death in colon cancer cells. *Zhejiang Med J* (2022) 44(10):1038–1041+1049+1126. doi: 10.12056/j.issn.1006-2785.2022.44.10.2021-1480

35. Yajun L. LINC01606 via SCD1 Wnt/ β- Effect and mechanism of catenin-TFE3 signal on biological function of colon cancer cells [D]. Chongqing Medical University (2022).

36. Xiaoyi Z. Echinoside A induces colon cancer cell apoptosis and inhibits its migration and invasion by down-regulation of VEGFA/VEGFR2/ERK pathway [D]. Qingdao University (2021).

37. Huijie Z. A new tubulin inhibitor TH320 inhibits the proliferation of human colon cancer HT-29 cells and its mechanism [D]. Henan University (2021).

38. Hao K. Wuhan University (2021).

39. Chen L, Tianfeng Z, Yu W, Longyun W, Wuyang B. miR-212 regulates tumor stem cell like properties and immune response of colon cancer SW480 by targeting NRP1. *Chin J Immunol* (2022) 38(14):1734–8.

40. Lichao C, Ying B, Shitao D, Qi W, Xiaoping L, Hezi Z. Exploring immune related prognostic factors in the tumor microenvironment of colon cancer based on TCGA and GEO database. *J Clin Lab* (2022) 40(06):466–74. doi: 10.13602/j.cnki.jcls.2022.06.14

41. Hong T, Fudao W, Xiangli Z, Jiangping F, Xiaojing Z. Effect of bevacizumab combined with oxaliplatin and capecitabine on the efficacy, immune function and tumor effect of bevacizumab combined with oxaliplatin and capecitabine on the efficacy, immune function and tumor markers of patients with advanced colon cancer. *Int J Lab Med* (2022) 43(12):1500–3. doi: 10.3969/j.issn.1673-4130.2022.12.020

42. Qinbo Z, Xuexin L, Senyao L. Effect of yangzheng huaji decoction combined with chemotherapy on tumor markers and immune function of advanced colon cancer. *New Chin Med* (2022) 54(11):194–7. doi: 10.13457/j.cnki.jncm.2022.11.042

43. Shuran C, Rui D, Huazhang W, Mulin L. FOLFOX resistance related gene is a potential biomarker to predict the prognosis of colon cancer patients. *Chongqing Med J* (2022) 51(17):3016–24. doi: 10.3969/j.issn.1671-8348.2022.17.029

44. Xia X, Xinyu T, Ye Q. Effect of rapid rehabilitation surgery combined with early nutrition management on the surgical outcome, immune function and postoperative rehabilitation of colon cancer patients. *Gen Nurs* (2022) 20(13):1812–5. doi: 10.12104/j.issn.1674-4748.2022.13.022

45. Zheng W. Peking Union Medical College (2022).

46. Yuqing W, Yue Z, Wen X, Zhongqi C. Construction and clinical application of a prognosis risk model of iron death related lncRNA colon cancer. *Lab Med* (2022) 37 (08):720–8. doi: 10.3969/j.issn.1673-8640.2022.08.004

47. Tao Z, Shiying L, Mengyuan W, Zihao L, Shuangshuang J, Yifei W, et al. Prognostic analysis of colon cancer patients based on the characteristics of iron death related long chain non coding RNA. *Cancer Res Clin* (2022) 34(05):338–45. doi: 10.3760/cma.j.cn115355-20211125-00537

48. Taniguchi H, Nakamura Y, Kotani D, Yukami H, Mishima S, Sawada K, et al. CIRCULATE-Japan: circulating tumor DNA-guided adaptive platform trials to refine adjuvant therapy for colorectal cancer. *Cancer Sci* (2021) 112(7):2915–20. doi: 10.1111/cas.14926

49. Planellas P, Marinello F, Elorza G, Golda T, Farrés R, Espín-Basany, et al. Extended versus standard complete mesocolon excision in sigmoid colon cancer: a multicenter randomized controlled Trial. *Ann Surg* (2022) 275(2):271–80. doi: 10.1097/SLA.0000000000005161

50. Taieb J, Taly V, Henriques J, Bourreau C, Mineur L, Bennouna J, et al. Prognostic value and relation with adjuvant treatment duration of ctDNA in stage III colon cancer: a *Post hoc* analysis of the PRODIGE-GERCOR IDEA-France Trial. *Clin Cancer Res* (2021) 27(20):5638–46. doi: 10.1158/1078-0432.CCR-21-0271

51. Di Buono G, Buscemi S, Cocorullo G, Sorce V, Amato G, Bonventre G, et al. Feasibility and safety of laparoscopic complete mesocolic excision (CME) for right-sided colon cancer: a randomized clinical Study. *Ann Surg* (2021) 274(1):57–62. doi: 10.1097/SLA.0000000000004557

52. Xu L, Su X, He Z, Zhang C, Lu J, Zhang G, et al. RELARC study group. short-term outcomes of complete mesocolic excision versus D2 dissection in patients undergoing laparoscopic colectomy for right colon cancer (RELARC): a randomised, controlled, phase 3, superiority trial. *Lancet Oncol* (2021) 22(3):391–401. doi: 10.1016/S1470-2045(20)30685-9

53. Politi L, Monasta L, Rigressi MN, Princivalle A, Gonfiotti A, Camiciottoli G, et al. Discriminant profiles of volatile compounds in the alveolar air of patients with squamous cell lung cancer, lung adenocarcinoma or colon cancer. *Molecules* (2021) 26 (3):550. doi: 10.3390/molecules26030550

frontiers | Frontiers in Medicine

TYPE Original Research
PUBLISHED 31 January 2024
DOI 10.3389/fmed.2024.1301487

OPEN ACCESS

EDITED BY
Muhammad Suleman,
Qatar University, Qatar

REVIEWED BY
Pralay Mukhopadhyay,
GlaxoSmithKline, United States
Zafar Ali,
University of Swat, Pakistan

*CORRESPONDENCE
Yunlong Pan
✉ tpanyl@jnu.edu.cn
Jun Lyu
✉ lyujun2020@jnu.edu.cn

†These authors have contributed equally to this work

RECEIVED 25 September 2023
ACCEPTED 08 January 2024
PUBLISHED 31 January 2024

CITATION
Su H, Xie S, Wang S, Huang L, Lyu J and Pan Y (2024) New findings in prognostic factor assessment for adenocarcinoma of transverse colon: a comparison study between competing-risk and COX regression analysis.
Front. Med. 11:1301487.
doi: 10.3389/fmed.2024.1301487

New findings in prognostic factor assessment for adenocarcinoma of transverse colon: a comparison study between competing-risk and COX regression analysis

Hongbo Su[1†], Shuping Xie[2†], Shanshan Wang[3], Liying Huang[4], Jun Lyu[4,5*] and Yunlong Pan[1*]

[1]Department of General Surgery, The First Affiliated Hospital of Jinan University, Guangzhou, Guangdong, China, [2]Department of Health Statistics, School of Public Health, Shanxi Medical University, Taiyuan, China, [3]Section of Occupational Medicine, Department of Special Medicine, Shanxi Medical University, Taiyuan, Shanxi, China, [4]Department of Clinical Research, The First Affiliated Hospital of Jinan University, Guangzhou, Guangdong, China, [5]Guangdong Provincial Key Laboratory of Traditional Chinese Medicine Informatization, Guangzhou, Guangdong, China

Purpose: Competing-risk analysis was used to accurately assess prognostic factors for cancer-specific death in patients with adenocarcinoma of transverse colon (ATC), and the results were compared with those from a conventional Cox regression analysis.

Materials and Methods: Patients diagnosed with ATC between 2000 and 2019 were selected from the Surveillance, Epidemiology, and End Results database. The crude mortality rates of patients with ATC were calculated and their differences were tested using the Gray's test, respectively. In performing multivariate analysis, the Cox regression model and the subdistribution hazard function (SD) in competing risk analysis were utilized, respectively.

Results: This study included 21,477 eligible patients. The SD model indicated that age, etc. are actual independent prognostic factors. In contrast to previous recognition, the results of the Cox regression showed false-positives for sex and Carcinoembryonic antigen, and underestimated point-estimates in the stage and American Joint Committee on Cancer stage due to competing events. A detailed comparison of treatment revealed that the larger surgical scopes were prognostic risk factors compared with the smaller scope of local tumor excision, partial colectomy, or segmental resection. Patients treated with external proton beam radiotherapy had an increased risk compared with those with no radiotherapy and internal radiotherapy.

Conclusions: After comparing the results of the two methods and mitigating the significant bias introduced by Cox regression, we found independent factors that really affect the prognosis of ATC. On the other hand, in terms of ATC, a larger surgical scope and external proton beam radiotherapy may not improve the

long-term survival of patients. Therefore, when faced with ATC patients, these differences should be noted and treated differently from common colorectal cancer patients. Thus, clinicians are able to give more targeted treatment plans and prognostic assessments.

KEYWORDS

adenocarcinoma of transverse colon, competing-risk analysis, SEER, Cox regression, subdistribution hazard function

Introduction

Cancer has become the impediment to human longevity and high quality of life. According to the latest global cancer statistics from GLOBOCAN 2020, colorectal cancer ranked third in terms of new cases, with 1.93 million accounting for 10% of all new cancers, and second in terms of deaths, with 940,000 accounting for 9.4% of all deaths due to cancer in that year (1).

Transverse colon cancer has been reported to account for about 10% of colorectal cancers (2). The transverse colon is located in a special high position, in the middle and anterior part of the entire colon, between the ascending and descending colon, excluding the hepatic and splenic flexures. It has a maximum length of about 50 cm. Since the transverse colon differs from the rest of the colon in terms of embryonic development, anatomical structure, blood supply, and pathogenetic characteristics, it is necessary to clearly delineate the different segments of the colon and to provide precise and individualized treatments according to the specific characteristics of the transverse colon, which is also in line with contemporary medical concepts. However, most studies on colorectal cancer have focused on the ascending and descending colon, which have obvious differences. The transverse colon, which is the link between the two, has received little attention in research. Adenocarcinoma arises from the glandular epithelium, ducts, or secretory epithelium, and is characterized by adenoid structure formation. It is the most common clinical type of colon cancer, accounting for 90–95% of cases, and has a better prognosis than other pathological types. Research on adenocarcinoma of transverse colon (ATC) would therefore be helpful for improving the clinical outcomes.

Kaplan-Meier (KM) analyses and Cox proportional-hazards models are the classical statistical analysis methods used in investigation of the prognostic factors for colorectal cancer. However, advances in medicine and statistical methods are increasing the demand for more-accurate results. It needs to be remembered that dying from cancer is only one of the causes of death for cancer patients, since deaths due to noncancerous diseases and accidents also account for a significant proportion of the causes of death (3). It is therefore necessary to consider cancer and non-cancer factors separately when estimating patient mortality. Non-cancer deaths are often considered competing events, and their presence makes the Cox proportional-hazards model inaccurate. Therefore, when analyzing the factors affecting the prognosis of patients with ATC, using a competing-risk analysis will reduce bias and increase the accuracy of the results, thereby more accurately reflecting the true situation.

This study extracted data from the Surveillance, Epidemiology, and End Results (SEER) database on patients diagnosed with ATC (4), performed a competing-risk analysis, and compared the results with those of a Cox regression analysis. This protocol allowed for a more-accurate determination of the factors affecting the prognosis of ATC.

Materials and methods

Data collection and patient selection

Surveillance, Epidemiology, and End Results is one of the most-authoritative large oncology registry databases (5). We used SEER*Stat software (version 8.4.0) and selected the "Incidence–SEER Research Plus Data, 17 Registries, Nov 2021 Sub (2000–2019)" database, which is derived from 17 registration stations and covers 26.5% of the entire US population. Basic and medical information on patients diagnosed with ATC was extracted, specifically demographic information such as age and race, clinical information such as type of pathology and surgical modality, and survival status. The following inclusion criteria were applied: age $\geq$ 18 years, diagnosed between 2000 and 2019, tumor located in the transverse colon (C18.4, excluding the hepatic flexure and splenic flexure), microscopy confirmation, and adenocarcinoma (including signet-ring-cell carcinoma). The exclusion criteria were no surgery, survival time 0 months or unknown, multiple primary malignant tumors, not the first tumor, not a primary malignant tumor, or too many incomplete variables (**Figure 1**). Since the causes of death and survival status of patients are documented in detail in the SEER database, we classify all patients into colon cancer-specific deaths, competing events (other causes of death), and survival (6). Applying the inclusion and exclusion criteria resulted in 21,477 patients being included in this study.

Statistical analyses

The variables in the baseline data were described using number (N) and percentage values. In the competing-risk analysis, death from ATC and death from other causes was regarded as a competitive relationship. The cumulative-risk rate was estimated in the single-factor analysis using the cumulative incidence function (CIF) described by $\mathrm{CIF}k(t) = \Pr(T \leq t, D = k)$, where function $\mathrm{CIF}k(t)$ represents the probability of the k-th event occurring before

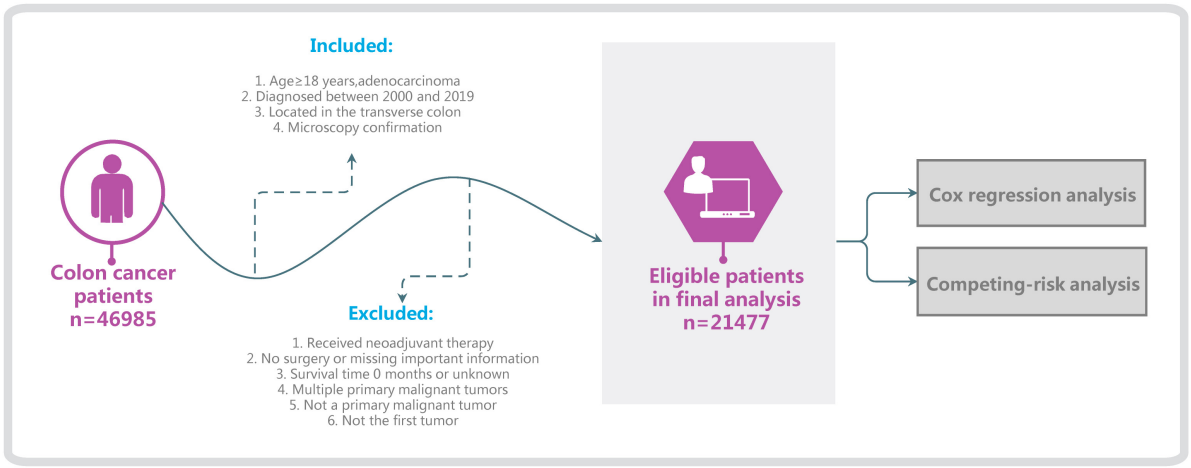

FIGURE 1
Flow chart of patient selection and study development.

time t and other class events, and D represents the type of events that occur (7). Gray's test was used to perform between-group comparisons (8). When no competing events exist, we used Cox regression for the multivariate analyses with the formula $\log[\lambda(t)] = \log[\lambda 0(t)] + \chi\beta^2$, where $\lambda 0(t)$ is the net risk and $\lambda(t)$ is the baseline risk function; that is, the risk function when the covariate vector is 0, which can be written as $\lambda(t) = \lambda 0(t)\exp(\chi\beta)$ (7).

When competing events are present and the deletion-independence condition is not satisfied (9), we provide the results of both the subdistribution hazard function (SD) and cause-specific (CS) hazard function belonging to competing-risk models (10). The formula used for the SD model was $\lambda_K^{SD}(t) = \lim_{\Delta t\to 0}\frac{P[t \le T < t+\Delta t, D=k|T>t \cup (T<t \cap K \ne k)]}{\Delta t}$, where SD represents the instantaneous probability of the occurrence of the k-th event being observed in the individual at time t (11). The formula used for the CS model was $\lambda_K^{CS}(t) = \lim_{\Delta t\to 0}\frac{P(t \le T < t+\Delta t, D=k|T \ge t)}{\Delta t}$, where CS represents the instantaneous probability of a class-k event being observed in the individual who did not experience any event at time t (12). The interpretation and usage differ between the above two models, and so the results of both models need to be provided at the same time (13). Lau et al. and Koller et al. proposed that the SD model only focus on the absolute incidence of events of interest (14, 15), and tends to be used in individual risk-prediction studies to estimate the risk and prognosis of a disease, and is suitable for establishing clinical prediction models and risk scores (4); The CS model favors etiological studies, with regression coefficients reflecting the relative effects of covariates on the increased incidence of events of interest in subjects in the event-free risk set (16). Therefore, the present study mainly adopted the conclusions from the SD model.$\lambda_k(t)$ in the formulas for the SD and CS models is the crude risk rate, which is not equal to the net risk rate when competing events are present, and so the hazards ratio (HR) value and 95% confidence interval (CI) obtained using traditional Cox analysis are biased (17). In view of this, we also compared the results of the competing-risk analysis with those of classical Cox analysis (18).

R Studio software (version 2022.02.3) was used for all statistical analyses. All statistical tests were two-sided, with a probability value of $P < 0.05$ considered to indicate statistical significance (19). The SEER database can be accessed free of charge, and this study was exempted from the need to obtain informed consent from the included patients by the institutional research committee of the First Affiliated Hospital of Jinan University.

Results

Clinical characteristics of patients and survival outcomes

Among the 21,477 patients with ATC who were screened, 10,867 (50.6%) died: (5,923 from ATC and 4,944 from other causes). The survival time was 64.67 ± 58.68 months.

For continuous variables, the average age of the sample was 68.08 ± 13.93 years, number of lymph nodes examined 17.78 ± 11.44, number of positive lymph nodes 1.63 ± 3.44. Table 1 lists the classification variables.

Univariate analyses

In the presence of competing-risk, we performed univariate analyses using the CIF and Gray's test, with the results showing that race, marital status, grade of differentiation, summary stage, AJCC stage, surgery of primary site and other site, radiotherapy and chemotherapy status, tumor size, CEA, status of bone metastasis, brain metastasis, liver metastasis, lung metastasis, distant lymph node metastasis, other site metastasis, and neuro invasion exerted significant effects on the prognosis of ATC ($P < 0.05$). Analyzing the CIF of each variab le at 1 year, 3 years, and 5 years revealed that the CIF of almost all variables increased over time. Among the ordinal classification variables such as grade, the CIF also increased gradually with increasing degree. Detailed data are provided in Table 2. Because age at diagnosis, the number of lymph nodes examined or positive are continuous variables, they were directly

TABLE 1 Basic characteristics of patients in this study.

Variable	All patients (%)	Censored (%)	Concerned (%)	Competition (%)
Total number	21,477	10,610	5,923	4,944
Race				
White people	16,934 (78.85)	8,160 (76.91)	4,630 (78.17)	4,144 (83.82)
Black people	2,613 (12.17)	1,274 (12.01)	840 (14.18)	499 (10.09)
Other	1,930 (8.99)	1,176 (11.08)	301 (5.08)	453 (9.16)
Sex				
Male	10,105 (47.05)	5,126 (48.31)	2,771 (46.78)	2,208 (44.66)
Female	11,372 (52.95)	5,484 (51.69)	3,152 (53.22)	2,736 (55.34)
Marital status				
Married	11,316 (52.69)	6,177 (58.22)	2,945 (49.72)	2,194 (44.38)
Unmarried	10,161 (47.31)	4,433 (41.78)	2,978 (50.28)	2,750 (55.62)
Grade				
I	1,774 (8.26)	1,045 (9.85)	283 (4.78)	446 (9.02)
II	14,460 (67.33)	7,528 (70.95)	3,521 (59.45)	3,411 (68.99)
III	4,243 (19.76)	1,611 (15.18)	1,761 (29.73)	871 (17.62)
IV	496 (2.31)	191 (1.8)	213 (3.6)	92 (1.86)
Unknown	504 (2.35)	235 (2.21)	145 (2.45)	124 (2.51)
Stage				
Localized	7,801 (36.32)	4,874 (45.94)	681 (11.5)	2,246 (45.43)
Regional	10,624 (49.47)	5,253 (49.51)	2,871 (48.47)	2,500 (50.57)
Distant	3,048 (14.19)	483 (4.55)	2,370 (40.01)	195 (3.94)
Unknown	4 (0.02)	0 (0)	1 (0.02)	3 (0.06)
AJCC				
0	186 (0.87)	127 (1.2)	11 (0.19)	48 (0.97)
I	3,787 (17.63)	2,489 (23.46)	208 (3.51)	1,090 (22.05)
II	8,068 (37.57)	4,515 (42.55)	1,220 (20.6)	2,333 (47.19)
III	6,433 (29.95)	3,010 (28.37)	2,140 (36.13)	1,283 (25.95)
IV	2,995 (13.95)	468 (4.41)	2,343 (39.56)	184 (3.72)
Unknown	8 (0.04)	1 (0.01)	1 (0.02)	6 (0.12)
LymphExcision				
Yes	21,149 (98.47)	10,456 (98.55)	5,826 (98.36)	4,867 (98.44)
No	313 (1.46)	151 (1.42)	89 (1.5)	73 (1.48)
Unknown	15 (0.07)	3 (0.03)	8 (0.14)	4 (0.08)
OthersiteSurgery				
No	19,932 (92.81)	10,062 (94.84)	5,141 (86.8)	4,729 (95.65)
Single resection	1,151 (5.36)	400 (3.77)	612 (10.33)	139 (2.81)
Combination	81 (0.38)	27 (0.25)	43 (0.73)	11 (0.22)
Surgery, NOS	231 (1.08)	106 (1.0)	82 (1.38)	43 (0.87)
Unknown	82 (0.38)	15 (0.14)	45 (0.76)	22 (0.44)
PrimSiteSurg				
LPS	8,617 (40.12)	4,111 (38.75)	2,310 (39)	2,196 (44.42)
SCH	11,977 (55.77)	6,074 (57.25)	3,313 (55.93)	2,590 (52.39)
TP	504 (2.35)	287 (2.7)	142 (2.4)	75 (1.52)
Surgery, NOS	379 (1.76)	138 (1.3)	158 (2.67)	83 (1.68)

(Continued)

TABLE 1 (Continued)

Variable	All patients (%)	Censored (%)	Concerned (%)	Competition (%)
Radiotherapy				
No	21,300 (99.18)	10,560 (99.53)	5,814 (98.16)	4,926 (99.64)
Beam radiation	144 (0.67)	37 (0.35)	94 (1.59)	13 (0.26)
Internal radiotherapy	9 (0.04)	4 (0.04)	4 (0.07)	1 (0.02)
Radiotherapy, NOS	7 (0.03)	2 (0.02)	3 (0.05)	2 (0.04)
Unknown	17 (0.08)	7 (0.07)	8 (0.14)	2 (0.04)
Chemotherapy				
Yes	7,212 (33.58)	3,645 (34.35)	2,773 (46.82)	794 (16.06)
No/unknown	14,265 (66.42)	6,965 (65.65)	3,150 (53.18)	4,150 (83.94)
MetsBone				
Yes	35 (0.16)	3 (0.03)	31 (0.52)	1 (0.02)
No	10,992 (51.18)	7,395 (69.7)	2,217 (37.43)	1,380 (27.91)
Unknown	10,450 (48.66)	3,212 (30.27)	3,675 (62.05)	3,563 (72.07)
MetsBrain				
Yes	7 (0.03)	1 (0.01)	5 (0.08)	1 (0.02)
No	11,018 (51.30)	7,397 (69.72)	2,242 (37.85)	1,379 (27.89)
Unknown	10,452 (48.67)	3,212 (30.27)	3,676 (62.06)	3,564 (72.09)
MetsLiver				
Yes	938 (4.37)	229 (2.16)	662 (11.18)	47 (0.95)
No	10,102 (47.04)	7,168 (67.56)	1,599 (27.0)	1,335 (27.0)
Unknown	10,437 (48.60)	3,213 (30.28)	3,662 (61.83)	3,562 (72.05)
MetsLung				
Yes	179 (0.83)	28 (0.26)	144 (2.43)	7 (0.14)
No	10,849 (50.51)	7,370 (69.46)	2,107 (35.57)	1,372 (27.75)
Unknown	10,449 (48.65)	3,212 (30.27)	3,672 (62.0)	3,565 (72.11)
MetsDistLN				
Yes	55 (0.26)	25 (0.24)	29 (0.49)	1 (0.02)
No	4,421 (20.58)	3,738 (35.23)	476 (8.04)	207 (4.19)
Unknown	17,001 (79.16)	6,847 (64.53)	5,418 (91.47)	4,736 (95.79)
MetsOther				
Yes	4,313 (20.08)	3,680 (34.68)	429 (7.24)	204 (4.13)
No	161 (0.75)	82 (0.77)	75 (1.27)	4 (0.08)
Unknown	17,003 (79.17)	6,848 (64.54)	5,419 (91.49)	4,736 (95.79)
TumorSize				
≤4 cm	10,378 (48.32)	5,511 (51.94)	2,255 (38.07)	2,612 (52.83)
>4 cm	11,099 (51.68)	5,099 (48.06)	3,668 (61.93)	2,332 (47.17)
CEA				
Negative	7,092 (33.02)	4,130 (38.93)	1,612 (27.22)	1,350 (27.31)
Border	60 (0.28)	31 (0.29)	16 (0.27)	13 (0.26)
Positive	5,701 (26.54)	2,945 (27.76)	1,648 (27.82)	1,108 (22.41)
Unknown	8,624 (40.15)	3,504 (33.03)	2,647 (44.69)	2,473 (50.02)

(Continued)

TABLE 1 (Continued)

Variable	All patients (%)	Censored (%)	Concerned (%)	Competition (%)
NeuroInvasion				
Yes	1,539 (7.17)	729 (6.87)	583 (9.84)	227 (4.59)
No	12,347 (57.49)	7,411 (69.85)	2,711 (45.77)	2,225 (45.0)
Unknown	7,591 (35.34)	2,470 (23.28)	2,629 (44.39)	2,492 (50.4)

Censored: Patients who are alive; Concerned: Patients who died of ATC; Competition: Patients who died of competing events; Unmarried, including single, widowed, divorced and separated. Stage: the most basic way of categorizing how far a cancer has spread from its point of origin. AJCC: American Joint Committee on Cancer; LymphExcision: if regional lymph nodes was removed; Single resection: removal of only regional metastases, or distant lymph nodes, or distant metastases; combination: Any combination of Single resection; Surgery, NOS: Surgery was performed but method is unknown; PrimSiteSurg: Surgery of Primary Site. LPS: Local tumor excision or Partial colectomy or Segmental resection; SCH: Subtotal colectomy or hemicolectomy; TP: Total colectomy or proctocolectomy; Internal radiotherapy: Radioactive implants or Radioisotopes; Radiotherapy, NOS: Radiotherapy was performed but method is unknown; Mets: metastases; MetsBone: bone metastases; CEA: carcinoembryonic antigen.

included in the multivariate analyses rather than in univariate analyses.

Multivariate analyses

All variables that were statistically significant in the univariate analyses ($P < 0.05$) were entered into a Cox regression analysis and a competing-risk analysis for the multivariate analyses (20). Since sex and regional lymphadenectomy were important demographic and surgical information, respectively, they also needed to be added to the multivariate analyses even though they were not statistically significant in univariate analyses (21).

Both the Cox regression analysis and the SD model indicated that age, race, grade, stage, AJCC, lymph node excision status, surgery of primary site, radiotherapy and chemotherapy status, marital status, tumor size, the number of lymph nodes examined or positive, status of bone metastasis, lung metastasis, liver metastasis, and neuro invasion were independent factors affecting the prognosis of ATC, and the results for each subgroup were basically consistent in different models. When analyzing the surgery of primary site, the HR values of subtotal colectomy or hemicolectomy, and total colectomy or proctocolectomy gradually increased with the expansion of surgical scope. The same phenomenon was observed in patients who received external proton-beam radiation. Beam radiation became a risk factor, but there was no statistically significant difference between those who did and did not receive internal radiotherapy (22). It was particularly interesting that being female and CEA-positive were risk factors in the Cox regression analysis. But in the SD model, there was no statistical difference between male and female and CEA-positive was also not a risk factor. There was no significant difference between patients with CEA-borderline and those who were CEA-negative. Most of the results from the CS model were consistent with those from the SD model. Since the CS model is often used to explore etiological issues, it only played an auxiliary role in the competing-risk analysis of this study, and so is not considered in detail (see **Table 3** for more details).

Discussion

Colorectal cancer is becoming more and more common. In terms of anatomical sites, there have been many studies about the ascending colon, descending colon, and sigmoid colon, while research into the transverse colon is rare, and so many aspects of this part are still uncertain. Adenocarcinoma is one of the most common types. Therefore, it is necessary to perform further related investigations.

The findings of the present study were consistent with previous studies finding that age, etc., are independent factors influencing the prognosis (23). The HR values and *p*-values for tumor size were consistent in the three models, which also confirms the results of previous studies, indicating that patients with tumors larger than 4 cm have a relatively poorer prognosis (24). There is general agreement that racial disparities in health insurance and medical care result in black people having a higher risk. The conclusion that other races have a better prognosis than white people in this study may differ from the results of some other studies, which may be caused by genetic differences under similar medical conditions. The grade of differentiation also significantly affected the prognosis. In addition to moderate differentiation (grade II), grades III and IV had significant effects on the survival rate compared with well differentiation (grade I). Some previous studies on a similar topic have applied competing-risk analyses, and found a significant difference between grades I and II in SD and CS models, but not in the Cox model, which can be interpreted as a false-negative result (7). Whereas, the results obtained in the present study for the three models indicated no significant difference between grades II and I. We believe that this discrepancy is attributable to differences in the characteristics or sizes of the selected samples, and it could also be due to inherent characteristics of ATC itself.

The statistical results of above variables are consistent in the range of *P*-values in the three models of this study. The correlation direction of risk factors and results was consistent. HR and 95% CI in Cox regression were slightly lower but still basically similar. It is worth noting that the point estimation and interval estimation of some factors differed markedly among the three models. For example, Cox regression analysis underestimated the risk of each level of AJCC by almost half, compared with the HR values for the SD and CS models, and the 95% CI were also correspondingly lower. This echoes what other researchers have found (25). Compared with the results of Cox regression and competing-risk analysis in the "stage-distant" group, the degree of risk underestimation was surprisingly similar. Obviously, due to the existence of competing events (26), Cox regression deviates markedly in both point estimation and interval estimation, whereas the results of the competing-risk analysis are more accurate (27).

TABLE 2 Univariate analysis of prognostic factors in patients with ATC.

Variable	Gray's test	*p*-value	CIF		
			1 year	3 years	5 years
Race	**37.77**	**<0.0001**			
White people			0.107	0.218	0.267
Black people			0.102	0.249	0.321
Other			0.078	0.182	0.233
Sex	**0.02**	**0.8825**			
Male			0.098	0.212	0.273
Female			0.109	0.224	0.269
Marital status	**41.62**	**<0.0001**			
Married			0.093	0.201	0.253
Unmarried			0.117	0.238	0.290
Grade	**743.54**	**<0.0001**			
I			0.045	0.107	0.152
II			0.077	0.181	0.235
III			0.207	0.369	0.417
IV			0.231	0.373	0.4
Unknown			0.102	0.235	0.283
Stage	**7027.36**	**<0.0001**			
Localized			0.022	0.048	0.071
Regional			0.084	0.200	0.261
Distant			0.383	0.713	0.805
Unknown			0.197	0.25	0.311
AJCC	**7418.21**	**<0.0001**			
0			0.016	0.036	0.044
I			0.013	0.027	0.042
II			0.043	0.097	0.133
III			0.105	0.253	0.329
IV			0.385	0.718	0.811
Unknown			0.113	0.146	0.213
LymphExcision	**4.05**	**0.132**			
Yes			0.104	0.218	0.271
No			0.105	0.209	0.262
Unknown			0.267	0.4	0.478
OthersiteSurgery	**517.84**	**<0.0001**			
No			0.097	0.202	0.252
Single resection			0.197	0.454	0.537
Combination			0.198	0.451	0.534
Surgery, NOS			0.120	0.288	0.329
Unknown			0.298	0.486	0.499
PrimSiteSurg	**42.48**	**<0.0001**			
LPS			0.101	0.209	0.258
SCH			0.104	0.221	0.274
TP			0.107	0.235	0.302
Surgery, NOS			0.173	0.329	0.401
Radiotherapy	**128.16**	**<0.0001**			
No			0.103	0.216	0.268
Beam radiation			0.324	0.569	0.636
Internal radiotherapy			0.467	0.802	0.893
Radiotherapy, NOS			0.143	0.356	0.429
Unknown			0.118	0.397	0.548
Chemotherapy	**619.72**	**<0.0001**			
Yes			0.104	0.301	0.386
No/unknown			0.104	0.177	0.213
MetsBone	**290.15**	**<0.0001**			
Yes			0.771	0.9	0.95
No			0.082	0.185	0.237
Unknown			0.124	0.246	0.298
MetsBrain	**133.84**	**<0.0001**			
Yes			0.857	0.862	0.875
No			0.084	0.187	0.23866
Unknown			0.124	0.247	0.29829
MetsLiver	**1,829**	**<0.0001**			
Yes			0.343	0.707	0.8069
No			0.060	0.139	0.18581
Unknown			0.123	0.246	0.29749
MetsLung	**654.06**	**<0.0001**			
Yes			0.473	0.830	0.90761
No			0.078	0.177	0.22818
Unknown			0.124	0.246	0.29798
MetsDistLN	**142.06**	**<0.0001**			
Yes			0.296	0.818	0.874
No			0.069	0.158	0.235
Unknown			0.112	0.228	0.279
MetsOther	**245.65**	**<0.0001**			
Yes			0.283	0.734	0.875
No			0.064	0.145	0.237
Unknown			0.112	0.228	0.279
TumorSize	**402.69**	**<0.0001**			
≤4 cm			0.067	0.158	0.209
>4 cm			0.139	0.275	0.329
CEA	**71.57**	**<0.0001**			

(Continued)

TABLE 2 (Continued)

Variable	Gray's test	*p*-value	CIF		
			1 year	3 years	5 years
Negative			0.085	0.184	0.235
Border			0.124	0.230	0.276
Positive			0.114	0.246	0.301
Unknown			0.113	0.228	0.279
NeuroInvasion	252.55	<0.0001			
Yes			0.149	0.342	0.425
No			0.085	0.186	0.234
Unknown			0.126	0.245	0.296

CIF, cumulative incidence function.

All of the independent related factors mentioned above have been widely recognized in previous studies. Our study not only further supports these conclusions, but also has produced some new findings by using competing-risk analysis. Many previous studies of colorectal cancer considered being female as a protective factor, and the present Cox regression analysis produced the same result. Based on the large population, this was not the case for the SD model, which indicated no difference in prognosis between males and females with ATC. Our analysis suggests that the incidence is slightly lower in females than males, but no difference was found in prognosis. This is consistent with the findings of Cheung et al. (28). We therefore consider this to be a false-positive result caused by competing events.

In terms of treatment, surgery has previously been considered a protective factor, but differences among specific surgical methods have not been discussed. Based on the records in the SEER database, we divided the surgical procedures into three categories. For all three models, SCH and TP with a larger surgical scope did not appear to benefit patients with ATC, but the risk increased as the surgical scope expanded relative to LPS covering a smaller scope. A larger surgical scope may tend to be applied more when the disease advanced, and is also associated with a greater tissue damage, resulting in a poor prognosis (29). Compared with the ascending colon and descending colon, the operation method of transverse colon is not so fixed, since a small deviation of the scope of hemicolectomy forward or backward can involve the ascending or descending colon (30). Sometimes the prognosis varies markedly depending on whether or not the middle colon artery is preserved (31). The results of the present competing-risk analysis further confirmed the results of the Cox regression analysis, hence making the results more robust and reliable.

The same was true for the variable of radiotherapy. Previous studies have only cared about whether patients received radiotherapy or not, and their conclusions are controversial. Some researchers have suggested that radiotherapy improves survival (32). However, studies that found radiotherapy to not be beneficial for long-term survival did not explore the underlying reasons. In contrast, the present study analyzed detailed information on radiotherapy, and found that the increased risk is mainly due to the use of external proton beam, which is the most common type of external radiotherapy, while internal radiotherapy such as I^{125} did not affect the prognosis. This may be due to external radiotherapy killing some tumor cells, reducing the tumor load, relieving symptoms, and improving short-term survival. However, due to the side effects of external radiotherapy, such as perforation, bleeding, and pancytopenia, and the generally late stage of patients who need radiotherapy, the long-term prognosis might not be improved (33). The present competing-risk analysis confirmed the results of the Cox regression analysis again.

Carcinoembryonic antigen is considered to be an important tumor marker for the diagnosis and monitoring of recurrence and metastasis, which has become a broad clinical consensus, but it often presents false-positive or false-negative results. Regarding the effect of CEA on prognosis, there is still a lot of controversy. The Cox regression analysis and the competing-risk analysis performed in this study produced different results. Elevated CEA was considered a risk factor for a poor prognosis in Cox regression, but no such difference was observed in the SD model. CEA assessment plays an important role in postoperative follow-up, in terms of detecting recurrence and metastasis early, thus improving the excision rate. However, this does not mean a higher or lower survival rate. It often needs to be combined with other indicators to evaluate the prognosis. Relevant studies by Ohlsson et al. (34) in Sweden and Kjeldsen et al. (35) in Denmark have confirmed this conclusion. Based on our results, particularly the findings from the SD model, it is evident that CEA cannot be used for prognostic prediction. This aligns with the prevailing views among most clinical experts and scholars. The clinical utility of CEA is therefore limited to the two points mentioned above. Our results once again validate the conclusions drawn by the majority of scholars. Relying solely on the results of Cox regression, however, can lead to significant errors. The Cox regression incorrectly estimates *P*-values due to the existence of competing events, and the results of competing-risk analysis will be more consistent with reality. It is well known that the location of colorectal cancer is closely related to the biological characteristics, genetic and epigenetic characteristics, pathological characteristics, and the prognosis of tumor cells (36). Tumors vary by site over time, and various features of tumors will also change gradually along the colon segment.

The transverse colon is quite special because it is located between the ascending colon and descending colons, traverses the upper abdomen, and entangled by the transverse mesocolon, which is an internal peritoneal organ. It abuts many important organs which differ from that of the ascending colon and descending colon. In addition, it is mainly supplied by the middle colon artery, and the type of surgical method is directly related to whether the artery is preserved or not. Regional lymph nodes are mainly distributed along the middle colonic artery (37), which makes lymph node dissection in this region a considerable surgical challenge. Therefore, the above-mentioned new findings in this study cannot only be attributed to the advantages of competing-risk analysis, but also reflect potential differences between ATC and cancers in other parts of the colon.

The classic KM and Cox methods rely on the assumption that censoring time and failure time are independent (38); that is, there is a single endpoint without competing events. However, in reality, clinical research data often contains a substantial amount of right-censored data due to loss of follow-up and other reasons, leading to multiple outcomes with competitive relationships. Using classical KM for univariate analyses without considering these biases will overestimate cumulative mortality, while using Cox regression for multivariate analyses can lead to further biases. (39). Our study

TABLE 3 Multivariate analysis of 3 models of prognostic factors in patients with ATC.

	COX model				SD model				CS model			
Prognostic factors	*p*-value	HR	95% CI		*p*-value	HR	95% CI		*p*-value	HR	95% CI	
Age	<0.0001	1.04	1.038	1.042	<0.0001	1.012	1.01	1.015	<0.0001	1.018	1.016	1.021
Sex												
Male	Reference				Reference				Reference			
Female	<0.0001	0.828	0.796	0.862	0.0897	0.954	0.903	1.007	0.0112	0.933	0.884	0.984
Race												
White people	Reference				Reference				Reference			
Black people	0.0009	1.105	1.042	1.172	0.0157	1.099	1.018	1.187	0.0108	1.103	1.023	1.19
Other	<0.0001	0.797	0.74	0.859	0.0255	0.893	0.808	0.986	0.0038	0.866	0.786	0.955
Marital status												
Married	Reference				Reference				Reference			
Unmarried	<0.0001	1.266	1.216	1.318	0.0032	1.088	1.029	1.15	<0.0001	1.143	1.083	1.207
Grade												
I	Reference				Reference				Reference			
II	0.15	1.058	0.98	1.144	0.1467	1.094	0.969	1.235	0.1698	1.089	0.964	1.231
III	<0.0001	1.29	1.185	1.404	<0.0001	1.487	1.307	1.693	<0.0001	1.508	1.326	1.714
IV	<0.0001	1.518	1.324	1.739	<0.0001	1.652	1.368	1.996	<0.0001	1.735	1.448	2.079
Unknown	0.0074	1.212	1.053	1.395	0.0002	1.483	1.203	1.828	<0.0001	1.513	1.238	1.851
Stage												
Localized	Reference				Reference				Reference			
Regional	<0.0001	1.186	1.109	1.267	<0.0001	1.489	1.326	1.672	<0.0001	1.525	1.358	1.712
Distant	<0.0001	1.848	1.377	2.481	<0.0001	3.149	2.104	4.714	<0.0001	3.25	2.279	4.634
Unknown	0.8369	0.854	0.191	3.828	<0.0001	3800.637	442.08	32674.75	0.9062	4105.527	0	5.01E+63
AJCC												
0	Reference				Reference				Reference			
I	0.1761	1.199	0.922	1.559	0.9826	1.007	0.555	1.826	0.9167	1.033	0.562	1.898
II	0.0065	1.441	1.107	1.875	0.0105	2.157	1.197	3.887	0.0077	2.263	1.241	4.129
III	<0.0001	2.054	1.568	2.691	<0.0001	4.297	2.368	7.796	<0.0001	4.77	2.598	8.756
IV	<0.0001	4.435	2.989	6.58	<0.0001	7.54	3.705	15.347	<0.0001	9.116	4.555	18.246
Unknown	0.0652	2.983	0.934	9.529	<0.0001	0.001	0	0.003	0.9199	0.001	0	9.97E+56
LymphExcision												
Yes	Reference				Reference				Reference			
No	0.0276	1.191	1.019	1.392	0.0255	1.275	1.03	1.579	0.0067	1.337	1.084	1.65
Unknown	0.0024	2.462	1.375	4.408	<0.0001	4.157	2.427	7.121	<0.0001	4.51	2.231	9.117
PrimSiteSurg												
LPS	Reference				Reference				Reference			
SCH	0.017	1.05	1.009	1.093	0.0004	1.108	1.047	1.172	<0.0001	1.126	1.065	1.189
TP	<0.0001	1.358	1.183	1.559	0.0001	1.444	1.198	1.741	<0.0001	1.496	1.26	1.776
Surgery, NOS	0.0417	1.146	1.005	1.305	0.0989	1.161	0.972	1.386	0.0129	1.229	1.045	1.447
Radiotherapy												
no	Reference				Reference				Reference			
Beam radiation	0.0019	1.367	1.122	1.667	<0.0001	1.515	1.239	1.854	0.0002	1.489	1.206	1.839
Internal radiotherapy	0.8319	1.1	0.455	2.658	0.6201	0.834	0.408	1.707	0.8044	0.883	0.329	2.369

(Continued)

TABLE 3 (Continued)

Prognostic factors	COX model			SD model			CS model		
	p-value	HR	95% CI	*p*-value	HR	95% CI	*p*-value	HR	95% CI
Radiotherapy, NOS	0.388	0.679	0.282 1.636	0.8544	0.868	0.191 3.947	0.6929	0.796	0.256 2.475
Unknown	0.9054	0.963	0.517 1.793	0.5205	1.315	0.57 3.033	0.5833	1.215	0.606 2.436
Chemotherapy									
Yes	Reference			Reference			Reference		
No/unknown	<0.0001	1.471	1.4 1.545	<0.0001	1.244	1.166 1.327	<0.0001	1.461	1.375 1.552
LymphExamed	<0.0001	0.983	0.981 0.985	<0.0001	0.983	0.98 0.986	<0.0001	0.979	0.976 0.982
LymphPositive	<0.0001	1.066	1.061 1.072	<0.0001	1.059	1.052 1.066	<0.0001	1.069	1.063 1.075
MetsBone									
Yes	Reference			Reference			Reference		
No	0.0471	0.679	0.463 0.995	0.034	0.668	0.46 0.97	0.0468	0.673	0.455 0.994
Unknown	0.1702	0.598	0.287 1.247	0.8796	0.942	0.432 2.054	0.3958	0.724	0.344 1.525
MetsLiver									
Yes	Reference			Reference			Reference		
No	<0.0001	0.793	0.72 0.873	0.0004	0.82	0.735 0.915	<0.0001	0.813	0.732 0.903
Unknown	0.4724	0.844	0.531 1.34	0.8765	0.956	0.539 1.695	0.4963	0.846	0.522 1.371
MetsLung									
Yes	Reference			Reference			Reference		
No	<0.0001	0.703	0.591 0.837	0.0091	0.751	0.606 0.931	<0.0001	0.694	0.58 0.831
Unknown	0.1152	0.666	0.402 1.104	0.0874	0.564	0.292 1.088	0.0265	0.553	0.327 0.933
TumorSize									
≤4 cm	Reference			Reference			Reference		
>4 cm	<0.0001	1.138	1.09 1.187	<0.0001	1.154	1.088 1.223	<0.0001	1.194	1.126 1.265
CEA									
Negative	Reference			Reference			Reference		
Border	0.3052	1.211	0.84 1.748	0.35	1.259	0.777 2.039	0.4315	1.219	0.744 1.999
Positive	0.0002	1.104	1.048 1.163	0.094	1.063	0.99 1.143	0.0171	1.088	1.015 1.166
Unknown	0.0024	1.08	1.028 1.134	0.3634	1.033	0.964 1.106	0.0836	1.062	0.992 1.136
NeuroInvasion									
Yes	Reference			Reference			Reference		
No	0.0002	0.863	0.799 0.931	0.0314	0.896	0.81 0.99	0.0038	0.872	0.795 0.957
Unknown	0.0006	0.863	0.794 0.939	0.1045	0.91	0.811 1.02	0.0307	0.889	0.799 0.989

HR, hazard radio; CI, confidence interval; CS, cause-specific hazard; SD, subdistribution hazard function.

has confirmed this theory. Some Cox regression results may have false-positives and biased effect estimates due to serious bias at a proportion of competing events exceeding 10%, with lower proportions also potentially resulting in false-positive or false-negative results (7). Competing-risk analysis can overcome these shortcomings by establishing the dependence between correlation degree and covariates, which can better and more accurately explain the effect of covariates and standardize the distribution function for different types of competing risk (7). It is noteworthy that the HR and 95% CI values obtained from the SD model were similar to those derived from the CS model, with consistent direction of associations and effect sizes that are basically consistent with the theory of SD ≤ CS; however, some results were inconsistent, which is also consistent with some studies. For instance, *P*-values for some factors in the SD and CS models were consistent, while others were not. This highlights the importance of obtaining results using both models in a competing-risk analysis, which helps to further differentiate the role of risk factors (39). Broadly speaking, CS addresses upstream epidemiological questions related to disease etiology, while SD focuses on downstream clinical event rates. The SD model is primarily used for prognostic analysis, risk scoring, and clinical prediction modeling. Therefore, it is crucial to use competing-risk analysis when analyzing the prognostic risk factors of patients where competing events are present (40).

As far as we know, this study is the first to report on the competing-risk analysis of prognostic factors for ATC, specifically using the largest number of samples and variables. It is based on the high-quality and large SEER database (41), allowing for the identification of accurate prognostic factors for specific diseases like ATC. Moreover, it provides valuable insights for clinicians in assessing prognosis and avoiding harmful treatment strategies. Additionally, it serves as a reminder to researchers about the significant inaccuracies associated with the use of Cox regression. The study also has some limitations. First, we only selected patients from 2000 to 2019, which may have introduced bias due to the short time span. Second, although the SEER database contains a significant amount of variable information, it does not cover all information that may affect patient survival, such as gene expression (42). Thus, further research is still needed to address these limitations.

Conclusion

Upon comparative analysis of the two methodologies, it provided conclusive evidence that age, etc. are the actual prognostic factors for ATC. However, sex and CEA do not qualify as independent prognostic factors. When analyzing prognostic factors with multiple endpoints, competing-risk analysis is more accurate and reliable than COX regression, which is prone to significant bias in the presence of competing events. Additionally, larger surgical scopes and external proton-beam radiotherapy may not improve long-term survival outcomes for patients with ATC. Therefore, clinicians should take note of these differences when treating ATC patients and may need to approach them differently from common cases of colorectal cancer. This study specifically examined ATC patients in detail, in contrast to previous crude analyses of prognostic factors for colorectal cancer. These results will contribute to a deeper understanding of ATC, as well as to diagnostic, therapeutic, and clinical decision-making processes.

Data availability statement

Publicly available datasets were analyzed in this study. This data can be found here: seer.cancer.gov/.

Ethics statement

Ethical approval was not required for the study involving humans in accordance with the local legislation and institutional requirements. Written informed consent to participate in this study was not required from the participants or the participants' legal guardians/next of kin in accordance with the national legislation and the institutional requirements.

Author contributions

HS: Data curation, Formal analysis, Software, Visualization, Writing—original draft, Writing—review and editing. SX: Software, Writing—review and editing. SW: Writing—review and editing. LH: Investigation, Visualization, Writing—review and editing. JL: Conceptualization, Writing—review and editing. YP: Conceptualization, Writing—review and editing.

Funding

The author(s) declare financial support was received for the research, authorship, and/or publication of this article. This work was supported by the Guangzhou Science and Technology Plan City-School Joint Funding Project (202201020084 and 202201020065), the Clinical Frontier Technology Program of the First Affiliated Hospital of Jinan University, China (No. JNU1AF-CFTP-2022a01223), and the Guangdong Provincial Key Laboratory of Traditional Chinese Medicine Informatization (2021B1212040007).

Acknowledgments

We thank the Surveillance, Epidemiology, and End Results (SEER) program staff for providing open access to the database.

Conflict of interest

The authors declare that the research was conducted in the absence of any commercial or financial relationships that could be construed as a potential conflict of interest.

Publisher's note

References

1. Sung, H, Ferlay J, Siegel R, Laversanne M, Soerjomataram I, Jemal A, et al. Global Cancer Statistics 2020: GLOBOCAN estimates of incidence and mortality worldwide for 36 cancers in 185 Countries. *CA*. (2021) 71: 209–49.

2. West N, Kobayashi H, Takahashi K, Perrakis A, Weber K, Hohenberger W, et al. Understanding optimal colonic cancer surgery: comparison of Japanese D3 resection and European complete mesocolic excision with central vascular ligation. *J Clin Oncol*. (2012) 30(15):1763–9.

3. Baudino T. Targeted cancer therapy: the next generation of cancer treatment. *Curr Drug Discov Technol.* (2015) 12:3–20.

4. Yang J, Pan Z, He Y, Zhao F, Feng X, Liu Q, et al. Competing-risks model for predicting the prognosis of penile cancer based on the SEER database. *Cancer Med.* (2019) 8:7881–9.

5. Lei S, Ge Y, Tian S, Cai B, Gao X, Wang N, et al. Colorectal cancer metastases to brain or bone and the relationship to primary tumor location: a population-based study. *J. Gastrointest Surg.* (2020) 24: 1833–42.

6. Wu W, Li Y, Feng A, Li L, Huang T, Xu A, et al. Data mining in clinical big data: the frequently used databases, steps, and methodological models. *Military Med Res.* (2021) 8:44.

7. Wu W, Yang J, Li D, Huang Q, Zhao F, Feng X, et al. Competitive risk analysis of prognosis in patients with cecum cancer: a population-based study. *Cancer Control.* (2021) 28:1073274821989316.

8. Haller B, Schmidt G, Ulm K. Applying competing risks regression models: an overview. *Lifetime Data Analysis.* (2013) 19:33–58.

9. Merrill R, Capocaccia R, Feuer E, Mariotto A. Cancer prevalence estimates based on tumour registry data in the Surveillance, Epidemiology, and End Results (SEER) Program. *Int J Epidemiol.* (2000) 29:197–207.

10. Goodwin J, Samet J, Hunt W. Determinants of survival in older cancer patients. *J Natl Cancer Inst.* (1996) 88:1031–8.

11. Wong C, Liew T, Hanzo L. Turbo coded burst by burst adaptive wideband modulation with blind modem mode detection. *Proceedings of the IEEE Transactions on Vehicular Technology*. Sorrento: IEEE (1999). p. 303–8.

12. Yang J, Li Y, Liu Q, Li L, Feng A, Wang T, et al. Brief introduction of medical database and data mining technology in big data era. *J Evid Based Med.* (2020) 13:57–69.

13. Esnaola N, Gebregziabher M, Finney C, Ford M. Underuse of surgical resection in black patients with nonmetastatic colorectal cancer: location, location, location. *Ann Surg.* (2009) 250:549–57.

14. Lau B, Cole S, Gange S. Competing risk regression models for epidemiologic data. *Am J Epidemiol.* (2009) 170:244–56.

15. Koller M, Raatz H, Steyerberg E, Wolbers M. Competing risks and the clinical community: irrelevance or ignorance? *Stat Med.* (2012) 31:1089–97.

16. Liang C, Heagerty PJ. A risk-based measure of time-varying prognostic discrimination for survival models. *Biometrics.* (2017) 73:725–34.

17. Islami F, Kamangar F, Boffetta P. Grand challenges in cancer epidemiology and prevention. *Front Oncol.* (2011) 1:3. doi: 10.3389/fonc.2011.00003

18. Avis P. Pressure homogenisation of mammalian cells. 2nd ed. In: Birnie G editor. *Subcellular Components*. Oxford: Butterworth-Heinemann (1972). p. 1–13.

19. Hashim D, Weiderpass E. Cancer survival and survivorship. 3rd ed. In: Boffetta P, Hainaut P editors. *Encyclopedia of Cancer*. Oxford: Academic Press (2019). p. 250–9.

20. Flick K, Sublette C, Yip-Schneider M, Maatman T, Colgate C, Soufi M, et al. Insurance type and marital status impact hospital length of stay after pancreatoduodenectomy. *J Surg Res.* (2021) 257:587–92.

21. Distaso A, Abatangelo L, Maglietta R, Creanza T, Piepoli A, Carella M, et al. Biological and functional analysis of statistically significant pathways deregulated in colon cancer by using gene expression profiles. *Int J Biol Sci.* (2008) 4: 368–78.

22. Longo C, De Robertis R, Valdo M, Montemezzi S. A case of acute bilateral iodine-induced submandibular sialadenitis: ultrasound findings. *J Clin Ultrasound.* (2022) 50:70–3.

23. Chottanapund S, Chamroonsawasdi K, Tunyasitthisundhorn P, Aekplakorn W, Silpasuwan P, Anantachoti P, et al. Modifiable factors and colon cancer risk in Thai population. *Asian Pac J Cancer Prevent.* (2021) 22: 37–43.

24. Liang, Y, Li Q, He D, Chen Y, Li J. Tumor size improves the accuracy of the prognostic prediction of T4a stage colon cancer. *Sci Rep.* (2021) 11:16264.

25. Hu C, Cao J, Zeng L, Luo Y, Fan H. Prognostic factors for squamous cervical carcinoma identified by competing-risks analysis: a study based on the SEER database. *Medicine.* (2022) 101:e30901.

26. Liang P, Chen T, Giovannucci E. Cigarette smoking and colorectal cancer incidence and mortality: systematic review and meta-analysis. *Int J Cancer.* (2009) 124:2406–15.

27. Zhao X, Kallakury B, Chahine J, Hartmann D, Zhang Y, Chen Y, et al. Surgical resection of SCLC: prognostic factors and the tumor microenvironment. *J Thoracic Oncol.* (2019) 14:914–23.

28. Cheung W, Shi Q, O'Connell M, Cassidy J, Blanke C, Kerr D, et al. The predictive and prognostic value of sex in early-stage colon cancer: a pooled analysis of 33,345 patients from the ACCENT database. *Clin Colorectal Cancer.* (2013) 12:179–87.

29. Su H, Wang S, Xie S, Huang L, Pan Y, Lyu J. Prediction of death probability in adenocarcinoma of the transverse colon: competing-risk nomograms based on 21,469 patients. *J Cancer Res Clin Oncol.* (2023) 149:10435–52.

30. Murphy C, Harlan L, Lund J, Lynch C, Geiger A. Patterns of colorectal cancer care in the United States: 1990-2010. *J Natl Cancer Inst.* (2015) 107:djv198.

31. Andersen B, Stimec B, Edwin B, Kazaryan A, Maziarz P, Ignjatovic D. Re-interpreting mesenteric vascular anatomy on 3D virtual and/or physical models: positioning the middle colic artery bifurcation and its relevance to surgeons operating colon cancer. *Surg Endoscopy.* (2022) 36:100–8.

32. Guan X, Jiang Z, Ma T, Liu Z, Hu H, Zhao Z, et al. Radiotherapy dose led to a substantial prolongation of survival in patients with locally advanced rectosigmoid junction cancer: a large population based study. *Oncotarget.* (2016) 7:28408–19.

33. Rijkmans E, van Triest B, Nout R, Kerkhof E, Buijsen J, Rozema T, et al. Evaluation of clinical and endoscopic toxicity after external beam radiotherapy and endorectal brachytherapy in elderly patients with rectal cancer treated in the HERBERT study. *Radiother Oncol.* (2018) 126:417–23.

34. Ohlsson B, Breland U, Ekberg H, Graffner H, Tranberg K. Follow-up after curative surgery for colorectal carcinoma. Randomized comparison with no follow-up. *Dis Colon Rectum.* (1995) 38:619–26.

35. Kjeldsen B, Kronborg O, Fenger C, Jørgensen OD. A prospective randomized study of follow-up after radical surgery for colorectal cancer. *Br J Surg.* (1997) 84:666–9.

36. Young S, Golzarian J. Primary tumor location in colorectal cancer: comparison of right- and left-sided colorectal cancer characteristics for the interventional radiologist. *Cardiovasc Intervent Radiol.* (2018) 41:1819–25.

37. Langman G, Patel A, Bowley D. Size and distribution of lymph nodes in rectal cancer resection specimens. *Dis Colon Rectum.* (2015) 58:406–14.

38. Giaccone G, Soria J-C. *Targeted Therapies in Oncology*. 2nd ed. Boca Raton, FL: CRC Press (2013).

39. Nie Z. A new perspective of clinical survival data: competitive risk model. *Chin J Epidemiol.* (2017) 38:1127–31.

40. Jung K, Won Y, Hong S, Kong H, Lee E. Prediction of cancer incidence and mortality in Korea, 2020. *Cancer Res Treat.* (2020) 52:351–8.

41. Zhang J, Yang J, Wang H, Pan Z, Yan X, Hu C, et al. Development and validation of a nomogram for osteosarcoma-specific survival: a population-based study. *Medicine.* (2019) 98:e15988.

42. Subramaniam D, Liu S, Giaccone G. Novel approaches in cancer immunotherapy. *Discov Med.* (2016) 21:267–74.

frontiers | Frontiers in Molecular Biosciences

TYPE Original Research
PUBLISHED 07 May 2024
DOI 10.3389/fmolb.2024.1351641

OPEN ACCESS

EDITED BY
Georgina Gonzalez-Avila,
National Institute of Respiratory Diseases-Mexico (INER), Mexico

REVIEWED BY
Pratibha Sharma,
University of Texas MD Anderson Cancer Center, United States
Jin Gan,
Boston Children's Hospital and Harvard Medical School, United States

*CORRESPONDENCE
Alexey Morozov,
runkel@inbox.ru

RECEIVED 06 December 2023
ACCEPTED 31 January 2024
PUBLISHED 07 May 2024

CITATION
Burov A, Grigorieva E, Lebedev T, Vedernikova V, Popenko V, Astakhova T, Leonova O, Spirin P, Prassolov V, Karpov V and Morozov A (2024), Multikinase inhibitors modulate non-constitutive proteasome expression in colorectal cancer cells. *Front. Mol. Biosci.* 11:1351641. doi: 10.3389/fmolb.2024.1351641

Multikinase inhibitors modulate non-constitutive proteasome expression in colorectal cancer cells

Alexander Burov[1], Ekaterina Grigorieva[1,2], Timofey Lebedev[3], Valeria Vedernikova[2,3], Vladimir Popenko[3], Tatiana Astakhova[4], Olga Leonova[3], Pavel Spirin[3], Vladimir Prassolov[3], Vadim Karpov[1] and Alexey Morozov[1]*

[1]Laboratory of Regulation of Intracellular Proteolysis, Engelhardt Institute of Molecular Biology, Russian Academy of Sciences, Moscow, Russia, [2]Moscow Institute of Physics and Technology, National Research University, Dolgoprudny, Russia, [3]Department of Cancer Cell Biology, Engelhardt Institute of Molecular Biology, Russian Academy of Sciences, Moscow, Russia, [4]Laboratory of Biochemistry of Ontogenesis Processes, Koltzov Institute of Developmental Biology, Russian Academy of Sciences, Moscow, Russia

Introduction: Proteasomes are multi-subunit protein complexes responsible for protein degradation in cells. Immunoproteasomes and intermediate proteasomes (together non-constitutive proteasomes) are specific forms of proteasomes frequently associated with immune response, antigen presentation, inflammation and stress. Expression of non-constitutive proteasome subunits has a prognostic value in several types of cancer. Thus, factors that modulate non-constitutive proteasome expression in tumors are of particular interest. Multikinase inhibitors (MKIs) demonstrate promising results in treatment of cancer. At the same time, their immunomodulatory properties and effects on non-constitutive proteasome expression in colorectal cancer cells are poorly investigated.

Methods: Proteasome subunit expression in colorectal cancer was evaluated by bioinformatic analysis of available datasets. Two colorectal cancer cell lines, expressing fluorescent non-constitutive proteasomes were treated with multikinase inhibitors: regorafenib and sorafenib. The proteasome subunit expression was assessed by real-time PCR, Western blotting and flow cytometry. The proteasome activity was studied using proteasome activity-based probe and fluorescent substrates. Intracellular proteasome localization was revealed by confocal microscopy. Reactive oxygen species levels following treatment were determined in cells. Combined effect of proteasome inhibition and treatment with MKIs on viability of cells was estimated.

Results: Expression of non-constitutive proteasomes is increased in BRAF-mutant colorectal tumors. Regorafenib and sorafenib stimulated the activity and synthesis of non-constitutive proteasomes in examined cell lines. MKIs induced oxidative stress and redistribution of proteasomes within cells. Sorafenib stimulated formation of cytoplasmic aggregates, containing proteolyticaly active non-constitutive proteasomes, while regorafenib had no such effect. MKIs caused no synergistic action when were combined with the proteasome inhibitor.

Discussion: Obtained results indicate that MKIs might affect the crosstalk between cancer cells and immune cells via modulation of intracellular proteasome pool. Observed phenomenon should be considered when MKI-based therapy is applied.

KEYWORDS

ubiquitin-proteasome system, non-constitutive proteasomes, multikinase inhibitors, regorafenib, sorafenib

1 Introduction

Cancer cells are highly dependent on the proper functioning of the ubiquitin-proteasome system (UPS) which supports homeostasis via degradation of most cellular proteins (Tsvetkov et al., 2018). The UPS provide a cascade of reactions leading to the post-translational modification of the substrate protein with a small protein–ubiquitin. This tag is recognized by the multisubunit protein complex, known as the 26S proteasome, where the protein degradation takes place (Ciechanover and Scwartz, 1998). The 26S proteasome consists of the 19S regulator/s which specifically recognizes the ubiquitinated substrates and the 20S proteasome that contains proteolytic centers (reviewed in (Morozov and Karpov, 2019)). With no attached 19S regulator/s the 20S proteasome is incapable to selectively degrade ubiqitinated proteins, but still can break down certain substrates including oxidized and damaged proteins (Kumar Deshmukh et al., 2019). Within the constitutive 20S proteasome, three subunits perform proteolysis and cleave peptide bonds after acidic (subunit β1), basic (subunit β2) and hydrophobic (subunit β5) amino acids. These subunits can be substituted by analogs (β1i, β2i and β5i), known as the immune subunits during the proteasome assembly, leading to the formation of the immunoproteasome or an intermediate proteasome, if not all constitutive catalytic subunits are replaced (Guillaume et al., 2010). These proteasomes, together non-constitutive proteasomes, demonstrate altered activity profile and thus, generate altered sets of peptides, which are further presented on the cell surface by the MHCI molecules (Winter et al., 2017). Consequently, along with other functions, these proteasomes facilitate antigen presentation; mice lacking immunoproteasomes display 50% different repertoire of presented peptides and altered response to viral infection (Kincaid et al., 2011). Non-constitutive proteasomes are abundant in the immune cells. In somatic cells the quantity of these proteasomes may rise drastically in conditions of stress, inflammation or following stimulation with pro-inflammatory cytokines including IFN-γ and TNF-α (Aki et al., 1994).

UPS-directed approach for cancer treatment includes mostly utilization of proteasome inhibitors or their combinations with other drugs. Indeed, bortezomib (Velcade), carfilzomib (Kyprolis) and ixazomib (Ninlaro) targeting both constitutive and non-constitutive proteasomes are effective against multiple myeloma and mantle cell lymphoma, but against solid tumors their efficacy is limited (Astakhova et al., 2018; Roeten et al., 2018). Interestingly, increased expression of immunoproteasome subunits in cancer cells has a prognostic value for several different types of solid tumors (Rouette et al., 2016; Tripathi et al., 2016; Lee et al., 2019). Though increased levels of immunoproteasome subunits in cancers could be associated with immune cells infiltration, modulation of non-constitutive proteasome subunit expression and activity in cancer cells might affect the tumor-immune system interactions and consequently the outcome of the disease. Recently, inhibitors directed specifically to immune proteasome subunits were developed and their derivatives are now being evaluated in clinical trials (Huber and Groll, 2021). Except use of pro-inflammatory cytokines with pleiotropic effects, currently, no specific drugs that facilitate immunoproteasome synthesis are known. At the same time, several reports indicate altered immunoproteasome subunit expression following treatment of cancer cells with other types of anti-cancer drugs - protein kinase inhibitors that are currently widely used in clinical practice (Burov et al., 2021; Takahashi et al., 2021).

Here, we specifically addressed the effect of two multikinase inhibitors (MKIs) on the proteasome activity, expression and intracellular localization of non-constitutive proteasomes using two genetically modified colorectal cancer cell lines, engineered to express fluorescently labeled non-constitutive proteasome subunit β5i.

2 Materials and methods

2.1 Bioinformatics analysis of publicly available datasets

The dataset E-MTAB-10089 (Rohr et al., 2021) was used to compare gene expression in normal tissue, adenoma and colorectal cancer. One-way ANOVA test was used to determine significant differences with Benjamini-Hochberg correction for multiple comparisons. The GSE39582 dataset (Marisa et al., 2013) was used for Kaplan-Meier analysis, comparison of gene expression in molecular subtypes of colon cancer and calculation of Spearman correlation between *CD274* and *PSMB1-10* genes expression. For each molecular subtype samples from GSE39582 were divided into mutant/deficient and wild type/proficient categories and compared using Mann-Whitney non-parametric test with Benjamini-Hochberg correction for comparisons of multiple genes. Proteomic dataset for HCT-116 cells treated with small molecule inhibitors (Mitchell et al., 2023) was used to identify drugs which can affect proteasome levels in colorectal cancer cells (Supplementary Table S1). All data was downloaded from R2: Genomics Analysis and Visualization Platform.[1] Kaplan-Meier analysis was performed using online tool from R2: Genomics Analysis and Visualization Platform. Correlations analyses, ANOVA tests and Benjamini-Hochberg corrections were performed using custom Python codes available in (Lebedev et al., 2022; Lebedev et al., 2022).

1 https://r2.amc.nl/

2.2 Correlation of dependency data with drug sensitivity

Average dependency scores were calculated using shRNA and CRISPR gene scores from DepMap data[2] described in (Lebedev et al., 2022). For each cell line we also calculated mean dependency score across all *PSMB1-10* genes. Drug sensitivity data was downloaded from CTRP database.[3] Briefly, for each colorectal cell line present in DepMap we calculated averaged dependency scores for each of the *PSMB1-10* genes and extracted AUC values from the dataset (Basu et al., 2013). AUC values were converted into sensitivity values as the reverse values and then we calculated Spearman correlation for each drug-gene pair with Benjamini-Hochberg correction. Drugs for the analysis were selected using the ChEMBL database[4] via searching for compounds that at least entered the phase-2 clinical trials and have indications for colorectal neoplasms. Heatmaps were constructed using ComplexHeatmap package for R (Gu et al., 2016).

2.3 Cell culture

Human colorectal adenocarcinoma cell line SW480 and embryonic kidney HEK 293T cell line were kindly provided by Dr. Vladimir Prassolov. The SW620B8-mCherry cell line was obtained previously (Burov et al., 2021). The SW480, SW480B8-mCherry and SW620B8-mCherry and HEK 293T cells were maintained in DMEM (Thermo Fisher Scientific, Paisley, Renfrewshire, Scotland, UK). Cell culture media contained 10% of fetal calf serum (FCS) (Hyclone, Logan, UT, USA), 100 U/mL of penicillin and 100 μg/mL of streptomycin. Cells were incubated at 37°C and 5% CO_2.

2.4 Cell viability assay and treatment of cells with MKIs

The SW480B8-mCherry, SW620B8-mCherry and HEK 293T cells were treated with 0.1–250 μM of regorafenib (MedChemExpress, Monmouth Junction, NJ, USA) and 0.1–500 μM of sorafenib (Sigma-Aldrich, Burlington, MA, USA). Cellular viability was assessed 72 h post-drug-treatment using trypan blue exclusion in Neubauer chamber. To evaluate the effects of MKIs, SW480B8-mCherry were incubated with 1, 5, or 10 μM of regorafenib or sorafenib, while the SW620B8-mCherry cells were treated with 0.5, 2.5, 5 μM of the drugs.

2.5 Transfection and cell sorting

The plasmid encoding Cas9D10A, GFP and gRNAs, the donor plasmid used for recombination, as well as the protocol for validation of the obtained cell line were generated previously (Burov et al., 2021). SW480 cells were co-transfected with the plasmids using Mirus TransIT-LT1 reagent (Mirus Bio LLC, Madison, WI, USA) according to manufacturer's instructions. Forty-eight hours post transfection cells were washed with PBS, detached from the plates using trypsin-EDTA solution (Pan-Eko, Moscow, Russia), centrifuged and resuspended in 1 mL of PBS. Then the FACSAria III cell sorter (BD Biosciences, Franklin Lakes, NJ, USA) was used to obtain the population of cells with considerable GFP fluorescence. After that, cells were cultured for 2 weeks and then stimulated with 1000 U/mL of recombinant human IFN-γ and 500 U/mL of recombinant human TNF-α (both from R&D systems, Minneapolis, MN, USA) for 72 h. Finally, cells with mCherry fluorescence were collected using the FACSAria III cell sorter (BD Biosciences, Franklin Lakes, NJ, USA) and propagated as described above.

2.6 Isolation of genomic DNA, total RNA; PCR and real-time PCR

Genomic DNA and total RNA were isolated using GeneJET Genomic DNA Purification Kit (Thermo Scientific, Waltham, MA, USA) and RNA Solo Kit (Evrogen, Moscow, Russia), according to the manufacturer's recommendations. The concentration and purity of nucleic acids were determined using NanoDrop spectrophotometer (Thermo Scientific, Waltham, MA, USA).

To verify the presence of specific insert in the genome of SW480B8-mCherry cells we used two sets of primers that were obtained previously (Burov et al., 2021) (Supplementary Table S2). The fragments of genomic DNA were amplified with primer pairs A-B and C-D (Burov et al., 2021) using Q5 High-Fidelity DNA polymerase (New England Biolabs, Ipswich, MA, USA). The nucleotide sequence integrity was confirmed by bi-directional sequencing.

The cDNA was obtained from two microgram of total RNA using oligo(dT)20 primer and Magnus Reverse Transcriptase (Evrogen, Moscow, Russia). To estimate chimeric gene (*PSMB8-mCherry*) expression levels we used the G-H pair of primers (Burov et al., 2021) (Supplementary Table S2). For the amplification of the wild-type *PSMB8*, *PSMB5*, *PSMB9* and *PSMB10* genes fragments, primer pairs reported in (Morozov et al., 2019) were utilized (Supplementary Table S2). qPCR reactions were performed as described in (Morozov et al., 2019). The β-Actin (*ACTB*) gene expression was used for normalization. The calculation of the relative expression levels of studied genes was performed using the ΔΔCt method.

2.7 Preparation of lysates and Western blotting

Cells were washed two times with PBS, collected and lysed for 10 min on ice in the NP-40 cell lysis buffer (50 mM Tris-Cl (pH 8.0), 150 mM NaCl, 1.0% NP-40), followed by centrifugation for 10 min at 13000×g. Cell supernatants were collected and stored at −80°C before use. Alternatively, cells were lysed directly in the SDS-PAGE Sample buffer (Invitrogen, Waltham, MA, USA). Proteins were separated in 12% Tris-glycine polyacrylamide gels and transferred

2 https://depmap.org/portal/

3 https://portals.broadinstitute.org/ctrp.v2.1/

4 https://www.ebi.ac.uk/chembl/

onto 0.45 μm nitrocellulose membranes (Bio-Rad, Hercules, CA, USA). The membranes were incubated with primary rabbit anti-β1i (Abcam, Cambridge, UK, RRID:AB_303707), or rabbit anti-β2i (Abcam, Cambridge, UK, AB_2895211) or rabbit anti-β5i (Abcam, Cambridge, UK, RRID:AB_303708), or rabbit anti-mCherry (Cell Signaling, Danvers, MA, USA, RRID:AB_2799246), or mouse anti-20S proteasome alpha1,2,3,5,6,7 (Enzo, Farmingdale, NY, USA, RRID:AB_10541045) antibodies and secondary HRP-labeled anti-rabbit or anti-mouse conjugates (Abcam, Cam-bridge, UK, RRID:AB_10679899 or Enzo, Farmingdale, NY, USA, RRID:AB_10540652, respectively). Blots were developed using SuperSignal West Femto Maximum Sensitivity Substrate (Thermo Scientific, Waltham, MA, USA). For signal normalization membranes were striped and treated with mouse anti-β-actin antibodies (Abcam, Cambridge, UK, RRID:AB_306371) and HRP-labeled anti-mouse conjugates. Blots were developed as described.

2.8 Immunoprecipitation of proteasomes

For the immunoprecipitation of proteasomes the Proteasome purification kit (Enzo, Farmingdale, NY, USA) was used according to the manufacturer's instructions. The homogenization of cells was performed in a binding buffer (25 mM HEPES, pH 7.4, 10% glycerol, 5 mM $MgCl_2$, 1 mM ATP, 1 mM DTT) via consecutive freezing/thawing. Cells were centrifuged for 30 min at 13,000×g and the supernatants were collected. Obtained samples were incubated with the proteasome purification matrix at 4°C overnight. After brief centrifugation at 5,000×g the supernatants (unbound fraction) were collected. The pellet was washed three times in binding buffer and the proteasomes were eluted using the SDS-PAGE Sample buffer (Invitrogen, Waltham, MA, USA).

2.9 Detection of catalytically active proteasome subunits

To detect catalytically active proteasome subunits we used proteasome activity probe—Me4BodipyFL-Ahx3Leu3VS (UbiQbio, Amsterdam, Netherlands) according to the protocol described in (De Jong et al., 2012). Obtained lysates (app. 20 μg of total protein) were mixed with 0.5 μL of probe and incubated for 1 h at 37°C. SDS-PAGE was performed and catalytically active proteasome subunits were revealed by using ChemiDoc XRS+ imaging system (Bio-Rad, Hercules, CA, USA) (excitation wavelength 480 nm and emission wavelength 530 nm). To ensure an equal protein load the gel was incubated with the ROTI®Blue quick protein stain (Carl Roth, Karlsruhe, Germany).

2.10 Determination of proteasome activity

Overall proteasome activity was determined using a Me4BodipyFL-Ahx3Leu3VS (UbiQbio, Amsterdam, The Netherlands) proteasome activity probe according to the published protocol (De Jong et al., 2012). Briefly, cells were cultivated in 12 well plates, treated with MKIs and following 72 h the probe was added into the culture media to achieve final concentration of 200 nM. Cells were incubated for 2 hours. After that, cells were washed with PBS and detached from the culture plate using a trypsin solution (PanEco, Moscow, Russia). Then, cells were fixed by continuous shaking in buffer containing 1% of FBS and 0.5% formaldehyde. Detection of fluorescence intensity was performed using LSRFortessa flow cytometer (BD Biosciences, Franklin Lakes, NJ, USA). For the determination of proteasome activity using fluorogenic substrates 72 h after treatment with the MKIs cells were washed with PBS, detached from the surface of the plate using the rubber scrapper, centrifuged and washed again. Cells were homogenized by consecutive freezing/thawing. Chymotrypsyn-like and β5i-specific proteasome activities were measured as described elsewhere (Vagapova et al., 2021) using Suc-LLVY-AMC (Sigma, St. Louis, MO, USA) and Ac-ANW-AMC (Boston Biochem, Cambridge, MA, USA) fluorogenic substrates, correspondingly. Control reactions with 100 nM of the proteasome inhibitor Bortezomib (Selleckchem, Houston, TX, USA) or 1 mM of another proteasome inhibitor MG132 (Santa Cruz Biotechnology Inc., Dallas, Texas, USA) were performed to test nonspecific degradation of substrates. The activities were estimated at the excitation wavelength 380 nm and emission wavelength 440 nm using VersaFluor Fluorometer (Bio-Rad, Hercules, CA, USA). Relative activity levels were obtained following subtraction of the activity levels in samples with proteasome inhibitors from the values detected in lysates.

2.11 Confocal microscopy

The SW480, SW480B8-mCherry and SW620B8-mCherry cells were grown on Clip-max culture flasks (TPP, Trasadingen, Switzerland). Twenty-four hours after seeding cells were stimulated with 1000 U/mL of recombinant human IFN-γ (R&D systems, Minneapolis, MN, USA) and 500 U/mL of recombinant human TNF-α (R&D systems, Minneapolis, MN, USA), or regorafenib (MedChemExpress, Monmouth Junction, NJ, USA), or sorafenib (Sigma-Aldrich, Burlington, MA, USA) and incubated for additional 72 h. Prior analysis, cells were incubated for 2 h with 200 nM of the probe Me4BodipyFL-Ahx3Leu3VS (UbiQbio, Amsterdam, The Netherlands). The cells were washed and fixed with 4% PFA (BosterBio, Pleasanton, CA, USA), washed again with PBS and incubated with NucBlue Fixed Cell ReadyProbe (Thermo Scientific, Waltham, MA, USA) for 15 min to stain the nuclei. After that, slides were covered with a SlowFade™ Gold Antifade Mountant (Thermo Scientific, Waltham, MA, USA) and cover slips (Thermo Scientific, Waltham, MA, USA). Samples were analyzed using Leica DMI 6000 CS microscope equipped with a Leica TCS SP5 laser scan unit (Leica, Wetzlar, Germany). All images were acquired in "sequential scan mode" to completely avoid the "bleed-through" effect. A quantitative comparison of label intensities was made by measuring the mean intensity value of pixels (0-255 for 8-bit images) within cytoplasm and nucleus regions using FIJI (ImageJ) software.[5]

5 https://imagej.nih.gov/ij/

2.12 Detection of oxidative stress

The SW480B8-mCherry and SW620B8-mCherry cells were grown on 12-well culture plates (TPP, Trasadingen, Switzerland). Twenty-four hours after seeding cells were stimulated with regorafenib (MedChemExpress, Monmouth Junction, NJ, USA) or sorafenib (Sigma-Aldrich, Burlington, MA, USA) and incubated for additional 72 h. Five micromoles of the drugs were used to stimulate SW620B8-mCherry cells and 10 μmol were used in the case of SW480B8-mCherry cell line. The oxidative stress was measured using ROS-ID Hypoxia/Oxidative stress detection kit (Enzo, Farmingdale, NY, USA) according to the manufacturer's instructions. Briefly, cells were detached from the plate, washed with PBS and incubated for 30 min at 37°C and 5% CO_2 with the Oxidative stress detection mix. After that, cells were washed with PBS and cellular fluorescence was analyzed by flow cytometry. Control reactions with no oxidative stress detection mix, or 200 μM of the ROS inducer (pyocyanin) were performed. Alternatively, following incubation with MKIs the Oxidative stress detection mix was added directly to the wells, cells were incubated for 30 min at 37°C and 5% CO_2. Then cells were washed and analyzed using Leica DMi 8 fluorescent microscope (Leica, Wetzlar, Germany).

2.13 Flow cytometry

To estimate the sensitivity of the obtained SW480B8-mCherry cell line, the cells were treated with 50, 100, 200, 500 or 1000 U/mL of IFN-γ (R&D systems, Minneapolis, MN, USA), or a combination of 500 U/mL of IFN-γ and 500 U/mL of TNF-α, or 1000 U/mL of IFN-γ and 500 U/mL of TNF-α (R&D systems, Minneapolis, MN, USA). To evaluate the effects of MKIs, SW480B8-mCherry and SW620B8-mCherry cells were treated with the above mentioned concentrations of regorafenib and sorafenib. Following 72 h of incubation, mCherry fluorescence was detected using LSRFortessa flow cytometer (BD Biosciences, Franklin Lakes, NJ, USA). Flow cytometry results were analyzed using FlowJo version 10.0.7 (FlowJo LLC, Ashland, OR, USA; RRID:SCR_008520) and GraphPad Prism version 8.4.3. (GraphPad Software, San Diego, CA, USA; RRID: SCR_002798) software.

2.14 Drug combination analysis

To determine the drug combination responses, SW480B8-mCherry and SW620B8-mCherry cells were seeded in 96-well plates in concentrations of 2500 and 5000 cells per well, respectively. After 24 h cells were treated with bortezomib in combination with sorafenib or regorafenib and incubated for additional 72 h. AbiCell Resazurin Cytotoxicity Assay Kit (Abisense, Sirius, Russia) was used for measurement of cell viability. Supernatant was removed and Resazurin in a ratio of 1: 100 in DMEM was added to cells. Resazurin assay was measured by 570 nm absorbance and 620 nm reference using Multiskan FC (Thermo Scientific, Waltham, MA, USA) after 4 h incubation at 37°C and 5% CO_2, reference signal for each well and mean signal for wells containing only growth medium and Resazurin were subtracted before normalization. ZIP synergy scores of drug combinations were calculated using SynergyFinder 3.0 software.[6]

2.15 Statistical analyses

The experiments were performed at least in triplicates. Bar carts depicts mean values ±standard deviation for experimental replicates. If other is not indicated, the unpaired two-tailed t-test was used to evaluate the statistical significance of differences between the experimental groups. For all the experiments, p values less than 0.05 were regarded as statistically significant. Asterisks indicate: $^{*}p < 0.05$; $^{**}p < 0.01$; $^{***}p < 0.001$; $^{****}p < 0.0001$.

3 Results

3.1 The expression of non-constitutive proteasomes is increased in BRAF-mutant colorectal tumors

First, we investigated colorectal carcinoma-associated patterns of expression of genes that encode 20S proteasome beta subunits (*PSMB1-10*). Using the dataset E-MTAB-10089 (Rohr et al., 2021) the expression levels of relevant genes in normal tissues (n = 231), non-malignant colon adenomas (n = 132) and colorectal cancer (n = 342) were compared. Most of the *PSMB1-10* genes were upregulated in adenomas and cancer compared to normal tissue, however only expression of the *PSMB9* (encodes immune subunit β1i) was significantly higher in colorectal cancer compared to non-malignant adenomas (Figure 1A). To further elucidate the link between *PSMB1-10* genes expression and colorectal cancer we compared gene expression in different molecular subtypes of colorectal cancer from GSE39582 dataset (Marisa et al., 2013): tumors with BRAF, KRAS, or TP53 mutations, CpG island methylator phenotype (CIMP), DNA mismatch repair deficiency (MMR), or chromosomal instability (CIN). Most of the *PSMB1-10* genes, including immune subunit genes *PSMB8* (encodes immune subunit β5i), *PSMB9*, and *PSMB10* (encodes immune subunit β2i) were upregulated in BRAF mutant, CIMP positive and MMR deficient tumors, with *PSMB6* (encodes constitutive subunit β1) and *PSMB9* having the highest difference (Figure 1B). For TP53 and KRAS mutant tumors we found no statistical difference in expression of any of the *PSMB1-10* genes. Tumors with chromosomal instability had lower expression of *PSMB5* (encodes constitutive subunit β5), *PSMB6* and *PSMB10* genes (Supplementary Figure S1). Interestingly, upregulation of *PSMB9* was associated with more favorable relapse-free survival as was revealed by Kaplan-Meier analysis (Figure 1C).

Next, we used gene fitness data from DepMap database (Tsherniak et al., 2017; McFarland et al., 2018; Behan et al., 2019) to investigate the role of proteasome genes in colorectal cancer cell survival. For each of 67 colorectal cell lines and *PSMB1-10* genes we calculated an averaged gene dependency

6 https://synergyfinder.fimm.fi

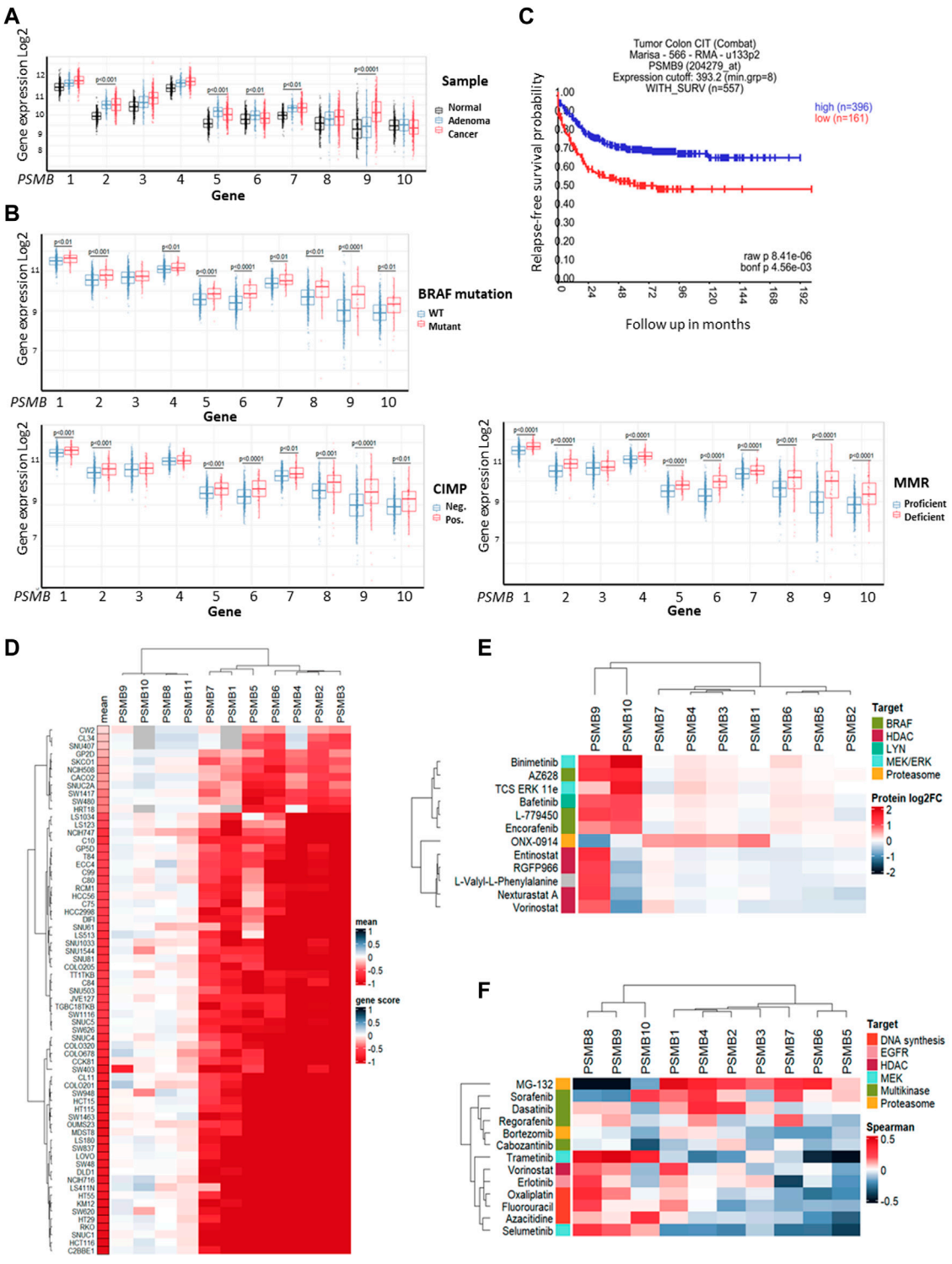

FIGURE 1
Proteasome genes expression in colorectal cancer and cell lines. **(A)** The *PSMB1-10* expression in normal colon tissue, non-malignant adenoma and colorectal carcinoma. Gene expression data was taken from E-MTAB-10089 dataset and statistical significance was determined using one-way ANOVA test with Benjamini-Hochberg correction. **(B)** Comparison of *PSMB1-10* expression in molecular subtypes of colorectal cancer from GSE39582 dataset. Statistical significance was determined using Mann-Whitney non-parametric test with Benjamini-Hochberg correction. CIMP- CpG island methylator phenotype, MMR—DNA mismatch repair. **(C)** Kaplan-Meier analysis of relapse-free survival for patients with high and low *PSMB9* expression in colorectal tumors. Survival data was taken from GSE39582 dataset and analyzed in R2: Genomics Analysis and Visualization Platform. **(D)** Heatmap of gene dependency scores for colorectal cell lines and *PSMB1-10* genes. Dependency score was calculated based on combined results from DepMap shRNA and CRISPR gene fitness screens. Negative values indicate reduced cell proliferation/survival after gene depletion. For each cell line the mean gene scores across all *PSMB1-10* genes was calculated. **(E)** Heatmap showing protein levels change in HCT-116 cells treated with selected drugs. The data was acquired from proteomic dataset (Mitchell et al., 2023). **(F)** Heatmap showing Sperman's correlation coefficients for each pair of *PSMB1-10* expression
(*Continued*)

FIGURE 1 (Continued)
and sensitivity to selected drugs. Cell lines, drugs and genes were clustered using Ward D2 method and heatmaps were generated using ComplexHeatmap package.

score (Lebedev et al., 2022) that represents how gene expression reduction by shRNA or CRISPR/Cas-9 system affected cell proliferation and survival. The *PSMB1-7* were essential for most colorectal cancer cell lines, while only few cell lines dependent on expression of immune subunits *PSMB8-10* (Figure 1D). Since non-constitutive proteasome subunits expression has the most pronounced changes in BRAF-mutant tumors, we sought to identify which drugs can affect immune proteasome subunits. We used proteome data for HCT-116 cells treated with 875 drugs (Mitchell et al., 2023) and selected drugs which changed β1i or β2i (the β5i levels were not included in the dataset) levels at least two-fold (Supplementary Table S1). Among 815 drugs we found 12 drugs which affect non-constitutive proteasome protein levels: ONX-0914, HDAC inhibitors entinostat, nexturastat-a, RGFP-996, and vorinostat, RAF inhibitors encorafenib, AZ-628, and L-779450, MEK inhibitor MEK-162, ERK1/2 inhibitor TCS-ERK-11e and LYN inhibitor bafetinib. Notably, only RAF, MEK and LYN inhibitors increased both β1i and β2i and did not affect protein levels of other subunits (Figure 1E). These findings suggest that although non-constitutive proteasomes are not essential for colorectal cell survival their protein levels change specifically in response to BRAF inhibitors, pointing on their role in drug response.

As the next step we analyzed the correlation of *PSMB1-10* gene expression in colorectal cell lines with their sensitivity to selected 11 drugs from ChEMBL database (https://www.ebi.ac.uk/chembl) that are approved for colorectal cancer treatment or undergo clinical trials from CTRP dataset (Basu et al., 2013). We also included two proteasome inhibitors MG-132 and bortezomib, and as expected, the sensitivity to proteasome inhibitor MG-132 positively correlated with expression of constitutive subunits. Multikinase inhibitors (MKIs) sorafenib, dasatinib, regorafenib and cabozantinib were clustered with proteasome inhibitors bortezomib and MG-132 (Figure 1F). Sensitivity to sorafenib, which also inhibits BRAF kinase, negatively correlated with *PSMB8* and *PSMB9* expression, suggesting that BRAF-mutant tumors with high *PSMB9* expression might be less sensitive to BRAF inhibitors and BRAF inhibitors may modulate the expression of non-constitutive proteasomes.

3.2 Generation of SW480B8-mCherry cell line

To investigate the effect of MKIs on the expression of non-constitutive proteasomes we used previously obtained cell line SW620B8-mCherry (Burov et al., 2021). The cells synthesize proteasomes containing the immune subunit β5i (a component of immunoproteasomes and most types of intermediate proteasomes (Guillaume et al., 2010)) fused with a red fluorescent protein mCherry. The unique feature of SW620 cell line is that it was derived from metastasis of patient with colorectal carcinoma and there is a cell line (SW480) that was obtained from the primary tumor of the same patient. Combination of these two cell lines allows studying late phases of colon cancer progression (Hewitt et al., 2000). Although these cell lines belong to the same patient they displayed different dependencies on proteasome expression: SW480 had one of the lowest dependencies on proteasome expression, while SW620 had one of the highest dependencies (Figure 1D). Therefore, we sought to investigate and compare the effect of MKIs on both cell lines. In this regard, we demonstrated that SW480 cells express β5i (Figure 2A) and performed the same genetic modifications with SW480 cells, as we did with SW620 cell line to label non-constitutive proteasomes (Burov et al., 2021). Using CRISPR/Cas9 system we introduced gene encoding the mCherry in the same open reading frame to the 3' end of the last exon of the *PSMB8* gene which encodes the β5i subunit. The SW480 cells were transfected with previously obtained plasmids and treated as described in (Burov et al., 2021). The presence of the insert in genomic DNA of SW480B8-mCherry cells was confirmed by PCR with two sets of primers (Figure 2B). Then, using real-time PCR it has been shown that combination of IFN-γ and TNF-α (cytokines that activate immunoproteasome subunit expression (Aki et al., 1994)) induce comparable increase in the level of *PSMB8* transcripts in wild-type SW480 cells and *PSMB8-mCherry* transcripts in SW480B8-mCherry cells, indicating conservation of endogenous regulatory mechanisms of *PSMB8* expression in modified cells (Figure 2C). The protein with molecular mass (~52 kDa) corresponding to a β5i–mCherry chimera was revealed in lysates of SW480B8-mCherry, but not control SW480 cells using antibodies to both β5i and mCherry (Figure 2D). Importantly, no free mCherry was detected in lysates of modified cells. To verify that the chimeric subunit is integrated into proteasomes we performed immunoprecipitation with antibodies to the non-catalytic proteasome subunit α4. We demonstrated presence of the chimeric protein in the precipitate obtained from IFN-γ and TNF-α-stimulated SW480B8-mCherry cells (Figure 2E). In order to verify that the chimeric subunit is catalytically active, cytokine-stimulated control and modified cells were incubated with Me4BodipyFL-Ahx3Leu3VS proteasome activity probe. The probe allows visualization of proteolytic proteasome subunits via binding to the N-terminal catalytic threonine residue (Berkers et al., 2007; De Jong et al., 2012). The interaction of the probe with the 52 kDa protein was observed in lysates of SW480B8-mCherry cells (Figure 2F). To estimate the sensitivity of the cell line to modulators that affect expression of the immune subunits, we incubated SW480 and SW480B8-mCherry cells for 72 h with different concentrations of IFN-γ and combinations of IFN-γ with TNF-α. Cell fluorescence was analyzed by flow cytometry. The significant difference ($p < 0.01$, t-test) in mCherry fluorescence between control and cytokine-stimulated SW480B8-mCherry cells was observed when 100 U/mL of IFN-γ was used. It should be mentioned that after incubation of cells with 50 U/mL the difference in

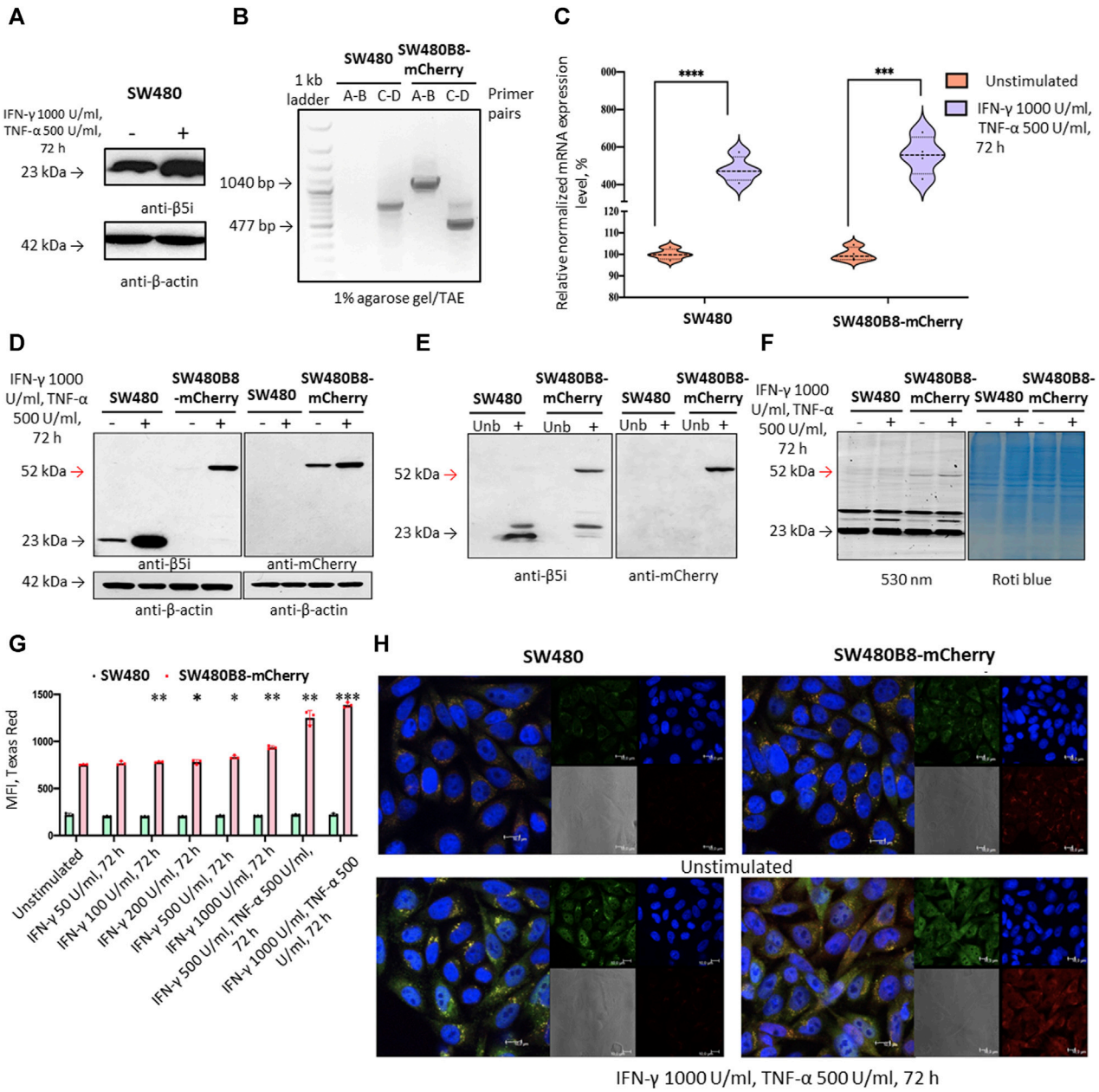

FIGURE 2
The mCherry gene is integrated into the genome and expressed in modified cells. The β5i-mCherry chimera is integrated into the proteasome and is an active proteasome subunit in SW480B8-mCherry cells. **(A)** Western blotting of lysates obtained from SW480 cells and SW480 cells treated with 1000 U/mL IFN-γ and 500 U/mL of TNF-α for 72 h. Membrane was incubated with anti- β5i, stripped and incubated with anti-β-actin antibodies. **(B)** Modification of the genomic DNA in SW480B8-mCherry cells was confirmed by PCR with two sets of primers (**(A–D)** (Supplementary Table S2) (Burov et al., 2021)). The amplicons of the anticipated size (1040 and 477 bp) were observed in samples from SW480B8-mCherry cells, but not control SW480 cells. **(C)** The relative expression levels of *PSMB8* and *PSMB8-mCherry* mRNA in unstimulated SW480 and SW480B8-mCherry cells and cells treated with IFN-γ (1000 U/mL) and TNF-α (500 U/mL) for 72 h, correspondingly. **(D)** Western blot of lysates obtained from unstimulated SW480 and SW480B8-mCherry, and cells treated with 1000 U/mL IFN-γ and 500 U/mL of TNF-α for 72 h. The membranes were incubated with either anti-β5i or anti-mCherry antibodies. **(E)** Immunoprecipitation of proteasomes from lysates of IFN-γ and TNF-α- stimulated SW480 and SW480B8-mCherry cells. Proteasomes were precipitated using agarose immobilized anti-α4 antibodies (Enzo, Farmingdale, NY, USA). Western blot of immunoprecipitated proteasomes. The membranes were incubated with either anti-β5i or anti-mCherry antibodies. **(F)** The β5i-mCherry is catalytically active subunit within the proteasomes of SW480B8-mCherry cells. Homogenates of unstimulated control and cytokine-stimulated (1000 U/mL of IFN-γ and 500 U/mL of TNF-α for 72 h) modified cells were incubated for 1 h at 37°C with the Me4BodipyFL-Ahx3Leu3VS probe. The fluorescence of proteasome subunits was analyzed in 13% Tris-Glycine polyacrylamide gel. The analysis was performed at the excitation wavelength 480 nm and emission wavelength 530 nm (left panel). The same gel stained with Roti blue quick protein stain is shown on the right panel. **(G)** The fluorescence of SW480 and SW480B8-mCherry cells treated with different concentrations of IFN-γ or combinations of IFN-γ and TNF-α for 72 h. Tests were performed in triplicates. Median fluorescence intensity (MFI) for 10000 of cells is shown. **(H)** Proteasomes with β5i-mCherry subunit were revealed in the nucleus and cytoplasm of SW480B8-mCherry cells. Confocal microscopy of unstimulated and cytokine-treated (1000 U/mL IFN-γ and 500 U/mL TNF-α) SW480 and SW480B8-mCherry cells. Proteasomes containing subunits with fused mCherry could be detected by red fluorescence. To reveal the proteasome activity within cells, cells were incubated for 2 h with Me4BodipyFL-Ahx3Leu3VS (green fluorescence). In addition fixed cell nuclei were stained with NucBlue Fixed Cell ReadyProbe (seen as the blue fluorescence). Ns- not significant; *$p < 0.05$; **$p < 0.01$; ***$p < 0.001$; t-test.

10.3389/fmolb.2024.1351641

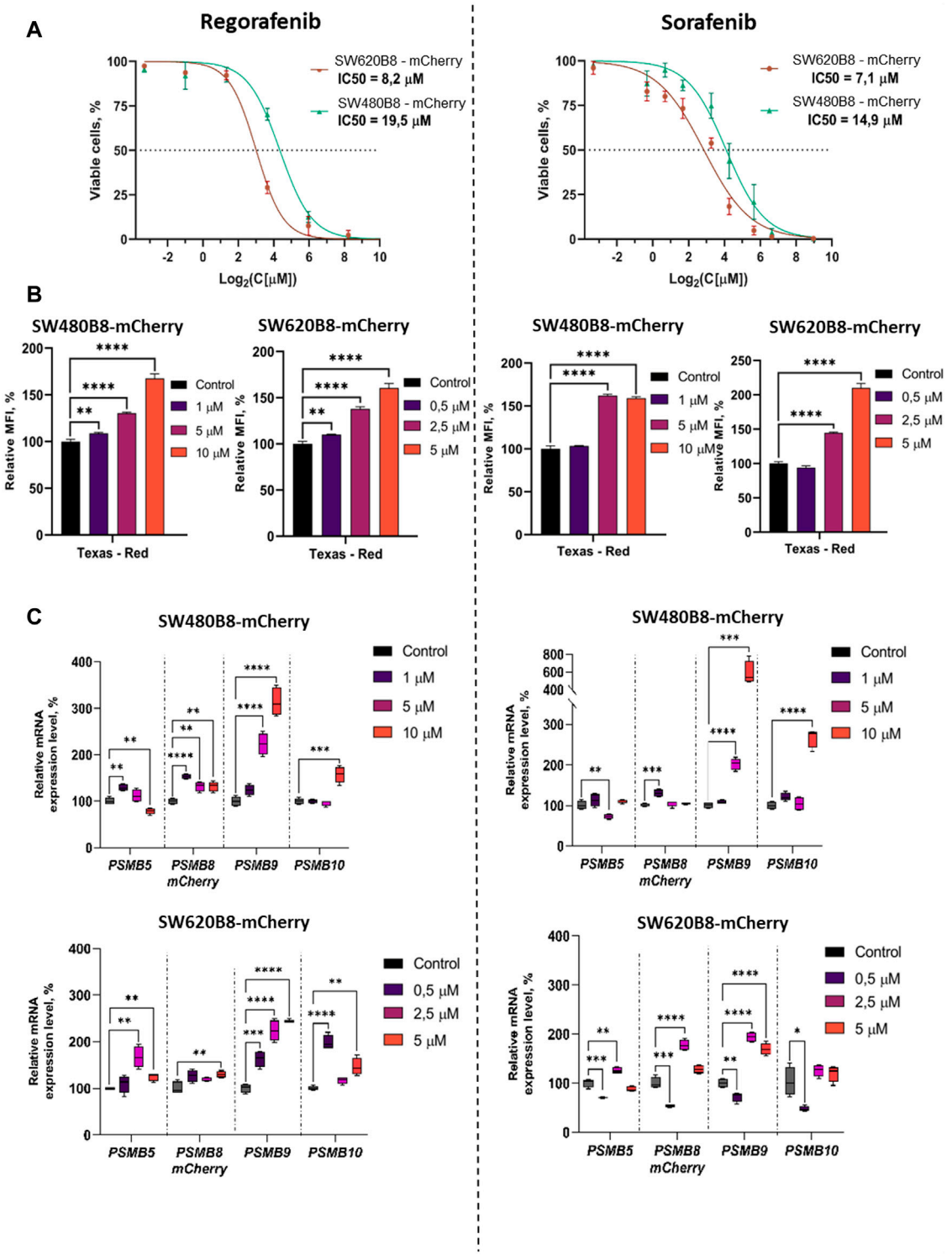

FIGURE 3
Regorafenib and sorafenib modulate expression of proteasome subunits genes in SW620B8-mCherry and SW480B8-mCherry cells. **(A)** Viability of cells treated with regorafenib or sorafenib. SW620B8-mCherry and SW480B8-mCherry cells were treated with 0.1–250 μM of regorafenib (left panel) and 0.1–500 μM of sorafenib (right panel). Cellular viability was evaluated 72 h post drug-treatment using trypan-blue exclusion. Data represents mean ± SEM of three independent experiments. **(B)** Effects of regorafenib and sorafenib on mCherry fluorescence in SW620B8-mCherry and SW480B8-mCherry cells evaluated by flow cytometry. The SW480B8-mCherry cells were treated with 1, 5 10 μM of regorafenib (left panel) or sorafenib (right panel) and SW620B8-mCherry cells were treated with 0.5, 2.5, 5 μM of regorafenib (left panel) or sorafenib (right panel) for 72 h. The mCherry fluorescence was measured using LSRFortessa flow cytometer (BD Biosciences, Franklin Lakes, NJ, United States). Yellow-green laser and Texas Red filter were used. Normalized median fluorescence intensity (MFI) of 10000 cells is shown. **(C)** Proteasome gene expression levels in cells treated with the MKIs. The relative expression levels of *PSMB5*, *PSMB8-mCherry*, *PSMB9* and *PSMB10* mRNA were determined by qPCR after 72 h-long incubation with the MKIs. *—$p < 0.05$; **—$p < 0.01$; ***—$p < 0.001$; ***—$p < 0.001$; ****—$p < 0.0001$, t-test.

fluorescence was close to significant (p = 0.067) indicating high sensitivity of the obtained cell line to modulation of the immune subunit expression (Figure 2G). No difference in fluorescence was observed when control SW480 cells were incubated with different concentrations of cytokines. The localization of non-constitutive proteasomes in SW480B8-mCherry was studied by confocal microscopy (Figure 2H). Within the unstimulated cells, proteasomes with mCherry-labelled β5i were mostly localized in the cytoplasm where they were either equally dispersed or formed small optically dense aggregates (Figure 2H). Stimulation of cells with IFN-γ and TNF-α lead to a significant increase of fluorescence and relocation of certain amount of non-constitutive proteasomes into cell nuclei. Proteasome-containing aggregates were still observed in the cytoplasm of treated cells (Figure 2H). Taken together, a new genetically-modified cell line was obtained, validated and could be used to address the effect of MKIs on non-constitutive proteasome expression and localization.

3.3 Regorafenib and sorafenib modulate non-constitutive proteasome subunit expression in colorectal cancer cells

Kinase inhibitors were used in cancer treatment since approval of imatinib in 2001 (Lee et al., 2023). Currently there are 77 FDA-approved small molecule protein kinase inhibitors (as of 19 September 2023, www.brimr.org/PKI/PKIs.htm) and new inhibitors are on the way. Based on the analysis of published datasets, BRAF and multikinase inhibitors were top candidates that could affect non-constitutive proteasome levels (Figure 1E), thus we selected multikinase inhibitors sorafenib and regorafenib which can target BRAF for further experiments.

We initially studied the viability of SW480B8-mCherry and SW620B8-mCherry cells after incubation with different concentrations of regorafenib and sorafenib. Comparing with the SW480B8-mCherry cells, SW620B8-mCherry cells were considerably more sensitive to regorafenib (IC50: 19.5 vs. 8.2 μM) (Figure 3A). When cell lines were incubated with sorafenib, SW620B8-mCherry cells were also found to be more sensitive with the IC50 of 7.1 μM (Figure 3A). The IC50 value for SW480B8-mCherry cells after sorafenib treatment was 14.9 μM (Figure 3A). Therefore, for the subsequent experiments we used 1, 5, 10 μM of drugs for SW480B8-mCherry cells and 0.5, 2.5, 5 μM of drugs–for SW620B8-mCherry cells. Importantly, used concentrations match the concentrations observed in plasma of patients under treatment with the inhibitors (Fucile et al., 2015; Kobayashi et al., 2021). We also tested the viability of non-cancerous HEK 293T cells following treatment with the inhibitors. It was demonstrated that when cells were incubated with different concentrations of sorafenib the IC50 was estimated as 32.7μM, while incubation with regorafenib yielded IC50 value of 44.6 μM (Supplementary Figure S2).

To investigate the effect of MKIs on the expression of non-constitutive proteasomes SW480B8-mCherry and SW620B8-mCherry cells treated for 72 h with selected concentrations of the drugs were firstly analyzed by flow cytometry. It was demonstrated that 1 μM and 0.5 μM of regorafenib induced increased fluorescence of mCherry in SW480B8-mCherry and SW620B8-mCherry cells, respectively (t-test, $^{**}p < 0.01$) (Figure 3B). At the same time, these concentrations of sorafenib had no statistically significant effect on the cell lines (Figure 3B). Higher concentrations of both drugs induced statistically significant increase (up to 2.1 fold) of the median fluorescence intensity (MFI) of cells (t-test, $^{****}p < 0.0001$) (Figure 3B). Obtained data indicated activated expression of the β5i subunit in studied cell lines upon treatment with MKIs.

To verify the results and to explore how the expression of other proteasome subunits is modulated, we performed qPCR to estimate the mRNA levels of *PSMB8-mCherry*, *PSMB5*, *PSMB9*, *PSMB10* genes encoding chimeric subunit (β5i-mCherry), constitutive proteasome subunit β5 and immune proteasome subunits β1i and β2i, respectively. Increased levels of immunoproteasome subunit mRNAs were revealed in cells following the 72 h incubation with both regorafenib and sorafenib. The expression of *PSMB9* was activated the most and increased up to 6 folds (t-test, $^{****}p < 0.0001$), *PSMB10* transcripts levels were increased by 2.9 folds (t-test, $^{****}p < 0.0001$) and *PSMB8-mCherry*—by 1.8 folds (t-test, $^{****}p < 0.0001$) (Figure 3C). The changes of the *PSMB5* expression were less pronounced reaching maximum 1.6 folds (t-test, $^{**}p < 0.01$) in SW620B8-mCherry cells incubated with regorafenib (Figure 3C). In SW480B8-mCherry cells a modest decrease of the *PSMB5* expression level was observed following the incubation with 10 μM of regorafenib and 5 μM of sorafenib (t-test, $^{**}p < 0.01$) (Figure 3C).

Revealed alterations of immune subunits expression were further confirmed by Western blotting of cytoplasmic lysates, as we observed drastic increase in the amount of β1i, β2i and β5i-mCherry subunits in SW620B8-mCherry, as well as the β1i and β5i-mCherry, in SW480B8-mCherry cells treated with regorafenib (Figure 4A). The proteasome subunits are synthesized as precursor molecules and undergo autocatalytic cleavage of propeptides during the late stages of proteasome assembly. Interestingly, we detected lower amounts of processed β1i and β2i subunits in unstimulated SW620B8-mCherry cells comparing to SW480B8-mCherry cells, highlighting differing proteasome pools and prevalence of intermediate proteasomes in SW620B8-mCherry cells. After treatment with regorafenib, however, the quantity of these two subunits rose significantly, favoring increase in the amount of "classical" immunoproteasomes in SW620B8-mCherry cells (Figures 4A, B). Of note, the quantity of precursor protein and processed β1i also increased considerably in SW480B8-mCherry cells indicating rearrangement of the proteasome pool in these cells as well (Figures 4A, B). The sorafenib stimulated accumulation of β1i and β5i-mCherry subunits in both cell lines and the β2i in SW480B8-mCherry cells. Importantly, we detected no differences in the amount of structural alpha proteasome subunits in cytoplasmic lysates, as well as the modest alterations (except decrease following treatment with regorafenib of SW480B8-mCherry cells) in the amount of constitutive β5 subunit indicating that overall quantity of proteasomes changes insignificantly following the exposure to MKIs and rather the rearrangement of the proteasome pool takes place (Figures 4A, B).

3.4 Regorafenib and sorafenib modulate proteasome activity and localization in colorectal cancer cells

Obtained data indicated possible modulation of proteasome activity by selected MKIs. Thus, we sought to evaluate

10.3389/fmolb.2024.1351641

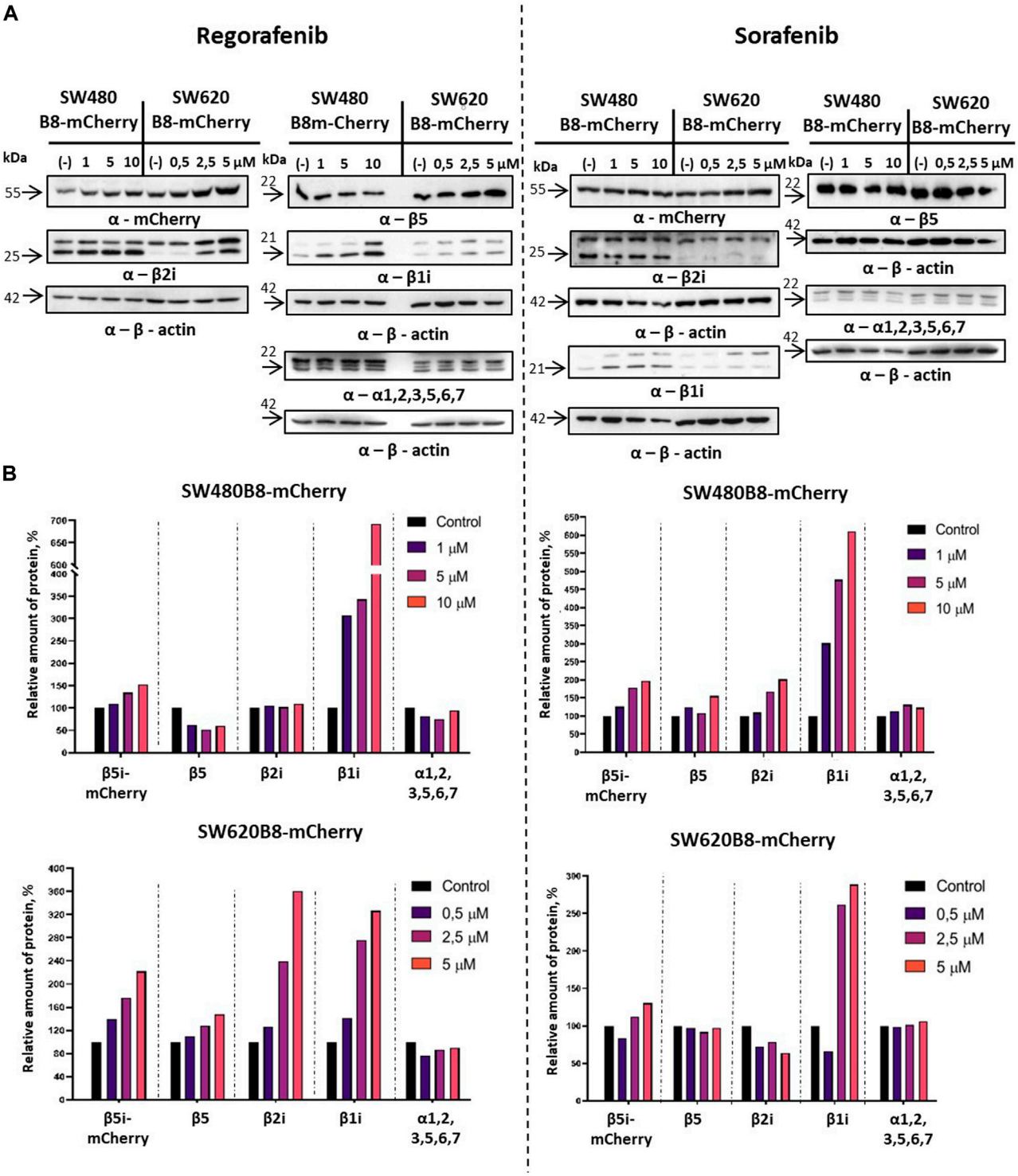

FIGURE 4
Regorafenib and sorafenib activate synthesis of non-constitutive proteasomes in SW620B8mCherry and SW480B8-mCherry cells. Western blotting of lysates obtained from SW480B8-mCherry and SW620B8-mCherry cells treated with different concentrations of regorafenib (left panel), or sorafenib (right panel) for 72 h **(A)**. Lysates were obtained using the NP-40 lysis buffer. Membranes were incubated with either anti-β1i, or anti-β2i, or anti-β5, or anti-mCherry, or anti-20S proteasome α1,2,3,5,6,7 antibodies, stripped and incubated with anti-β-actin antibodies. **(B)** Evaluation of **(A)** data using the ImageJ software.

chymotrypsin-like and β5i-specific proteasome activities in homogenates of treated cells. It was demonstrated that following treatment with regorafenib both activities were increased in SW620B8-mCherry and SW480B8-mCherry (Figure 5A). Interestingly, the β5i-specific activity in SW480B8-mCherry cells was increased by 2.8 folds (t-test, $^{***}p < 0.001$) and

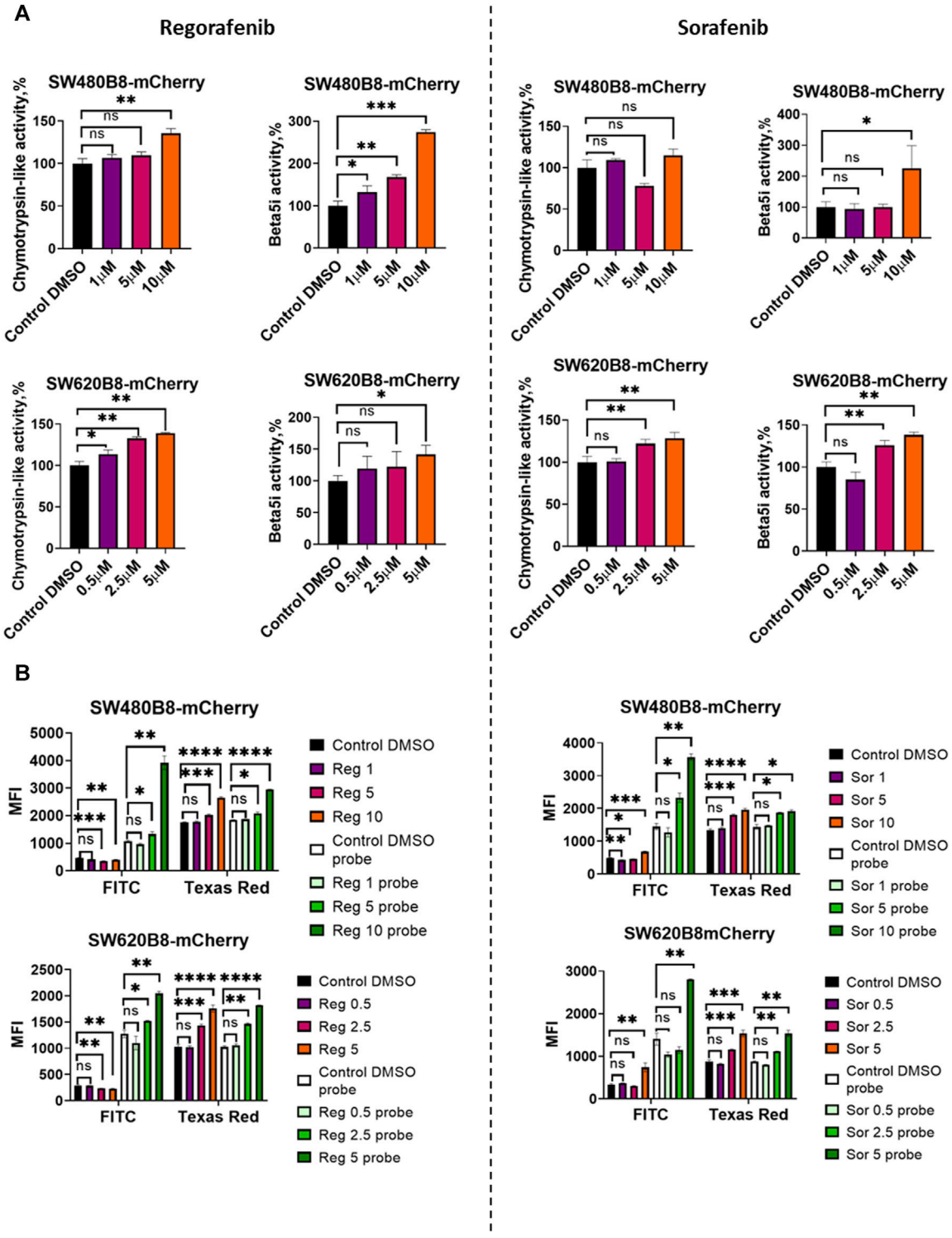

FIGURE 5
Regorafenib and sorafenib modulate activity of proteasomes in SW620B8mCherry and SW480B8-mCherry cells. **(A)** Chymotrypsin-like and β5i-specific proteasome activity in homogenates of SW480B8-mCherry and SW620B8-mCherry cells treated with different concentrations of regorafenib (left panel), or sorafenib (right panel) for 72 h. The activity was determined using Suc-LLVY-AMC and Ac-ANW-AMC fluorogenic substrates, correspondingly. **(B)** Analysis of BodipyFL and β5i-mCherry fluorescence and proteasome activity in modified cells following incubation with different concentrations of regorafenib (left) and sorafenib (right) by flow cytometry. Treated cells were incubated for 2 h with Me4BodipyFL-Ahx3Leu3VS probe before being analyzed. The BodipyFL and mCherry fluorescence was measured using LSRFortessa flow cytometer (BD Biosciences, Franklin Lakes, NJ, United States). Blue, yellow-green lasers, FITC and Texas Red filters were used, correspondingly. Tests were performed in triplicates. Ns - not significant; *—$p < 0.05$; **—$p < 0.01$; ***—$p < 0.001$; ***—$p < 0.001$; ****—$p < 0.0001$, t-test.

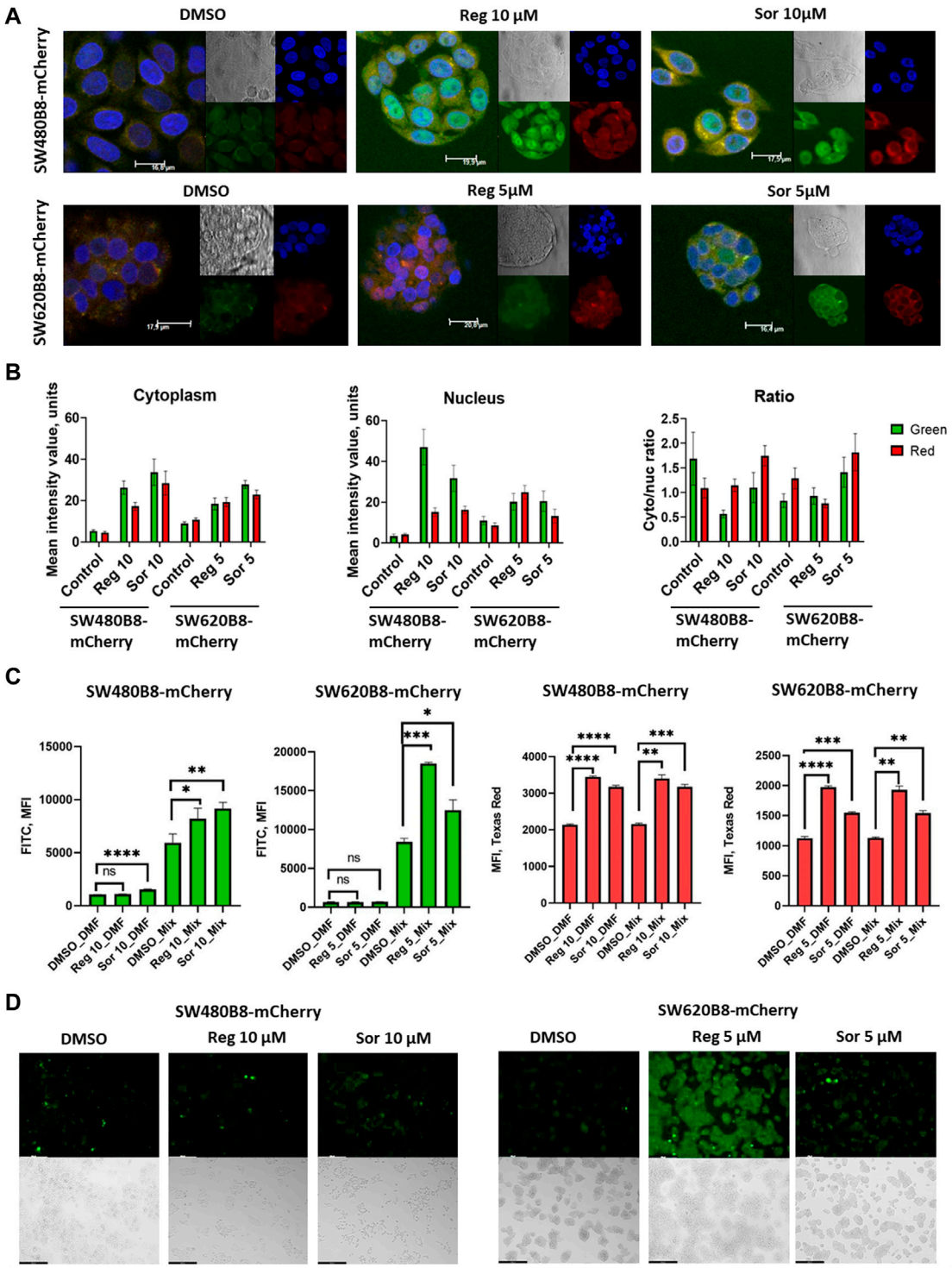

FIGURE 6
Regorafenib and sorafenib modulate localization of proteasomes and induce oxidative stress in SW620B8mCherry and SW480B8-mCherry cells. **(A)** Activity and localization of proteasomes is altered in modified cells incubated with regorafenib and sorafenib. Confocal microscopy of unstimulated or treated with 10 μM of regorafenib or sorafenib SW480B8-mCherry cells (upper panel). Confocal microscopy of unstimulated or treated with 5 μM of regorafenib or sorafenib SW620B8-mCherry cells (lower panel). Prior microscopy cells were additionally incubated for 2 h with proteasome activity probe Me4Bodipy FL-Ahx3Leu3VS (green fluorescence). The mCherry fluorescence is shown in red, while cell nuclei were visualized using NucBlue Fixed Cell ReadyProbe (blue fluorescence). **(B)** Quantification of mean fluorescence intensity of the probe Me4BodipyFL-Ahx3Leu3VS (green) and the mCherry (red) within cytoplasm and nucleus of the cells shown in **(A)**. Additionally Cytoplasm/nucleus fluorescence ratio was calculated (right panel). Calculations were performed using at least 6 representative cells using the ImageJ software. Analysis of oxidative stress in sorafenib and regorafenib treated cells **(C, D)**. Twenty-four hours after seeding the SW480B8-mCherry and SW620B8-mCherry cells were stimulated with regorafenib or sorafenib and incubated for additional 72 h. The SW480B8-mCherry were incubated with 10 μM of regorafenib or sorafenib, while the SW620B8-mCherry cells were treated with 5 μM of the drugs. Control cells were treated with DMSO. The oxidative stress was measured using ROS-ID Hypoxia/Oxidative stress detection kit (Enzo, Farmingdale, NY, USA) according to the manufacturer's
(*Continued*)

FIGURE 6 (Continued)
instructions. Cellular fluorescence was analyzed by flow cytometry **(C)** or fluorescent microscopy **(D)**. Reactive oxygen species production can be deduced from changes in green fluorescence, while β5i-mCherry expression is revealed by mCheery fluorescence. For the evaluation of cellular fluorescence by flow cytometry the LSRFortessa flow cytometer (BD Biosciences, Franklin Lakes, NJ, United States) equipped with blue, yellow-green lasers, FITC and Texas Red filters was used. Median fluorescence intensity (MFI) for 10000 of cells is shown. Tests were performed in triplicates. Ns - not significant; *—$p < 0.05$; **—$p < 0.01$; ***—$p < 0.001$; ***—$p < 0.001$; ****—$p < 0.0001$, t-test. Scale bar—250 μm.

in SW620B8-mCherry–by 1.4 folds (t-test, *$p < 0.05$) following incubation with the highest concentration of the MKI. Sorafenib treatment of SW480B8-mCherry cells resulted in increased β5i-specific activity (by 2.1 folds, t-test, *$p < 0.05$) but minimally affected chymotrypsin-like activity in cellular homogenates (Figure 5A). At the same time, both activities were increased in SW620B8-mCherry cells following the incubation with sorafenib (t-test, **$p < 0.01$) (Figure 5A). We further evaluated overall proteasome activity using the proteasome activity probe - Me4BodipyFL-Ahx3Leu3VS and flow cytometry. It was demonstrated that 5 μM of regorafenib induced significant elevation (t-test, *$p < 0.05$) of proteasome activity in SW480B8-mCherry cells, 2.5 μM of regorafenib increased the activity in SW620B8-mCherry cells (t-test, *$p < 0.05$), while maximal concentrations of regorafenib or sorafenib induced up to 3.5 folds (t-test, **$p < 0.01$) elevation of proteasome activity in both cell lines (Figure 5B). Confocal microscopy of cells treated with Me4BodipyFL-Ahx3Leu3VS and 5 and 10 μM of regorafenib or sorafenib, respectively revealed significant increase of BodipyFL and mCherry fluorescence (Figures 6A, B). Interestingly, following the treatment with regorafenib the ratio of cytoplasmic/nuclear mCherry fluorescence (comparing to control) did not change (SW480B8-mCherry cells) or was decreased (SW620B8-mCherry cells). At the same time, SW480B8-mCherry cells demonstrated decreased ratio of cytoplasmic/nuclear BodipyFL fluorescence following treatment with regorafenib. Accumulation of nuclear BodipyFL fluorescence in SW480B8-mCherry cells together with decreased amount of constitutive β5 subunit in the cytoplasmic lysates might indicate accumulation of large amount of constitutive proteasomes in the nuclei of the cells following treatment with regorafenib. In contrast to regorafenib effects, after incubation with sorafenib the cytoplasmic/nuclear mCherry fluorescence was increased in both cell lines, indicating different localization of non-constitutive proteasomes following treatment with different MKIs (Figure 6B). In SW480B8-mCherry cells, as after the treatment with regorafenib, a decreased ratio of cytoplasmic/nuclear Bodipy fluorescence was observed following incubation with sorafenib. Thus, at least in the case of sorafenib treatment of SW480B8-mCherry cells a translocation of constitutive proteasomes into the nuclei might take place, but more prominent (comparing to regorafenib) retention of non-constitutive proteasomes in the cytoplasm is observed, likely indicating separation of proteasome pool (Figures 6A, B). Interestingly, active non-constitutive proteasomes were revealed in aggregate-like structures near the nuclei and within the cytoplasm of sorafenib-treated cells (Figure 6A). Obtained results indicate putative specific role of non-constitutive proteasomes following the treatment with MKIs and especially sorafenib.

3.5 MKIs stimulate production of reactive oxygen species in colorectal cancer cells

Formation of proteasome-containing intracellular aggregates is frequently observed in stress conditions (Enenkel et al., 2022). Thus, we investigated if regorafenib and sorafenib induce the oxidative stress in SW620B8-mCherry and SW480B8-mCherry cells. Cells were treated with 5 μM, or 10 μM of the drugs, respectively for 72 h. It has been shown that both sorafenib and regorafenib stimulated production of reactive oxygen species (ROS). Depending on the cell line, the elevation of ROS concentration was from 1.4 folds (t-test, *$p < 0.05$; SW480B8-mCherry cells treated with 10 μM of regorafenib) to 2.2 folds (t-test, ***$p < 0.001$; SW620B8-mCherry cells treated with 5 μM of regorafenib) (Figures 6C, D). Thus, our results indicate that MKIs induce oxidative stress in studied cell lines.

3.6 Sorafenib or regorafenib cause no synergistic or additive action when combined with bortezomib

Rearrangements within cellular proteasome pool can potentially affect the responsiveness of cancer cells to proteasome inhibitors. Thus, we studied the viability of cells treated with bortezomib in combination with sorafenib or regorafenib. Although all the inhibitors significantly affected the survival of cells when added separately, we did not found increase or even addition of cytotoxic effects when introduced sorafenib or regorafenib in combination with bortezomib (Figures 7A–D). As an example, treatment of SW480B8-mCherry cells with sorafenib added in low toxic concentration of 6.25 μM lead to 30% decrease of cell survival. Treatment of cells with low toxic concentration of bortezomib (12.5 nM) lead to approximately 20% decrease of cell survival. When used in combination no synergistic or even statistically significant additive actions on cell viability were detected (Figure 7A). Next, we studied effects of drug combinations taken in a broad range of concentrations on the viability of both cell lines. The dose-response matrixes were obtained and analyzed using Synergy Finder 3.0 software. The ZIP scores were calculated for combination of sorafenib with bortezomib (ZIP score: −3.405) and regorafenib with

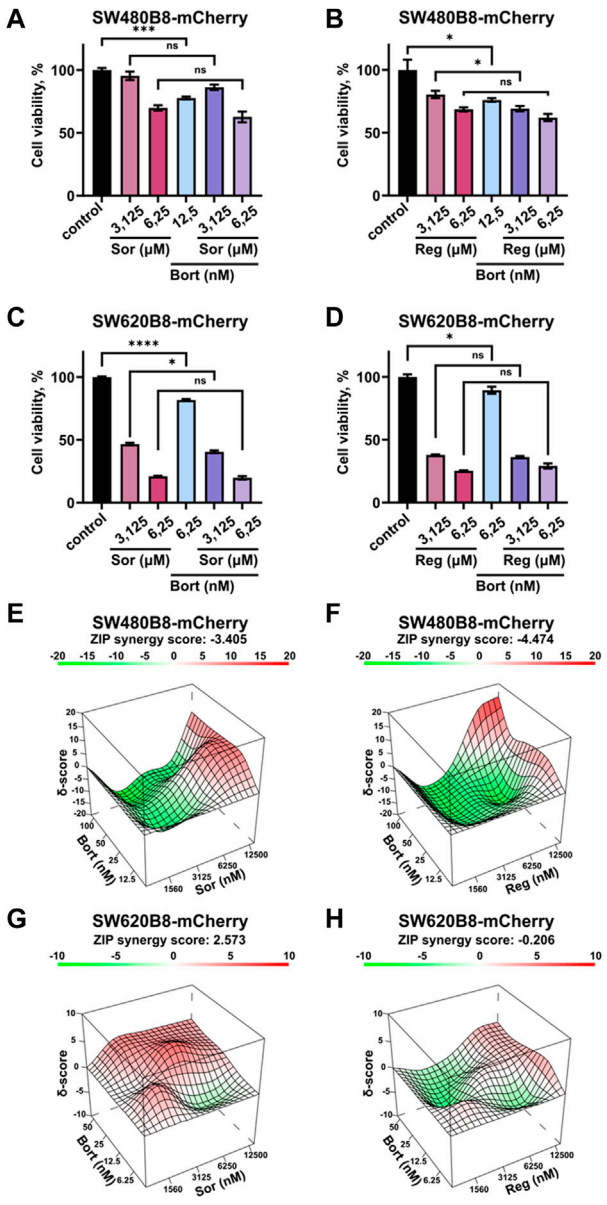

FIGURE 7
Sorafenib or regorafenib cause no synergistic or additive action when combined with bortezomib. The SW480B8-mCherry and SW620B8-mCherry cells were treated with bortezomib (Bort) in combination with sorafenib (Sor) or regorafenib (Reg). Viability was measured 72 h after treatment. **(A–D)** The bar-charts represent the viability of SW480B8-mCherry **(A, B)** and SW620B8-mCherry **(C, D)** cells treated with sorafenib/regorafenib in 2 concentrations and bortezomib alone or in combinations with the MKIs. The experiment was performed in three replicates. SEM is shown for each bar. *p*-value was determined by Unpaired t-test. Asterisks: ns -p>0.05, *- $p < 0.05$, **- $p < 0.01$, ***- $p < 0.001$, ****- $p < 0.0001$. **(E–H)** Synergy 3D plots represent the effect of drug combinations (synergism–red area; additive effect–white area; antagonism–green area) which was calculated and visualized using SynergyFinder 3.0 software.

bortezomib (ZIP score: −4.474) when added to SW480B8-mCherry cells (Figures 7E, F). When sorafenib and regorafenib were added to SW620B8-mCherry cells in combination with bortezomib the ZIP scores were 2.573 and −0.206, respectively (Figures 7G, H). When ZIP score is more than 10 it may be interpreted as synergistic action, when less 10 and more than 0 as additive action, ZIP scores less than 0 – antagonistic action. Based on the obtained scores, it may be concluded that sorafenib or regorafenib cause most likely antagonistic action when combined with bortezomib.

4 Discussion

Multikinase inhibitors (MKIs) modulate signaling pathways that control survival and proliferation of cells and, therefore, widely used in the therapy of cancer. Regorafenib and sorafenib are among the most effective MKIs, utilized to treat solid tumors. Both inhibitors target different kinases including VEGFRs, PDGFRs, BRAF, RET and c-kit (Kannaiyan and Mahadevan, 2018). Structurally regorafenib and sorafenib are almost identical with the only difference–the presence of a fluorine atom in the central phenyl ring of regorafenib, which leads to certain differences in properties between the two compounds (Wilhelm et al., 2011). The regorafenib is approved for the treatment of metastatic colorectal carcinoma (Grothey et al., 2013), while sorafenib is mostly used for the treatment of hepatocellular carcinoma, renal cell carcinoma and differentiated thyroid cancer (Lee et al., 2023), however several publications indicate its applicability for the treatment of colorectal cancer (Kacan et al., 2016; Martchenko et al., 2016; Jeong et al., 2020). Importantly, MKIs were shown to induce immunomodulatory effects. For instance, previous studies demonstrated that exposure to MKIs including sorafenib and regorafenib can stimulate MHCI synthesis and expression of other components of the antigen presentation pathway in cancer cells and, consequently, stimulate their elimination by cytotoxic lymphocytes (Kwilas et al., 2014; Tsai et al., 2017; Takahashi et al., 2021). At the same time, little is known regarding the effect of MKIs on specifically the expression of non-constitutive proteasomes in cancer in general and in colorectal cancer in particular. Since immunoproteasomes and intermediate proteasomes substantially broad the repertoire of MHCI-presented peptides including those derived from cancer antigens (Vigneron et al., 2017), their expression is an essential parameter that can affect the outcome of the disease. Here, we found strong relation between BRAF mutations in colorectal cancer and expression of non-constitutive proteasomes. We demonstrated that regorafenib and sorafenib stimulate reactive oxygen species production, increase proteasome activity, upregulate expression and modulate non-constitutive proteasome localization in two colorectal cancer cell lines.

The clinical implication of the observed MKIs effects might be dichotomous. Indeed, upregulation of constitutive and non-constitutive proteasomes, which is frequently observed in cancer, could be both beneficial and detrimental for the tumor (Rouette et al., 2016; Leister et al., 2021; Chen et al., 2023).

From one side, as indicated above the expression of non-constitutive proteasomes may facilitate presentation of certain cancer antigens and stimulate elimination of tumor cells by the immune system (Vigneron et al., 2017). Concordantly, overexpression of immune proteasome subunits is a favorable prognostic marker for breast, endometrial and urothelial cancer,

as well as non-small cell lung carcinoma (Rouette et al., 2016; Tripathi et al., 2016; Lee et al., 2019,[7],[8]). Increased levels of immunoproteasomes in tumors might be associated with activation of their expression in cancer cells, or infiltration of the immune cells, or both. Importantly, non-constitutive proteasome expression is enhanced through secretion of IFN-γ by tumor-infiltrating lymphocytes. Indeed, considerably higher expression of immuno-proteasome subunits was shown in melanoma tissue infiltrated with $CD3^+$ T-cells (Woods et al., 2016). IFN-γ-induced stimulation of MHC I and immunoproteasome subunit expression was in turn augmented by MKIs in hepatocellular carcinoma cells (Takahashi et al., 2021). Thus, treatment with such inhibitors affect generation and presentation of cancer antigens acting in a synergic manner with endogenous immune molecules and by this mean stimulate recognition of cancer cells by the immune system.

On the other hand, non-constitutive proteasomes are involved in degradation of tumor suppressor proteins (Chen et al., 2023). Along these lines, upregulation of *PSMB9* is an unfavorable prognostic marker in renal cancer.[9] Moreover, immunoproteasomes promote production of pro-inflammatory cytokines (Basler et al., 2010) and their inhibition with non-constitutive proteasome inhibitor ONX-0914 was sufficient to suppress the growth of inflammation-induced colorectal cancer (Koerner et al., 2017; Vachharajani et al., 2017). Furthermore, in PSMB8-10KO mice no colitis-associated cancer development was observed (Leister et al., 2021), highlighting that non-constitutive proteasome gene expression may stimulate tumor growth via involvement in inflammatory response and likely in other more complex interactions of cancer cells with the immune system. Interestingly, one of the mechanisms of tumor cell adaptation to immune system pressure is associated with increased expression of programmed death-ligand 1 (PD-L1), a transmembrane protein known to suppress the activation of T-cells (Wang et al., 2016). Colorectal carcinomas with BRAF mutations show higher expression of PD-L1 (Srivastava et al., 2021), which can contribute to immune evasion of cancer cells and in turn nuclear PD-L1 promotes cell cycle progression of BRAF mutant cells (Ma et al., 2022). PD-L1 inhibition by sparatlizumab improved effectivity of combined inhibition of BRAF and MEK with dabrafenib and trametinib in phase 2 clinical trial for colorectal cancer (Tian et al., 2023). Along these lines, we calculated the correlation of proteasome gene expression with expression of PD-L1 in colorectal tumors. We found that *PSMB1-10* genes had significant correlation with PD-L1, however non-constitutive subunit genes *PSMB9*, *PSMB10* and *PSMB8* demonstrated the strongest Spearman correlations: R = 0.57, 0.43, 0.38, respectively and $p < 0.0001$ (Supplementary Figure S3). Moreover, we revealed modest upregulation of the *CD274* (encodes PD-L1) gene expression in cells treated with sorafenib (Supplementary Figure S4). Thus, activation of PD-L1 gene expression coincided with the activation of immunoproteasome subunit expression following treatment with the inhibitor. Here it should be mentioned that upregulated *PSMB8/9* expression correlated with increased efficacy of immune checkpoint inhibitors in melanoma (Kalaora et al., 2020) and lower-grade glioma (Liu et al., 2022). Interestingly, it has been shown that mutated forms of BRAF, NRAS, and KRAS can upregulate non-constitutive proteasome expression and reduce endoplasmic reticulum stress in multiple myeloma (Shirazi et al., 2020).

Moreover, cancer cells are constantly exposed to different stresses (Chen and Xie, 2018). Increased expression of non-constitutive proteasomes might help to deal with the consequences of stress-induced build-up of potentially toxic protein aggregates and facilitate their adaptation (Grune et al., 2011; Pickering et al., 2012; Johnston-Carey et al., 2015). Though we did not specifically address the mechanism that stands behind activation of immunoproteasome subunit expression following the incubation with the MKIs, it is well established that non-constitutive proteasome expression is increased in various stress conditions including oxidative stress (Johnston-Carey et al., 2015; Petersen and Zetterberg, 2016; Raynes et al., 2016; Wang et al., 2023). MKIs were demonstrated to induce various types of stress (Wang et al., 2023). Specifically, sorafenib was shown to induce oxidative stress, endoplasmic reticulum stress and inflammation (Rahmani et al., 2007; Wei et al., 2021; Wang et al., 2023). Regorafenib was also shown to induce endoplasmic reticulum stress (Sui et al., 2023), as well as the oxidative stress in colon cancer cells (Yu et al., 2023). Our results indicate that both drugs stimulate production of reactive oxygen species and hence, most likely—oxidative stress in studied colorectal cancer cell lines (Figures 6C, D). Thus, it could not be ruled out that stimulation of immunoproteasome subunit expression following treatment with the MKIs might involve stress-induced activation of relevant signaling pathways.

Another interesting consequence of different stresses is formation of intracellular membraneless inclusions containing proteasomes (Enenkel et al., 2022). Current findings indicate that most of these structures serve to sequester damaged proteins, facilitate their proteasomal degradation in order to cope with the consequence of stress and disappear when stress is relieved. Following treatment with MKIs, we observed re-localization of proteasomes. Upon exposure to regorafenib the distribution of non-constitutive proteasomes was not significantly altered in SW480B8-mCherry cells, but decreased cytoplasmic/nuclear ratio was observed in SW620B8-mCherry cells. However, especially in SW480B8-mCherry cells we revealed considerably higher proteasome activity in the nucleus comparing to the cytoplasm (Figure 6A). It has been shown that following different stresses proteasome-containing foci accumulate in the nucleus where proteolysis of unassembled orphan RPs and various ubiquitinated defective proteins that accumulate in stress conditions is performed (Yasuda et al., 2020; Fu et al., 2021; Uriarte et al., 2021). At least some of these structures were shown to contain p62 and heat-shock proteins and to stimulate degradation of defective proteins that accumulate following heat or oxidative stress (Fu et al., 2021). Thus, these assemblies seemingly perform protein quality control in the nucleus and their accumulation in the nucleus of regorafenib-treated cells might be a consequence of oxidative stress induced by this MKI. At the same time, following treatment with sorafenib, we revealed upregulation of proteasome activity in the nuclei but, surprisingly,

7 https://www.proteinatlas.org/ENSG00000204264-PSMB8/pathology

8 https://www.proteinatlas.org/ENSG00000205220-PSMB10/pathology

9 https://www.proteinatlas.org/ENSG00000240065-PSMB9/pathology

non-constitutive proteasomes accumulated in the cytoplasm of both cell lines (Figure 6A). This indicates that in that case proteasome-containing foci and protein quality control mechanisms in the nuclei are likely mostly associated with constitutive proteasomes. We revealed optically dense structures containing active non-constitutive proteasomes in the area close to the nuclei of treated cells. Previously, sorafenib was shown to induce formation of stress granules (Adjibade et al., 2015; Dai et al., 2023). Formation of stress granules induced by sorafenib was suggested to promote cyclooxygenase-2 expression and survival of renal cancer cells (Dai et al., 2023). Though stress granules mainly contain RNA, ribosomal components and RNA-binding proteins, they were recently shown to participate in sequestration of misfolded proteins in the cytoplasm preventing their accumulation in the nucleus and protecting from perturbations in the nuclear proteostasis (Xu et al., 2023). Another study indicates that 26S proteasomes concentrate in perinuclear aggresomes that contain defective protein aggregates and facilitate autophagic clearance of these structures (Hao et al., 2013). Moreover, upon stress induced by proteasome inhibition, proteasomes and soluble ubiquitinated misfolded proteins aggregated in juxtanuclear compartment (JUNQ) (Kaganovich et al. 2008)

Recently, a Bcl2-associated athanogene 2 (BAG2) –containing phase-separated membraneless organelles were identified (Carrettiero et al., 2022). These structures were formed in response to by hyperosmotic, proteasome inhibition, temperature or oxidative stresses and except BAG2 were shown to contain heat-shock protein Hsp-70 and 20S proteasomes capped with 11S regulators (Carrettiero et al., 2022). These granules were rather small and demonstrated more or less equal distribution within the cytoplasm. Proteasome containing structures that we observed in sorafenib-treated cells resembled BAG2 granules, but also formed larger aggregates at the proximity to the nuclei. Since we did not specify other components of the aggregates we suppose that sorafenib may stimulate formation of various proteasome-containing assemblies including BAG2 granules, JUNQ-associated aggregates or perinuclear aggresomes. Moreover, these structures contain large amount of non-constitutive proteasomes. Different localization of constitutive and non-constitutive proteasomes in these cells indicates specialized role of non-constitutive proteasomes in adaptation to stress induced by sorafenib. Concordantly, a role of β5i-containing proteasomes in degradation of α-synuclein was proposed (Ugras et al., 2018). Induction of another immunoproteasome subunit β1i was recently shown to facilitate adaptation to mitochondrial stress and prevent formation of intracellular aggregates (Kim et al., 2023). In β5iKO mice, impaired proteostasis with accumulation of ubiquitinated proteins was revealed in microglia (Cetin et al., 2022). These findings are in line with the role of immunoproteasome in prevention of aggregate formation after stress (Seifert et al., 2010). Together, induction of non-constitutive proteasomes and proteasome-containing structures may represent an adaptation to oxidative stress induced by MKIs. At the same time, different localization of proteasomes following treatment with regorafenib or sorafenib indicates differences in response to the inhibitors.

It should be mentioned that the proteasome activity was significantly elevated in colorectal cells treated with both MKIs. Importantly, this was not associated with the increased amount of proteasomes within cells at least within the cytoplasm (Figure 4A). Except increase in number, the activity of proteasomes might be modulated by several factors: association with regulators, interactions with several proteins (other than classical regulators), capable to affect proteasome activity and post-translational modifications of proteasome/regulator subunits (Kors et al., 2019). It has been shown that tyrosine-kinase inhibitors prevent Src-dependent phosphorylation of the Rpt2 (19S regulator subunit) at Y439, affecting the association of the regulator with the 20S proteasome and hence, its activity (Chen et al., 2021). Although regorafenib and sorafenib do not directly target Src, the activation of the latter is induced by receptor tyrosine kinases (e.g., PDGFR, VEGFR), which are targets of selected MKIs. Another kinase that could be influenced by Src and can affect proteasome activity is the c-Abl. Thus, a c-Abl and Arg-kinase dependent phosphorylation of the structural proteasome subunit α4 at Y153 was shown to reduce the proteasome activity (Liu et al., 2006). Moreover, regorafenib and sorafenib target several kinases of the MAPK pathway. It has been shown that phosphorylation of Rpt5 subunit of the 19S proteasome regulator by the apoptosis-regulating kinase ASK1 a member of the MAPK family inhibited the ATPase and overall activity of the 26S proteasome (Um et al., 2010). Importantly, ASK1 is activated and negatively regulates the 26S proteasome in oxidative stress (Um et al., 2010). In stress conditions the phosphorylation of Y273 of another 19S regulator subunit Rpn2 was induced by p38 MAPK. This in turn reduced the proteasome activity and facilitated accumulation of polyubiquitinated proteins in cells (Lee et al., 2010). Accordingly, MAPK inhibitors were shown to stimulate proteasome activity (Lee et al., 2010) and interestingly, no increased abundance of proteasome subunits was detected. Moreover, silencing of other components of MAPK pathway: ASK1, MKK6 (MAP kinase kinase 6), as well as the p38 MAPK target protein MK2 also stimulated proteasome activity (Leestemaker et al., 2017). Thus, one cannot exclude that MKIs can stimulate the activity of proteasomes via modulation of post-translational modification pattern of 19S regulator and 20S proteasome subunits, facilitating the adaptation of colorectal cells to stress conditions induced by the inhibitors. Although this issue should be specifically addressed, it indicates that MKIs can affect the efficacy of proteasome inhibitors if used in combination. In previous publications sorafenib demonstrated a synergistic effect in combination with proteasome inhibitors against multiply myeloma (Ramakrishnan et al., 2010) and hepatocellular carcinoma (Honma et al., 2014). Therefore we tested whether the combinations of proteasome inhibitor (bortezomib) with either sorafenib or regorafenib might be effective against colorectal cancer cell lines. Using both cell lines it has been shown that sorafenib and regorafenib do not demonstrate synergy or additive effect with bortezomib. Moreover, certain combinations of MKIs and proteasome inhibitor revealed antagonistic effect (Figure 7). Obtained results indicate that stimulation of proteasome activity and rearrangement of proteasome pool induced by MKIs can affect cellular responsiveness to proteasome inhibition which might in turn affect the outcome of combined therapy.

Taken together, our results demonstrate that regorafenib and sorafenib modulate the activity and localization of proteasomes, as well as the expression of non-constitutive proteasomes in colorectal cancer cells. This might affect presentation of tumor antigens and could be associated with the adaptation of cancer cells to the oxidative stress induced by the inhibitors. Revealed phenomenon contributes to the understanding of immunomodulatory action of MKIs and mechanisms of the crosstalk between tumor and the

immune system. At the same time, our results indicate that stimulation of proteasome activity with the MKIs can reduce the efficacy of proteasome inhibitors showing that specific tests are needed to determine the applicability of such combination for the therapy of a particular tumor. Finally, the non-constitutive proteasome expression and activity can be considered as potential markers for such therapy effectiveness.

Data availability statement

The original contributions presented in the study are included in the article/Supplementary Material, further inquiries can be directed to the corresponding author.

Ethics statement

Ethical approval was not required for the studies on humans in accordance with the local legislation and institutional requirements because only commercially available established cell lines were used.

Author contributions

AB: Data curation, Formal Analysis, Investigation, Writing–review and editing, Validation. EG: Data curation, Formal Analysis, Investigation, Validation, Writing–review and editing. TL: Conceptualization, Data curation, Formal Analysis, Investigation, Software, Validation, Writing–original draft, Writing–review and editing. VV:Formal Analysis, Investigation, Writing–review and editing. VP: Data curation, Formal Analysis, Investigation, Software, Visualization, Writing–review and editing. TA: Data curation, Formal Analysis, Investigation, Validation, Writing–review and editing. OL: Data curation, Formal Analysis, Investigation, Validation, Visualization, Writing–review and editing. PS: Formal Analysis, Investigation, Methodology, Writing–review and editing. VP: Investigation, Methodology, Resources, Supervision, Writing–review and editing. VK: Conceptualization, Funding acquisition, Investigation, Project administration, Resources, Supervision, Writing–review and editing. AM: Conceptualization, Data curation, Formal Analysis, Investigation, Methodology, Supervision, Validation, Writing–original draft, Writing–review and editing.

Funding

The author(s) declare financial support was received for the research, authorship, and/or publication of this article. This research was funded by Russian Science Foundation, grant #23-14-00224.

Acknowledgments

We would like to thank Vishnyakova Afina and Anastasia Kravchenko for the evaluation of *CD274* gene expression levels.

Conflict of interest

The authors declare that the research was conducted in the absence of any commercial or financial relationships that could be construed as a potential conflict of interest.

Publisher's note

Supplementary material

The Supplementary Material for this article can be found online at: https://www.frontiersin.org/articles/10.3389/fmolb.2024.1351641/full#supplementary-material

References

Adjibade, P., St-Sauveur, V. G., Quevillon Huberdeau, M., Fournier, M. J., Savard, A., Coudert, L., et al. (2015). Sorafenib, a multikinase inhibitor, induces formation of stress granules in hepatocarcinoma cells. *Oncotarget* 6 (41), 43927–43943. doi:10.18632/oncotarget.5980

Aki, M., Shimbara, N., Takashina, M., Akiyama, K., Kagawa, S., Tamura, T., et al. (1994). Interferon-gamma induces different subunit organizations and functional diversity of proteasomes. *J. Biochem.* 115, 257–269. doi:10.1093/oxfordjournals.jbchem.a124327

Astakhova, T. M., Morozov, M. V., Erokhov, P. A., Mikhailovskaya, M. I., Akopov, S. B., Chupikova, I., et al. (2018). Combined effect of bortezomib and menadione sodium bisulfite on proteasomes of tumor cells: the dramatic decrease of bortezomib toxicity in a preclinical trial. *Cancers* 10, 351. doi:10.3390/cancers10100351

Basler, M., Dajee, M., Moll, C., Groettrup, M., and Kirk, C. J. (2010). Prevention of experimental colitis by a selective inhibitor of the immunoproteasome. *J. Immunol.* 185, 634–641. doi:10.4049/jimmunol.0903182

Basu, A., Bodycombe, N. E., Cheah, J. H., Price, E. V., Liu, K., Schaefer, G. I., et al. (2013). An interactive resource to identify cancer genetic and lineage dependencies targeted by small molecules. *Cell* 154 (5), 1151–1161. doi:10.1016/j.cell.2013.08.003

Behan, F. M., Iorio, F., Picco, G., Gonçalves, E., Beaver, C. M., Migliardi, G., et al. (2019). Prioritization of cancer therapeutic targets using CRISPR-Cas9 screens. *Nature* 568 (7753), 511–516. doi:10.1038/s41586-019-1103-9

Berkers, C. R., van Leeuwen, F. W., Groothuis, T. A., Peperzak, V., van Tilburg, E. W., Borst, J., et al. (2007). Profiling proteasome activity in tissue with fluorescent probes. *Mol. Pharm.* 4 (5), 739–748. doi:10.1021/mp0700256

Burov, A., Funikov, S., Vagapova, E., Dalina, A., Rezvykh, A., Shyrokova, E., et al. (2021). A cell-based Platform for the investigation of immunoproteasome subunit β5i expression and biology of β5i-containing proteasomes. *Cells* 10 (11), 3049. doi:10.3390/cells10113049

Carrettiero, D. C., Almeida, M. C., Longhini, A. P., Rauch, J. N., Han, D., Zhang, X., et al. (2022). Stress routes clients to the proteasome via a BAG2 ubiquitin-independent degradation condensate. *Nat. Commun.* 13 (1), 3074. doi:10.1038/s41467-022-30751-4

Çetin, G., Studencka-Turski, M., Venz, S., Schormann, E., Junker, H., Hammer, E., et al. (2022). Immunoproteasomes control activation of innate immune signaling and microglial function. *Front. Immunol.* 13, 982786. doi:10.3389/fimmu.2022.982786

Chen, B., Zhu, H., Yang, B., and Cao, J. (2023). The dichotomous role of immunoproteasome in cancer: friend or foe? *Acta Pharm. Sin. B* 13 (5), 1976–1989. doi:10.1016/j.apsb.2022.11.005

Chen, L., Zhang, Y., Shu, X., Chen, Q., Wei, T., Wang, H., et al. (2021). Proteasome regulation by reversible tyrosine phosphorylation at the membrane. *Oncogene* 40 (11), 1942–1956. doi:10.1038/s41388-021-01674-z

Chen, M., and Xie, S. (2018). Therapeutic targeting of cellular stress responses in cancer. *Thorac. Cancer* 9 (12), 1575–1582. doi:10.1111/1759-7714.12890

Ciechanover, A., and Schwartz, A. L. (1998). The ubiquitin-proteasome pathway: the complexity and myriad functions of proteins death. *Proc. Natl. Acad. Sci. U. S. A.* 95 (6), 2727–2730. doi:10.1073/pnas.95.6.2727

Dai, H., Wang, G., Cao, W., Qi, W., Chen, W., and Guo, H. (2023). Stress granules affect the sensitivity of renal cancer cells to sorafenib by sequestering and stabilizing COX-2 mRNA. *Oncol. Lett.* 25 (6), 274. doi:10.3892/ol.2023.13860

De Jong, A., Schuurman, K. G., Rodenko, B., Ovaa, H., and Berkers, C. R. (2012). Fluorescence-based proteasome activity profiling. *Methods Mol. Biol.* 803, 183–204. doi:10.1007/978-1-61779-364-6_13

Enenkel, C., Kang, R. W., Wilfling, F., and Ernst, O. P. (2022). Intracellular localization of the proteasome in response to stress conditions. *J. Biol. Chem.* 298 (7), 102083. doi:10.1016/j.jbc.2022.102083

Fu, A., Cohen-Kaplan, V., Avni, N., Livneh, I., and Ciechanover, A. (2021). p62-containing, proteolytically active nuclear condensates, increase the efficiency of the ubiquitin-proteasome system. *Proc. Natl. Acad. Sci. U. S. A.* 118 (33), e2107321118. doi:10.1073/pnas.2107321118

Fucile, C., Marenco, S., Bazzica, M., Zuccoli, M. L., Lantieri, F., Robbiano, L., et al. (2015). Measurement of sorafenib plasma concentration by high-performance liquid chromatography in patients with advanced hepatocellular carcinoma: is it useful the application in clinical practice? A pilot study. *Med. Oncol.* 32 (1), 335. doi:10.1007/s12032-014-0335-7

Grothey, A., Van Cutsem, E., Sobrero, A., Siena, S., Falcone, A., Ychou, M., et al. (2013). Regorafenib monotherapy for previously treated metastatic colorectal cancer (CORRECT): an international, multicentre, randomised, placebo-controlled, phase 3 trial. *Lancet* 381 (9863), 303–312. doi:10.1016/S0140-6736(12)61900-X

Grune, T., Catalgol, B., Licht, A., Ermak, G., Pickering, A. M., Ngo, J. K., et al. (2011). HSP70 mediates dissociation and reassociation of the 26S proteasome during adaptation to oxidative stress. *Free Radic. Biol. Med.* 51, 1355–1364. doi:10.1016/j.freeradbiomed.2011.06.015

Gu, Z., Eils, R., and Schlesner, M. (2016). Complex heatmaps reveal patterns and correlations in multidimensional genomic data. *Bioinformatics* 32 (18), 2847–2849. doi:10.1093/bioinformatics/btw313

Guillaume, B., Chapiro, J., Stroobant, V., Colau, D., Van Holle, B., Parvizi, G., et al. (2010). Two abundant proteasome subtypes that uniquely process some antigens presented by HLA class I molecules. *Proc. Natl. Acad. Sci. U. S. A.* 107 (43), 18599–18604. doi:10.1073/pnas.1009778107

Hao, R., Nanduri, P., Rao, Y., Panichelli, R. S., Ito, A., Yoshida, M., et al. (2013). Proteasomes activate aggresome disassembly and clearance by producing unanchored ubiquitin chains. *Mol. Cell* 51 (6), 819–828. doi:10.1016/j.molcel.2013.08.016

Hewitt, R. E., McMarlin, A., Kleiner, D., Wersto, R., Martin, P., Tsokos, M., et al. (2000). Validation of a model of colon cancer progression. *J. Pathol.* 192 (4), 446–454. doi:10.1002/1096-9896(2000)9999:9999<::AID-PATH775>3.0.CO;2-K

Honma, Y., Shimizu, S., Takehara, T., and Harada, M. (2014). Sorafenib enhances proteasome inhibitor-induced cell death via inactivation of Akt and stress-activated protein kinases. *J. Gastroenterol.* 49 (3), 517–526. doi:10.1007/s00535-013-0796-z

Huber, E. M., and Groll, M. (2021). A nut for every bolt: subunit-selective inhibitors of the immunoproteasome and their therapeutic potential. *Cells* 10 (8), 1929. doi:10.3390/cells10081929

Jeong, K. Y., Park, M., Sim, J. J., and Kim, H. M. (2020). Combination antitumor effect of sorafenib via calcium-dependent deactivation of focal adhesion kinase targeting colorectal cancer cells. *Molecules* 25 (22), 5299. doi:10.3390/molecules25225299

Johnston-Carey, H. K., Pomatto, L. C., and Davies, K. J. (2015). The Immunoproteasome in oxidative stress, aging, and disease. *Crit. Rev. Biochem. Mol. Biol.* 51 (4), 268–281. doi:10.3109/10409238.2016.1172554

Kacan, T., Nayir, E., Altun, A., Kilickap, S., Babacan, N. A., Ataseven, H., et al. (2016). Antitumor activity of sorafenib on colorectal cancer. *J. Oncol. Sci.* 2 (2–3), 53–57. doi:10.1016/j.jons.2016.07.008

Kaganovich, D., Kopito, R., and Frydman, J. (2008). Misfolded proteins partition between two distinct quality control compartments. *Nature* 454 (7208), 1088–1095. doi:10.1038/nature07195

Kalaora, S., Lee, J. S., Barnea, E., Levy, R., Greenberg, P., Alon, M., et al. (2020). Immunoproteasome expression is associated with better prognosis and response to checkpoint therapies in melanoma. *Nat. Commun.* 11 (1), 896. doi:10.1038/s41467-020-14639-9

Kannaiyan, R., and Mahadevan, D. (2018). A comprehensive review of protein kinase inhibitors for cancer therapy. *Expert Rev. Anticancer Ther.* 18 (12), 1249–1270. doi:10.1080/14737140.2018.1527688

Kim, M., Serwa, R. A., Samluk, L., Suppanz, I., Kodroń, A., Stępkowski, T. M., et al. (2023). Immunoproteasome-specific subunit PSMB9 induction is required to regulate cellular proteostasis upon mitochondrial dysfunction. *Nat. Commun.* 14 (1), 4092. doi:10.1038/s41467-023-39642-8

Kincaid, E. Z., Che, J. W., York, I., Escobar, H., Reyes-Vargas, E., Delgado, J. C., et al. (2011). Mice completely lacking immunoproteasomes show major changes in antigen presentation. *Nat. Immunol.* 13 (2), 129–135. doi:10.1038/ni.2203

Kobayashi, K., Sugiyama, E., Shinozaki, E., Wakatsuki, T., Tajima, M., Kidokoro, H., et al. (2021). Associations among plasma concentrations of regorafenib and its metabolites, adverse events, and ABCG2 polymorphisms in patients with metastatic colorectal cancers. *Cancer Chemother. Pharmacol.* 87 (6), 767–777. doi:10.1007/s00280-021-04237-x

Koerner, J., Brunner, T., and Groettrup, M. (2017). Inhibition and deficiency of the immunoproteasome subunit LMP7 suppress the development and progression of colorectal carcinoma in mice. *Oncotarget* 8, 50873–50888. doi:10.18632/oncotarget.15141

Kors, S., Geijtenbeek, K., Reits, E., and Schipper-Krom, S. (2019). Regulation of proteasome activity by (Post-)transcriptional mechanisms. *Front. Mol. Biosci.* 6, 48. doi:10.3389/fmolb.2019.00048

Kumar Deshmukh, F., Yaffe, D., Olshina, M. A., Ben-Nissan, G., and Sharon, M. (2019). The contribution of the 20S proteasome to proteostasis. *Biomolecules* 9 (5), 190. doi:10.3390/biom9050190

Kwilas, A. R., Ardiani, A., Donahue, R. N., Aftab, D. T., and Hodge, J. W. (2014). Dual effects of a targeted small-molecule inhibitor (cabozantinib) on immune-mediated killing of tumor cells and immune tumor microenvironment permissiveness when combined with a cancer vaccine. *J. Transl. Med.* 12, 294. doi:10.1186/s12967-014-0294-y

Lebedev, T., Buzdin, A., Khabusheva, E., Spirin, P., Suntsova, M., Sorokin, M., et al. (2022a). Subtype of neuroblastoma cells with high KIT expression are dependent on KIT and its knockdown induces compensatory activation of pro-survival signaling. *Int. J. Mol. Sci.* 23 (14), 7724. doi:10.3390/ijms23147724

Lebedev, T. D., Khabusheva, E. R., Mareeva, S. R., Ivanenko, K. A., Morozov, A. V., Spirin, P. V., et al. (2022b). Identification of cell type-specific correlations between ERK activity and cell viability upon treatment with ERK1/2 inhibitors. *J. Biol. Chem.* 298 (8), 102226. doi:10.1016/j.jbc.2022.102226

Lee, M., Song, I. H., Heo, S. H., Kim, Y. A., Park, I. A., Bang, W. S., et al. (2019). Expression of immunoproteasome subunit LMP7 in breast cancer and its association with immune-related markers. *Cancer Res. Treat.* 51, 80–89. doi:10.4143/crt.2017.500

Lee, P. Y., Yeoh, Y., and Low, T. Y. (2023). A recent update on small-molecule kinase inhibitors for targeted cancer therapy and their therapeutic insights from mass spectrometry-based proteomic analysis. *FEBS J.* 290 (11), 2845–2864. doi:10.1111/febs.16442

Lee, S. H., Park, Y., Yoon, S. K., and Yoon, J. B. (2010). Osmotic stress inhibits proteasome by p38 MAPK-dependent phosphorylation. *J. Biol. Chem.* 285 (53), 41280–41289. doi:10.1074/jbc.M110.182188

Leestemaker, Y., de Jong, A., Witting, K. F., Penning, R., Schuurman, K., Rodenko, B., et al. (2017). Proteasome activation by small molecules. *Cell Chem. Biol.* 24 (6), 725–736. doi:10.1016/j.chembiol.2017.05.010

Leister, H., Luu, M., Staudenraus, D., Lopez Krol, A., Mollenkopf, H.-J., Sharma, A., et al. (2021). Pro- and antitumorigenic capacity of immunoproteasomes in shaping the tumor microenvironment. *Cancer Immunol. Res.* 9, 682–692. doi:10.1158/2326-6066.CIR-20-0492

Liu, J., Yang, X., Ji, Q., Yang, L., Li, J., Long, X., et al. (2022). Immune characteristics and prognosis analysis of the proteasome 20S subunit beta 9 in lower-grade gliomas. *Front. Oncol.* 12, 875131. doi:10.3389/fonc.2022.875131

Liu, X., Huang, W., Li, C., Li, P., Yuan, J., Li, X., et al. (2006). Interaction between c-Abl and Arg tyrosine kinases and proteasome subunit PSMA7 regulates proteasome degradation. *Mol. Cell* 22 (3), 317–327. doi:10.1016/j.molcel.2006.04.007

Ma, R., Liu, Y., Che, X., Li, C., Wen, T., Hou, K., et al. (2022). Nuclear PD-L1 promotes cell cycle progression of BRAF-mutated colorectal cancer by inhibiting THRAP3. *Cancer Lett.* 527, 127–139. doi:10.1016/j.canlet.2021.12.017

Marisa, L., de Reyniès, A., Duval, A., Selves, J., Gaub, M. P., Vescovo, L., et al. (2013). Gene expression classification of colon cancer into molecular subtypes: characterization, validation, and prognostic value. *PLoS Med.* 10 (5), e1001453. doi:10.1371/journal.pmed.1001453

Martchenko, K., Schmidtmann, I., Thomaidis, T., Thole, V., Galle, P. R., Becker, M., et al. (2016). Last line therapy with sorafenib in colorectal cancer: a retrospective analysis. *World J. Gastroenterol.* 22 (23), 5400–5405. doi:10.3748/wjg.v22.i23.5400

McFarland, J. M., Ho, Z. V., Kugener, G., Dempster, J. M., Montgomery, P. G., Bryan, J. G., et al. (2018). Improved estimation of cancer dependencies from large-scale RNAi screens using model-based normalization and data integration. *Nat. Commun.* 9 (1), 4610. doi:10.1038/s41467-018-06916-5

Mitchell, D. C., Kuljanin, M., Li, J., Van Vranken, J. G., Bulloch, N., Schweppe, D. K., et al. (2023). A proteome-wide atlas of drug mechanism of action. *Nat. Biotechnol.* 41 (6), 845–857. doi:10.1038/s41587-022-01539-0

Morozov, A. V., Burov, A. V., Astakhova, T. M., Spasskaya, D. S., Margulis, B. A., and Karpov, V. L. (2019). Dynamics of the functional activity and expression of proteasome subunits during cellular adaptation to heat shock. *Mol. Biol. Mosk.* 53 (4), 638–647. doi:10.1134/S0026898419040086

Morozov, A. V., and Karpov, V. L. (2019). Proteasomes and several aspects of their heterogeneity relevant to cancer. *Front. Oncol.* 9, 761. doi:10.3389/fonc.2019.00761

Petersen, A., and Zetterberg, M. (2016). The immunoproteasome in human lens epithelial cells during oxidative stress. *Investig. Ophthalmol. Vis. Sci.* 57 (11), 5038–5045. doi:10.1167/iovs.16-19536

Pickering, A. M., Linder, R. A., Zhang, H., Forman, H. J., and Davies, K. J. (2012). Nrf2-dependent induction of proteasome and Pa28αβ regulator are required for adaptation to oxidative stress. *J. Biol. Chem.* 287, 10021–10031. doi:10.1074/jbc.M111.277145

Rahmani, M., Davis, E. M., Crabtree, T. R., Habibi, J. R., Nguyen, T. K., Dent, P., et al. (2007). The kinase inhibitor sorafenib induces cell death through a process involving induction of endoplasmic reticulum stress. *Mol. Cell Biol.* 27 (15), 5499–5513. doi:10.1128/MCB.01080-06

Ramakrishnan, V., Timm, M., Haug, J. L., Kimlinger, T. K., Wellik, L. E., Witzig, T. E., et al. (2010). Sorafenib, a dual raf kinase/vascular endothelial growth factor receptor inhibitor has significant anti-myeloma activity and synergizes with common anti-myeloma drugs. *Oncogene* 29, 1190–1202. doi:10.1038/onc.2009.403

Raynes, R., Pomatto, L. C., and Davies, K. J. (2016). Degradation of oxidized proteins by the proteasome: distinguishing between the 20S, 26S, and immunoproteasome proteolytic pathways. *Mol. Asp. Med.* 50, 41–55. doi:10.1016/j.mam.2016.05.001

Roeten, M. S. F., Cloos, J., and Jansen, G. (2018). Positioning of proteasome inhibitors in therapy of solid malignancies. *Cancer Chemother. Pharmacol.* 81 (2), 227–243. doi:10.1007/s00280-017-3489-0

Rohr, M., Beardsley, J., Nakkina, S. P., Zhu, X., Aljabban, J., Hadley, D., et al. (2021). A merged microarray meta-dataset for transcriptionally profiling colorectal neoplasm formation and progression. *Sci. Data* 8 (1), 214. doi:10.1038/s41597-021-00998-5

Rouette, A., Trofimov, A., Haberl, D., Boucher, G., Lavallee, V. P., D'angelo, G., et al. (2016). Expression of immunoproteasome genes is regulated by cell-intrinsic and -extrinsic factors in human cancers. *Sci. Rep.* 6, 34019. doi:10.1038/srep34019

Seifert, U., Bialy, L. P., Ebstein, F., Bech-Otschir, D., Voigt, A., Schröter, F., et al. (2010). Immunoproteasomes preserve protein homeostasis upon interferon-induced oxidative stress. *Cell* 142 (4), 613–624. doi:10.1016/j.cell.2010.07.036

Shirazi, F., Jones, R. J., Singh, R. K., Zou, J., Kuiatse, I., Berkova, Z., et al. (2020). Activating KRAS, NRAS, and BRAF mutants enhance proteasome capacity and reduce endoplasmic reticulum stress in multiple myeloma. *Proc. Natl. Acad. Sci. U. S. A.* 117 (33), 20004–20014. doi:10.1073/pnas.2005052117

Srivastava, P., Husain, N., Shukla, S., Chauhan, S., Pandey, A., and Masood, S. (2021). PD-L1 Expression in colorectal carcinoma and its correlation with clinicopathological parameters, microsatellite instability and BRAF mutation. *Indian J. Pathol. Microbiol.* 64 (3), 490–496. doi:10.4103/IJPM.IJPM_521_20

Sui, H., Xiao, S., Jiang, S., Wu, S., Lin, H., Cheng, L., et al. (2023). Regorafenib induces NOX5-mediated endoplasmic reticulum stress and potentiates the anti-tumor activity of cisplatin in non-small cell lung cancer cells. *Neoplasia* 39, 100897. doi:10.1016/j.neo.2023.100897

Takahashi, A., Umemura, A., Yano, K., Okishio, S., Kataoka, S., Okuda, K., et al. (2021). Tyrosine kinase inhibitors stimulate HLA class I expression by augmenting the ifnγ/STAT1 signaling in hepatocellular carcinoma cells. *Front. Oncol.* 11, 707473. doi:10.3389/fonc.2021.707473

Tian, J., Chen, J. H., Chao, S. X., Pelka, K., Giannakis, M., Hess, J., et al. (2023). Combined PD-1, BRAF and MEK inhibition in BRAFV600E colorectal cancer: a phase 2 trial. *Nat. Med.* 29 (2), 458–466. doi:10.1038/s41591-022-02181-8

Tripathi, S. C., Peters, H. L., Taguchi, A., Katayama, H., Wang, H., Momin, A., et al. (2016). Immunoproteasome deficiency is a feature of non-small cell lung cancer with a mesenchymal phenotype and is associated with a poor outcome. *Proc. Natl. Acad. Sci. U. S. A.* 113, E1555–E1564. doi:10.1073/pnas.1521812113

Tsai, K. A., Khan, Y. A., Worgo, E. C., Wang, L. L., Liang, Y., and Davila, E. (2017). A multikinase and DNA-PK inhibitor combination immunomodulates melanomas, suppresses tumor progression, and enhances immunotherapies. *Cancer Immunol. Res.* 5, 790–803. doi:10.1158/2326-6066.CIR-17-0009

Tsherniak, A., Vazquez, F., Montgomery, P. G., Weir, B. A., Kryukov, G., Cowley, G. S., et al. (2017). Defining a cancer dependency map. *Cell* 170 (3), 564–576. doi:10.1016/j.cell.2017.06.010

Tsvetkov, P., Adler, J., Myers, N., Biran, A., Reuven, N., and Shaul, Y. (2018). Oncogenic addiction to high 26S proteasome level. *Cell Death Dis.* 9 (7), 773. doi:10.1038/s41419-018-0806-4

Ugras, S., Daniels, M. J., Fazelinia, H., Gould, N. S., Yocum, A. K., Luk, K. C., et al. (2018). Induction of the immunoproteasome subunit Lmp7 links proteostasis and immunity in α-synuclein aggregation disorders. *EBioMedicine* 31, 307–319. doi:10.1016/j.ebiom.2018.05.007

Um, J. W., Im, E., Park, J., Oh, Y., Min, B., Lee, H. J., et al. (2010). ASK1 negatively regulates the 26 S proteasome. *J. Biol. Chem.* 285 (47), 36434–36446. doi:10.1074/jbc.M110.133777

Uriarte, M., Sen Nkwe, N., Tremblay, R., Ahmed, O., Messmer, C., Mashtalir, N., et al. (2021). Starvation-induced proteasome assemblies in the nucleus link amino acid supply to apoptosis. *Nat. Commun.* 12, 6984. doi:10.1038/s41467-021-27306-4

Vachharajani, N., Joeris, T., Luu, M., Hartmann, S., Pautz, S., Jenike, E., et al. (2017). Prevention of colitis-associated cancer by selective targeting of immunoproteasome subunit LMP7. *Oncotarget* 8, 50447–50459. doi:10.18632/oncotarget.14579

Vagapova, E., Burov, A., Spasskaya, D., Lebedev, T., Astakhova, T., Spirin, P., et al. (2021). Immunoproteasome activity and content determine hematopoietic cell sensitivity to ONX-0914 and to the infection of cells with lentiviruses. *Cells* 10, 1185. doi:10.3390/cells10051185

Vigneron, N., Abi Habib, J., and Van Den Eynde, B. J. (2017). Learning from the proteasome how to fine-tune cancer immunotherapy. *Trends Cancer* 3, 726–741. doi:10.1016/j.trecan.2017.07.007

Wang, H., Wang, Y., Li, J., He, Z., Boswell, S. A., Chung, M., et al. (2023b). Three tyrosine kinase inhibitors cause cardiotoxicity by inducing endoplasmic reticulum stress and inflammation in cardiomyocytes. *BMC Med.* 21 (1), 147. doi:10.1186/s12916-023-02838-2

Wang, X., Teng, F., Kong, L., and Yu, J. (2016). PD-L1 expression in human cancers and its association with clinical outcomes. *Onco Targets Ther.* 9, 5023–5039. doi:10.2147/OTT.S105862

Wang, X., Zhang, H., Wang, Y., Bramasole, L., Guo, K., Mourtada, F., et al. (2023a). DNA sensing via the cGAS/STING pathway activates the immunoproteasome and adaptive T-cell immunity. *EMBO J.* 42 (8), e110597. doi:10.15252/embj.2022110597

Wei, J., Wang, Z., Wang, W., Liu, X., Wan, J., Yuan, Y., et al. (2021). Oxidative stress activated by sorafenib alters the temozolomide sensitivity of human glioma cells through autophagy and JAK2/STAT3-AIF Axis. *Front. Cell Dev. Biol.* 9, 660005. doi:10.3389/fcell.2021.660005

Wilhelm, S. M., Dumas, J., Adnane, L., Lynch, M., Carter, C. A., Schutz, G., et al. (2011). Regorafenib (BAY 73–4506): a new oral multikinase inhibitor of angiogenic, stromal and oncogenic receptor tyrosine kinases with potent preclinical antitumor activity. *Int. J. Cancer* 129 (1), 245–255. doi:10.1002/ijc.25864

Winter, M. B., La Greca, F., Arastu-Kapur, S., Caiazza, F., Cimermancic, P., Buchholz, T. J., et al. (2017). Immunoproteasome functions explained by divergence in cleavage specificity and regulation. *Elife* 6, e27364. doi:10.7554/eLife.27364

Woods, K., Knights A, J., Anaka, M., Schittenhelm, R. B., Purcell, A. W., Behren, A., et al. (2016). Mismatch in epitope specificities between IFNγ inflamed and uninflamed conditions leads to escape from T lymphocyte killing in melanoma. *J. Immunother. Cancer* 4, 10. doi:10.1186/s40425-016-0111-7

Xu, S., Gierisch, M. E., Schellhaus, A. K., Poser, I., Alberti, S., Salomons, F. A., et al. (2023). Cytosolic stress granules relieve the ubiquitin-proteasome system in the nuclear compartment. *EMBO J.* 42 (3), e111802. doi:10.15252/embj.2022111802

Yasuda, S., Tsuchiya, H., Kaiho, A., Guo, Q., Ikeuchi, K., Endo, A., et al. (2020). Stress- and ubiquitylation-dependent phase separation of the proteasome. *Nature* 578 (7794), 296–300. doi:10.1038/s41586-020-1982-9

Yu, Y., Wu, T., Zhang, X., Li, P., Ye, L., Kuang, J., et al. (2023). Regorafenib activates oxidative stress by inhibiting SELENOS and potentiates oxaliplatin-induced cell death in colon cancer cells. *Eur. J. Pharmacol.* 957, 175986. doi:10.1016/j.ejphar.2023.175986

frontiers | Frontiers in Immunology

TYPE Review
PUBLISHED 28 June 2024
DOI 10.3389/fimmu.2024.1375730

OPEN ACCESS

EDITED BY
Shahid Ali,
University of Swat, Pakistan

REVIEWED BY
Arshad Iqbal,
University of Swat, Pakistan
Silvia Giunco,
University of Padova, Italy

*CORRESPONDENCE
Wei Zhang
weizhang2000cn@163.com
Guanyu Yu
yuguanyu0451@163.com
Leqi Zhou
richard12@126.com

†These authors have contributed equally to this work

RECEIVED 24 January 2024
ACCEPTED 17 June 2024
PUBLISHED 28 June 2024

CITATION
Zhang T, Wen R, Fan H, Yu Y, Jia H, Peng Z, Zhou L, Yu G and Zhang W (2024) Impact and potential value of immunosenescence on solid gastrointestinal tumors.
Front. Immunol. 15:1375730.
doi: 10.3389/fimmu.2024.1375730

Impact and potential value of immunosenescence on solid gastrointestinal tumors

Tianshuai Zhang†, Rongbo Wen†, Hao Fan†, Yue Yu, Hang Jia, Zhiying Peng, Leqi Zhou*, Guanyu Yu* and Wei Zhang*

Department of Colorectal Surgery, Shanghai Changhai Hospital, Naval Medical University, Shanghai, China

Solid gastrointestinal tumors often respond poorly to immunotherapy for the complex tumor microenvironment (TME), which is exacerbated by immune system alterations. Immunosenescence is the process of increased diversification of immune genes due to aging and other factors, leading to a decrease in the recognition function of the immune system. This process involves immune organs, immune cells, and the senescence-associated secretory phenotype (SASP). The most fundamental change is DNA damage, resulting in TME remodeling. The main manifestations are worsening inflammation, increased immunosuppressive SASP production, decreased immune cell antitumor activity, and the accumulation of tumor-associated fibroblasts and myeloid-derived suppressor cells, making antitumor therapy less effective. Senotherapy strategies to remove senescent cells and block key senescence processes can have synergistic effects with other treatments. This review focuses on immunoenescence and its impact on the solid TME. We characterize the immunosenescent TME and discuss future directions for antitumor therapies targeting senescence.

KEYWORDS

gastrointestinal tumors, colorectal cancer, immunosenescence, tumor microenvironment, immunotherapy

Background

Health problems caused by population aging are among the great challenges the world is facing today. Nearly half of the global disease burden (92 diseases (including 35 cancers), accounting for 51.3%, 95% uncertainty interval, 48.5–53.9) is considered age-related (1). These include colorectal cancer, a solid tumor of the gastrointestinal tract with the third-highest incidence and second-highest mortality rate globally (2). Cancer morbidity and mortality rates are the highest in individuals over 50 years of age, suggesting that aging may play a significant role in cancer development and progression (3). Studies on the mechanisms of aging and tumor development have shown that some hallmarks of aging

(including genomic instability, epigenetic alterations, chronic inflammation, and dysbiosis) promote oncogenesis and progression, whereas others have shown antagonistic (telomere attrition and stem cell exhaustion) or ambivalent effects (disabled macroautophagy and cellular senescence) on tumors (4). Therefore, the effects of aging on tumors need to be specifically explored at the systemic, microenvironmental, and cellular levels.

The immune system constitutes the body's defensive barrier by monitoring, protecting, and eliminating threats (5). However, the interaction between adaptive and innate immune cells can lead to chronic inflammation and increase the likelihood of cancer development, and different types of infiltrating immune cells can have opposite effects on tumor prognosis (6). In addition, immune system function decreases with age, known as immunosenescence, which increases the risk of cancer and is a key player in cancer development (7). It was Roy Walford who first elucidated the link between immunity and aging and coined the term "immunosenescence," which refers to increased immunogenetic diversification due to aging, leading to a progressive decrease in the recognition function of the immune system (8, 9). Immune aging is not simply a one-way process that leads to dysfunction and other harmful effects, but a dynamic balance between adaptation and maladaptation (10).

Changes in the immune senescence process will further complicate the immune features of the tumor microenvironment (TME) and may therefore have diverse impacts on tumor development and immunotherapy. The TME is composed of multiple types of immune cells, cancer-associated fibroblasts, endothelial cells, pericytes, various tissue-resident cell types, and extracellular matrix (ECM) (11). The complexity of the TME lies in the fact that immune cells are recruited to and infiltrate the TME through the action of cytokines and chemokines secreted from cancer cells to play an antitumor role, but simultaneously produce additional features of the TME that facilitate immunosuppression and limit antitumor immune responses (12–14). Particularly in colorectal cancer, slight alterations in the TME will trigger complex immunotherapy changes (15). Increasing evidence suggests that both innate and adaptive immune cells in the TME have a facilitative effect on tumor progression, while crosstalk with cancer cells enhances the recruitment of suppressive immune cells, including myeloid-derived suppressor cells (MDSCs) and tumor-associated macrophages (16–18). In addition, a decrease in antitumor immune cell infiltration and function, together with the accumulation of immunosuppressive cells and upregulation of ligands that bind to inhibitory receptors on immune cells, may contribute to immune escape and consequently lead to poor immunotherapy results (19, 20).

Although remarkable research advancements have been made for both immunosenescence and the TME in the past decades, the impact of their interaction on different constituents and tumor progression remains to be further explored. This review focuses on the process of immunosenescence and the role of TME regulation. In addition, we discuss the impact of immunosenescence on tumor progression and immunotherapy. Finally, we describe future directions for limiting tumor progression by intervening in immunosenescence.

The process of immunosenescence

The process of immune aging involves three distinct but interrelated components, i.e., the immune organs, immune cells, and circulating factors (chemokines, cytokines, and other soluble molecules), which change during aging and produce corresponding effects (Figure 1) (21). Immune system aging ultimately results in increased incidence of infectious diseases and mortality, reduced responsiveness to vaccines, accelerated aging of other organs, and increased risk of tumors (22–25) Immunosenescence is a complex and well-integrated process.

The aging of immune organs is the most noticeable change. For example, thymus function degenerates in nearly all species. Thymic involution begins in childhood and reaches its peak in adolescence. While excessive energy use is reduced in this process, age-related degeneration is detrimental to the organism (26, 27). During this process, thymus cells are gradually replaced by adipocytes, which results in a decrease in the proportion of undifferentiated T cells produced by the thymus (e.g., naïve T cells) and an increase in that of terminally differentiated cells (e.g., memory or depleted phenotypic T cells) (28). Such changes are also observed in neonates with early thyme resection, suggesting that they are a sign of immune deficiency (29). In conclusion, thymic degeneration is associated with the age-related immune decline and makes one prone to age-related diseases.

The key factors in promoting and mediating immunosenescence are alterations in circulating factors (chemokines, cytokines, and other soluble molecules). Immunosenescence causes the body to gradually enter an age-related pro-inflammatory state, while simultaneously, the body exerts anti-inflammatory effects through low-level, sterile chronic inflammation to adapt and remodel the immune system (30). During this process, senescent cells secrete inflammatory, extracellular modifying, and growth factors as signaling and acting molecules collectively referred to as the senescence-associated secretory phenotype (SASP) (31).

The SASP is expressed upon exposure to excessive stresses, such as repetitive cell division, oxidative stress, mitochondrial degradation, oncogene expression, and other stresses that cause DNA damage (Figure 2) (32). As an inflammatory response, the regulation of SASP is strongly associated with nuclear factor kappa-light-chain-enhancer of activated B cells (NF-κB) activation. As a classical DNA damage response pathway, the p38 MAPK pathway is activated by oxidative stress and DNA damage and regulates NF-κB through the $p16^{INK4A}$, p53, and DNA damage checkpoint kinase CHK1/CHK2 mechanisms, which in turn produce the SASP (33–37). Another DNA damage response-related pathway, the ATM/ATR pathway, is thought to mediate NF-κB action via the key molecule GATA4 to produce the SASP (38). In addition, the downregulation of DNase (DNase2/TREX1) expression in senescent cells leads to the accumulation of DNA in the cytoplasm, which in turn leads to abnormal cGAS-STING pathway activation and SASP production through IFN-mediated NF-κB activation (39). Another pathway validated to produce SASP via NF activation is regulated by IL-1α, which phosphorylates IRAK1 via IRAK4 after binding to the IL-1 receptor and eventually activates NF-κB (40). Another signaling

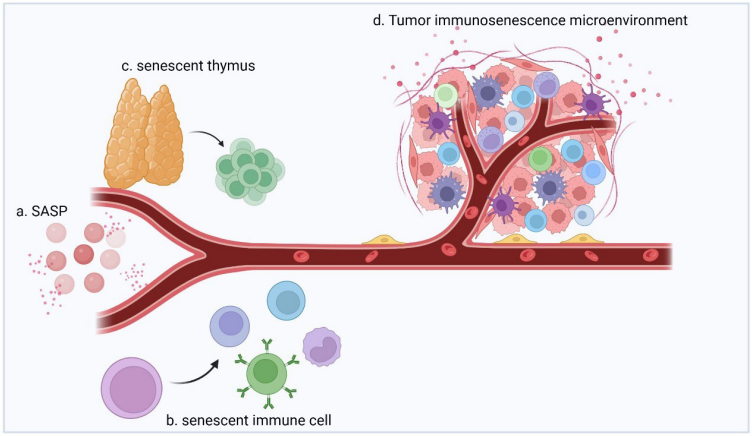

FIGURE 1
The immunosenescence process involves immune organs, immune cells, and circulating factors (chemokines, cytokines, and other soluble molecules) as three distinct but interrelated components that undergo changes during aging, with corresponding effects. **(A)** During aging, senescent cells secrete signaling and action molecules such as inflammatory, extracellular modifying, and growth factors, collectively known as SASP, which are key factors in facilitating and mediating immunosenescence. **(B)** Immune cells produced by senescent hematopoietic stem cells interact with SASPs and are characterized by increased numbers, increased secretion of inflammatory factors, decreased self-renewal capacity, diminished homing effects, and decreased energy metabolism. **(C)** During aging, thymus cells are gradually replaced by adipocytes, which results in a decrease in the proportion of undifferentiated T cells produced by the thymus (e.g., naïve T cells). **(D)** Multiple factors act together to shape the immunosenescent TME and exhibit strong immunosuppressive effects.

molecule that can regulate SASP is NOTCH1, which acts synergistically with NF-κB by activating the NOTCH-JAG1 pathway to produce TGF-β to induce aging while inhibiting C/EBPβ (41). In recent years, JAK/STAT pathway activation by signaling molecules including phospholipase A2 receptor 1 (PLA2R1), tumor necrosis factor (TNF)-α, and interferon (IFN)-γ has been shown to also induce SASP production (42, 43). The SASP generated through multiple pathways will profoundly impact immune cell function and ultimately restructure the TME.

Alterations in immune cells are the most complex part of immune aging and produce direct effects. Such alterations are mainly due to two aspects: on the one hand, as mentioned above, the SASP plays a regulatory role in immune cell senescence, and on the other hand, hematopoietic stem cell (HSC) senescence is considered to be the basis of immunosenescence (44). Inflammation is a major factor in HSC aging, as inflammatory factors such as IL-1, IFNα/γ, and TNF-α drive HSC aging (45–47). Aging HSCs and immune cells differentiated from HSCs are increased in numbers and show increased inflammatory factor secretion, reduced self-renewal capacity, diminished homing effects, and reduced energy metabolism (44). Aging immune cells interact with soluble factors, including the SASP, in the TME to

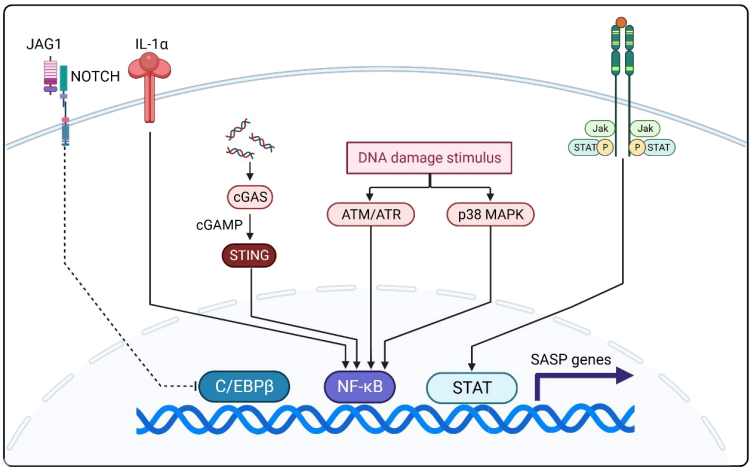

FIGURE 2
NF-κB activation is closely related to SASP regulation and activation. The p38 MAPK, ATM/ATR, and cGAS-STING pathways and aberrant IL-1α activation mediate SASP production by NF-κB. The NOTCH-JAG1 pathway can synergize with NF-κB to activate SASP production by inhibiting C/EBPβ. In recent years, JAK/STAT pathway activation by signaling molecules including phospholipase A2 receptor 1 (PLA2R1), TNF-production by iN-γ has been shown to also induce SASP production.

influence tumor progression and therapeutic efficacy, reflecting the impact of immunosenescence on cancer.

Impact of immunosenescence on TME alterations and tumor progression

The TME consists of various components that can be classified into a non-cancerous cellular fraction, including fibroblasts, neurons, adipocytes, and immune cells (adaptive and innate), and a non-cellular fraction, including ECM, chemokines, growth factors, cytokines, and vesicles (48). According to the characteristics of each component, the TME can also be subdivided into tumor immune microenvironment, tumor biophysical microenvironment, tumor microbe microenvironment, etc. (49–51) We propose the term "immunosenescence microenvironment" as a new TME component to reflect the impact of senescent immune-related cells and signaling molecules in the TME on tumor development (Table 1). By analyzing the individual components of the immunosenescent TME, we can more clearly the delineate the role of immunosenescence on tumor development.

SASP

A large number of SASP signaling molecules originate from the ECM, which plays a microenvironmental regulatory role in the immunosenescent TME, and these molecules determine the overall state of the TME (52). The SASP, derived from senescent cells, plays an important regulatory role in antitumor immunity in the ECM. Its effects are generally mediated by the paracrine way and have both positive and negative effects on tumor progression (53).

Various factors of the interleukin (IL) family involved in the SASP, such as IL-6, IL-8, and IL1α/β, function in microenvironment regulation. The IL-6/JAK/STAT3 signaling pathway drives tumor cell proliferation, invasion and metastasis and suppresses anti-tumor immune responses by reducing tumor antigen expression and decreasing responses to genotoxicity (54–57, 103). IL-6 as well as IL-8 can enhance tumor metastasis by promoting neoangiogenesis (58–61). IL-1β mediates immunosuppression by NLRP3 by inducing the expansion of MDSCs, leading to a decrease in the activity of natural killer (NK) cells and CD8+ T cells and an increase in the number of inhibitory antitumor immune cells, such as regulatory T (Treg) cells and M2 macrophages, in the TME (62, 63). Similarly, IL-1α/β secreted by tumor cells also induces fibroblasts to release pro-tumorigenic chemokines including CXCL9 and CXCL10 (65).

Chemokines involved in the SASP are another important type of regulatory molecules in the TME. CCL5, CXCL1, CXCL2, CXCL5, and CXCL12 are chemokines produced by senescent cells that have opposite effects on tumor development (66). Chemokines such as CCL5 recruit antitumor immune cells to enhance antitumor immunity while recruiting immunosuppressive lymphocytes such as Treg cells, leading to tumor immune escape (64, 67, 68). On the contrary, CXCL5, CXCL1 and CXCL2 have a tumor-promoting effect because they recruit MDSCs, which can play an

TABLE 1 Changes in components of the tumor immunosenescence microenvironment.

Components		Specific changes and impacts	Ref.
SASP	IL-6	Drive tumor cell proliferation, invasion, and metastasis; reduce tumor antigen expression as well as genotoxic stress; promote neoangiogenesis.	(50–54)
	IL-8	Drive tumor cell proliferation, invasion, and metastasis.	(55–57)
	IL-1α/β	Induce the expansion of myeloid-derived suppressor cells (MDSC); decrease the activity of NK cells and CD8+ T cells; increase inhibitory anti-tumor immune cells such as Treg cells and M2 macrophages.	(58–60)
	CCL5	Recruit immunosuppressive lymphocytes such as Treg cells.	(61)
	CXCL1	Recruit MDSCs; reduce CD8+ T cells.	(61–64)
	CXCL2	Recruit MDSCs; reduce CD8+ T cells.	(61–64)
	CXCL5	Recruit MDSCs.	(61, 64–66)
	CXCL12	Attenuates T-cell infiltration and tumor cell killing ability; increases tumor angiogenesis and immune resistance.	(61, 67–69)
	TNF-α	Mediate cell death.	(70)
	VEGF	Promote tumor angiogenesis.	(71)
	GM-CSF	Induce immune cell depletion	(72)
T cell		Competitive grape depletion with Treg cells.	(73, 74)
		Tumor-derived cyclic adenosine monophosphate (cAMP) and some genotoxins of pathogenic bacteria can induce senescence of T cells through DNA damage.	(75–77)
		DNA damage produced by this process is mainly regulated by the MAPK and STAT pathways.	(78–80)
		TNFα and proteases are the main components of SASP secreted by T cells.	(81)
		Down-regulation of CD27, CD28, and the up-regulation of CD57.	(82–85)
		Decreased production of perforin, which reduces cytolysis and tumor cell killing.	(86)
B cell		Deterioration of the inflammatory state of the	(87, 88)

(Continued)

TABLE 1 Continued

Components		Specific changes and impacts	Ref.
		tumor microenvironment by a class of B cells called age-associated B cells (ABCs).	
		IgD CD27 double-negative B cells (DN cells) accumulate in areas of chronic inflammation and exacerbate the inflammatory microenvironment by producing pro-inflammatory factors.	(89, 90)
NK cell		The proportion of CD56dim increases while the proportion of CD56bright decreases.	(91)
		Cytotoxicity was attenuated by decreased perforin production and decreased degranulation.	(92, 93)
Other cells	DCs	The endocytosis, and presentation of antigens by dendritic cells are diminished, while more pro-inflammatory cytokines are secreted.	(94)
		Reduced ability to activate T cells.	(95, 96)
	MDSCs	Produce inflammatory molecules such as IL-10 and TGF-β with inhibitory antigen presentation or immunosuppressive effects.	(97–99)
		Enhancement of oxidative stress in the microenvironment by generation of reactive oxygen species and inhibition of immune checkpoint protein-mediated contact between T cells and tumor cells	(100–102)

immunosuppressive role by suppressing the immune function of lymphocytes through the secretion of Arg-1 and iNOS, and CXCL1 and CXCL2 also reduce the number of CD8+ T cells (69–72, 75, 76). CXCL12 attenuates T-cell infiltration and tumor cell-killing ability and increases tumor angiogenesis and immune resistance via CXCR4/CXCL12 (73, 74, 77).

Other important modulations of tumor progression by the SASP include TNF-α-mediated cell death, vascular endothelial growth factor-promoted tumor angiogenesis, and granulocyte macrophage colony-stimulating factor-induced immune-cell depletion, which inhibits antitumor immunity and promotes tumor progression (78, 79, 104).

T cells

Tumor cells and Treg cells are thought to induce T-cell senescence directly, and some senescent cells secrete SASPs that may have a consistent effect. Tumor-derived cyclic adenosine monophosphate can cause DNA damage and senescence in both CD4+ T cells and CD8+ T cells and immunoglobulin-like transcript 4 and its derivative PIR-B induce T cell senescence by increasing the fatty acid synthesis and lipid accumulation in tumor cells via MAPK ERK1/2 signaling (80). In $CD4^+$ T cells, AMPK can trigger p38 phosphorylation via the scaffolding protein TAB1, which in turn activates the MAPK signaling pathway to induce senescence (81). While in CD8+ T cells, activation of the p38 MAPK pathway leads to the secretion of SASP (82).

Treg cells also play an essential role in inducing T-cell senescence. Treg cells have a selective metabolic profile that accelerates glucose depletion compared to effector T cells and suppresses responding T cells and induces senescence through cross-talk (83). This is because metabolic competition controls DNA damage in effector T cells through ERK1/2 and p38 signaling in cooperation with STAT1 and STAT3, leading to senescence and functional changes that are molecularly distinct from energy and exhaustion (105). Some genotoxins from pathogenic bacteria can also induce $CD4^+$ T-cell senescence through DNA damage, suggesting that the gastrointestinal microbiota may complicate the tumor immunosenescence microenvironment (84).

$CD8^+$ T cells are key immune cells that exert tumor-cell killing; therefore, their senescence significantly affects antitumor capacity. Changes in surface costimulatory molecules such as CD27, CD28, and CD57 reduce the tumor-associated antigen recognition ability of $CD8^+$ T cells, resulting in decreased antitumor activity of $CD8^+$ T cells (85, 86, 106). Further, decreased perforin production by senescent $CD8^+$ T cells reduces cytolysis and decreases their tumor cell-killing function (107). However, a recent study came to the opposite conclusion, suggesting that the effect of aging on the ability of $CD8^+$ T cells to kill tumor cells needs to be further explored (108). Research on T-cell senescence is limited, but some hallmarks of T-cell senescence have been identified (109). The DNA damage produced during the process is mainly regulated by the MAPK and STAT pathways (81, 87, 110). TNFα and proteases are the main SASP components secreted by senescent T cells (82). Changes in T-cell surface proteins, including the downregulation of CD27 and CD28 and the upregulation of CD57, are one of the hallmarks (88, 89). Further, senescent T cells enter cell-cycle arrest after T-cell receptor stimulation (83, 90, 91, 111).

B cells

B cells in TME can produce antibodies that bind to tumor-associated antigens and exert antitumor effects of antigen presentation (92). Their senescence arises predominantly from a decrease in B-cell differentiation and maturation in the bone marrow due to HSC senescence, as well as the reorganization of peripheral B-cell subsets (112, 113).

The impact of senescent B cells on TME is reflected not only in a decrease in antigen-presenting capacity but also in the pro-inflammatory effects derived from a class of B cells known as "age-associated B cells", which are thought to be associated with TNFα secretion (93, 94, 114). IgD CD27 double-negative B cells,

which play an immunosuppressive role, are another type of B cell that expands in aging populations (95). These cells are more likely to aggregate in areas of chronic inflammation due to surface expression of CCR6 and CCR7 after senescence and exacerbate the inflammatory microenvironment through pro-inflammatory factor production, worsening the immunosuppressive function of the TME (96, 97).

NK cells

NK cells are a key innate immune component of the TME that exerts antitumor immunity. These cells are more environmentally sensitive, as evidenced by the fact that passive transfer to environments of different age states can have a significant effect on cytotoxicity (115).

In senescent NK cells, the proportion of $CD56^{dim}$ increases, whereas that of $CD56^{bright}$ declines, which in turn leads to diminished immunocyte function (116). Senescent NK cells appear to enter a silent phase, as cytotoxicity after senescence is attenuated by reduced perforin production and decreased degranulation, and even the production of cytokines such as IFN-γ, MIP-1α, and IL-8 after stimulation is lower than that in nonsenescent NK cells (117–120).

Other cells

Dendritic cells are important antigen-presenting cells that play an important coordinating role in the immune response (121). However, as a result of immune senescence, the endocytosis and presentation of antigens by dendritic cells are diminished, while more pro-inflammatory cytokines are secreted (98). In addition, the ability of dendritic cells to activate T cells is reduced by senescence (99, 100).

MDSCs are a class of immunosuppressive cells recruited by the chronic inflammatory tumor immunosenescence microenvironment (101). MDSCs can inhibit the anti-tumor function of T cells and NK cells by expressing immune checkpoint molecules such as PD-L1 (102, 122, 123). In addition, MDSCs can affect the normal amino acid metabolism of T cells by depriving them of cysteine. This process affects the utilization of tryptophan by T cells and produces the immunosuppressive metabolite l-kynurenine, which ultimately induces T cell loss of function and promotes Treg cell differentiation (124, 125).

MDSCs drive immunosenescence and structure the immunosuppressive microenvironment, which are correlated with their multiple immunosuppressive functions (126). Upon the activation of MDSC amplification due to chronic inflammation caused by tumors and aging, certain chemokines, such as CCL2, CXCL1, and CXCR2, can recruit them to the TME, and this process can be enhanced by the complex gastrointestinal bacterial environment (127–132). Inflammatory molecules in the TME activate the immunosuppressive function of MDSCs mainly via JAK-STAT and NF-κB signaling, causing MDSCs to produce inflammatory molecules such as IL-10 and TGF-β that have antigen presentation-inhibitory or immunosuppressive effects (101, 133, 134). In addition, the immunosuppressive effects of MDSCs are reflected in the enhanced oxidative stress state in the microenvironment via the active generation of reactive oxygen species and the inhibition of immune checkpoint protein-mediated contact between T cells and tumor cells (135–137).

Other cells such as macrophages and neutrophils also exhibit immunosuppressive effects in the immunosenescent TMEby exacerbating chronic inflammation and increasing pro-tumorigenic M2-type macrophages (138). These molecular and cellular changes in the TME in the context of immune senescence promote tumor progression to a certain extent, and more importantly, influence antitumor therapy.

Immunosenescence and tumor therapy

The relationship between immunosenescence and antitumor therapy reflects the fact that there always are two sides to the same coin. On the one hand, for gastrointestinal solid tumors such as colorectal tumors, radiotherapy, chemotherapy, and immunotherapy are important antitumor treatments besides surgery; however, these treatments induce immune senescence, termed "treatment-induced immune senescence."

Radiotherapy and chemotherapy can cause cancer-associated fibroblasts to expand in the TME and exacerbate the inflammatory state, leading to immune senescence (139). In addition, radiotherapy and chemotherapy can accelerate cellular senescence by directly causing DNA damage (140–142). Immunotherapies such as immune checkpoint inhibitors can also induce senescence in TME components by inducing increased production of senescence-related cytokines (143).

Senotherapy strategies targeting immunosenescence

On the other hand, senescence can be exploited as a new target in antitumor therapies (Table 2) (144, 145). This is explained by the fact that senescent cells continue to secrete SASP and lead to the presence of a pro-tumoral tumor microenvironment. Thus, senotherapy refers to the rational use of treatments that target senescent cells to fight tumors (146).

One senotherapeutic strategy is the removal of senescent cells by using anti-aging cell drugs that complement other antitumor therapies by mitigating the negative effects of treatment-induced senescence. Some drugs are used after senescence-inducing cancer therapies to target senescent tumor cells for clearance (147). BCL family inhibitors (e.g., ABT-737 and ABT-263) are representative of this class of drugs; they scavenge senescent cells by inhibiting the anti-apoptotic BCL protein family (148, 149). The tyrosine kinase inhibitor dasatinib combined with quercetin selectively kills senescent cells by inhibiting the pro-survival network that is upregulated in senescent cells (150). In addition, there are immunotherapeutic drugs and antibody-drug combinations that

TABLE 2 Therapeutic strategies to counteract the immunosenescent microenvironment of tumors.

Treatment strategy		Key points	Ref.
Senotherapy	Removal of senescent tumor cells.	Inhibit the senescent cell anti-apoptotic protein BCL family.	(132, 133)
	Extensively removes senescent cells.	Inhibit the pro-survival network that is upregulated in senescent cells	(134)
	Removal of senescent cells using cellular engineering.	Using CAR-T cells to target the characteristic protein urokinase-type fibrinogen activator receptor (uPAR) on the surface of senescent cells.	(137)
	Clearance of tumor cells after active induction of senescence.	Selective induction of TP53-mutated cancer cell senescence using the DNA replication kinase CDC7 allows subsequent inhibitors of mTOR signaling to sustainably suppress and kill tumor cells.	(138)
	Mitigate the negative effects of SASP.	Inhibit SASP-producing pathways such as the previously mentioned p38 MAPK, NF-κB, and JAK/STAT	(139, 140)
Enhancing anti-tumor immune efficacy in the tumor immunosenescence microenvironment		Increased $CD8^+$ T-cell infiltration using photochemotherapy.	(141)
		Δ133p53α TCR-T cell enhances fitness and effector functions of senescent T cells by modulation of p53 isoforms	(142)

can similarly remove senescent cells and synergize with senescence-inducing antitumor treatments (151, 152). Engineered CAR-T cells targeting urokinase-type plasminogen activator receptor, a characteristic protein on the surface of senescent cells, can be used as a therapeutic modality to remove senescent cancer cells (153). Another senotherapeutic strategy is to induce senescence of tumor cells and then target them for elimination. The key to this strategy is to find corresponding drugs that can be targeted to induce tumor-cell senescence. For example, the DNA replication kinase CDC7 can selectively induce senescence in TP53-mutated hepatocellular carcinoma cells, which can subsequently be killed by mTOR signaling inhibitors (154). Mitigating the negative effects of the SASP is another senotherapeutic strategy. This approach is mainly based on the inhibition of SASP-producing pathways, such as the above-mentioned p38 MAPK, NF-κB, and JAK/STAT pathways (155, 156).

Other therapeutic approaches, such as the use of engineered tumor-targeting TCR-T cells or of photochemotherapy to increase immune cell infiltration, have been successful in countering the immunosenescent TME by enhancing antitumor immune efficacy (157, 158).These diverse therapeutic approaches combined can exert a more significant antitumor effect by targeting the immunosenescent environment from different angles.

Emerging biomarkers of immunosenescence in gastrointestinal tumors

Although the molecular biology of immunosenescence has been explored and therapeutic strategies for tumors have been optimized based on its action mechanisms, the timely identification of immunosenescent phenotypes is more clinically relevant, which provides an opportunity for early intervention (159, 160).

Since aging occurs in the immune system, accordingly, the type of biomarker that most readily comes to mind is the senescent phenotype of immune cells. Of these, both $CD8^+$ TEMRA ($CD45RA^+CCR7^-CD28^-CD27^-$) and $CD4^+$ TEMRA are markers of immunosenescence, with increased proportions and absolute numbers in colorectal cancer patients, reflecting low value-added potential and anti-apoptotic properties (161, 162). However, these markers are cell surface receptors and must be assayed using flow cytometry, which requires fresh blood samples. In contrast, the soluble form of immunosenescence markers are more stable and can be measured from stored serum, making them promising candidates as soluble markers of immunosenescence. However, these markers are less specific, as they can also be detected during acute inflammation. The soluble markers sCD163, sCD28 and sCTLA-4 have great potential for application as biomarkers of immunosenescence (163–165). These soluble markers can be detected using ELISA methods, but further studies are needed to compare the diagnostic performance of these markers with the gold standard (cell surface receptor) assay. In addition, some mutations in genes associated with immunosenescence such as PIK3CA, TP53, NF-κB, AMPK, mTOR, and P53 may also serve as biomarkers of the aging process (166–169).

Conclusions

Immunosenescence, as a feature of this stage, increases the risk of infectious diseases and tumors while decreasing antitumor immune functions. This is because immune senescence results in changes in immune organs, immune cells, and the SASP, which all interact with each other. Such changes significantly impact solid tumors of the gastrointestinal tract, such as colorectal cancer, which have a complex TME, and ultimately lead to the formation of an

immunosuppressive tumor immunosenescence microenvironment. In such an environment, immunosuppression is manifested in multiple aspects, including immunosuppressive cell recruitment, increased secretion of inhibitory cytokines, and diminished antitumor immune cell function. These changes allow the tumor to develop and deteriorate, and increase its tendency to invade, and affect antitumor therapy, which in itself induces immune senescence and induces immunosuppressive changes. Therefore, senotherapy, a new therapy targeting immune senescence, has been developed on the basis of various antitumor therapies to remove senescent tumor cells and restore the antitumor capacity of immune cells from a different perspective. However, more in-depth studies on the tumor immune senescence microenvironment need to be conducted to paint a more complete picture of immunosuppression and explore the mechanisms by which immunosenescence attenuates antitumor immunity. This will enable the development of antitumor drugs and different therapeutic strategies for aging characteristics. However, the therapeutic effects remain to be verified in long-term experiments.

Author contributions

TZ: Conceptualization, Investigation, Writing – original draft. RW: Conceptualization, Investigation, Methodology, Writing – original draft. HF: Conceptualization, Investigation, Writing – original draft. YY: Conceptualization, Formal Analysis, Writing – original draft. HJ: Data curation, Writing – original draft. ZP: Data curation, Writing – original draft. LZ: Investigation, Supervision, Writing – review & editing. GY: Funding acquisition, Supervision, Writing – review & editing. WZ: Funding acquisition, Project administration, Supervision, Writing – review & editing.

Funding

The author(s) declare financial support was received for the research, authorship, and/or publication of this article. National Natural Science Foundation of China (82072750, 82203137), Shanghai Sailing Program (21YF1459300), Shanghai Municipal Health Commission Health Industry Clinical Research Project (20224Y0348).

Conflict of interest

The authors declare that the research was conducted in the absence of any commercial or financial relationships that could be construed as a potential conflict of interest.

Publisher's note

References

1. Chang AY, Skirbekk VF, Tyrovolas S, Kassebaum NJ, Dieleman JL. Measuring population ageing: an analysis of the Global Burden of Disease Study 2017. *Lancet Public Health*. (2019) 4:e159–67. doi: 10.1016/S2468-2667(19)30019-2

2. Sung H, Ferlay J, Siegel RL, Laversanne M, Soerjomataram I, Jemal A, et al. Global cancer statistics 2020: GLOBOCAN estimates of incidence and mortality worldwide for 36 cancers in 185 countries. *CA Cancer J Clin*. (2021) 71:209–49. doi: 10.3322/caac.21660

3. Lin L, Li Z, Yan L, Liu Y, Yang H, Li H. Global, regional, and national cancer incidence and death for 29 cancer groups in 2019 and trends analysis of the global cancer burden, 1990-2019. *J Hematol Oncol*. (2021) 14:197. doi: 10.1186/s13045-021-01213-z

4. López-Otín C, Pietrocola F, Roiz-Valle D, Galluzzi L, Kroemer G. Meta-hallmarks of aging and cancer. *Cell Metab*. (2023) 35:12–35. doi: 10.1016/j.cmet.2022.11.001

5. Parkin J, Cohen B. An overview of the immune system. *Lancet*. (2001) 357:1777–89. doi: 10.1016/S0140-6736(00)04904-7

6. de Visser KE, Eichten A, Coussens LM. Paradoxical roles of the immune system during cancer development. *Nat Rev Cancer*. (2006) 6:24–37. doi: 10.1038/nrc1782

7. Lian J, Yue Y, Yu W, Zhang Y. Immunosenescence: a key player in cancer development. *J Hematol Oncol*. (2020) 13:151. doi: 10.1186/s13045-020-00986-z

8. RL WALFORD. THE IMMUNOLOGIC THEORY OF AGING. *Gerontologist*. (1964) 4:195–7. doi: 10.1093/geront/4.4.195

9. Effros RB. Roy Walford and the immunologic theory of aging. *Immun Ageing*. (2005) 2:7. doi: 10.1186/1742-4933-2-7

10. Fulop T, Larbi A, Hirokawa K, Cohen AA, Witkowski JM. Immunosenescence is both functional/adaptive and dysfunctional/maladaptive. *Semin Immunopathol*. (2020) 42:521–36. doi: 10.1007/s00281-020-00818-9

11. Chen J, Zhu H, Yin Y, Jia S, Luo X. Colorectal cancer: Metabolic interactions reshape the tumor microenvironment. *Biochim Biophys Acta Rev Cancer*. (2022) 1877:188797. doi: 10.1016/j.bbcan.2022.188797

12. DePeaux K, Delgoffe GM. Metabolic barriers to cancer immunotherapy. *Nat Rev Immunol*. (2021) 21:785–97. doi: 10.1038/s41577-021-00541-y

13. Weulersse M, Asrir A, Pichler AC, Lemaitre L, Braun M, Carrié N, et al. Eomes-dependent loss of the co-activating receptor CD226 restrains CD8(+) T cell anti-tumor functions and limits the efficacy of cancer immunotherapy. *Immunity*. (2020) 53:824–39.e10. doi: 10.1016/j.immuni.2020.09.006

14. Vignali P, DePeaux K, Watson MJ, Ye C, Ford BR, Lontos K, et al. Hypoxia drives CD39-dependent suppressor function in exhausted T cells to limit antitumor immunity. *Nat Immunol*. (2023) 24:267–79. doi: 10.1038/s41590-022-01379-9

15. Ganesh K. Optimizing immunotherapy for colorectal cancer. *Nat Rev Gastroenterol Hepatol*. (2022) 19:93–4. doi: 10.1038/s41575-021-00569-4

16. Hinshaw DC, Shevde LA. The tumor microenvironment innately modulates cancer progression. *Cancer Res*. (2019) 79:4557–66. doi: 10.1158/0008-5472.CAN-18-3962

17. Jou E, Rodriguez-Rodriguez N, Ferreira AF, Jolin HE, Clark PA, Sawmynaden K, et al. An innate IL-25-ILC2-MDSC axis creates a cancer-permissive microenvironment for Apc mutation-driven intestinal tumorigenesis. *Sci Immunol*. (2022) 7:eabn0175. doi: 10.1126/sciimmunol.abn0175

18. Huang C, Wang X, Wang Y, Feng Y, Wang X, Chen S, et al. Sirpα on tumor-associated myeloid cells restrains antitumor immunity in colorectal cancer independent of its interaction with CD47. *Nat Cancer*. (2024) 5:500–16. doi: 10.1038/s43018-023-00691-z

19. DeBerardinis RJ. Tumor microenvironment, metabolism, and immunotherapy. *N Engl J Med*. (2020) 382:869–71. doi: 10.1056/NEJMcibr1914890

20. Yang L, Li A, Lei Q, Zhang Y. Tumor-intrinsic signaling pathways: key roles in the regulation of the immunosuppressive tumor microenvironment. *J Hematol Oncol*. (2019) 12:125. doi: 10.1186/s13045-019-0804-8

21. Nikolich-Žugich J. The twilight of immunity: emerging concepts in aging of the immune system. *Nat Immunol*. (2018) 19:10–9. doi: 10.1038/s41590-017-0006-x

22. Yousefzadeh MJ, Flores RR, Zhu Y, Schmiechen ZC, Brooks RW, Trussoni CE, et al. An aged immune system drives senescence and ageing of solid organs. *Nature*. (2021) 594:100–5. doi: 10.1038/s41586-021-03547-7

23. Müller L, Andrée M, Moskorz W, Drexler I, Walotka L, Grothmann R, et al. Age-dependent immune response to the biontech/pfizer BNT162b2 coronavirus disease 2019 vaccination. *Clin Infect Dis*. (2021) 73:2065–72. doi: 10.1093/cid/ciab381

24. Akbar AN, Gilroy DW. Aging immunity may exacerbate COVID-19. *Science*. (2020) 369:256–7. doi: 10.1126/science.abb0762

25. Bottazzi B, Riboli E, Mantovani A. Aging, inflammation and cancer. *Semin Immunol*. (2018) 40:74–82. doi: 10.1016/j.smim.2018.10.011

26. Elyahu Y, Monsonego A. Thymus involution sets the clock of the aging T-cell landscape: Implications for declined immunity and tissue repair. *Ageing Res Rev*. (2021) 65:101231. doi: 10.1016/j.arr.2020.101231

27. Xu L, Wei C, Chen Y, Wu Y, Shou X, Chen W, et al. IL-33 induces thymic involution-associated naive T cell aging and impairs host control of severe infection. *Nat Commun*. (2022) 13:6881. doi: 10.1038/s41467-022-34660-4

28. Park JE, Botting RA, Domínguez Conde C, Popescu DM, Lavaert M, Kunz DJ, et al. A cell atlas of human thymic development defines T cell repertoire formation. *Science*. (2020) 367:eaay3224. doi: 10.1126/science.aay3224

29. Deya-Martinez A, Flinn AM, Gennery AR. Neonatal thymectomy in children-accelerating the immunologic clock. *J Allergy Clin Immunol*. (2020) 146:236–43. doi: 10.1016/j.jaci.2020.02.028

30. Santoro A, Bientinesi E, Monti D. Immunosenescence and inflammaging in the aging process: age-related diseases or longevity. *Ageing Res Rev*. (2021) 71:101422. doi: 10.1016/j.arr.2021.101422

31. Faget DV, Ren Q, Stewart SA. Unmasking senescence: context-dependent effects of SASP in cancer. *Nat Rev Cancer*. (2019) 19:439–53. doi: 10.1038/s41568-019-0156-2

32. Coppé JP, Desprez PY, Krtolica A, Campisi J. The senescence-associated secretory phenotype: the dark side of tumor suppression. *Annu Rev Pathol*. (2010) 5:99–118. doi: 10.1146/annurev-pathol-121808-102144

33. Xu Y, Li N, Xiang R, Sun P. Emerging roles of the p38 MAPK and PI3K/AKT/mTOR pathways in oncogene-induced senescence. *Trends Biochem Sci*. (2014) 39:268–76. doi: 10.1016/j.tibs.2014.04.004

34. Freund A, Patil CK, Campisi J. p38MAPK is a novel DNA damage response-independent regulator of the senescence-associated secretory phenotype. *EMBO J*. (2011) 30:1536–48. doi: 10.1038/emboj.2011.69

35. Xinxing Z, Beijia H, Fengting Z, Jie L, Lixiang H, Yangxia Z, et al. p38-mediated FOXN3 phosphorylation modulates lung inflammation and injury through the NF-κB signaling pathway. *Nucleic Acids Res*. (2023) 51:2195–214. doi: 10.1093/nar/gkad057

36. Hao M, Ding C, Peng X, Chen H, Dong L, Zhang Y, et al. Ginseng under forest exerts stronger anti-aging effects compared to garden ginseng probably via regulating PI3K/AKT/mTOR pathway, SIRT1/NF-κB pathway and intestinal flora. *Phytomedicine*. (2022) 105:154365. doi: 10.1016/j.phymed.2022.154365

37. Sayegh S, Fantecelle CH, Laphanuwat P, Subramanian P, Rustin M, Gomes D, et al. Vitamin D(3) inhibits p38 MAPK and senescence-associated inflammatory mediator secretion by senescent fibroblasts that impacts immune responses during ageing. *Aging Cell*. (2024) 23:e14093. doi: 10.1111/acel.14093

38. Kang C, Xu Q, Martin TD, Li MZ, Demaria M, Aron L, et al. The DNA damage response induces inflammation and senescence by inhibiting autophagy of GATA4. *Science*. (2015) 349:aaa5612. doi: 10.1126/science.aaa5612

39. Takahashi A, Loo TM, Okada R, Kamachi F, Watanabe Y, Wakita M, et al. Downregulation of cytoplasmic DNases is implicated in cytoplasmic DNA accumulation and SASP in senescent cells. *Nat Commun*. (2018) 9:1249. doi: 10.1038/s41467-018-03555-8

40. Orjalo AV, Bhaumik D, Gengler BK, Scott GK, Campisi J. Cell surface-bound IL-1alpha is an upstream regulator of the senescence-associated IL-6/IL-8 cytokine network. *Proc Natl Acad Sci U.S.A*. (2009) 106:17031–6. doi: 10.1073/pnas.0905299106

41. Hoare M, Ito Y, Kang TW, Weekes MP, Matheson NJ, Patten DA, et al. NOTCH1 mediates a switch between two distinct secretomes during senescence. *Nat Cell Biol*. (2016) 18:979–92. doi: 10.1038/ncb3397

42. Beaulieu D, Attwe A, Breau M, Lipskaia L, Marcos E, Born E, et al. Phospholipase A2 receptor 1 promotes lung cell senescence and emphysema in obstructive lung disease. *Eur Respir J*. (2021) 58:2000752. doi: 10.1183/13993003.00752-2020

43. Renuka K, Xiaomeng Y, Tamar T, Martin George M, Kirkland James L, Junko O. TNF-α/IFN-γ synergy amplifies senescence-associated inflammation and SARS-CoV-2 receptor expression via hyper-activated JAK/STAT1. *Aging Cell*. (2022) 21:e13646. doi: 10.1111/acel.13646

44. Li X, Li C, Zhang W, Wang Y, Qian P, Huang H. Inflammation and aging: signaling pathways and intervention therapies. *Signal Transduct Target Ther*. (2023) 8:239. doi: 10.1038/s41392-023-01502-8

45. Mitchell CA, Verovskaya EV, Calero-Nieto FJ, Olson OC, Swann JW, Wang X, et al. Stromal niche inflammation mediated by IL-1 signalling is a targetable driver of haematopoietic ageing. *Nat Cell Biol*. (2023) 25:30–41. doi: 10.1038/s41556-022-01053-0

46. Pioli PD, Casero D, Montecino-Rodriguez E, Morrison SL, Dorshkind K. Plasma cells are obligate effectors of enhanced myelopoiesis in aging bone marrow. *Immunity*. (2019) 51:351–66.e6. doi: 10.1016/j.immuni.2019.06.006

47. Chen J, Feng X, Desierto MJ, Keyvanfar K, Young NS. IFN-γ-mediated hematopoietic cell destruction in murine models of immune-mediated bone marrow failure. *Blood*. (2015) 126:2621–31. doi: 10.1182/blood-2015-06-652453

48. Xiao Y, Yu D. Tumor microenvironment as a therapeutic target in cancer. *Pharmacol Ther*. (2021) 221:107753. doi: 10.1016/j.pharmthera.2020.107753

49. Ma J, Huang L, Hu D, Zeng S, Han Y, Shen H. The role of the tumor microbe microenvironment in the tumor immune microenvironment: bystander, activator, or inhibitor. *J Exp Clin Cancer Res*. (2021) 40:327. doi: 10.1186/s13046-021-02128-w

50. Fu T, Dai LJ, Wu SY, Xiao Y, Ma D, Jiang YZ, et al. Spatial architecture of the immune microenvironment orchestrates tumor immunity and therapeutic response. *J Hematol Oncol*. (2021) 14:98. doi: 10.1186/s13045-021-01103-4

51. Zhang T, Jia Y, Yu Y, Zhang B, Xu F, Guo H. Targeting the tumor biophysical microenvironment to reduce resistance to immunotherapy. *Adv Drug Delivery Rev*. (2022) 186:114319. doi: 10.1016/j.addr.2022.114319

52. Huang J, Zhang L, Wan D, Zhou L, Zheng S, Lin S, et al. Extracellular matrix and its therapeutic potential for cancer treatment. *Signal Transduct Target Ther*. (2021) 6:153. doi: 10.1038/s41392-021-00544-0

53. D'Ambrosio M, Gil J. Reshaping of the tumor microenvironment by cellular senescence: An opportunity for senotherapies. *Dev Cell*. (2023) 58:1007–21. doi: 10.1016/j.devcel.2023.05.010

54. Johnson DE, O'Keefe RA, Grandis JR. Targeting the IL-6/JAK/STAT3 signalling axis in cancer. *Nat Rev Clin Oncol*. (2018) 15:234–48. doi: 10.1038/nrclinonc.2018.8

55. Meraviglia-Crivelli D, Villanueva H, Zheleva A, Villalba-Esparza M, Moreno B, Menon AP, et al. IL-6/STAT3 signaling in tumor cells restricts the expression of frameshift-derived neoantigens by SMG1 induction. *Mol Cancer*. (2022) 21:211. doi: 10.1186/s12943-022-01679-6

56. Bent EH, Millán-Barea LR, Zhuang I, Goulet DR, Fröse J, Hemann MT. Microenvironmental IL-6 inhibits anti-cancer immune responses generated by cytotoxic chemotherapy. *Nat Commun*. (2021) 12:6218. doi: 10.1038/s41467-021-26407-4

57. Heichler C, Scheibe K, Schmied A, Geppert CI, Schmid B, Wirtz S, et al. STAT3 activation through IL-6/IL-11 in cancer-associated fibroblasts promotes colorectal tumour development and correlates with poor prognosis. *Gut*. (2020) 69:1269–82. doi: 10.1136/gutjnl-2019-319200

58. Chen RY, Yen CJ, Liu YW, Guo CG, Weng CY, Lai CH, et al. CPAP promotes angiogenesis and metastasis by enhancing STAT3 activity. *Cell Death Differ*. (2020) 27:1259–73. doi: 10.1038/s41418-019-0413-7

59. Sharma I, Singh A, Siraj F, Saxena S. IL-8/CXCR1/2 signalling promotes tumor cell proliferation, invasion and vascular mimicry in glioblastoma. *J BioMed Sci*. (2018) 25:62. doi: 10.1186/s12929-018-0464-y

60. Rolny C, Capparuccia L, Casazza A, Mazzone M, Vallario A, Cignetti A, et al. The tumor suppressor semaphorin 3B triggers a prometastatic program mediated by interleukin 8 and the tumor microenvironment. *J Exp Med*. (2008) 205:1155–71. doi: 10.1084/jem.20072509

61. Fousek K, Horn LA, Palena C. Interleukin-8: A chemokine at the intersection of cancer plasticity, angiogenesis, and immune suppression. *Pharmacol Ther*. (2021) 219:107692. doi: 10.1016/j.pharmthera.2020.107692

62. Tengesdal IW, Dinarello A, Powers NE, Burchill MA, Joosten L, Marchetti C, et al. Tumor NLRP3-derived IL-1β Drives the IL-6/STAT3 axis resulting in sustained MDSC-mediated immunosuppression. *Front Immunol*. (2021) 12:661323. doi: 10.3389/fimmu.2021.661323

63. Tengesdal IW, Menon DR, Osborne DG, Neff CP, Powers NE, Gamboni F, et al. Targeting tumor-derived NLRP3 reduces melanoma progression by limiting MDSCs expansion. *Proc Natl Acad Sci U.S.A*. (2021) 118:e2000915118. doi: 10.1073/pnas.2000915118

64. Korbecki J, Grochans S, Gutowska I, Barczak K, Baranowska-Bosiacka I. CC chemokines in a tumor: A review of pro-cancer and anti-cancer properties of receptors CCR5, CCR6, CCR7, CCR8, CCR9, and CCR10 ligands. *Int J Mol Sci*. (2020) 21:7619. doi: 10.3390/ijms21207619

65. Pein M, Insua-Rodríguez J, Hongu T, Riedel A, Meier J, Wiedmann L, et al. Metastasis-initiating cells induce and exploit a fibroblast niche to fuel Malignant colonization of the lungs. *Nat Commun*. (2020) 11:1494. doi: 10.1038/s41467-020-15188-x

66. Takasugi M, Yoshida Y, Ohtani N. Cellular senescence and the tumour microenvironment. *Mol Oncol*. (2022) 16:3333–51. doi: 10.1002/1878-0261.13268

67. Chang LY, Lin YC, Mahalingam J, Huang CT, Chen TW, Kang CW, et al. Tumor-derived chemokine CCL5 enhances TGF-β-mediated killing of CD8(+) T cells in colon cancer by T-regulatory cells. *Cancer Res*. (2012) 72:1092–102. doi: 10.1158/0008-5472.CAN-11-2493

68. Böttcher JP, Bonavita E, Chakravarty P, Blees H, Cabeza-Cabrerizo M, Sammicheli S, et al. NK Cells Stimulate Recruitment of cDC1 into the Tumor Microenvironment Promoting Cancer Immune Control. *Cell*. (2018) 172:1022–37.e14. doi: 10.1016/j.cell.2018.01.004

69. Taki M, Abiko K, Baba T, Hamanishi J, Yamaguchi K, Murakami R, et al. Snail promotes ovarian cancer progression by recruiting myeloid-derived suppressor cells via CXCR2 ligand upregulation. *Nat Commun*. (2018) 9:1685. doi: 10.1038/s41467-018-03966-7

70. Hu J, Zhao Q, Kong LY, Wang J, Yan J, Xia X, et al. Regulation of tumor immune suppression and cancer cell survival by CXCL1/2 elevation in glioblastoma multiforme. *Sci Adv*. (2021) 7:eabc2511. doi: 10.1126/sciadv.abc2511

71. Chen Y, Kim J, Yang S, Wang H, Wu CJ, Sugimoto H, et al. Type I collagen deletion in αSMA(+) myofibroblasts augments immune suppression and accelerates progression of pancreatic cancer. *Cancer Cell*. (2021) 39:548–565.e6. doi: 10.1016/j.ccell.2021.02.007

72. Sorrentino C, D'Antonio L, Ciummo SL, Fieni C, Landuzzi L, Ruzzi F, et al. CRISPR/Cas9-mediated deletion of Interleukin-30 suppresses IGF1 and CXCL5 and boosts SOCS3 reducing prostate cancer growth and mortality. *J Hematol Oncol*. (2022) 15:145. doi: 10.1186/s13045-022-01357-6

73. Garg B, Giri B, Modi S, Sethi V, Castro I, Umland O, et al. NFκB in pancreatic stellate cells reduces infiltration of tumors by cytotoxic T cells and killing of cancer cells, via up-regulation of CXCL12. *Gastroenterology*. (2018) 155:880–891.e8. doi: 10.1053/j.gastro.2018.05.051

74. Heidegger I, Fotakis G, Offermann A, Goveia J, Daum S, Salcher S, et al. Comprehensive characterization of the prostate tumor microenvironment identifies CXCR4/CXCL12 crosstalk as a novel antiangiogenic therapeutic target in prostate cancer. *Mol Cancer*. (2022) 21:132. doi: 10.1186/s12943-022-01597-7

75. Akiyama T, Yasuda T, Uchihara T, Yasuda-Yoshihara N, Tan B, Yonemura A, et al. Stromal reprogramming through dual PDGFRα/β Blockade boosts the efficacy of anti-PD-1 immunotherapy in fibrotic tumors. *Cancer Res*. (2023) 83:753–70. doi: 10.1158/0008-5472.CAN-22-1890

76. Ding D, Zhong H, Liang R, Lan T, Zhu X, Huang S, et al. Multifunctional nanodrug mediates synergistic photodynamic therapy and MDSCs-targeting immunotherapy of colon cancer. *Adv Sci (Weinh)*. (2021) 8:e2100712. doi: 10.1002/advs.202100712

77. Daniel SK, Seo YD, Pillarisetty VG. The CXCL12-CXCR4/CXCR7 axis as a mechanism of immune resistance in gastrointestinal Malignancies. *Semin Cancer Biol*. (2020) 65:176–88. doi: 10.1016/j.semcancer.2019.12.007

78. Cui Y, Liu H, Wang Z, Zhang H, Tian J, Wang Z, et al. Fructose promotes angiogenesis by improving vascular endothelial cell function and upregulating VEGF expression in cancer cells. *J Exp Clin Cancer Res*. (2023) 42:184. doi: 10.1186/s13046-023-02765-3

79. Arnold IC, Artola-Boran M, Gurtner A, Bertram K, Bauer M, Frangez Z, et al. The GM-CSF-IRF5 signaling axis in eosinophils promotes antitumor immunity through activation of type 1 T cell responses. *J Exp Med*. (2020) 217:e20190706. doi: 10.1084/jem.20190706

80. Gao A, Liu X, Lin W, Wang J, Wang S, Si F, et al. Tumor-derived ILT4 induces T cell senescence and suppresses tumor immunity. *J Immunother Cancer*. (2021) 9:e001536. doi: 10.1136/jitc-2020-001536

81. Lanna A, Henson SM, Escors D, Akbar AN. The kinase p38 activated by the metabolic regulator AMPK and scaffold TAB1 drives the senescence of human T cells. *Nat Immunol*. (2014) 15:965–72. doi: 10.1038/ni.2981

82. Callender LA, Carroll EC, Beal R, Chambers ES, Nourshargh S, Akbar AN, et al. Human CD8(+) EMRA T cells display a senescence-associated secretory phenotype regulated by p38 MAPK. *Aging Cell*. (2018) 17:e12675. doi: 10.1111/acel.12675

83. Ye J, Ma C, Hsueh EC, Dou J, Mo W, Liu S, et al. TLR8 signaling enhances tumor immunity by preventing tumor-induced T-cell senescence. *EMBO Mol Med*. (2014) 6:1294–311. doi: 10.15252/emmm.201403918

84. Mathiasen SL, Gall-Mas L, Pateras IS, Theodorou S, Namini M, Hansen MB, et al. Bacterial genotoxins induce T cell senescence. *Cell Rep*. (2021) 35:109220. doi: 10.1016/j.celrep.2021.109220

85. Chen X, Liu Q, Xiang AP. CD8+CD28- T cells: not only age-related cells but a subset of regulatory T cells. *Cell Mol Immunol*. (2018) 15:734–6. doi: 10.1038/cmi.2017.153

86. Hendriks J, Gravestein LA, Tesselaar K, van Lier RA, Schumacher TN, Borst J. CD27 is required for generation and long-term maintenance of T cell immunity. *Nat Immunol*. (2000) 1:433–40. doi: 10.1038/80877

87. Lanna A, Gomes DC, Muller-Durovic B, McDonnell T, Escors D, Gilroy DW, et al. A sestrin-dependent Erk-Jnk-p38 MAPK activation complex inhibits immunity during aging. *Nat Immunol*. (2017) 18:354–63. doi: 10.1038/ni.3665

88. Daniel L, Tassery M, Lateur C, Thierry A, Herbelin A, Gombert JM, et al. Allotransplantation is associated with exacerbation of CD8 T-cell senescence: the particular place of the innate CD8 T-cell component. *Front Immunol*. (2021) 12:674016. doi: 10.3389/fimmu.2021.674016

89. Fernandes JR, Pinto T, Arruda LB, da Silva C, de Carvalho C, Pinto R, et al. Age-associated phenotypic imbalance in TCD4 and TCD8 cell subsets: comparison between healthy aged, smokers, COPD patients and young adults. *Immun Ageing*. (2022) 19:9. doi: 10.1186/s12979-022-00267-y

90. Liu X, Hoft DF, Peng G. Senescent T cells within suppressive tumor microenvironments: emerging target for tumor immunotherapy. *J Clin Invest*. (2020) 130:1073–83. doi: 10.1172/JCI133679

91. Ye J, Ma C, Hsueh EC, Eickhoff CS, Zhang Y, Varvares MA, et al. Tumor-derived γδ regulatory T cells suppress innate and adaptive immunity through the induction of immunosenescence. *J Immunol*. (2013) 190:2403–14. doi: 10.4049/jimmunol.1202369

92. Laumont CM, Nelson BH. B cells in the tumor microenvironment: Multi-faceted organizers, regulators, and effectors of anti-tumor immunity. *Cancer Cell*. (2023) 41:466–89. doi: 10.1016/j.ccell.2023.02.017

93. Ratliff M, Alter S, Frasca D, Blomberg BB, Riley RL. In senescence, age-associated B cells secrete TNFα and inhibit survival of B-cell precursors. *Aging Cell*. (2013) 12:303–11. doi: 10.1111/acel.12055

94. Qin Y, Cai ML, Jin HZ, Huang W, Zhu C, Bozec A, et al. Age-associated B cells contribute to the pathogenesis of rheumatoid arthritis by inducing activation of fibroblast-like synoviocytes via TNF-α-mediated ERK1/2 and JAK-STAT1 pathways. *Ann Rheum Dis*. (2022) 81:1504–14. doi: 10.1136/ard-2022-222605

95. Chung M, Gong L, Kwong DL, Lee VH, Lee AW, Guan XY, et al. Functions of double-negative B cells in autoimmune diseases, infections, and cancers. *EMBO Mol Med*. (2023) 15:e17341. doi: 10.15252/emmm.202217341

96. Bulati M, Caruso C, Colonna-Romano G. From lymphopoiesis to plasma cells differentiation, the age-related modifications of B cell compartment are influenced by "inflamm-ageing". *Ageing Res Rev*. (2017) 36:125–36. doi: 10.1016/j.arr.2017.04.001

97. Bulati M, Buffa S, Martorana A, Gervasi F, Camarda C, Azzarello DM, et al. Double negative (IgG+IgD-CD27-) B cells are increased in a cohort of moderate-severe Alzheimer's disease patients and show a pro-inflammatory trafficking receptor phenotype. *J Alzheimers Dis*. (2015) 44:1241–51. doi: 10.3233/JAD-142412

98. Agrawal A, Gupta S. Impact of aging on dendritic cell functions in humans. *Ageing Res Rev*. (2011) 10:336–45. doi: 10.1016/j.arr.2010.06.004

99. Grolleau-Julius A, Harning EK, Abernathy LM, Yung RL. Impaired dendritic cell function in aging leads to defective antitumor immunity. *Cancer Res*. (2008) 68:6341–9. doi: 10.1158/0008-5472.CAN-07-5769

100. Gardner JK, Mamotte C, Jackaman C, Nelson DJ. Modulation of dendritic cell and T cell cross-talk during aging: The potential role of checkpoint inhibitory molecules. *Ageing Res Rev*. (2017) 38:40–51. doi: 10.1016/j.arr.2017.07.002

101. Veglia F, Sanseviero E, Gabrilovich DI. Myeloid-derived suppressor cells in the era of increasing myeloid cell diversity. *Nat Rev Immunol*. (2021) 21:485–98. doi: 10.1038/s41577-020-00490-y

102. Hsu J, Hodgins JJ, Marathe M, Nicolai CJ, Bourgeois-Daigneault MC, Trevino TN, et al. Contribution of NK cells to immunotherapy mediated by PD-1/PD-L1 blockade. *J Clin Invest*. (2018) 128:4654–68. doi: 10.1172/JCI99317

103. Jin Y, Kang Y, Wang M, Wu B, Su B, Yin H, et al. Targeting polarized phenotype of microglia via IL6/JAK2/STAT3 signaling to reduce NSCLC brain metastasis. *Signal Transduct Target Ther*. (2022) 7:52. doi: 10.1038/s41392-022-00872-9

104. Habtetsion T, Ding ZC, Pi W, Li T, Lu C, Chen T, et al. Alteration of tumor metabolism by CD4+ T cells leads to TNF-α-dependent intensification of oxidative stress and tumor cell death. *Cell Metab*. (2018) 28:228–42.e6. doi: 10.1016/j.cmet.2018.05.012

105. Liu X, Mo W, Ye J, Li L, Zhang Y, Hsueh EC, et al. Regulatory T cells trigger effector T cell DNA damage and senescence caused by metabolic competition. *Nat Commun*. (2018) 9:249. doi: 10.1038/s41467-017-02689-5

106. Song DG, Ye Q, Poussin M, Harms GM, Figini M, Powell DJ Jr.CD27 costimulation augments the survival and antitumor activity of redirected human T cells *in vivo*. *Blood*. (2012) 119:696–706. doi: 10.1182/blood-2011-03-344275

107. Gong Z, Jia Q, Chen J, Diao X, Gao J, Wang X, et al. Impaired cytolytic activity and loss of clonal neoantigens in elderly patients with lung adenocarcinoma. *J Thorac Oncol*. (2019) 14:857–66. doi: 10.1016/j.jtho.2019.01.024

108. Zöphel D, Angenendt A, Kaschek L, Ravichandran K, Hof C, Janku S, et al. Faster cytotoxicity with age: Increased perforin and granzyme levels in cytotoxic CD8(+) T cells boost cancer cell elimination. *Aging Cell*. (2022) 21:e13668. doi: 10.1111/acel.13668

109. Mittelbrunn M, Kroemer G. Hallmarks of T cell aging. *Nat Immunol*. (2021) 22:687–98. doi: 10.1038/s41590-021-00927-z

110. Wang X, Guo S, Zhou H, Sun Y, Gan J, Zhang Y, et al. Pan-cancer transcriptomic analysis identified six classes of immunosenescence genes revealed molecular links between aging, immune system and cancer. *Genes Immun*. (2023) 24:81–91. doi: 10.1038/s41435-023-00197-9

111. Ye J, Huang X, Hsueh EC, Zhang Q, Ma C, Zhang Y, et al. Human regulatory T cells induce T-lymphocyte senescence. *Blood*. (2012) 120:2021–31. doi: 10.1182/blood-2012-03-416040

112. Frasca D, Diaz A, Romero M, Garcia D, Blomberg BB. B cell immunosenescence. *Annu Rev Cell Dev Biol*. (2020) 36:551–74. doi: 10.1146/annurev-cellbio-011620-034148

113. Yu K, Ravoor A, Malats N, Pineda S, Sirota M. A pan-cancer analysis of tumor-infiltrating B cell repertoires. *Front Immunol*. (2021) 12:790119. doi: 10.3389/fimmu.2021.790119

114. Nickerson KM, Smita S, Hoehn KB, Marinov AD, Thomas KB, Kos JT, et al. Age-associated B cells are heterogeneous and dynamic drivers of autoimmunity in mice. *J Exp Med*. (2023) 220:e20221346. doi: 10.1084/jem.20221346

115. Chiu BC, Martin BE, Stolberg VR, Chensue SW. The host environment is responsible for aging-related functional NK cell deficiency. *J Immunol*. (2013) 191:4688–98. doi: 10.4049/jimmunol.1301625

116. Hazeldine J, Lord JM. The impact of ageing on natural killer cell function and potential consequences for health in older adults. *Ageing Res Rev*. (2013) 12:1069–78. doi: 10.1016/j.arr.2013.04.003

117. Hazeldine J, Hampson P, Lord JM. Reduced release and binding of perforin at the immunological synapse underlies the age-related decline in natural killer cell cytotoxicity. *Aging Cell*. (2012) 11:751–9. doi: 10.1111/j.1474-9726.2012.00839.x

118. Shehata HM, Hoebe K, Chougnet CA. The aged nonhematopoietic environment impairs natural killer cell maturation and function. *Aging Cell*. (2015) 14:191–9. doi: 10.1111/acel.12303

119. Mariani E, Pulsatelli L, Meneghetti A, Dolzani P, Mazzetti I, Neri S, et al. Different IL-8 production by T and NK lymphocytes in elderly subjects. *Mech Ageing Dev*. (2001) 122:1383–95. doi: 10.1016/S0047-6374(01)00270-6

120. Mariani E, Meneghetti A, Neri S, Ravaglia G, Forti P, Cattini L, et al. Chemokine production by natural killer cells from nonagenarians. *Eur J Immunol*. (2002) 32:1524–9. doi: 10.1002/1521-4141(200206)32:6<1524::AID-IMMU1524>3.0.CO;2-E

121. Wang Y, Xiang Y, Xin VW, Wang XW, Peng XC, Liu XQ, et al. Dendritic cell biology and its role in tumor immunotherapy. *J Hematol Oncol*. (2020) 13:107. doi: 10.1186/s13045-020-00939-6

122. Sun R, Xiong Y, Liu H, Gao C, Su L, Weng J, et al. Tumor-associated neutrophils suppress antitumor immunity of NK cells through the PD-L1/PD-1 axis. *Transl Oncol*. (2020) 13:100825. doi: 10.1016/j.tranon.2020.100825

123. Fleming V, Hu X, Weller C, Weber R, Groth C, Riester Z, et al. Melanoma extracellular vesicles generate immunosuppressive myeloid cells by upregulating PD-L1 via TLR4 signaling. *Cancer Res*. (2019) 79:4715–28. doi: 10.1158/0008-5472.CAN-19-0053

124. Mezrich JD, Fechner JH, Zhang X, Johnson BP, Burlingham WJ, Bradfield CA. An interaction between kynurenine and the aryl hydrocarbon receptor can generate regulatory T cells. *J Immunol*. (2010) 185:3190–8. doi: 10.4049/jimmunol.0903670

125. Frumento G, Rotondo R, Tonetti M, Damonte G, Benatti U, Ferrara GB. Tryptophan-derived catabolites are responsible for inhibition of T and natural killer cell proliferation induced by indoleamine 2,3-dioxygenase. *J Exp Med*. (2002) 196:459–68. doi: 10.1084/jem.20020121

126. Salminen A, Kaarniranta K, Kauppinen A. Immunosenescence: the potential role of myeloid-derived suppressor cells (MDSC) in age-related immune deficiency. *Cell Mol Life Sci*. (2019) 76:1901–18. doi: 10.1007/s00018-019-03048-x

127. Liao W, Overman MJ, Boutin AT, Shang X, Zhao D, Dey P, et al. KRAS-IRF2 axis drives immune suppression and immune therapy resistance in colorectal cancer. *Cancer Cell*. (2019) 35:559–572.e7. doi: 10.1016/j.ccell.2019.02.008

128. Chen H, Pan Y, Zhou Q, Liang C, Wong CC, Zhou Y, et al. METTL3 inhibits antitumor immunity by targeting m(6)A-BHLHE41-CXCL1/CXCR2 axis to promote colorectal cancer. *Gastroenterology*. (2022) 163:891–907. doi: 10.1053/j.gastro.2022.06.024

129. Wu P, Wu D, Ni C, Ye J, Chen W, Hu G, et al. γδT17 cells promote the accumulation and expansion of myeloid-derived suppressor cells in human colorectal cancer. *Immunity*. (2014) 40:785–800. doi: 10.1016/j.immuni.2014.03.013

130. Chun E, Lavoie S, Michaud M, Gallini CA, Kim J, Soucy G, et al. CCL2 promotes colorectal carcinogenesis by enhancing polymorphonuclear myeloid-derived suppressor cell population and function. *Cell Rep*. (2015) 12:244–57. doi: 10.1016/j.celrep.2015.06.024

131. Schneider KM, Mohs A, Gui W, Galvez E, Candels LS, Hoenicke L, et al. Imbalanced gut microbiota fuels hepatocellular carcinoma development by shaping the hepatic inflammatory microenvironment. *Nat Commun*. (2022) 13:3964. doi: 10.1038/s41467-022-31312-5

132. Zhang Z, Zheng Y, Chen Y, Yin Y, Chen Y, Chen Q, et al. Gut fungi enhances immunosuppressive function of myeloid-derived suppressor cells by activating PKM2-dependent glycolysis to promote colorectal tumorigenesis. *Exp Hematol Oncol*. (2022) 11:88. doi: 10.1186/s40164-022-00334-6

133. Ibrahim ML, Klement JD, Lu C, Redd PS, Xiao W, Yang D, et al. Myeloid-derived suppressor cells produce IL-10 to elicit DNMT3b-dependent IRF8 silencing to promote colitis-associated colon tumorigenesis. *Cell Rep*. (2018) 25:3036–3046.e6. doi: 10.1016/j.celrep.2018.11.050

134. Condamine T, Gabrilovich DI. Molecular mechanisms regulating myeloid-derived suppressor cell differentiation and function. *Trends Immunol*. (2011) 32:19–25. doi: 10.1016/j.it.2010.10.002

135. Redd PS, Ibrahim ML, Klement JD, Sharman SK, Paschall AV, Yang D, et al. SETD1B activates iNOS expression in myeloid-derived suppressor cells. *Cancer Res*. (2017) 77:2834–43. doi: 10.1158/0008-5472.CAN-16-2238

136. Conche C, Finkelmeier F, Pešić M, Nicolas AM, Böttger TW, Kennel KB, et al. Combining ferroptosis induction with MDSC blockade renders primary tumours and metastases in liver sensitive to immune checkpoint blockade. *Gut*. (2023) 72:1774–1782. doi: 10.1136/gutjnl-2022-327909

137. Ohl K, Tenbrock K. Reactive oxygen species as regulators of MDSC-mediated immune suppression. *Front Immunol*. (2018) 9:2499. doi: 10.3389/fimmu.2018.02499

138. Jackaman C, Tomay F, Duong L, Abdol Razak NB, Pixley FJ, Metharom P, et al. Aging and cancer: The role of macrophages and neutrophils. *Ageing Res Rev*. (2017) 36:105–16. doi: 10.1016/j.arr.2017.03.008

139. Nicolas AM, Pesic M, Engel E, Ziegler PK, Diefenhardt M, Kennel KB, et al. Inflammatory fibroblasts mediate resistance to neoadjuvant therapy in rectal cancer. *Cancer Cell*. (2022) 40:168–184.e13. doi: 10.1016/j.ccell.2022.01.004

140. Zhao Y, Tyshkovskiy A, Muñoz-Espín D, Tian X, Serrano M, de Magalhaes JP, et al. Naked mole rats can undergo developmental, oncogene-induced and DNA damage-induced cellular senescence. *Proc Natl Acad Sci U.S.A*. (2018) 115:1801–6. doi: 10.1073/pnas.1721160115

141. Han Z, Wei W, Dunaway S, Darnowski JW, Calabresi P, Sedivy J, et al. Role of p21 in apoptosis and senescence of human colon cancer cells treated with camptothecin. *J Biol Chem*. (2002) 277:17154–60. doi: 10.1074/jbc.M112401200

142. Jaiswal AS, Panda H, Law BK, Sharma J, Jani J, Hromas R, et al. NSC666715 and its analogs inhibit strand-displacement activity of DNA polymerase β and potentiate temozolomide-induced DNA damage, senescence and apoptosis in colorectal cancer cells. *PloS One*. (2015) 10:e0123808. doi: 10.1371/journal.pone.0123808

143. Ahmetlic F, Fauser J, Riedel T, Bauer V, Flessner C, Hömberg N, et al. Therapy of lymphoma by immune checkpoint inhibitors: the role of T cells, NK cells and cytokine-induced tumor senescence. *J Immunother Cancer*. (2021) 9:e001660. doi: 10.1136/jitc-2020-001660

144. Prasanna PG, Citrin DE, Hildesheim J, Ahmed MM, Venkatachalam S, Riscuta G, et al. Therapy-induced senescence: opportunities to improve anticancer therapy. *J Natl Cancer Inst*. (2021) 113:1285–98. doi: 10.1093/jnci/djab064

145. Wang B, Kohli J, Demaria M. Senescent cells in cancer therapy: friends or foes. *Trends Cancer*. (2020) 6:838–57. doi: 10.1016/j.trecan.2020.05.004

146. Sikora E, Bielak-Zmijewska A, Mosieniak G. Targeting normal and cancer senescent cells as a strategy of senotherapy. *Ageing Res Rev*. (2019) 55:100941. doi: 10.1016/j.arr.2019.100941

147. Wang L, Lankhorst L, Bernards R. Exploiting senescence for the treatment of cancer. *Nat Rev Cancer*. (2022) 22:340–55. doi: 10.1038/s41568-022-00450-9

148. Yosef R, Pilpel N, Tokarsky-Amiel R, Biran A, Ovadya Y, Cohen S, et al. Directed elimination of senescent cells by inhibition of BCL-W and BCL-XL. *Nat Commun*. (2016) 7:11190. doi: 10.1038/ncomms11190

149. Chang J, Wang Y, Shao L, Laberge RM, Demaria M, Campisi J, et al. Clearance of senescent cells by ABT263 rejuvenates aged hematopoietic stem cells in mice. *Nat Med*. (2016) 22:78–83. doi: 10.1038/nm.4010

150. Zhu Y, Tchkonia T, Pirtskhalava T, Gower AC, Ding H, Giorgadze N, et al. The Achilles' heel of senescent cells: from transcriptome to senolytic drugs. *Aging Cell*. (2015) 14:644–58. doi: 10.1111/acel.12344

151. Duro-Sánchez S, Nadal-Serrano M, Lalinde-Gutiérrez M, Arenas EJ, Bernadó Morales C, Morancho B, et al. Therapy-induced senescence enhances the efficacy of HER2-targeted antibody-drug conjugates in breast cancer. *Cancer Res*. (2022) 82:4670–9. doi: 10.1158/0008-5472.CAN-22-0787

152. Chaturvedi P, George V, Shrestha N, Wang M, Dee MJ, Zhu X, et al. Immunotherapeutic HCW9218 augments anti-tumor activity of chemotherapy via NK cell-mediated reduction of therapy-induced senescent cells. *Mol Ther*. (2022) 30:1171–87. doi: 10.1016/j.ymthe.2022.01.025

153. Amor C, Feucht J, Leibold J, Ho YJ, Zhu C, Alonso-Curbelo D, et al. Senolytic CAR T cells reverse senescence-associated pathologies. *Nature*. (2020) 583:127–32. doi: 10.1038/s41586-020-2403-9

154. Wang C, Vegna S, Jin H, Benedict B, Lieftink C, Ramirez C, et al. Inducing and exploiting vulnerabilities for the treatment of liver cancer. *Nature*. (2019) 574:268–72. doi: 10.1038/s41586-019-1607-3

155. Acosta JC, O'Loghlen A, Banito A, Guijarro MV, Augert A, Raguz S, et al. Chemokine signaling via the CXCR2 receptor reinforces senescence. *Cell*. (2008) 133:1006–18. doi: 10.1016/j.cell.2008.03.038

156. Toso A, Revandkar A, Di Mitri D, Guccini I, Proietti M, Sarti M, et al. Enhancing chemotherapy efficacy in Pten-deficient prostate tumors by activating the senescence-associated antitumor immunity. *Cell Rep*. (2014) 9:75–89. doi: 10.1016/j.celrep.2014.08.044

157. Sui D, Li C, Tang X, Meng X, Ding J, Yang Q, et al. Sialic acid-mediated photochemotherapy enhances infiltration of CD8(+) T cells from tumor-draining lymph nodes into tumors of immunosenescent mice. *Acta Pharm Sin B*. (2023) 13:425–39. doi: 10.1016/j.apsb.2022.06.005

158. Legscha KJ, Antunes Ferreira E, Chamoun A, Lang A, Awwad M, Ton G, et al. Δ133p53α enhances metabolic and cellular fitness of TCR-engineered T cells and promotes superior antitumor immunity. *J Immunother Cancer*. (2021) 9:e001846. doi: 10.1136/jitc-2020-001846

159. Pawelec G. The human immunosenescence phenotype: does it exist. *Semin Immunopathol*. (2020) 42:537–44. doi: 10.1007/s00281-020-00810-3

160. Bao H, Cao J, Chen M, Chen M, Chen W, Chen X, et al. Biomarkers of aging. *Sci China Life Sci*. (2023) 66:893–1066. doi: 10.1007/s11427-023-2305-0

161. Salumets A, Tserel L, Rumm AP, Türk L, Kingo K, Saks K, et al. Epigenetic quantification of immunosenescent CD8(+) TEMRA cells in human blood. *Aging Cell*. (2022) 21:e13607. doi: 10.1111/acel.13607

162. Zhang L, Chen X, Zu S, Lu Y. Characteristics of circulating adaptive immune cells in patients with colorectal cancer. *Sci Rep*. (2022) 12:18166. doi: 10.1038/s41598-022-23190-0

163. Aprilia A, Handono K, Sujuti H, Sabarudin A, Winaris N. sCD163, sCD28, sCD80, and sCTLA-4 as soluble marker candidates for detecting immunosenescence. *Immun Ageing*. (2024) 21:9. doi: 10.1186/s12979-023-00405-0

164. Arikan S, Gümüş A, Küçükhüseyin Ö, Coşkun C, Turan S, Cacina C, et al. The effect of CTLA-4 and CD28 gene variants and circulating protein levels in patients with gastric cancer. *Turk J Biochem*. (2017) 42(5):551–8. doi: 10.1515/tjb-2017-0024

165. Ding D, Song Y, Yao Y, Zhang S. Preoperative serum macrophage activated biomarkers soluble mannose receptor (sMR) and soluble haemoglobin scavenger receptor (sCD163), as novel markers for the diagnosis and prognosis of gastric cancer. *Oncol Lett*. (2017) 14:2982–90. doi: 10.3892/ol.2017.6547

166. Al-Danakh A, Safi M, Jian Y, Yang L, Zhu X, Chen Q, et al. Aging-related biomarker discovery in the era of immune checkpoint inhibitors for cancer patients. *Front Immunol*. (2024) 15:1348189. doi: 10.3389/fimmu.2024.1348189

167. Shah Y, Verma A, Marderstein AR, White J, Bhinder B, Garcia Medina JS, et al. Pan-cancer analysis reveals molecular patterns associated with age. *Cell Rep*. (2021) 37:110100. doi: 10.1016/j.celrep.2021.110100

168. Lee W, Wang Z, Saffern M, Jun T, Huang KL. Genomic and molecular features distinguish young adult cancer from later-onset cancer. *Cell Rep*. (2021) 37:110005. doi: 10.1016/j.celrep.2021.110005

169. Li CH, Haider S, Boutros PC. Age influences on the molecular presentation of tumours. *Nat Commun*. (2022) 13:208. doi: 10.1038/s41467-021-27889-y

frontiers | Frontiers in Molecular Biosciences

TYPE Original Research
PUBLISHED 30 July 2024
DOI 10.3389/fmolb.2024.1449197

OPEN ACCESS

EDITED BY
Valeria Guglielmi,
University of Rome Tor Vergata; Unit of Internal Medicine and Obesity Center, Italy

REVIEWED BY
Jolanta Dardzińska,
Medical University of Gdańsk, Poland
Maria Perticone,
University of Magna Graecia, Italy
Valeria Simonelli,
National Institute of Health (ISS), Italy

*CORRESPONDENCE
Alessio Molfino,
alessio.molfino@uniroma1.it

†These authors have contributed equally to this work and share first authorship

RECEIVED 14 June 2024
ACCEPTED 12 July 2024
PUBLISHED 30 July 2024

CITATION
Tambaro F, Imbimbo G, Pace V, Amabile MI, Rizzo V, Orlando S, Lauteri G, Ramaccini C, Catalano C, Nigri G, Muscaritoli M and Molfino A (2024), Circulating adipose-tissue miRNAs in gastrointestinal cancer patients and their association with the level and type of adiposity at body composition analysis. *Front. Mol. Biosci.* 11:1449197. doi: 10.3389/fmolb.2024.1449197

Circulating adipose-tissue miRNAs in gastrointestinal cancer patients and their association with the level and type of adiposity at body composition analysis

Federica Tambaro[1†], Giovanni Imbimbo[1†], Valentina Pace[1], Maria Ida Amabile[2], Veronica Rizzo[3], Simona Orlando[1], Giulia Lauteri[4], Cesarina Ramaccini[1], Carlo Catalano[3], Giuseppe Nigri[4], Maurizio Muscaritoli[1] and Alessio Molfino[1*]

[1]Deparment of Translational and Precision Medicine, Sapienza University of Rome, Rome, Italy, [2]Department of Surgery, Sapienza University of Rome, Rome, Italy, [3]Department of Radiological, Oncological and Pathological Sciences, Sapienza University of Rome, Rome, Italy, [4]Department of Medical and Surgical Sciences and Translational Medicine, Sapienza University of Rome, Rome, Italy

Background: Adipose tissue (AT) wasting in cancer is an early catabolic event with negative impact on outcomes. Circulating miRNAs may promote body weight loss and cachexia. We measured circulating miRNAs linked to AT alterations and compared their levels between i) gastrointestinal (GI) cancer patients and controls, ii) cachectic and non-cachectic cancer patients, and iii) according to adiposity level and its distribution.

Methods: Patients with GI cancer and subjects with benign diseases as controls were considered. Cachexia was assessed and adiposity evaluated by CT-scan for subcutaneous AT area (SAT), visceral AT area and the total AT area (TAT). MiRNAs involved were measured in plasma by RT-qPCR.

Results: 37 naïve GI cancer patients and 14 controls were enrolled. Patients with cachexia presented with lower SAT compared to non-cachectic ($p < 0.05$). In cancer patients, we found higher levels of miR-26a, miR-128, miR-155 and miR-181a vs. controls ($p < 0.05$). Cancer patients with BMI < 25 kg/m^2 showed higher levels of miR-26a vs. those with BMI ≥ 25 ($p = 0.035$). MiR-26a and miR-181a were higher in cachectic and non-cachectic vs. controls ($p < 0.05$). Differences between cachectic and controls were confirmed for miR-155 ($p < 0.001$) but not between non-cachectic vs. control ($p = 0.072$). MiR-155 was higher in cachectic patients with low TAT vs. those without cachexia and high TAT ($p = 0.036$).

Conclusion: Our data confirm a modulation of specific and different miRNAs involved in AT metabolism in cancer and cachexia. MiR-155 levels were higher in patients presenting with cachexia and low adiposity with

implications in the pathogenic mechanisms and clinical consequences of GI cancer patients.

KEYWORDS

adiposity, miRNAs, cachexia, cancer, CT-scan, body composition

1 Introduction

In the last years, adipose tissue derangements were indicated as active promoters of cachexia in cancer patients, with potential negative impact on patient's survival (Al-Sawaf et al., 2023). Strong evidence showed that adipose tissue wasting often precedes the clinical diagnosis of cancer representing an early event during the disease (Babic et al., 2023). Importantly, adipose tissue has several functions other than energy storing, including release of endocrine hormones, promoting inflammation and regulating the expression of different genes, as well as energy expenditure (Cypess, 2022). In parallel, modifications in terms of quantity and quality of adipose tissue were found in the cancer cachexia phenotype (Molfino et al., 2023a). Recently, data showed that patients with gastrointestinal cancer undergoing surgery for cancer resection presented deep histomorphological alterations of adipose tissue, as well as changes in molecular markers of browning and lipolysis (Molfino et al., 2022a; Molfino et al., 2023a; Tambaro et al., 2024). Also, Taylor J et al. (2023) evaluated the cancer capacity to manipulate the endothelium in white adipose tissue and found that the intracellular pathway signaling promoting adipose tissue wasting was modulated. In this light, cancer-released factors are promising agents to target for the treatment of cancer cachexia. Among them, miRNAs were extensively studied for their capacity to modulate gene expression. Also, miRNAs may act distally being transported in exosomes as endocrine factors and possibly serving as biomarkers in some clinical settings, including cancer (Belli et al., 2021). Importantly, Tomou T et al. showed that adipose tissue represents an important source of circulating exosomal miRNAs, acting as adipokines (Thomou et al., 2017).

In cancer, some miRNAs were found to be potentially implicated in adipose tissue metabolism and wasting. Recently, among others, miR-26a-5p, miR-128, miR-144, miR-181a-5p, and miR-155 were identified as potential regulator of adipose tissue metabolism, such as lipolysis, browning of WAT, and adipogenesis (Tao et al., 2015; Chen et al., 2018; Kim et al., 2020; Hongfang et al., 2023), all phenomena deeply involved in the development of cancer cachexia and therefore of interest in the setting of gastrointestinal cancer.

However, data on the association between these miRNAs and cancer cachexia and adipose tissue wasting in humans are still scanty or lacking.

For this reason, by this study we aimed to evaluate differences in specific circulating miRNAs profile, linked to adipose tissue alterations between i) cancer patients and controls, ii) cachectic and non-cachectic cancer patients, and iii) according to adiposity level (low or high) and distribution assessed by CT-scan.

2 Materials and methods

2.1 Study design and participant's enrollment

We conducted a cross-sectional study on patients with a new diagnosis of gastrointestinal cancer (gastric, colon and pancreatic cancer), known to be frequently associated with cachexia (Baracos et al., 2018), eligible for surgical tumor resection, and controls undergoing surgery for non-malignant diseases. The enrollment was carried out at the Department of Medical and Surgical Science of Sapienza University of Rome, Italy. The experiments were conducted at the Department of Translational and Precision Medicine of Sapienza University of Rome, Italy.

The inclusion criteria of this study were age ≥18 years; recent diagnosis of cancer (≤4 weeks); not having received anticancer or anti-inflammatory treatments before surgery; the ability to provide signed informed consent. Exclusion criteria were the presence of coexisting conditions inducing malnutrition such as infections, liver failure, renal failure, heart failure, rheumatologic disorders, clear signs of malabsorption or intestinal occlusion, as well as dysphagia. The study was conducted according to the Declaration of Helsinki and approved by the local Ethics Committee (Sapienza University, Azienda Sant'Andrea Hospital, Rome, Italy—prot. n. 167_2017). Written informed consent was obtained by all the participants enrolled in the study.

2.2 Clinical parameters, nutritional status and body composition analysis for adiposity

At first study visit, we collected demographic information and patient's medical history, as well as data on the staging and histology of the cancer. We registered body weight (kg) and height (m), calculated the body mass index (BMI, kg/m^2) and asked for usual weight and unvoluntary body weight loss in the previous 6 months. Cachexia was diagnosed according to the Fearon's criteria (Fearon et al., 2011).

In fasting condition, we obtained blood samples in EDTA tubes to measure inflammatory and nutritional biomarkers, such as serum C-reactive protein (CRP) and albumin with standard laboratory techniques.

Using CT scans, we measured the abdominal fat area at the level of the third lumbar vertebra (L3), quantifying both the total adipose tissue (TAT) and visceral adipose tissue (VAT), as previously shown (Erdem et al., 2019; Molfino et al., 2022b). The SAT area at the same level was calculated, subtracting VAT from TAT. We defined high or low level of adiposity based on the median values of SAT, VAT and TAT (over the median: high; below the median: low). This

10.3389/fmolb.2024.1449197

TABLE 1 Participant's characteristics.

Parameters	Cancer patients (n = 37)	Controls (n = 14)
Age, years *	71.6 ± 11.9	58.1 ± 14.2
Male, n (%)	23 (62)	8 (57)
Female, n (%)	14 (38)	6 (43)
Actual weight, kg	70.2 ± 12.6	72.0 ± 11.2
BMI, kg/m^2	24.1 ± 3.8	25.0 ± 3.3
Cachexia, n (%)	18 (49)	—
Blood parameters		
Hemoglobin, g/dL	12.0 ± 2.1	13.1 ± 1.8
C-reactive protein, mg/dL	4.8 (0.2; 11.7)	1.7 (0.6; 4.7)
Albumin, g/dL	3.4 ± 0.6	3.7 ± 0.4
Type of GI, n (%)		
Colon	32 (87)	—
Gastric	4 (11)	—
Pancreatic	1 (3)	—
Stage of the disease, n (%)		
I-II	24 (65)	—
III-IV	13 (35)	—

Variables are shown as mean ± SD and as median (inter-quartile range) for non-normally distributed values. No differences were shown between cancer patients and controls with exception of age ($^*p = 0.001$). Abbreviations: BMI, body mass index.

TABLE 2 Differences between cachectic and non-cachectic cancer patients in clinical and adiposity parameters.

Parameters	Cachexia (n = 18)	No cachexia (n = 19)
Age, years	72.8 ± 12.6	70.4 ± 11.4
Male, n (%)	13 (72)	10 (53)
Female, n (%)	5 (28)	9 (47)
BMI, kg/m^2 *	22.8 ± 3.8	25.3 ± 3.6
Stage of the diseases, n (%)		
I-II	10 (56)	14 (74)
III-IV	8 (44)	5 (26)
Body composition parameters		
SAT, cm$^{2\#}$	157.6 ± 63.7	206.2 ± 73.5
VAT, cm^2	145.8 ± 93.0	159.3 ± 82.3
TAT, cm^2	303.5 ± 149.1	365.5 ± 138.7

No differences were shown between cachectic and non-cachectic with exception of BMI, and SAT ($^*p = 0.044$; $\#p = 0.039$). Abbreviations: BMI, body mass index; SAT, subcutaneous adipose tissue area; VAT, visceral adipose tissue area; TAT, total adipose tissue area.

approach was previously implemented in the setting of adipose tissue wasting (Abdallah et al., 2023).

OsiriX Lite (v11.0.3, Bernex, Switzerland) was used for the abdominal fat composition analysis.

2.3 Plasma samples collection

To analyze circulating miRNAs profiles, fasting blood samples were collected prior to the surgical procedure in EDTA Vacutainer® tubes and centrifuged at 3,000 rpm for 15 min at 4°C. Supernatant plasma was immediately aliquoted into cryovials and stored at −80°C until further analysis.

2.4 Extraction, quantification and pre-amplification of circulating miRNAs

Total RNA was extracted from plasma samples (250 µL/sample) using miRNeasy Serum/Plasma Kit (Qiagen, Germantown, MD, United States) according to the manufacturer's instructions. RNA quantification was performed using Multiskan Sky spectrophotometer (Thermo Fisher Scientific, Waltham, MA, United States). cDNA was synthetized from 10 ng of total RNA using the TaqMan Advanced miRNA cDNA Synthesis kit (Applied Biosystems, Thermo Fisher Scientific, Waltham, MA, United States) following the manufacturer's instructions.

2.5 Analysis of circulating miRNAs profiles

Quantitative real-time PCR was performed with TaqMan Fast Advanced Master Mix (Applied Biosystems, Thermo Fisher Scientific, Waltham, MA, United States), using the QuantStudio® Real Time PCR (Applied Biosystems, Thermo Fisher Scientific, Waltham, MA, United States). Quantification was performed using the following specific TaqMan miRNA Assay (Applied Biosystems, Thermo Fisher Scientific, Waltham, MA, United States) probes: hsa-miR-26a-5p (478926_mir); hsa-miR-128-3p (477892_mir); hsa-miR-144-3p (477913_mir); has-miR-155-3p (477926_mir); hsa-miR-181a-5p (477857_mir). Data were normalized to hsa-miR-16-5p (477860_mir) used as the internal control. Resulting data were analyzed using SDS2.4 Software (Applied Biosystems, Bedford, MA, United States), and fold-change was determined by using the $2^{-\Delta\Delta CT}$, as previously described (Schmittgen and Livak, 2008). All reactions were performed using three biological replicates and all the experiments were performed in duplicate.

2.6 Statistical analyses

Data are presented as the mean ± standard deviation (SD) or standard error of the mean (SEM) and median with interquartile

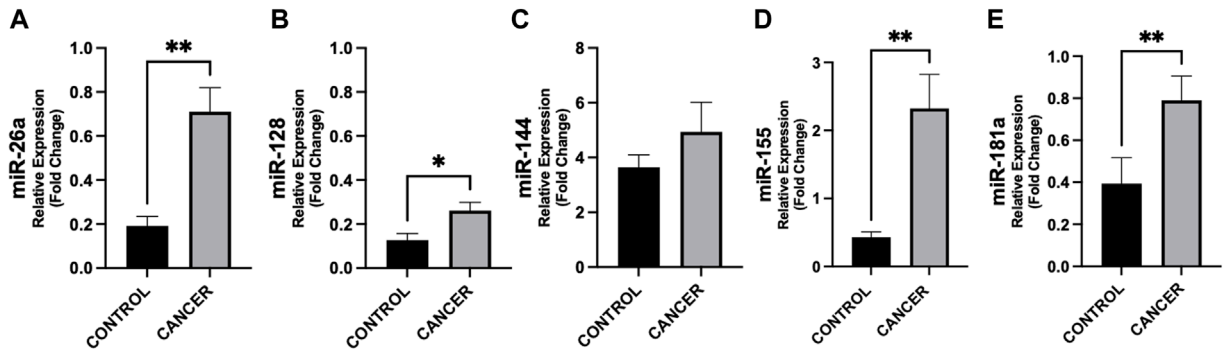

FIGURE 1
Differences in circulating miRNAs between cancer patients and controls. Circulating miRNAs levels were analyzed by quantitative Real Time PCR from gastrointestinal cancer patients (n = 37) and control group (n = 14). Data show higher expression of miR-26a ($p = 0.002$) **(A)**, –128 ($p = 0.047$) **(B)**, –155 ($p = 0.004$) **(D)**, and –181a ($p = 0.007$) **(E)** in cancer with respect to controls. No difference was observed in miR-144 levels in cancer patients vs. controls **(C)**. Data were normalized against the miR-16 from two biological replicates. $^{*}p < 0.05$, $^{**}p \leq 0.01$, $^{***}p \leq 0.001$.

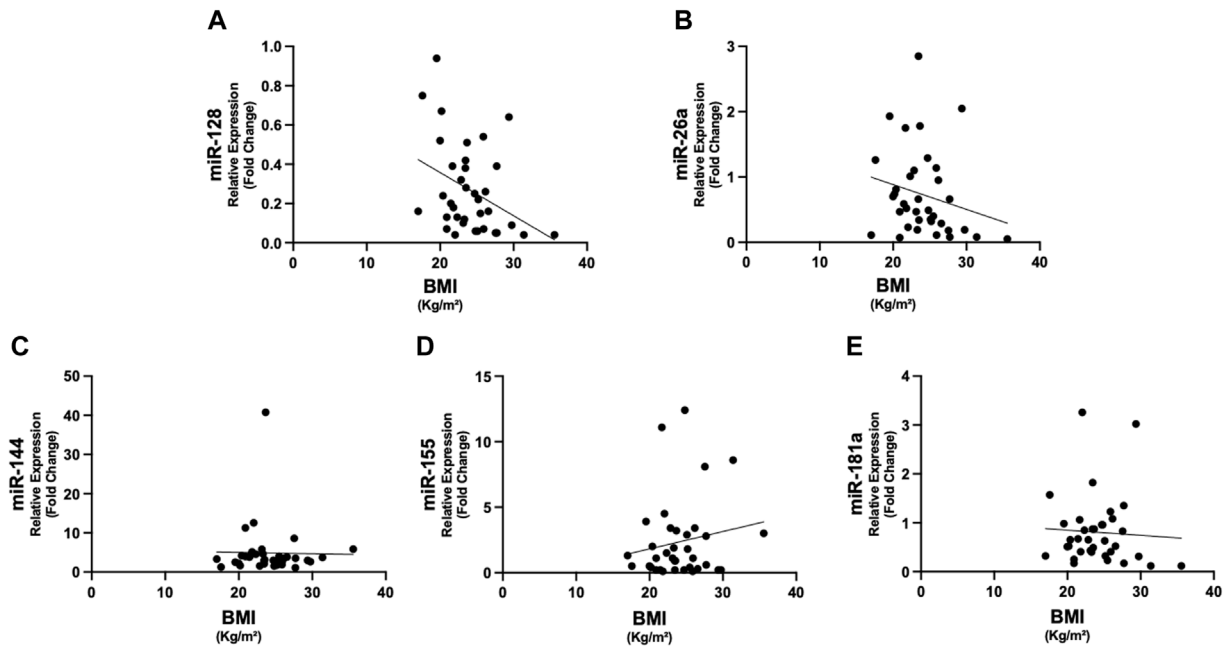

FIGURE 2
Correlations between circulating miRNAs and BMI in cancer patients. The expression of miR-128 showed negative correlation with BMI (rho = −0.380, $p = 0.022$) **(A)**. No significant correlations were present between the other miRNAs and BMI **(B–E)**. Abbreviations: BMI, body mass index.

range (25th and 75th percentile) for continuous normally and non-normally distributed variables, as appropriate. The normal/non-normal distribution was assessed by Shapiro-Wilk test. Student's t-test and One-way ANOVA test or Mann–Whitney test and Kruskal–Wallis test were used for normally distributed data or non-normally distributed data, respectively. The Spearman's coefficient was used to determine the correlation between miRNA expression and BMI. A p-value <0.05 was considered statistically significant. IBM®SPSS Statistics version 26 and Graphpad Prism 5.0 (San Diego, California, United States) were employed in the calculation.

3 Results

3.1 Clinical characteristics of cancer patients and controls

We enrolled a total of 37 gastrointestinal cancer patients (23 male), affected by colorectal (n = 32; 21 male), gastric (n = 4; 1 male) and pancreatic cancers (n = 1, male). The mean age was 71.6 ± 11.9 years, and BMI (kg/m^2) was 24.1 ± 3.8.

Control group included 14 patients undergoing surgery for benign diseases (including cholecystectomy, abdominal

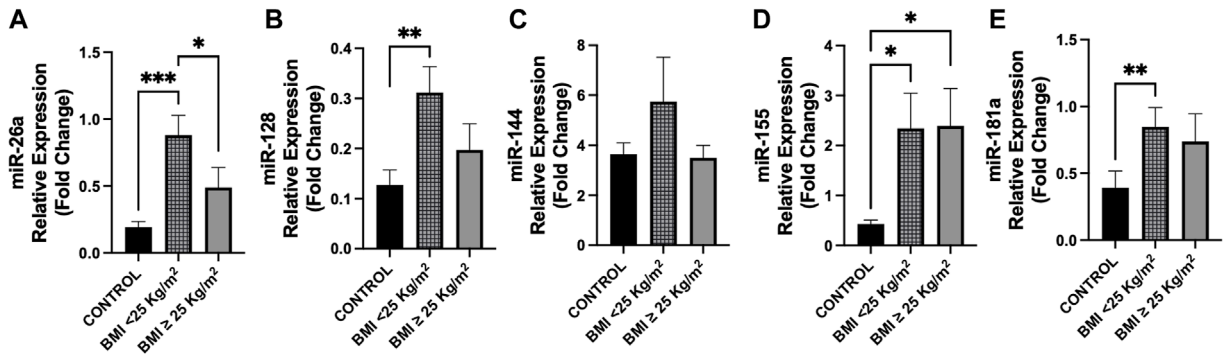

FIGURE 3
Differences in circulating miRNAs between cancer patients and controls according to BMI classes. Circulating miRNAs levels were analyzed in cancer patients according to BMI (kg/m^2) classes (BMI < 25, n = 22; BMI ≥ 25, n = 14) compared to control group (n = 14). **(A)** Expression levels of miR-26a were higher in cancer patients with BMI < 25 with respect to those with BMI ≥ 25 (p = 0.035) and vs. controls (p < 0.001). **(B)** MiR-128 showed overexpression in cancer patients with BMI < 25 vs. controls (p = 0.008), whereas no difference was observed with respect to those with BMI ≥ 25 (p = 0.071). **(D,E)** MiR-155 and miR-181a levels were higher in cancer patients with BMI < 25 compared to controls (p = 0.010 and p = 0.003, respectively), whereas miR-155 levels were higher in cancer patients with BMI ≥ 25 vs. controls (p = 0.017). **(C)** No differences were observed in miR-144 levels between groups. *p < 0.05, **p ≤ 0.01, ***p ≤ 0.001. Abbreviations: BMI, body mass index.

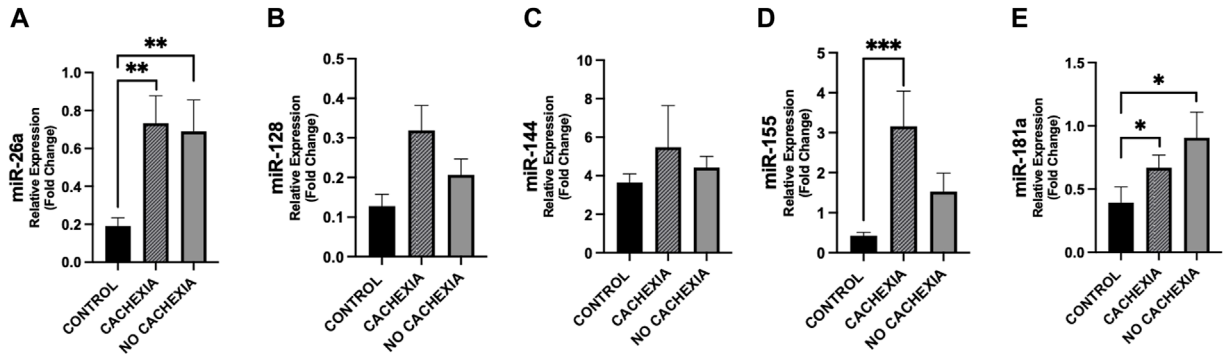

FIGURE 4
Differences in circulating miRNAs among cachectic and non-cachectic cancer patients and controls. Circulating miRNAs levels were analyzed in cancer patients with cachexia (n = 18), without cachexia (n = 19) and controls (n = 14). Data show higher expression of miR-26a **(A)**, miR-155 **(D)** and miR-181 **(E)** in patients with cachexia (p = 0.005, p = 0.001 and p = 0.023, respectively) with respect to controls and higher expression of miR-26a **(A)**, and miR-181 **(E)** in cancer patients without cachexia (p = 0.007 and p = 0.012, respectively) with respect to controls. For miR-128, we observed a trend of increased expression in cachectic patients vs. controls (p = 0.057) **(B)**. No difference was observed in miR-144 levels in cancer patients with/without cachexia vs. controls **(C)**. *p < 0.05, **p ≤ 0.01, ***p ≤ 0.001.

hernia and cysts), with a mean age of 58.1 ± 14.2 years and a BMI of 25.0 ± 3.3.

Cancer patients were older than controls (p = 0.001) and BMI was not different between the two groups. The participant's characteristics are shown in Table 1.

3.2 Prevalence of cachexia and assessment of adiposity by CT-scan

In cancer patients, cachexia was diagnosed in 18 out of 37 cancer patients (49%). Patients with cachexia compared to non-cachectic presented with a decreased BMI (22.8 ± 3.8 vs. 25.3 ± 3.6, p = 0.044).

The mean values (cm^2) of SAT, VAT and TAT in cancer patients were 182.6 ± 72.3, 152.8 ± 86.7 and 335.5 ± 145.2, respectively.

In cachectic patients, we observed lower SAT compared to non-cachectic (157.6 ± 63.7 vs. 206.2 ± 73.5, p = 0.039) (Table 2), but no difference was seen in VAT and TAT (Table 2).

In all cancer patients, BMI strongly and positively correlated with SAT (r = 0.77, p < 0.001), VAT (r = 0.64, p < 0.001) and TAT (r = 0.74, p < 0.001). Other clinical characteristics are shown in Table 2.

3.3 Differences in circulating miRNAs between cancer patients and controls

In Figure 1, we show the differences in plasma miRNAs between cancer patients and controls. In particular, in patients with cancer we found higher levels of miR-26a, miR-128, miR-155 and miR-181a with respect to controls (p < 0.05) (Figure 1). No differences were observed in miR-144 between the two groups (Figure 1). In addition,

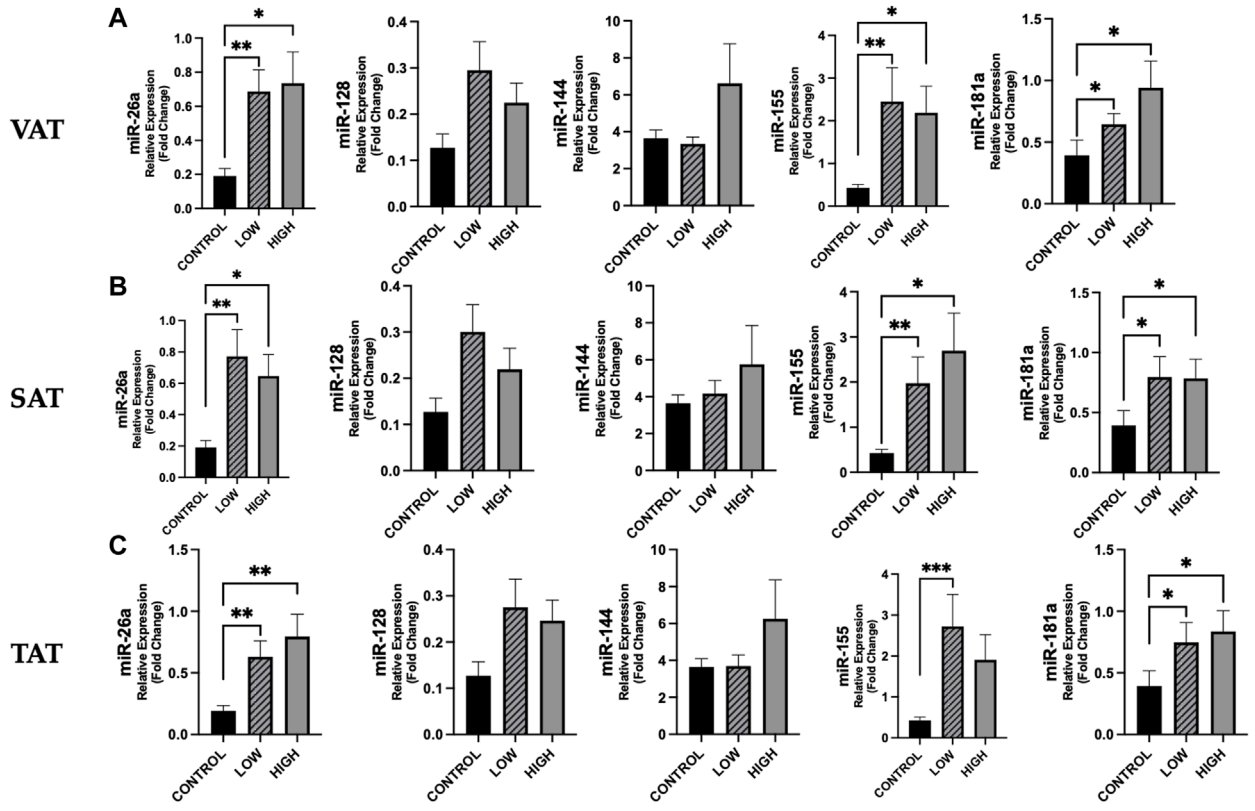

FIGURE 5
Differences in circulating miRNAs according to adiposity level among cancer patients and in controls. We analyzed the data according to the median level of adiposity, as follows: low (n = 19) vs. high (n = 18) of VAT (median: 130.70 cm^2), SAT (median: 167.57 cm^2), and TAT (median: 322.56 cm^2) and in controls (n = 14). **[(A)**, from left to right**]** Data show higher expression of miR-26a (p = 0.003), miR-155 (p = 0.004) and miR-181 (p = 0.023) in cancer patients with low VAT vs. controls and higher expression of these miRs in cancer patients with high VAT vs. controls (p = 0.011, p = 0.024, p = 0.012, respectively) **[(B)**, from left to right] Expression levels of miR-26a, miR-155 and miR-181 were higher in cancer patients with low SAT vs. controls (p = 0.004, p = 0.006 and p = 0.016, respectively) and were also significantly higher in cancer patients with high SAT vs. controls (p = 0.010, p = 0.019 and p = 0.018, respectively). **[(C)**, from left to right] Considering TAT, we observed that miR-26a, miR-155 and miR-181 were higher in cancer patients with low TAT vs. controls (p = 0.008, p = 0.001 and p = 0.022, respectively) and that miR-26a and miR-181a were higher in cancer patients with high TAT vs. controls (p = 0.004 and p = 0.012, respectively). $^*p < 0.05$, $^{**}p \leq 0.01$, $^{***}p \leq 0.001$. Abbreviations: VAT, visceral adipose tissue; SAT, subcutaneous adipose tissue; TAT, total adipose tissue.

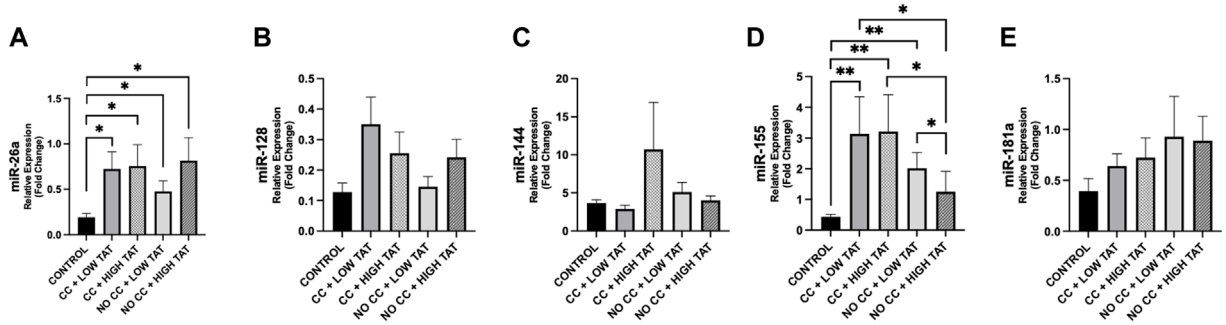

FIGURE 6
Differences in circulating miRNAs according to TAT in cachectic and non-cachectic cancer patients. We analyzed the circulating miRNAs according to the presence/absence of cancer cachexia and low/high levels of TAT (based on median value of 322.56 cm^2) in cancer patients vs. controls. Groups are the following: cancer patients with cachexia and low TAT (n = 12); cancer patients with cachexia and high TAT (n = 6); cancer patients without cachexia and low TAT (n = 7); cancer patients without cachexia and high TAT (n = 12); controls (n = 14). **(A)** MiR-26a showed different modulation in cancer groups vs. controls ($p < 0.05$). **(D)** MiR-155 showed different levels between cancer groups and controls ($p < 0.05$) and we observed a significant downregulation of this miRNAs between cancer patients with cachexia and high TAT vs. cancer patients without cachexia and high TAT (p = 0.031) and higher levels in cancer patients without cachexia and low TAT compared to those with high TAT (p = 0.036). **(B,C,E)** No significance was observed in other miRNAs. $^*p < 0.05$, $^{**}p \leq 0.01$, $^{***}p \leq 0.001$. Abbreviations: TAT, total adipose tissue; CC, cancer cachexia; NO CC, no cancer cachexia.

in cancer patients miR-128 negatively correlated with BMI (rho = −0.380, p = 0.022) (Figure 2), whereas no significant correlations were present between BMI and other miRNAs tested (Figure 2). No differences were observed in the miRNAs levels according to cancer stage (data not shown).

According to BMI classes, patients with BMI < 25 presented with higher plasma levels of miR-26a with respect to cancer patients with BMI ≥ 25 (p = 0.035), as well as vs. controls (p < 0.001) (Figure 3); a similar trend was observed for miR-128 in cancer group (p = 0.071) (Figure 3). No additional differences between BMI classes in cancer patients were observed for the other miRNAs (Figure 3).

3.4 Differences in circulating miRNAs among cachectic and non-cachectic cancer patients and controls

In Figure 4, we show the differences in plasma miRNAs between cancer patients with and without cachexia and controls. In particular, plasma levels of miR-26a resulted higher in cachectic patients (p = 0.007), as well as in non-cachectic (p = 0.005) vs. controls; this was also observed for miR-181a (p < 0.05) (Figure 4).

Differences between cachectic patients and controls were also found for miR-155 (p < 0.001) and did not reach the significance between non-cachectic and controls (p = 0.072) (Figure 4). Also, miR-155 showed a trend of increase in cachectic compared to non-cachectic patients (p = 0.087) (Figure 4). No significant differences were seen in miR-128 and miR-144 between groups (Figure 4).

3.5 Differences in circulating miRNAs according to adiposity level and distribution assessed by CT-scan in cachectic and non-cachectic cancer patients

According to adiposity level (low vs. high median values of VAT, SAT, and TAT, resulting as follows: 130.70, 167.57 and 322.56 cm^2), we observed for some miRNAs significant differences between cancer patients and controls (Figure 5). No differences were found between cancer patients with low vs. high adiposity (Figure 5).

Analyzing the differences between cachexia/no-cachexia groups with low or high TAT, we observed that miR-155 was higher in cachectic patients with low TAT compared to those without cachexia and high TAT (p = 0.036) (Figure 6). Finally, miR-155 was higher in cachectic patients, regardless of low or high TAT, when compared to controls (Figure 6). Moreover, miR-155 expression was increased in cancer patients without cachexia with low TAT compared to those non-cachectic with high TAT (Figure 6). These differences were not present for the other miRNAs (Figure 6).

4 Discussion

Our study confirms the presence of clinical and nutritional changes in patients with gastrointestinal cancer undergoing surgery for cancer resection. In fact, although the main nutritional (anthropometric) parameter routinely used in clinic - BMI - was not different between cancer patients and controls, the presence of cachexia was highly prevalent (49%) in cancer patients. This is of particular interest taking into account that the patients of the present cohort were at their first cancer diagnosis, eligible to surgery and did not yet receive anticancer treatments. Our results indicate that patients satisfying the Fearon's criteria for cachexia (Fearon et al., 2011) showed reduced SAT, suggesting the presence of adipose tissue metabolic derangements since the early phase of cancer disease. Interestingly, the phenomenon of adipose atrophy occurring in cancer was described even preceding the clinical diagnosis of pancreatic cancer (Babic et al., 2023). In another study, during the early phase of cancer disease, we described several histological alterations in SAT, including decreased adipocyte size, increased fibrosis and increased inflammatory infiltration in cachectic patients (Molfino et al., 2022b). Moreover, several evidence support that an increased lipolysis and browning of WAT are crucial in promoting cancer cachexia (Baracos et al., 2018; Hu et al., 2023; Geppert and Rohm, 2024).

Regarding the complex pathophysiology of adipose tissue changes and atrophy in cancer, the implication of circulating miRNAs has been recently supported by different studies (Di et al., 2021; Li et al., 2022; Hu et al., 2023). In our analyses, we found higher circulating levels of miR-26a, miR-128, miR-155 and miR-181a in cancer group compared to controls, and when observing the modulation of these miRNAs according to BMI classes, we found in patients with BMI < 25 kg/m^2 that miR-26a was overexpressed compared to those defined as overweight or obese based on BMI ≥ 25 kg/m^2, as well as to controls. No statistical difference was found for miR-128.

In line with our results, a recent study investigating circulating and visceral adipose miRNAs showed a downregulation of miR-26a in both plasma and VAT in patients with obesity compared with patients with normal weight, suggesting a potential role of this miRNA in regulating adiposity (Kim et al., 2020). However, in another study miR-128 overexpression was shown to play a regulatory role in adipose tissue metabolism, in particular by controlling adipogenesis and lipolysis (Chen et al., 2018). However, conclusive data on these miRNAs are still lacking in the literature.

In addition, we observed significant differences of miR-26 and miR-181a according to the presence of cachexia compared to controls, although the difference was also significant between non-cachectic and control groups. For this reason, at this time it is not possible to indicate a clear implication of these miRNAs in the pathophysiology of cancer cachexia. However, miR-155 showing a similar behavior of miR-26a and miR-181a tended to be modulated in cachectic when compared to non-cachectic patients, although this result should be verified in larger sample.

MiR-155 appears of particular interest in adipose tissue wasting based on the data showing a potential role in promoting derangements of adipose tissue metabolism, by the suppression of adipogenesis and promotion of browning process in gastrointestinal and breast cancers (Liu et al., 2022; Sun et al., 2023). Also, Yehia et al., showed upregulation of miR-155 in cachectic patients with lung and pancreatic cancer (Yehia et al., 2021).

Body composition analysis, specifically addressing the level of adiposity in our cancer group, revealed a significant reduction in

terms of SAT between cachectic and non-cachectic cancer patients. The absence of difference in VAT is likely due to the early stage of cancer disease. Our observation appears interesting considering that other authors found that SAT is implicated in wasting condition during the early phase of catabolic status. In fact, Sah et al. observed in patients with pancreatic cancer a loss of SAT that started 18 months before the cancer diagnosis, anticipating visceral adipose tissue and skeletal muscle atrophy (Sah et al., 2019). Atrophy of SAT was at least in part associated with an increased expression of UCP1 in SAT representing a potential biomarker of early adipose tissue metabolic derangements (Sah et al., 2019), but no information on miRNA profiling in this setting was available.

In our study, when assessing the differences between cachectic patients with low or high TAT, we found that only miR-155 was higher in those with low TAT compared to patients without cachexia and high adiposity. This may suggest an implication of miR-155 in patients with high catabolic status.

Our study has limitations, including the type of gastrointestinal cancer patients, mainly represented by colorectal cancer. Cancer group was older than controls and this difference in age may affect adipose tissue distribution. The inclusion of other gastrointestinal tract cancer, in particular stomach and pancreas, may reveal additional miRNAs modulation that may occur in cancer and in cachexia. The level of adiposity was not assessed in control group and this information may be clinically relevant when comparing adipose tissue changes and its distribution and miRNAs profile in non-catabolic/non cancer conditions. However, CT scan for body composition analysis was not possible for ethical reasons in our controls. We selected specific miRNAs for adipose tissue metabolism, but Next-generation Sequencing (NGS) panel may allow for the identification of a larger number of miRNAs potentially involved in changes in adipose tissue. However, our methodological approach based on analyzing specific miRNAs known to be implicated in biological processes was previously implemented (Lin et al., 2022; Molfino et al., 2023b). The analysis in the subgroups (e.g., cachectic with low or high adiposity) was conducted in small number of participants and need further verification.

5 Conclusion

In the present study, we observed modulations in specific miRNAs involved in adipose tissue metabolism and cachexia in plasma of cancer patients, according to the presence of cachexia and low adiposity. Among others, miR-155 was shown to be modulated according to the presence of both cachexia and low adiposity evaluated by CT scan. To unveil the involvement of miRNAs in the pathophysiology of cachexia may allow for a prompt and early diagnosis of nutritional and metabolic alterations in cancer providing the rationale for innovative treatments.

Data availability statement

The raw data supporting the conclusions of this article will be made available by the authors, without undue reservation.

Ethics statement

The studies involving humans were approved by Sapienza University of Rome - Azienda Policlinico Umberto I - Ospedale Sant'Andrea- Rome, Italy. The studies were conducted in accordance with the local legislation and institutional requirements. Written informed consent for participation in this study was provided by the participants' legal guardians/next of kin.

Author contributions

FT: Conceptualization, Data curation, Formal Analysis, Funding acquisition, Investigation, Methodology, Writing–original draft. GI: Data curation, Formal Analysis, Investigation, Software, Writing–original draft. VP: Formal Analysis, Investigation, Methodology, Writing–original draft. MA: Conceptualization, Data curation, Writing–original draft. VR: Formal Analysis, Software, Writing–original draft. SO: Methodology, Writing–original draft. GL: Investigation, Writing–original draft. CR: Methodology, Writing–original draft. CC: Software, Writing–original draft. GN: Investigation, Writing–review and editing. MM: Conceptualization, Supervision, Writing–review and editing. AM: Conceptualization, Formal Analysis, Funding acquisition, Investigation, Methodology, Resources, Supervision, Writing–original draft, Writing–review and editing.

Funding

The author(s) declare that financial support was received for the research, authorship, and/or publication of this article. This study was supported by intramural research grants from Sapienza University of Rome, Italy, received by AM (Grant n. RG120172B8DFB08E; Grant n. RG11816427B021CF; Grant n. RG1221816C673852) and Initial Grant Project received by FT (Grant n. AR1221816C72B9CD).

Acknowledgments

FT and SO contributed to this study as a recipient of the PhD program in Innovative Biomedical Technologies in Clinical Medicine, at Sapienza University of Rome, Italy. VP contributed as recipient of research scholarship from Sapienza University of Rome (PI: AM).

Conflict of interest

The authors declare that the research was conducted in the absence of any commercial or financial relationships that could be construed as a potential conflict of interest.

The author(s) declared that they were an editorial board member of Frontiers, at the time of submission. This had no impact on the peer review process and the final decision.

Publisher's note

References

Abdallah, N. H., Nagayama, H., Takahashi, N., Gonsalves, W., Fonder, A., Dispenzieri, A., et al. (2023). Muscle and fat composition in patients with newly diagnosed multiple myeloma. *Blood Cancer J.* 13, 185. doi:10.1038/s41408-023-00934-3

Al-Sawaf, O., Weiss, J., Skrzypski, M., Lam, J. M., Karasaki, T., Zambrana, F., et al. (2023). Body composition and lung cancer-associated cachexia in TRACERx. *Nat. Med.* 29, 846–858. doi:10.1038/s41591-023-02232-8

Babic, A., Rosenthal, M. H., Sundaresan, T. K., Khalaf, N., Lee, V., Brais, L. K., et al. (2023). Adipose tissue and skeletal muscle wasting precede clinical diagnosis of pancreatic cancer. *Nat. Commun.* 14, 4317. doi:10.1038/s41467-023-40024-3

Baracos, V. E., Martin, L., Korc, M., Guttridge, D. C., and Fearon, K. C. H. (2018). Cancer-associated cachexia. *Nat. Rev. Dis. Primer* 4, 17105. doi:10.1038/nrdp.2017.105

Belli, R., Ferraro, E., Molfino, A., Carletti, R., Tambaro, F., Costelli, P., et al. (2021). Liquid biopsy for cancer cachexia: focus on muscle-derived microRNAs. *Int. J. Mol. Sci.* 22, 9007. doi:10.3390/ijms22169007

Chen, C., Deng, Y., Hu, X., Ren, H., Zhu, J., Fu, S., et al. (2018). miR-128-3p regulates 3T3-L1 adipogenesis and lipolysis by targeting Pparg and Sertad2. *J. Physiol. Biochem.* 74, 381–393. doi:10.1007/s13105-018-0625-1

Cypess, A. M. (2022). Reassessing human adipose tissue. *N. Engl. J. Med.* 386, 768–779. doi:10.1056/NEJMra2032804

Di, W., Zhang, W., Zhu, B., Li, X., Tang, Q., and Zhou, Y. (2021). Colorectal cancer prompted adipose tissue browning and cancer cachexia through transferring exosomal miR-146b-5p. *J. Cell Physiol.* 236, 5399–5410. doi:10.1002/jcp.30245

Erdem, M., Möckel, D., Jumpertz, S., John, C., Fragoulis, A., Rudolph, I., et al. (2019). Macrophages protect against loss of adipose tissue during cancer cachexia. *J. Cachexia Sarcopenia Muscle* 10, 1128–1142. doi:10.1002/jcsm.12450

Fearon, K., Strasser, F., Anker, S. D., Bosaeus, I., Bruera, E., Fainsinger, R. L., et al. (2011). Definition and classification of cancer cachexia: an international consensus. *Lancet Oncol.* 12, 489–495. doi:10.1016/S1470-2045(10)70218-7

Geppert, J., and Rohm, M. (2024). Cancer cachexia: biomarkers and the influence of age. *Mol. Oncol.* doi:10.1002/1878-0261.13590

Hongfang, G., Khan, R., and El-Mansi, A. A. (2023). Bioinformatics analysis of miR-181a and its role in adipogenesis, obesity, and lipid metabolism through review of literature. *Mol. Biotechnol.* doi:10.1007/s12033-023-00894-w

Hu, Y., Liu, L., Chen, Y., Zhang, X., Zhou, H., Hu, S., et al. (2023). Cancer-cell-secreted miR-204-5p induces leptin signalling pathway in white adipose tissue to promote cancer-associated cachexia. *Nat. Commun.* 14, 5179. doi:10.1038/s41467-023-40571-9

Kim, N. H., Ahn, J., Choi, Y. M., Son, H. J., Choi, W. H., Cho, H. J., et al. (2020). Differential circulating and visceral fat microRNA expression of non-obese and obese subjects. *Clin. Nutr. Edinb Scotl* 39, 910–916. doi:10.1016/j.clnu.2019.03.033

Li, X., Du, L., Liu, Q., and Lu, Z. (2022). MicroRNAs: novel players in the diagnosis and treatment of cancer cachexia (Review). *Exp. Ther. Med.* 24, 446. doi:10.3892/etm.2022.11373

Lin, W., Wen, X., Li, X., Chen, L., Wei, W., Zhang, L., et al. (2022). MiR-144 regulates adipogenesis by mediating formation of C/EBPα-FOXO1 protein complex. *Biochem. Biophys. Res. Commun.* 612, 126–133. doi:10.1016/j.bbrc.2022.04.093

Liu, Y., Wang, M., Deng, T., Liu, R., Ning, T., Bai, M., et al. (2022). Exosomal miR-155 from gastric cancer induces cancer-associated cachexia by suppressing adipogenesis and promoting brown adipose differentiation *via* C/EPBβ. *Cancer Biol. Med.* 19, 1301–1314. doi:10.20892/j.issn.2095-3941.2021.0220

Molfino, A., Belli, R., Imbimbo, G., Carletti, R., Amabile, M. I., Tambaro, F., et al. (2022a). Evaluation of browning markers in subcutaneous adipose tissue of newly diagnosed gastrointestinal cancer patients with and without cachexia. *Cancers* 14, 1948. doi:10.3390/cancers14081948

Molfino, A., Beltrà, M., Amabile, M. I., Belli, R., Birolo, G., Belloni, E., et al. (2023b). Small non-coding RNA profiling in patients with gastrointestinal cancer. *J. Cachexia Sarcopenia Muscle* 14, 2692–2702. doi:10.1002/jcsm.13343

Molfino, A., Carletti, R., Imbimbo, G., Amabile, M. I., Belli, R., di Gioia, C. R. T., et al. (2022b). Histomorphological and inflammatory changes of white adipose tissue in gastrointestinal cancer patients with and without cachexia. *J. Cachexia Sarcopenia Muscle* 13, 333–342. doi:10.1002/jcsm.12893

Molfino, A., Imbimbo, G., and Muscaritoli, M. (2023a). Metabolic and histomorphological changes of adipose tissue in cachexia. *Curr. Opin. Clin. Nutr. Metab. Care* 26, 235–242. doi:10.1097/MCO.0000000000000923

Sah, R. P., Sharma, A., Nagpal, S., Patlolla, S. H., Sharma, A., Kandlakunta, H., et al. (2019). Phases of metabolic and soft tissue changes in months preceding a diagnosis of pancreatic ductal adenocarcinoma. *Gastroenterology* 156, 1742–1752. doi:10.1053/j.gastro.2019.01.039

Schmittgen, T. D., and Livak, K. J. (2008). Analyzing real-time PCR data by the comparative C(T) method. *Nat. Protoc.* 3, 1101–1108. doi:10.1038/nprot.2008.73

Sun, S., Wang, Z., Yao, F., Sun, K., Li, Z., Sun, S., et al. (2023). Breast cancer cell-derived exosome-delivered microRNA-155 targets UBQLN1 in adipocytes and facilitates cancer cachexia-related fat loss. *Hum. Mol. Genet.* 32, 2219–2228. doi:10.1093/hmg/ddad055

Tambaro, F., Imbimbo, G., Ferraro, E., Andreini, M., Belli, R., Amabile, M. I., et al. (2024). Assessment of lipolysis biomarkers in adipose tissue of patients with gastrointestinal cancer. *Cancer Metab.* 12, 1. doi:10.1186/s40170-023-00329-9

Tao, C., Huang, S., Wang, Y., Wei, G., Zhang, Y., Qi, D., et al. (2015). Changes in white and brown adipose tissue microRNA expression in cold-induced mice. *Biochem. Biophys. Res. Commun.* 463, 193–199. doi:10.1016/j.bbrc.2015.05.014

Taylor, J., Uhl, L., Moll, I., Hasan, S. S., Wiedmann, L., Morgenstern, J., et al. (2023). Endothelial Notch1 signaling in white adipose tissue promotes cancer cachexia. *Nat. Cancer* 4, 1544–1560. doi:10.1038/s43018-023-00622-y

Thomou, T., Mori, M. A., Dreyfuss, J. M., Konishi, M., Sakaguchi, M., Wolfrum, C., et al. (2017). Adipose-derived circulating miRNAs regulate gene expression in other tissues. *Nature* 542, 450–455. doi:10.1038/nature21365

Yehia, R., Schaalan, M., Abdallah, D. M., Saad, A. S., Sarhan, N., and Saleh, S. (2021). Impact of TNF-α gene polymorphisms on pancreatic and non-small cell lung cancer-induced cachexia in adult Egyptian patients: a focus on pathogenic trajectories. *Front. Oncol.* 11, 783231. doi:10.3389/fonc.2021.783231

frontiers | Frontiers in Immunology

TYPE Original Research
PUBLISHED 02 September 2024
DOI 10.3389/fimmu.2024.1450135

OPEN ACCESS

EDITED BY
Shahid Ali,
University of Swat, Pakistan

REVIEWED BY
Guoli Zhou,
Michigan State University, United States
Shanchun Guo,
Xavier University of Louisiana, United States

*CORRESPONDENCE
Hezi Zhang
hezizhang2020@163.com
Ying Ba
by@ngdna.com

RECEIVED 17 June 2024
ACCEPTED 19 August 2024
PUBLISHED 02 September 2024

CITATION
Cao L, Chen F, Xu L, Zeng J, Wang Y, Zhang S, Ba Y and Zhang H (2024) Prognostic cellular senescence-related lncRNAs patterns to predict clinical outcome and immune response in colon cancer.
Front. Immunol. 15:1450135.
doi: 10.3389/fimmu.2024.1450135

Prognostic cellular senescence-related lncRNAs patterns to predict clinical outcome and immune response in colon cancer

Lichao Cao[1,2,3], Fang Chen[1,2,3], Long Xu[4,5], Jian Zeng[6], Yun Wang[6], Shenrui Zhang[1,2,3], Ying Ba[1,2,3]* and Hezi Zhang[1,2,3]*

[1]Shenzhen Nucleus Gene Technology Co., Ltd., Shenzhen, Guangdong, China, [2]Shenzhen Nucleus Huaxi Medical Laboratory, Shenzhen, Guangdong, China, [3]Shanghai Nucleus Biotechnology Co., Ltd., Shanghai, China, [4]Department of Gastroenterology and Hepatology, Shenzhen University General Hospital, Shenzhen, Guangdong, China, [5]Marshall Laboratory of Biomedical Engineering, Shenzhen University, Shenzhen, Guangdong, China, [6]Longhua Innovation Institute for Biotechnology, College of Life Sciences and Oceanography, Shenzhen University, Shenzhen, Guangdong, China

Background: Cellular senescence (CS) is believed to be a major factor in the evolution of cancer. However, CS-related lncRNAs (CSRLs) involved in colon cancer regulation are not fully understood. Our goal was to create a novel CSRLs prognostic model for predicting prognosis and immunotherapy and exploring its potential molecular function in colon cancer.

Methods: The mRNA sequencing data and relevant clinical information of GDC TCGA Colon Cancer (TCGA-COAD) were obtained from UCSC Xena platform, and CS-associated genes was acquired from the CellAge website. Pearson correlation analysis was used to identify CSRLs. Then we used Kaplan–Meier survival curve analysis and univariate Cox analysis to acquire prognostic CSRL. Next, we created a CSRLs prognostic model using LASSO and multivariate Cox analysis, and evaluated its prognostic power by Kaplan–Meier and ROC curve analysis. Besides, we explored the difference in tumor microenvironment, somatic mutation, immunotherapy, and drug sensitivity between high-risk and low-risk groups. Finally, we verified the functions of MYOSLID in cell experiments.

Results: Three CSRLs (AC025165.1, LINC02257 and MYOSLID) were identified as prognostic CSRLs. The prognostic model exhibited a powerful predictive ability for overall survival and clinicopathological features in colon cancer. Moreover, there was a significant difference in the proportion of immune cells and the expression of immunosuppressive point biomarkers between the different groups. The high-risk group benefited from the chemotherapy drugs, such as Teniposide and Mitoxantrone. Finally, cell proliferation and CS were suppressed after MYOSLID knockdown.

Conclusion: CSRLs are promising biomarkers to forecast survival and therapeutic responses in colon cancer patients. Furthermore, MYOSLID, one of 3-CSRLs in the prognostic model, could dramatically regulate the proliferation and CS of colon cancer.

KEYWORDS

colon cancer, cellular senescence, lncRNAs, MYOSLID, immune response

1 Introduction

Colon cancer, one of the most-diagnosed cancer, is the second most common causes of cancer-related death globally (1). According to the latest cancer statistics from the American Cancer Society, there were 81,860 colon cancer cases in males and 71,160 cases in females, with 52,550 deaths in 2023 (2). Recently, despite the rapid development of cancer screening methods (3), the incidence of colon cancer remains high, and effective therapeutic targets are still few. In addition, the AJCC TNM staging system, as a prognostic signature for colon cancer patients, is constantly updated, but there are still differences in prognosis among patients with the same clinicopathologic characteristics (4, 5). Therefore, further exploration of specific and sensitive prognostic biomarkers and possible therapeutic targets is essential to ameliorate the clinical outcome and treatment of colon cancer.

Cellular senescence (CS) defined as a state of permanent cell cycle termination (6, 7). Currently, there are 8 types of CS phenotypes, which are mainly triggered by DNA damage response, involvement of cycle-related kinase inhibitors, enhanced secretion of pro-inflammatory factors and tissue repair factors, induction of anti-apoptotic genes, metabolic changes, and endoplasmic reticulum stress (8, 9). Recently, there has been increasing evidence that CS not only has a suppressor effect on tumor (10), but that senescent cells can also accelerate tumor growth by promoting immune escape (11, 12). In the third edition of cancer hallmarks proposed in 2022, senescent cells are recognized as one of novel cancer hallmarks (13). However, few reports have explored the role of CS in the occurrence, development and treatment of colon cancer (14). Therefore, further screening of CS-associated genes based on clinical samples is necessary for the diagnosis and prognosis of colon cancer.

Long noncoding RNA (lncRNA) with more than 200 nucleotides in length, do not have the ability to encode proteins (15). LncRNA has been revealed to play a key role in regulating the physiological activity of cancer cells (16, 17). Furthermore, lncRNA is an ideal tumor biomarker with high specificity and sensitivity that are easy to repeat detection (18). LncRNA plays a functional role in development of CS. Activation of p53 is a key initiating event in CS (19). Several lncRNAs has been reported as regulators or mediators of the p53 pathway, such as lncRNA-H19 and lncRNA DANCR (20, 21). Besides, lncRNA UCA1, as a pro-senescence agent, has been established as an oncogene in several malignancies (22). More importantly, CS-related lncRNAs (CSRLs) were regarded as potential biomarkers for assessing the prognosis of multiple cancers, such as hepatocellular carcinoma (23), lung adenocarcinoma (24), breast cancer (25). Moreover, some study demonstrated that lncRNA PURPL suppressed basal p53 levels, promoting tumorigenicity of colorectal cancer cells, thereby contributing to the pro-survival phenotype of senescent cells (26). However, there are currently few studies about CSRLs in colon cancer (27). Given this, the identification of prognostic CSRLs is important for the prognosis and treatment of colon cancer.

Here, we aimed to explore the prognostic significance of CSRLs in colon cancer. Specifically, a CSRLs prognostic model was constructed to evaluate the performance in the diagnosis, prognosis and therapeutic response for colon cancer.

2 Methods

2.1 Data acquiring and preparation

The RNA sequencing data of GDC TCGA Colon Cancer (TCGA-COAD) cohort (including 469 tumor tissues and 41 normal tissues) and corresponding clinical information, gene expression profiles and mutation profiling data were downloaded from the UCSC Xena platform (https://xenabrowser.net/datapages/). Then, we used the GENCODE website to identified 15,088 lncRNAs via the lncRNA annotation file. Subsequently, transcriptome profiles were used to extract expression matrixes for lncRNAs. In addition, CellAge (https://genomics.senescence.info/download.html#cellage) provided a list of 601 CS-related genes.

2.2 Identification of CSRLs

Differentially expressed genes (DEGs) between normal and cancer tissues were screened out according to $|\log_2$ fold change (FC)$| > 0.585$ and adjusted P-value < 0.05. Then, venn diagram was used to show

overlapping CS-related DEGs between DEGs and CS-related genes. Pearson correlation analysis was performed based on CS-related DEGs and lncRNAs expression levels to identify CSRLs with |Pearson correlation coefficient| > 0.5 and *P*-value of < 0.001 (28, 29).

2.3 Creation and validation of CSRLs prognostic model

Transcriptome expression data of 469 tumor samples in TCGA-COAD cohort were obtained, among which 37 samples without survival or phenotypic information were excluded. Remaining samples (n=432) considered as the entire cohort. The information of the entire cohort is showed in Supplementary Table 1. Then, the entire cohort was randomly classified into training (n=216) or test (n=216) sets at a 1:1 ratio. Next, a prognostic risk model was generated in the training cohort and validated in test and entire cohorts, respectively. First, the prognostic CSRLs were obtained by the association between the CSRLs expression level and patients' overall survival (OS) using Kaplan–Meier analysis ($p < 0.05$). Subsequently, univariate Cox regression with a *P*-value of < 0.05 was applied to further filtrate optimal prognostic CSRLs among the above filtered candidate prognostic CSRLs. The least absolute shrinkage and selection operator (LASSO) analysis was applied to the above prognostic CSRLs to avoid over-fitting. Then a CSRLs prognostic model was established by applying multivariate Cox regression analysis. The formula for the CSRLs prognostic model was built to forecast patient survival (28):

$$\text{risk core} = \sum Cox\ coefficient\ of\ gene\ x^i * expression\ value\ of gene\ x^i .$$

The regression coefficient was obtained from the multivariate Cox results.

The receiver operating characteristic (ROC) curve was applied to estimate the predictive accuracy of the prognostic model via the *survivalROC* R package, which was reflected by quantifying area-under-curve (AUC) for assessing the CSRLs prognostic model's sensitivity as well as specificity. Meantime, the optimum critical point of the ROC curve is regarded as the best cutoff value. Colon cancer patients were divided into the high-risk group and the low-risk group based on the cutoff value. Kaplan-Meier curves were plotted using the *survminer* R package to show the relationship between high-risk and low-risk groups and prognosis.

Besides, the test and entire cohorts were performed to assess the model feasibility, respectively. The verification measure was the same as above.

Additionally, the relationship between the CSRLs prognostic model and the pathological stages, microsatellite status, and TNM stages were examined by the Wilcoxon test and Kruskal-Wallis test.

2.4 Function analysis of the 3 prognostic CSRLs

EnrichR is a Gene Set Enrichment method that speculates biological information by enriching input gene sets that represent biological functions or functional pathways (30). We used the 'enrichR' package to perform Gene Ontology (GO) and Kyoto Encyclopedia of Genes and Genomes Enrichment (KEGG) enrichment analyses of the 3 lncRNAs-correlated CS-associated DEGs in R.

2.5 Relationship between immune cell infiltration and the model

Investigation the immune cell infiltration can provide prognostic value and guide immunotherapy in colon cancer (31). The CIBERSORT algorithm was performed to obtain the proportions of 22 types of tumor-infiltrating immune cells (32). The unpaired *t*-test was applied to compare the proportions of tumor-infiltrating immune cells between the high- and low-risk groups. Kaplan–Meier curve was performed to assess the correlation between OS and significant differential immune cell types (*P*-value < 0.01).

2.6 Genetic alterations analysis

Mutation data from colon cancer patients were obtained from TCGA and the R package "maftools" was used to visualize the gene mutation landscape in different subgroups.

2.7 Exploring immunotherapy response

Wilcoxon test was applied to compare the mRNA levels of CD274, PDCD1, CTLA4, HAVCR2, LAG3, and TIGIT between the high- and low-risk groups. Then, we calculated the tumor mutation burden (TMB) value of different subgroups using the R package "maftools" and performed immunotherapy analysis. Finally, the *oncoPredict* R package was applied to compare the IC50 values of 8 chemotherapeutic drugs between different risk groups.

2.8 Cell line culture and transfection

American Type Culture Collection (ATCC) provided HCT116 and SW480 cells. These cells were grown in McCoy's 5A or Leibovitz's L-15 medium (Gibco, United States) with 10% fetal bovine serum (Gibco, United States). All cells were cultured in a 37° C and 5% CO_2 cell incubator. Follow manufacturer's instructions, jetPRIME® (Polyplus, France) was performed to transfect cells with ASOs (Tsingke Biotech, Beijing, China). Sequences of ASOs were listed in Supplementary Table 2.

2.9 Quantitative real-time polymerase chain reaction

TRIzol reagent was applied to extract total RNA from cell lines. Then, the obtained RNAs were used for cDNA synthesis using the

Hifair® III 1st Strand cDNA Synthesis SuperMix (YESEN, Shanghai, China). Gene expression was quantified by conducted with Hieff® qPCR SYBR Green Master Mix (YESEN, Shanghai, China). The relative quantitative value were calculated with the $2^{-\Delta\Delta Ct}$ method. The primer sequences were shown in Supplementary Table 3.

2.10 Cell counting kit-8 assay

The cells were seeded into a 96-well plate at a density of 1000 cells/well for 24 h. Then, 10 μL CCK-8 reagent (Yeasen, Shanghai, China) was added to each well at the indicated time (24h, 48h, 72h, 96h) and incubated for 10 min. Absorbance was measured at 450nm.

2.11 Statistical analysis

GraphPad Prism 8.0 software was used to perform statistical analysis. Student's t test was applied to assess the differences between the two groups. Data were expressed as the mean ± standard deviations (SD). $P < 0.05$ was set as the significance level.

3 Results

3.1 Screening CSRLs in colon cancer

The detailed flowchart is shown in Figure 1. In this study, we acquired transcriptome data of 510 colon cancer samples (including 41 normal and 469 tumor samples) from the TCGA-COAD cohort. There were 572 DEGs (276 up-regulated and 296 down-regulated) between normal and tumor tissues (Supplementary Table 4). Then, we obtained 601 CS-related genes from CellAge database. The 8 overlapping genes were considered CS-related DEGs (Supplementary Figure S1). Subsequently, we performed a Pearson correlation analysis of the obtained 8 CS-related DEGs and 15,088 lncRNAs to obtain CSRLs (Supplementary Table 5). Finally, 237 CSRLs were identified.

3.2 Construction and validation of the CSRLs prognostic model

Using the Kaplan–Meier analysis, the expression levels of 21 CSRLs were significantly associated with patient's OS ($P < 0.05$; Supplementary Figure S2) in the training cohort. Then, univariate Cox regression analysis showed 7 CSRLs are associated with prognosis in the training cohort ($P < 0.05$; Figure 2A). LASSO regression analysis has confirmed 7 CSRLs have the maximum prognostic value (Figure 2B). Subsequently, the multivariate Cox regression analysis was applied to establish a senescence-related prognostic model composed of 3 CSRLs (AC025165.1, LINC02257 and MYOSLID) based on the training cohort (Figure 2C). Colon cancer patients were classified into high- and low-risk groups according to the cutoff value of ROC curves. Figure 2D showed patients with high-risk group has shorter survival times than those in low-risk group in the training cohort ($P < 0.0001$). Moreover, the AUC values at 1-, 3- and 5-year were 0.654, 0.707 and 0.742 in the training cohort, respectively (Figure 2E), demonstrating the predictive reliability of the CSRLs prognostic model. We also constructed

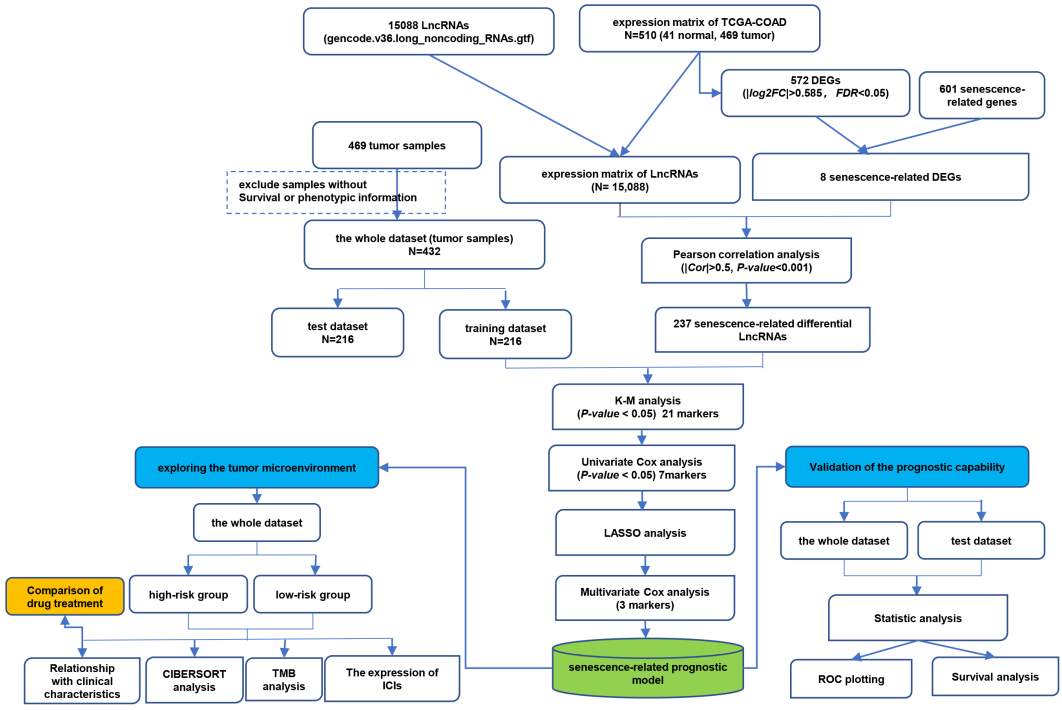

FIGURE 1
The technical flow chart of this study.

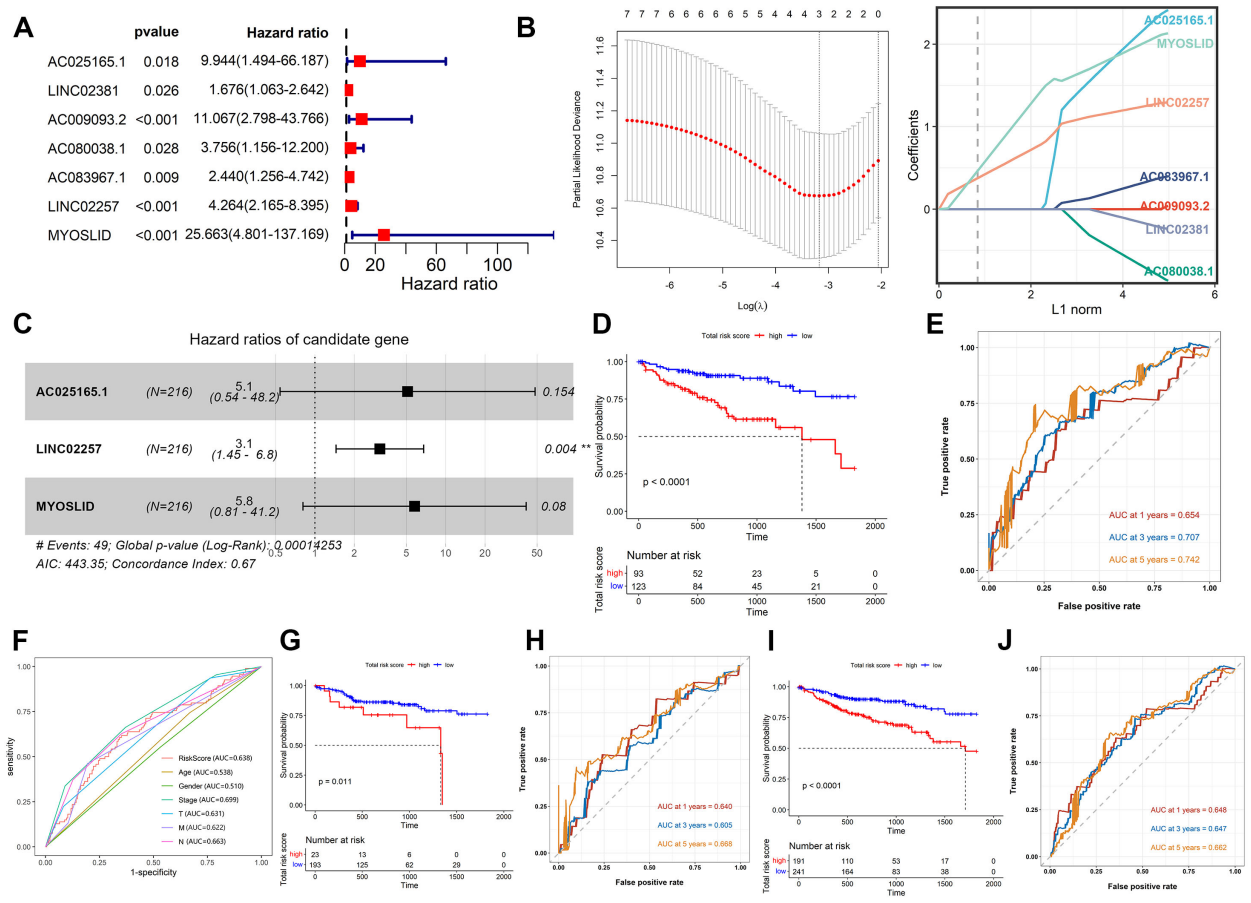

FIGURE 2
Construction and validation of the CSRLs prognostic model. **(A)** Univariate Cox regression analysis. **(B)** LASSO regression analysis. **(C)** Multivariate Cox regression analysis. Kaplan-Meier survival analyses of the CSRLs prognostic model in the **(D)** training cohort, **(G)** test cohort and **(I)** entire cohort. ROC curves indicated the potential of the CSRLs prognostic model in predicting 1-, 3- and 5-year OS in the **(E)** training cohort, **(H)** test cohort and **(J)** entire cohort. **(F)** ROC curves comparing the prognostic accuracy of the risk score and other clinical characteristics in the training cohort.

an ROC curve to validate the prognostic accuracy of this prognostic model compared to other clinical characteristics (Figure 2F). Furthermore, we also validated the prognostic power of the model in the test cohort and the entire cohort (Figures 2G–J). The AUC values at 0.64, 0.605, and 0.668 for 1-, 3- and 5-year in the test cohort, accordingly (Figure 2H); the AUC values at 0.648, 0.647, and 0.662 for 1-, 3- and 5-year in the entire cohort, respectively (Figure 2J). These results indicated that the CSRLs prognostic model can predict the prognosis of colon cancer.

3.3 Relationship between the CSRLs prognostic model and the clinicopathological characteristics

We further explored whether there were differences in risk scores for different clinical features. There was differences in risk scores among pathological stages (Stage I, Stage II, Stage III, Stage IV), T stages (T1, T2, T3, T4), M stages (M0, M1), and N stages (N0, N1, N2) (Figures 3A, C–E). In general, patients with advanced stage tumors also had higher risk scores. In contrast, the risk scores exhibited no differences between MSI-H and MSI-L (Figure 3B). These findings demonstrated that the CSRLs prognostic model has outstanding potential to predict clinical characteristics in patients with colon cancer.

3.4 Function analysis of the 3 prognostic CSRLs

Our results showed that AC025165.1, LINC02257 and MYOSLID may be involved in the regulation of 2 CS-related DEGs (ACKR1 and NOX4). The 2 CS-related DEGs were significantly enriched in the biological process terms inflammatory response and homocysteine metabolic process (Figure 4A). The 2 CS-related DEGs were significantly enriched in the molecular function terms NAD(P)H oxidase H2O2-forming activity and superoxide-generating NAD(P)H oxidase activity (Figure 4B). The 2 CS-related DEGs found to be involved in the Cellular Component: NADPH oxidase complex and endoplasmic reticulum membrane (Figure 4C). KEGG pathway showed 2 CS-related DEGs were enriched in AGE-RAGE signaling pathway in diabetic complications (Figure 4D).

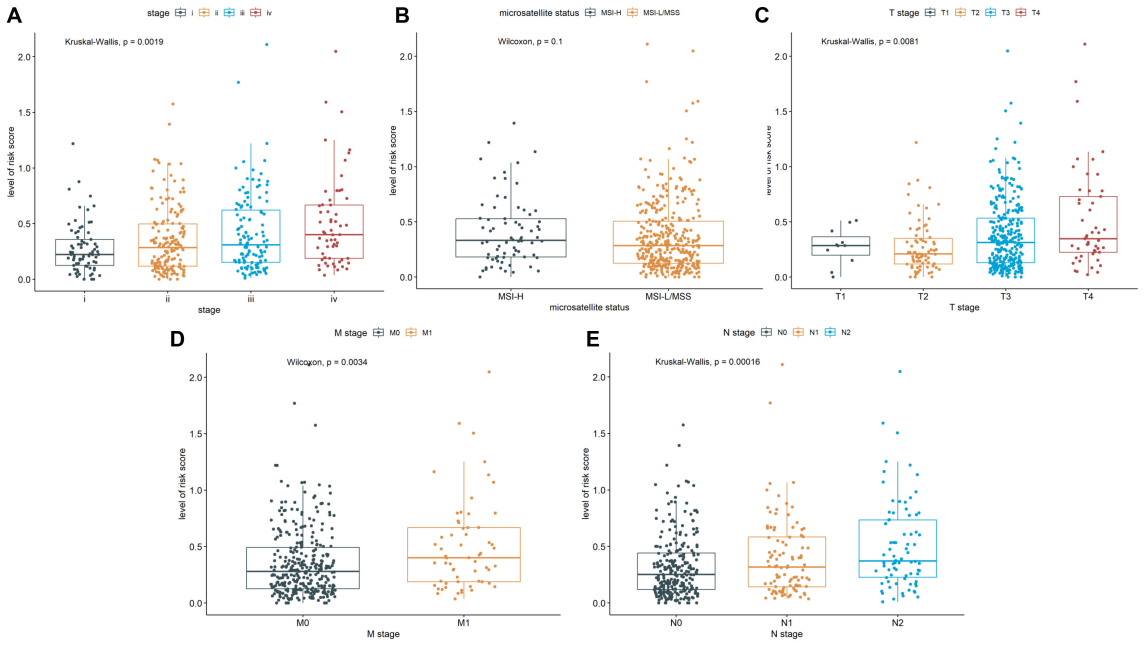

FIGURE 3
Correlation of the CSRLs prognostic model and the clinicopathological characteristics, such as **(A)** pathological stage, **(B)** microsatellite status, and **(C–E)** TNM stages based on the entire cohort.

3.5 Correlation of the CSRLs prognostic model with immune characteristics

Immune microenvironment is a key factor affecting tumor growth and patient prognosis (33). As shown in Figure 5A, there were the significant differences in naïve B cells, memory B cells, plasma cells, CD4 memory-resting T cells, CD4 memory-activated T cells, follicular helper T cell, resting NK cells, M0 macrophages, M2 macrophages, M3 macrophages, activated dendritic cell, resting mast cells and neutrophils between the low-risk group and high-risk group. Among them, the poor prognosis of patients was associated with the high level of M0 macrophages or resting NK cells (Figures 5B, C). Conversely, down-regulated M1 Macrophages or naïve B cells were associated with a poor prognosis (Figures 5D, E). These results suggested that the CSRLs prognostic model might reflect the immune microenvironment status in patients with colon cancer.

3.6 Cancer type-specific genomic variations in the CSRLs prognostic model

To investigate the gene mutation for the CSRLs prognostic model in colon cancer, we used *maftools* R package to explore the mutation profiles of the low-risk and high-risk groups. While the top 10 mutated genes in high-risk and low-risk groups were similar, their ranking differed. Additionally, the median number of mutations in high-risk group was higher than in low-risk group (116 vs. 102.5). In high-risk and low-risk groups, the most common variant classification was missense mutation, the most common variant type was single nucleotide polymorphisms (SNP), and the most common single nucleotide variants (SNVs) class was C>T (Figures 6A, B). Moreover, we also examined the top 20 significantly mutated genes in all patients (Figure 6C). Generally, APC, had a relatively higher mutation rate in the low-risk groups (79% vs. 66%), while TTN presented a relatively higher mutation rate in the high-risk group (58% vs. 48%) (Figure 6D). These genomic alterations may be associated with differences in senescence cells between low-risk and high-risk patients.

3.7 The role of CSRLs prognostic model in clinical treatment

Since immune checkpoint inhibitor (ICI) has been shown to have beneficial effects in the treatment of colon cancer in clinical trials, we further investigated the role of immunosuppressive point biomarkers in the model. The results showed that the expression of immunosuppressive point biomarkers in the high-risk group was higher than that those with a low-risk group (Figure 7A), suggesting that patients in high-risk group may be better candidates for immunosuppressive therapy. Additionally, TMB has been proved to be an important indicator for predicting the clinical benefits of immunotherapy. There was a significant difference in TMB between the high-risk and low-risk groups (Figure 7B). Similarly, the expression of immunosuppressive point biomarkers in the TMB-high group was higher than that those with a TMB-low group (Figure 7C). In addition to ICI treatment, chemotherapy is also a common treatment for colon cancer. The results demonstrated that the high-risk group marked clinical benefits from Teniposide (P=0.00041) and Mitoxantrone (P = 0.02204) compared to low-risk group, but no significant difference with other 6 chemotherapeutic

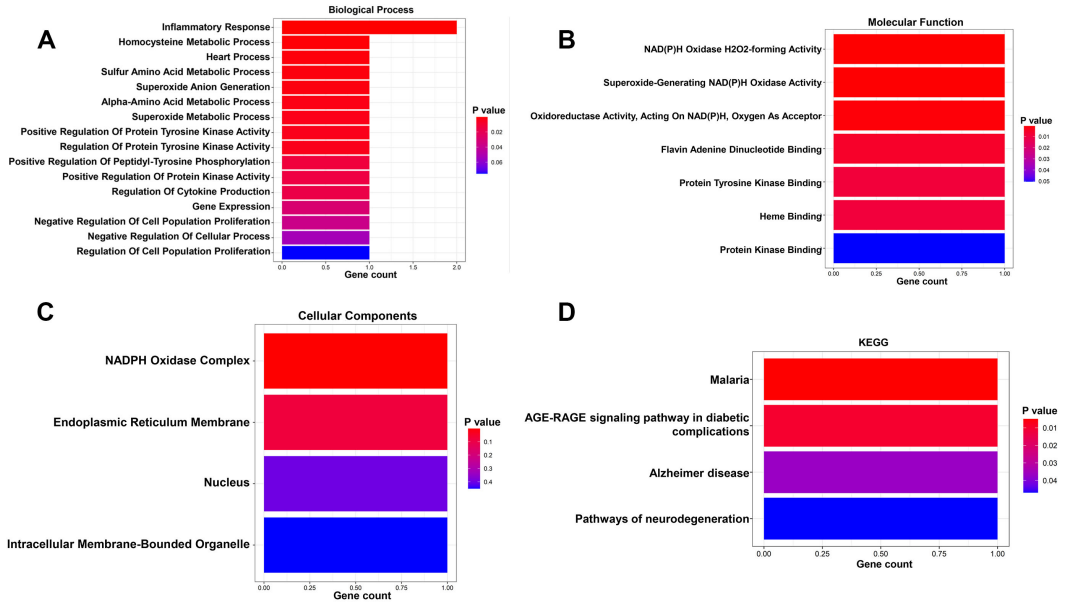

FIGURE 4
GO and KGEE analysis of the 3 prognostic CSRLs. **(A)** Biological process of the 3 CSRLs-associated DEGs. **(B)** Molecular function of the 3 CSRLs-associated DEGs. **(C)** Cellular components of the 3 CSRLs-associated DEGs. **(D)** KEGG of the 3 CSRLs-associated DEGs.

drugs between high-risk and low-risk groups (Figure 7D). Collectively, our prognostic model is suitable for providing immunotherapeutic strategies and predicting drug sensitivity for colon cancer patients.

3.8 Knockdown of MYSOLID inhibited the cell proliferation and CS of colon cancer

CS has been proved to depress the development of colon cancer cells (34) and can also enhance the progression of colon cancer (35), which may be correlated with the fact that it is highly heterogeneous (36). Here, we selected MYOSLID to examine the relationship between CS and colon cancer. MYOSLID has been revealed to be highly expressed in colon cancer cell lines (RKO and HCT116) and accelerate the malignant activity of colon cancer cells (37, 38). Therefore, we synthesized 3 pairs of ASO sequences and mixed them to interfere with MYOSLID expression. In both the HCT116 and RKO cell lines, MYOSLID dramatically reduced (Figures 8A, B). The activity of colon cancer cells was observably decreased following MYOSLID knockdown in HCT116 and RKO cell lines (Figures 8C, D), which is similarly to other reports (37). Subsequently, we further verified the effect of MYOSLID knockout on biomarkers of CS. The results demonstrated the expressions of KI67 and MCM2 were considerably increased following MYOSLID knockdown in HCT116 (Figure 8E). Similarly, MYOSLID knockdown dramatically up-regulated the expressions of KI67, LaminB1, and MCM2, and significantly reduced the expression of P16 in RKO cell lines (Figure 8F). Taken together, MYOSLID promoted cell proliferation and CS of colon cancer cells.

4 Discussion

Colon cancer is a recognized malignant tumor with a very high mortality rate. The occurrence of colon cancer is mainly associated with two types of precursor polyps produced by two distinct pathways (39). However, the progression of colon cancer is a multistep process involving changes in many endogenous and exogenous factors, such as tumor microenvironment (TME) (40), immune escape (41), alteration of intestinal flora (42), and environmental factors (43). Accumulating evidence indicated that CS is a key process in cancer progression and treatment (44). However, studies of CS and colon cancer are rare. Nowadays, lncRNA, as a stable expression biomarker with high detection sensitivity, have been used in the early diagnosis of a variety of cancers (45, 46). Therefore, we successfully established a CSRLs prognostic model and provided reliable early prognostic indicators for colon cancer.

Here, we comprehensively analyzed the expression profiles of TCGA-COAD cohort and Human Ageing Genomic Resources database, finally screened out 8 CS-related DEGs. Subsequently, we identified 237 CSRLs using the Pearson correlation method, 3 of which were prognostic CSRLs, named LINC02257, MYOSLID, and AC025165.1. LINC02257, as a enhancer RNA, has been demonstrated to be an independent prognostic factor for colon cancer patients (47). Moreover, LINC02257 was considered to be an independent prognostic biomarker for colorectal adenocarcinoma via the PI3K-Akt signaling pathway (48). A previous study reported MYOSLID was considered as an oncogene for gastric cancer (49). Besides, MYOSLID can be used to predict clinical outcomes in colon cancer patients (50). MYOSLID knockdown has been reported to lead to a decrease in CD4+ T cells in colorectal

10.3389/fimmu.2024.1450135

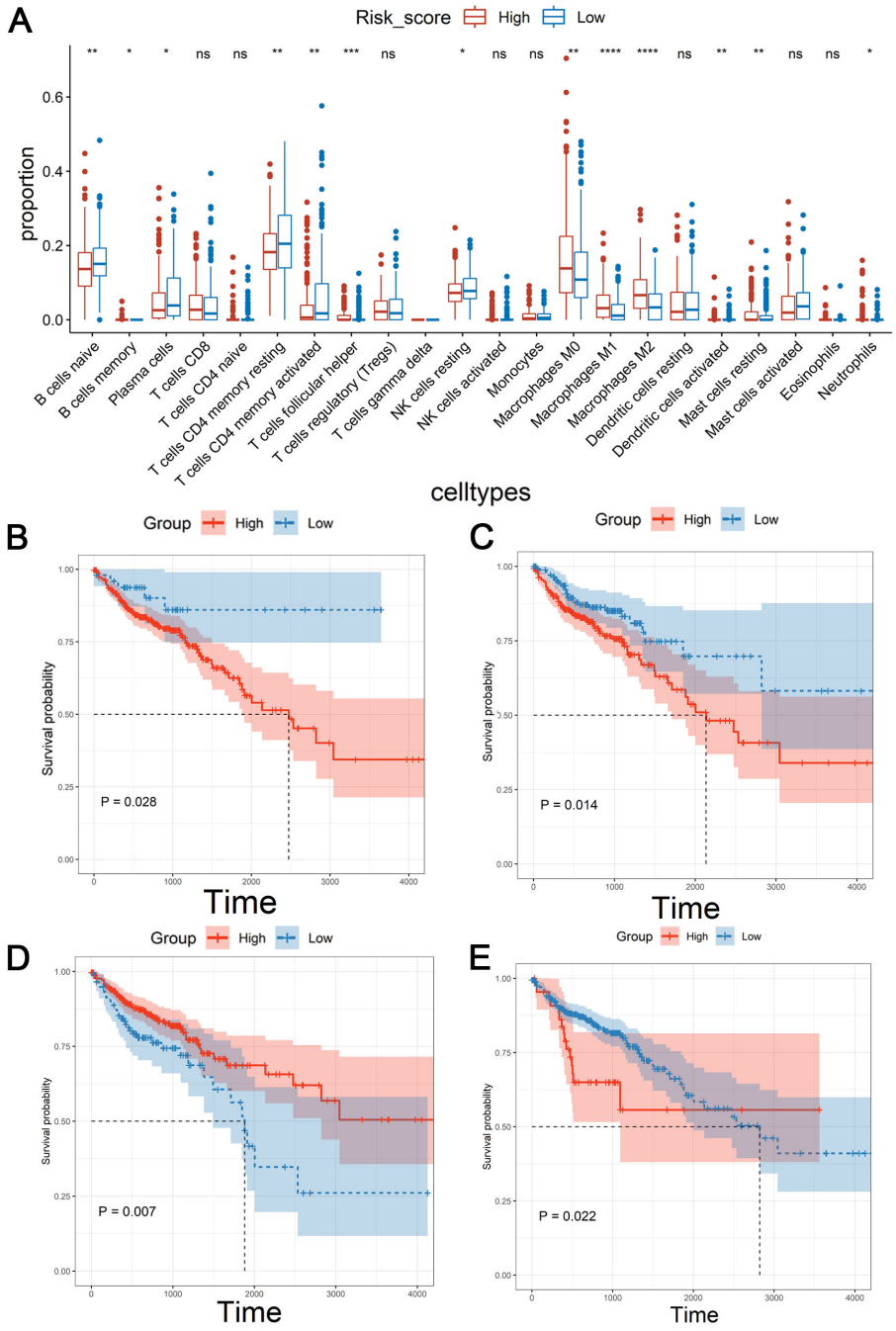

FIGURE 5
Correlation of the CSRLs prognostic model with immune microenvironment based on the entire cohort. **(A)** Immune cell infiltration analysis. * indicated *P*<0.05, ** indicated *P*<0.01, *** indicated *P*<0.001, **** indicated *P*<0.0001, ns indicated no significant difference. Kaplan-Meier survival analyses of the relationship between the level of **(B)** M0 macrophages, **(C)** resting NK cells, **(D)** M1 Macrophages, and **(E)** naïve B cells with patients' OS.

cancer cells, which may play a role in regulating immunity to colorectal cancer (37). However, to our knowledge, the correlation between AC025165.1 and colon cancer has not been reported.

We developed a novel prognostic 3-CSRLs model for colon cancer, which could provide an effective basis for clinicians to estimate the prognosis of colon cancer patients. Considering that senescent cells secrete a variety of proteins, such as inflammatory cytokines, chemokines, and growth factors, etc., which lead to an antitumor immune response through recruitment of immune cells (51, 52). Moreover, senescent cells can reshape surrounding tissue by regulating the properties of neighboring cells, including stromal and immune cells (53). Therefore, we also explored the immune microenvironment characteristics of CSRLs on colon cancer. Patients with low-risk had more immature immune cells such as naïve B cells or immunosuppressive cells such as regulatory T cells compared to those with high-risk. CD4+ T cells are known to play

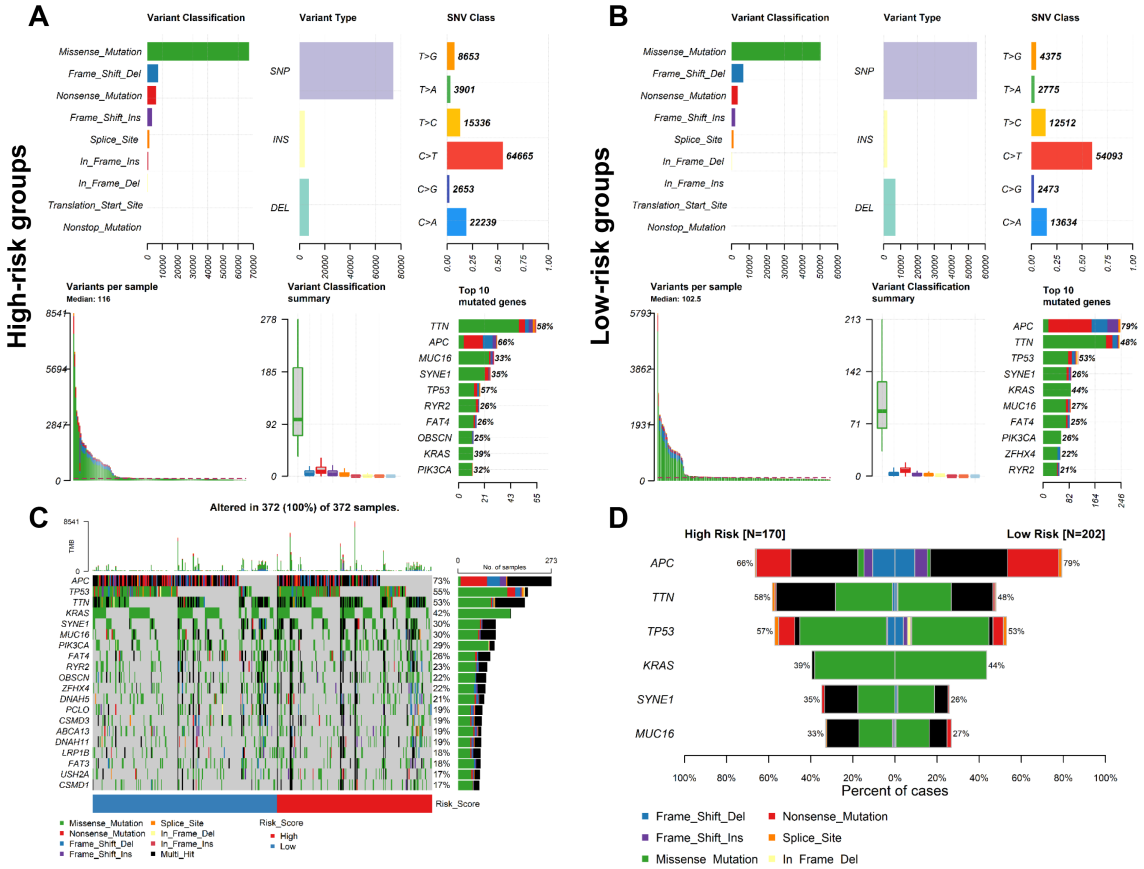

FIGURE 6
Analysis of mutation profiles in low- and high-risk groups based on the entire cohort. Mutation characteristics of **(A)** high- and **(B)** low-risk group. **(C)** The mutation profiles of all patients. **(D)** Comparison of the mutation rate between two risk groups.

an important role in tumor immunity, which offer a promising strategy for immunotherapy of colon cancer (54). NK cells, as cytotoxic innate lymphocytes that eradicate tumor cells, induce a durable anti-tumor immune response, which is a priority in cancer immunotherapy (55). We observed a significant decrease in CD4+ T cells and NK cells in the high-risk group, and we speculated that the function of CD4+ T cells and NK cells may be relatively suppressed in the high-risk group. In addition, high-risk patients had a high level of M0 Macrophages that is associated with unfavorable survival, meaning CSRLs prognostic model can predict patient outcomes at the immune cell level. Because it is unidentified in clinical work to determine which colon cancer patients benefit from chemotherapy, this often leads to the misuse of chemotherapy drugs. In our study, the expression levels of multiple immune checkpoints in high-risk group were higher than those in low-risk group. Thus, it may be possible to improve outcomes in high-risk patients by enhancing their immune reactivity (56). Taken together, the CSRLs prognostic model reflected a different immunological microenvironment in colon cancer patients with diverse prognosis, and had a better predictive performance for immunotherapy.

Aging and diet are two of the most important risk factors for colon cancer and can enhance an oxidative state in the colon (57). Guo et al. found that senescent cells promote the formation of colon cancer by secreting GDF15 (35). Similar to other studies (37, 38), our study showed MYOSLID promoted the proliferation of colon cancer cells, and overexpression of MYOSLID prognosticated poor prognosis in colon cancer patients. MYOSLID was first reported to promote vascular smooth muscle differentiation (58). Many studies have reported MYOSLID as a prognostic factor for multiple cancers, such as head and neck squamous cell carcinoma (59), gastric cancer (49), and osteosarcoma (60). MYOSLID has been reported as a prognostic factor for colorectal cancer as a hypoxia-related lncRNA (38). However, what role MYOSLID plays in CS have not yet been reported. To the best of our knowledge, our study was the first to demonstrate that MYOSLID as a prognostic CSRL for colon cancer, and that knockdown of MYOSLID inhibited CS and growth of colon cancer. As mentioned earlier, there are two sides of CS that promote or antagonize the progression of colon cancer (34, 35). Moreover, there is a strong relationship between CS and TME. Chen et al. suggested that overexpression of INHBA is positively associated with poor prognosis in colorectal cancer, as well as regulating CS of colorectal cancer cells by mediating immune evasion in TME (61). Recent study found that NOX4, as a CS-related gene in colorectal cancer, may be a key factor in driving colorectal cancer resistance by altering TME (62). These findings

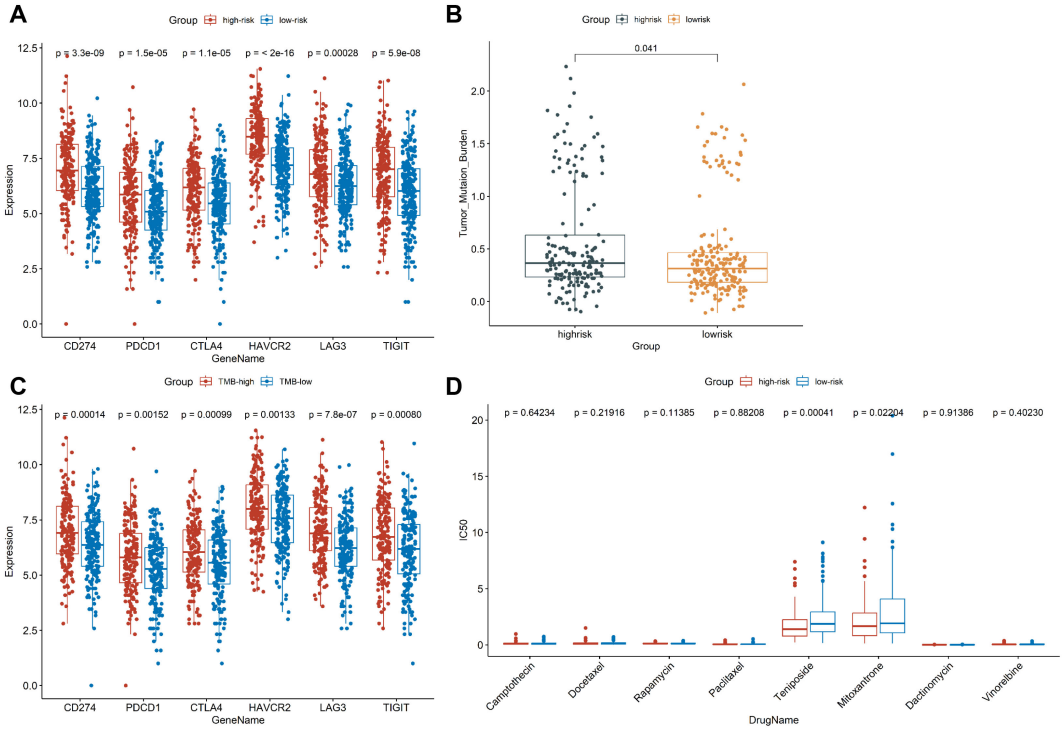

FIGURE 7
Exploring the role of CSRLs prognostic model in clinical treatment. **(A)** Comparison of the expression of immunosuppressive point biomarkers between low- and high-risk groups. **(B)** Comparison of TMB values between low- and high-risk groups. **(C)** Comparison of the expression of immunosuppressive point biomarkers between TMB-low and TMB-high groups. **(D)** Comparison of the IC50 values of chemotherapy drugs between low- and high-risk groups.

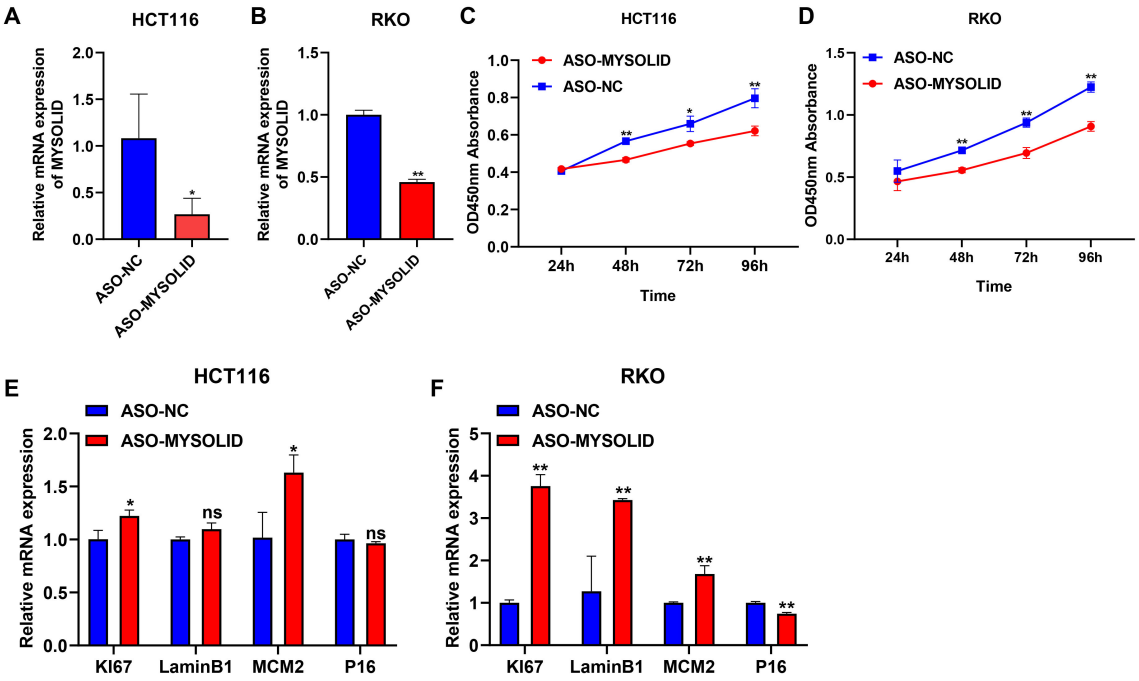

FIGURE 8
Exploring the role of MYSOLID in colon cancer. q-PCR verified the efficiency of MYSOLID knockdown in **(A)** HCT116 and **(B)** RKO cells. The activity of cells was markedly down-regulated following MYSOLID knockdown in **(C)** HCT116 and **(D)** RKO cells. q-PCR verified the expression of CS-related biomarkers following MYSOLID knockdown in **(E)** HCT116 and **(F)** RKO cells. * indicated $P<0.05$, ** indicated $P<0.01$, ns indicated no significant difference.

give a hint that MYOSLID may promote tumor proliferation by mediating CS through regulation of immune microenvironment, but more evidence is still needed.

The present research has some shortcomings. Firstly, the original data for establishing the CSRLs prognostic model were only retrieved from the TCGA database. Additionally, other external datasets and external validation with clinical data are still needed to confirm the reliability and accuracy of the model. Moreover, the prognostic efficacy and underlying mechanisms of this model still require further study through real clinical data and basic experiments. Lastly, the mechanism of how CS regulates the development of colon cancer is still unclear and needs to be explained through additional studies.

5 Conclusion

Overall, we established a CSRLs prognostic model that could prognosticate the survival outcomes of colon cancer. The CSRLs prognostic model could effectually reflect the immune microenvironment characteristics and genomic mutation of colon cancer and the effect of immunotherapy and chemotherapy drugs. Finally, we discovered that MYOSLID could influence the biological function and CS of colon cancer. These suggested that CSRLs could be new biomarkers in diagnosis and prognosis of colon cancer.

Data availability statement

Publicly available datasets were analyzed in this study. This data can be found here: All data sets used in this study are publicly available on the UCSC Xena platform.

Ethics statement

Ethical approval was not required for the studies on humans in accordance with the local legislation and institutional requirements because only commercially available established cell lines were used.

Author contributions

LC: Conceptualization, Data curation, Formal analysis, Writing – original draft. FC: Data curation, Methodology, Writing – original draft. LX: Formal analysis, Software, Writing – original draft. JZ: Data curation, Visualization, Writing – original draft. YW: Funding acquisition, Writing – original draft. SZ: Software, Validation, Writing – original draft. YB: Conceptualization, Project administration, Writing – review & editing. HZ: Conceptualization, Project administration, Writing – review & editing.

Funding

The author(s) declare that financial support was received for the research, authorship, and/or publication of this article. This work was supported by Technology and Innovation Commission of Shenzhen Municipality (KCXFZ202002011006448).

Conflict of interest

LC, FC, SZ, HZ and YB were employed by Shenzhen Nucleus Gene Technology Co., Ltd., and Shanghai Nucleus Biotechnology Co., Ltd.

The remaining authors declare that the research was conducted in the absence of any commercial or financial relationships that could be construed as a potential conflict of interest.

Publisher's note

Supplementary material

The Supplementary Material for this article can be found online at: https://www.frontiersin.org/articles/10.3389/fimmu.2024.1450135/full#supplementary-material

SUPPLEMENTARY FIGURE 1
Kaplan-Meier survival analyses of the relationship between the expressions of CSRLs with patients' OS.

SUPPLEMENTARY FIGURE 2
Venn diagram.

SUPPLEMENTARY TABLE 1
The clinical information of the entire cohort.

SUPPLEMENTARY TABLE 2
The sequences of MYSOLID-ASOs.

SUPPLEMENTARY TABLE 3
The primer sequences used for q-PCR.

SUPPLEMENTARY TABLE 4
The information of 572 DEGs between normal and tumor tissues.

SUPPLEMENTARY TABLE 5
The relationship between CS-related DEGs and lncRNAs.

References

1. Wu Z, Lu Z, Li L, Ma M, Long F, Wu R, et al. Identification and validation of ferroptosis-related lncRNA signatures as a novel prognostic model for colon cancer. *Front Immunol*. (2021) 12:783362. doi: 10.3389/fimmu.2021.783362

2. Siegel RL, Miller KD. Cancer statistics, 2023. *CA Cancer J Clin Cancer Res*. (2023) 73:17–48. doi: 10.3322/caac.21763

3. Issa IA, Noureddine M. Colorectal cancer screening: An updated review of the available options. *World J Gastroenterol*. (2017) 23:5086–96. doi: 10.3748/wjg.v23.i28.5086

4. Lino-Silva LS, Xinaxtle DL, Salcedo-Hernández RA. Tumor deposits in colorectal cancer: the need for a new "pN" category. *Ann Transl Med*. (2020) 8:733. doi: 10.21037/atm.2020.03.175

5. Ren X, Chen B, Hong Y, Liu W, Jiang Q, Yang J, et al. The challenges in colorectal cancer management during COVID-19 epidemic. *Ann Transl Med*. (2020) 8:498. doi: 10.21037/atm.2020.03.158

6. Mathon NF, Lloyd AC. Cell senescence and cancer. *Nat Rev Cancer*. (2001) 1:203–13. doi: 10.1038/35106045

7. Zhang R, Chen HZ, Liu DP. The four layers of aging. *Cell Syst*. (2015) 1:180–6. doi: 10.1016/j.cels.2015.09.002

8. Dai L, Wang X, Bai T, Liu J, Chen B, Yang W. Cellular senescence-related genes: predicting prognosis in gastric cancer. *Front Genet*. (2022) 13:909546. doi: 10.3389/fgene.2022.909546

9. Lu C, Wang Y, Nie L, Chen L, Li M, Qing H, et al. Comprehensive analysis of cellular senescence-related genes in the prognosis, tumor microenvironment, and immunotherapy/chemotherapy of clear cell renal cell carcinoma. *Front Immunol*. (2022) 13:934243. doi: 10.3389/fimmu.2022.934243

10. Collado M, Blasco MA, Serrano M. Cellular senescence in cancer and aging. *Cell*. (2007) 130:223–33. doi: 10.1016/j.cell.2007.07.003

11. Prieto LI, Baker DJ. Cellular senescence and the immune system in cancer. *Gerontology*. (2019) 65:505–12. doi: 10.1159/000500683

12. Krizhanovsky V, Yon M, Dickins RA, Hearn S, Simon J, Miething C, et al. Senescence of activated stellate cells limits liver fibrosis. *Cell*. (2008) 134:657–67. doi: 10.1016/j.cell.2008.06.049

13. Hanahan D. Hallmarks of cancer: new dimensions. *Cancer Discovery*. (2022) 12:31–46. doi: 10.1158/2159-8290.cd-21-1059

14. Dai L, Wang X, Bai T, Liu J, Chen B, Li T, et al. Identification of a novel cellular senescence-related signature for the prediction of prognosis and immunotherapy response in colon cancer. *Front Genet*. (2022) 13:961554. doi: 10.3389/fgene.2022.961554

15. Bhan A, Soleimani M, Mandal SS. Long noncoding RNA and cancer: A new paradigm. *Cancer Res*. (2017) 77:3965–81. doi: 10.1158/0008-5472.can-16-2634

16. Li J, Meng H, Bai Y, Wang K. Regulation of lncRNA and its role in cancer metastasis. *Oncol Res*. (2016) 23:205–17. doi: 10.3727/096504016x14549667334007

17. Peng WX, Koirala P, Mo YY. LncRNA-mediated regulation of cell signaling in cancer. *Oncogene*. (2017) 36:5661–7. doi: 10.1038/onc.2017.184

18. Brunner AL, Beck AH, Edris B, Sweeney RT, Zhu SX, Li R, et al. Transcriptional profiling of long non-coding RNAs and novel transcribed regions across a diverse panel of archived human cancers. *Genome Biol*. (2012) 13:R75. doi: 10.1186/gb-2012-13-8-r75

19. Mijit M, Caracciolo V, Melillo A, Amicarelli F, Giordano A. Role of p53 in the regulation of cellular senescence. *Biomolecules*. (2020) 10(3):420. doi: 10.3390/biom10030420

20. Zhuang Y, Li T, Xiao H, Wu J, Su S, Dong X, et al. LncRNA-H19 drives cardiomyocyte senescence by targeting miR-19a/socs1/p53 axis. *Front Pharmacol*. (2021) 12:631835. doi: 10.3389/fphar.2021.631835

21. Sun D, Wang Y, Sun N, Jiang Z, Li Z, Wang L, et al. LncRNA DANCR counteracts premature ovarian insufficiency by regulating the senescence process of granulosa cells through stabilizing the interaction between p53 and hNRNPC. *J Ovarian Res*. (2023) 16:41. doi: 10.1186/s13048-023-01115-3

22. Wang H, Guan Z, He K, Qian J, Cao J, Teng L. LncRNA UCA1 in anti-cancer drug resistance. *Oncotarget*. (2017) 8:64638–50. doi: 10.18632/oncotarget.18344

23. Huang H, Yao H, Wei Y, Chen M, Sun J. Cellular senescence-related long noncoding ribonucleic acids: Predicting prognosis in hepatocellular carcinoma. *Cancer Rep (Hoboken)*. (2023) 6:e1791. doi: 10.1002/cnr2.1791

24. Liu A, Wang X, Hu L, Yan D, Yin Y, Zheng H, et al. A predictive molecular signature consisting of lncRNAs associated with cellular senescence for the prognosis of lung adenocarcinoma. *PloS One*. (2023) 18:e0287132. doi: 10.1371/journal.pone.0287132

25. Yin F, Zhao W, Ding C, Hou C, Wang S, Sun C, et al. A novel cellular senescence-related lncRNA signature for predicting the prognosis of breast cancer patients. *J Cancer*. (2024) 15:4700–16. doi: 10.7150/jca.96107

26. Casella G, Munk R, Kim KM, Piao Y, De S, Abdelmohsen K, et al. Transcriptome signature of cellular senescence. *Nucleic Acids Res*. (2019) 47:7294–305. doi: 10.1093/nar/gkz555

27. Xu C, Li F, Liu Z, Yan C, Xiao J. A novel cell senescence-related lncRNA survival model associated with the tumor immune environment in colorectal cancer. *Front Immunol*. (2022) 13:1019764. doi: 10.3389/fimmu.2022.1019764

28. Cao L, Zhang S, Ba Y, Zhang H. Identification of m6A-related lncRNAs as prognostic signature within colon tumor immune microenvironment. *Cancer Rep (Hoboken)*. (2023) 6:e1828. doi: 10.1002/cnr2.1828

29. Wang K, Yu J, Xu Q, Peng Y, Li H, Lu Y, et al. Disulfidptosis-related long non-coding RNA signature predicts the prognosis, tumor microenvironment, immunotherapy, and antitumor drug options in colon adenocarcinoma. *Apoptosis*. (2024). doi: 10.1007/s10495-024-02011-x

30. Kuleshov MV, Jones MR, Rouillard AD, Fernandez NF, Duan Q, Wang Z, et al. Enrichr: a comprehensive gene set enrichment analysis web server 2016 update. *Nucleic Acids Res*. (2016) 44:W90–7. doi: 10.1093/nar/gkw377

31. Shum B, Larkin J, Turajlic S. Predictive biomarkers for response to immune checkpoint inhibition. *Semin Cancer Biol*. (2022) 79:4–17. doi: 10.1016/j.semcancer.2021.03.036

32. Newman AM, Liu CL, Green MR, Gentles AJ, Feng W, Xu Y, et al. Robust enumeration of cell subsets from tissue expression profiles. *Nat Methods*. (2015) 12:453–7. doi: 10.1038/nmeth.3337

33. Salmon H, Remark R, Gnjatic S, Merad M. Host tissue determinants of tumor immunity. *Nat Rev Cancer*. (2019) 19:215–27. doi: 10.1038/s41568-019-0125-9

34. Cho YY, Kim DJ, Lee HS, Jeong CH, Cho EJ, Kim MO, et al. Autophagy and cellular senescence mediated by Sox2 suppress Malignancy of cancer cells. *PloS One*. (2013) 8:e57172. doi: 10.1371/journal.pone.0057172

35. Guo Y, Ayers JL, Carter KT, Wang T, Maden SK, Edmond D, et al. Senescence-associated tissue microenvironment promotes colon cancer formation through the secretory factor GDF15. *Aging Cell*. (2019) 18:e13013. doi: 10.1111/acel.13013

36. Sikora E, Bielak-Zmijewska A, Mosieniak G. A common signature of cellular senescence; does it exist? *Ageing Res Rev*. (2021) 71:101458. doi: 10.1016/j.arr.2021.101458

37. Wu Z, Zhang F, Wang Y, Lu Z, Lin C. Identification and Validation of the lncRNA MYOSLID as a Regulating Factor of Necroptosis and Immune Cell Infiltration in Colorectal Cancer following Necroptosis-Related LncRNA Model Establishment. *Cancers (Basel)*. (2022) 14(18):4364. doi: 10.3390/cancers14184364

38. Zhong X, He X, Wang Y, Hu Z, Yu D, Huang H, et al. A hypoxia-related lncRNA signature correlates with survival and tumor microenvironment in colorectal cancer. *J Immunol Res*. (2022) 2022:9935705. doi: 10.1155/2022/9935705

39. Cappell MS. Pathophysiology, clinical presentation, and management of colon cancer. *Gastroenterol Clin North Am*. (2008) 37:1–24. doi: 10.1016/j.gtc.2007.12.002

40. Jahanafrooz Z, Mosafer J, Akbari M, Hashemzaei M, Mokhtarzadeh A. Colon cancer therapy by focusing on colon cancer stem cells and their tumor microenvironment. *J Cell Physiol*. (2020) 235(5):4153–66. doi: 10.1002/jcp.29337

41. Ruan H, Leibowitz BJ, Zhang L. Immunogenic cell death in colon cancer prevention and therapy. *Mol Carcinog*. (2020) 59(7):783–93. doi: 10.1002/mc.23183

42. Chattopadhyay I, Dhar R, Pethusamy K, Seethy A, Srivastava T, Sah R, et al. Exploring the role of gut microbiome in colon cancer. *Appl Biochem Biotechnol*. (2021) 193(6):1780–99. doi: 10.1007/s12010-021-03498-9

43. Birt DF, Phillips GJ. Diet, genes, and microbes: complexities of colon cancer prevention. *Toxicol Pathol*. (2014) 42:182–8. doi: 10.1177/0192623313506791

44. Nardella C, Clohessy JG, Alimonti A, Pandolfi PP. Pro-senescence therapy for cancer treatment. *Nat Rev Cancer*. (2011) 11:503–11. doi: 10.1038/nrc3057

45. Zhang G, Sun J, Zhang X. A novel Cuproptosis-related LncRNA signature to predict prognosis in hepatocellular carcinoma. *Sci Rep*. (2022) 12:11325. doi: 10.1038/s41598-022-15251-1

46. Song J, Sun Y, Cao H, Liu Z, Xi L, Dong C, et al. A novel pyroptosis-related lncRNA signature for prognostic prediction in patients with lung adenocarcinoma. *Bioengineered*. (2021) 12(1):5932–49. doi: 10.1080/21655979.2021.1972078

47. Chen M, Li C, Luo Q. LncRNA LINC02257: A potential biomarker for diagnosis and prognosis of colorectal cancer. *J Oncol*. (2022) 2022:4330630. doi: 10.1155/2022/4330630

48. Xiao J, Liu Y, Yi J, Liu X. LINC02257, an enhancer RNA of prognostic value in colon adenocarcinoma, correlates with multi-omics immunotherapy-related analysis in 33 cancers. *Front Mol Biosci*. (2021) 8:646786. doi: 10.3389/fmolb.2021.646786

49. Han Y, Wu N, Jiang M, Chu Y, Wang Z, Liu H, et al. Long non-coding RNA MYOSLID functions as a competing endogenous RNA to regulate MCL-1 expression by sponging miR-29c-3p in gastric cancer. *Cell Prolif*. (2019) 52(6):e12678. doi: 10.1111/cpr.12678

50. Lin Y, Xiao Y, Liu S, Hong L, Shao L, Wu J. Role of a lipid metabolism-related lncRNA signature in risk stratification and immune microenvironment for colon cancer. *BMC Med Genomics*. (2022) 15:221. doi: 10.1186/s12920-022-01369-8

51. Yasuda T, Baba H, Ishimoto T. Cellular senescence in the tumor microenvironment and context-specific cancer treatment strategies. *FEBS J*. (2023) 290(5):1290–302. doi: 10.1111/febs.16231

52. Rao SG, Jackson JG. SASP: tumor suppressor or promoter? Yes! *Trends Cancer*. (2016) 2:676–87. doi: 10.1016/j.trecan.2016.10.001

53. Takasugi M, Yoshida Y, Ohtani N. Cellular senescence and the tumor microenvironment. *Mol Oncol.* (2022) 16(18):3333–51. doi: 10.1002/1878-0261.13268

54. Waldner M, Schimanski CC, Neurath MF. Colon cancer and the immune system: the role of tumor invading T cells. *World J Gastroenterol.* (2006) 12:7233–8. doi: 10.3748/wjg.v12.i45.7233

55. Lu L, Yang C, Zhou X, Wu L, Hong X, Li W, et al. STING signaling promotes NK cell antitumor immunity and maintains a reservoir of TCF-1(+) NK cells. *Cell Rep.* (2023) 42:113108. doi: 10.1016/j.celrep.2023.113108

56. Cristescu R, Mogg R, Ayers M, Albright A, Murphy E, Yearley J, et al. Pan-tumor genomic biomarkers for PD-1 checkpoint blockade-based immunotherapy. *Science.* (2018) 362(6411):eaar3593. doi: 10.1126/science.aar3593

57. Stone WL, Krishnan K, Campbell SE, Palau VE. The role of antioxidants and pro-oxidants in colon cancer. *World J Gastrointest Oncol.* (2014) 6:55–66. doi: 10.4251/wjgo.v6.i3.55

58. Zhao J, Zhang W, Lin M, Wu W, Jiang P, Tou E, et al. MYOSLID is a novel serum response factor-dependent long noncoding RNA that amplifies the vascular smooth muscle differentiation program. *Arterioscler Thromb Vasc Biol.* (2016) 36:2088–99. doi: 10.1161/atvbaha.116.307879

59. Xiong HG, Li H, Xiao Y, Yang QC, Yang LL, Chen L, et al. Long noncoding RNA MYOSLID promotes invasion and metastasis by modulating the partial epithelial-mesenchymal transition program in head and neck squamous cell carcinoma. *J Exp Clin Cancer Res.* (2019) 38:278. doi: 10.1186/s13046-019-1254-4

60. Yang S, Chen M, Lin C. A novel lncRNA MYOSLID/miR-1286/RAB13 axis plays a critical role in osteosarcoma progression. *Cancer Manag Res.* (2019) 11:10345–51. doi: 10.2147/cmar.s231376

61. Chen S, Gong Y, Shen Y, Liu Y, Fu Y, Dai Y, et al. INHBA is a novel mediator regulating cellular senescence and immune evasion in colorectal cancer. *J Cancer.* (2021) 12:5938–49. doi: 10.7150/jca.61556

62. Yue Y, She X, Ding W, Chen S, Xiao Q, Pan B, et al. A novel Senescence-Based prognostic model unveils tumor interactions and drug resistance in colorectal cancer. *Int Immunopharmacol.* (2024) 134:112197. doi: 10.1016/j.intimp.2024.112197

frontiers | Frontiers in Molecular Biosciences

TYPE Original Research
PUBLISHED 21 January 2025
DOI 10.3389/fmolb.2024.1448792

OPEN ACCESS

EDITED BY
Muhammad Suleman,
University of Swat, Pakistan

REVIEWED BY
Xiangwei Zhao,
Southeast University, China
Dhanya Sooraj,
Monash University, Australia

*CORRESPONDENCE
Maxim Sorokin,
sorokin@oncobox.com
Ye Wang,
yewangsd@163.com

RECEIVED 13 June 2024
ACCEPTED 20 December 2024
PUBLISHED 21 January 2025

CITATION
Sorokin M, Lyadov V, Suntsova M, Garipov M, Semenova A, Popova N, Guguchkin E, Heydarov R, Zolotovskaia M, Zhao X, Yan Q, Wang Y, Karpulevich E and Buzdin A (2025) Detection of fusion events by RNA sequencing in FFPE versus freshly frozen colorectal cancer tissue samples. *Front. Mol. Biosci.* 11:1448792. doi: 10.3389/fmolb.2024.1448792

Detection of fusion events by RNA sequencing in FFPE versus freshly frozen colorectal cancer tissue samples

Maxim Sorokin[1,2,3,4]*, Vladimir Lyadov[5,6,7], Maria Suntsova[3], Marat Garipov[5], Anna Semenova[5], Natalia Popova[5], Egor Guguchkin[8], Rustam Heydarov[3], Marianna Zolotovskaia[4], Xiaowen Zhao[9], Qing Yan[9], Ye Wang[9]*, Evgeny Karpulevich[8] and Anton Buzdin[2,4,10,11]

[1]OmicsWay Corp., Covina, CA, United States, [2]PathoBiology Group, European Organization for Research and Treatment of Cancer (EORTC), Brussels, Belgium, [3]Institute of Personalized Oncology, I.M. Sechenov First Moscow State Medical University, Moscow, Russia, [4]Moscow Center for Advanced Studies, Moscow, Russia, [5]Moscow State Budgetary Healthcare Institution "Moscow City Oncological Hospital N1, Moscow Healthcare Department", Moscow, Russia, [6]Federal State Budgetary Educational Institution of Further Professional Education "Russian Medical Academy of Continuous Professional Education" of the Ministry of Healthcare of the Russian Federation, Moscow, Russia, [7]Novokuznetsk State Institute for Advanced Training of Physicians – Branch of RMACPE, Novokuznetsk, Russia, [8]Institute for System Programming of RAS, Moscow, Russia, [9]Core lab, Qingdao Central Hospital, University of Health and Rehabilitation Sciences, Qingdao, China, [10]Group for Genomic Regulation of Cell Signaling Systems, Shemyakin-Ovchinnikov Institute of Bioorganic Chemistry, Moscow, Russia, [11]World-Class Research Center "Digital Biodesign and Personalized Healthcare", Sechenov First Moscow State Medical University, Moscow, Russia

Gene fusion events result in chimeric proteins that are frequently found in human cancers. Specific targeted therapies are available for several types of cancer fusions including receptor tyrosine kinase gene moieties. RNA sequencing (RNAseq) can directly be used for detection of gene rearrangements in a single test, along with multiple additional biomarkers. However, tumor biosamples are usually formalin-fixed paraffin-embedded (FFPE) tissue blocks where RNA is heavily degraded, which in theory may result in decreased efficiency of fusion detection. Here, for the first time, we compared the efficacy of gene fusion detection by RNAseq for matched pairs of freshly frozen in RNA stabilizing solution (FF) and FFPE tumor tissue samples obtained from 29 human colorectal cancer patients. We detected no statistically significant difference in the number of chimeric transcripts in FFPE and FF RNAseq profiles. The known fusion *KANSL1-ARL17A/B* occurred with a high frequency in 69% of the patients. We also detected 93 new fusion genes not mentioned in the literature or listed in the ChimerSeq database. Among them, 11 were found in two or more patients, suggesting their potential role in carcinogenesis. Most of the fusions detected most probably represented read-through, microdeletion or local duplication events. Finally, in one patient, we detected a potentially clinically actionable in-frame fusion

of *LRRFIP2* and *ALK* genes not previously described in colorectal cancer with an intact tyrosine kinase domain that can be potentially targeted by ALK inhibitors.

KEYWORDS

colorectal cancer, formalin-fixed paraffin-embedded tumor tissue samples, FFPE, RNA sequencing, RNAseq, new cancer fusion genes, chimeric transcripts, detection of gene rearrangements

Introduction

Clinical relevance of fusion genes

Fusion genes are frequently found in cancer cell genomes (Li et al., 2023; Sorokin et al., 2022). Some types of oncogenic fusions, especially those involving receptor tyrosine kinase (RTK) genes, are considered clinically applicable because they can be targeted by specific, clinically approved therapeutic agents (Sorokin et al., 2022). In most cases, the role of RTK fusion partner genes is to drive RTK moiety expression at abnormally high levels (Sorokin et al., 2022). This leads to a significant enhancement of proliferation and survival signaling, which promotes tumor development (Schubert et al., 2023; Shreenivas et al., 2023). In turn, relevant RTK activities can be detected, targeted and inhibited by specific drugs. For example, the first-generation ALK inhibitor crizotinib, as well as second- and third-generation drugs such as brigatinib, lorlatinib, alectinib, and ceritinib, have been included in guidelines for the treatment of lung cancer patients with *ALK* gene fusions (Wu et al., 2016). In addition, crizotinib is also approved for the treatment of *ROS1* fusion-positive cancers (Shaw et al., 2014). Entrectinib and larotrectinib are used to treat *NTRK* family fusion-positive solid tumors, marking the first indication for use in cancer based on the detection of a specific type of gene fusion (Doebele et al., 2020; Drilon et al., 2018). The presence of *FGFR2* gene fusion in cholangiocarcinoma is an indication for the administration of infigratinib (Javle et al., 2021) or pemigatinib (Walden et al., 2022). Erdafitinib has been approved for the treatment of urothelial carcinomas with *FGFR2* or *FGFR3* fusion (Loriot et al., 2019). Finally, selpercatinib and pralcetinib are effective in the treatment of solid tumors with *RET* gene rearrangement (Subbiah et al., 2022a; Subbiah et al., 2022b). In addition, many oncogenic fusions are associated with prognosis or may serve as diagnostic biomarkers (Haley et al., 2021; Huang et al., 2023; Zhu et al., 2019). Thus, reliable detection of gene fusions is a high priority in modern cancer treatment.

Detection of fusion genes

Oncogenic fusion events can be detected with varying degrees of efficiency by whole genome or target DNA sequencing, reverse transcription PCR, immunohistochemistry, or fluorescence *in situ* hybridization (FISH) (Sorokin et al., 2022). Alternatively, these events can be directly detected by analyzing RNA sequencing data by identifying fragments of the corresponding chimeric transcripts (Dorney et al., 2023). RNA analysis offers the advantage of detecting multiple cancer biomarkers in a single test. Indeed, RNA sequencing results can be used to determine tumor mutational burden (Sorokin et al., 2021), assess the status of key immunohistochemistry biomarkers (Sorokin et al., 2020a), evaluate microsatellite instability, measure the expression of molecular targets of anticancer drugs (Buzdin et al., 2020), and interrogate various clinically relevant gene signatures (Lazar et al., 2023; Sorokin et al., 2020b).

Several bioinformatic tools have been developed to detect fused transcripts in RNA sequencing data (Haas et al., 2019). However, there is a certain degree of discrepancy between different such tools (Hafstað et al., 2023). Most of these tools have been tested on fresh tissue samples, which allows the isolation and sequencing of long, high-quality RNA molecules. Although fresh tumor tissue is undoubtedly favorable for nucleic acid molecular analysis, cancer biomaterials are mostly stored as formalin-fixed, paraffin-embedded (FFPE) tissue blocks where RNA undergoes severe degradation, resulting in shorter RNA sequencing reads (Suntsova et al., 2019).

Despite these theoretical considerations, to the best of our knowledge, no study has yet been published that directly compares the efficiency of fusion gene detection in fresh tissue samples compared to FFPE samples. Here, we performed such an analysis for the first time using RNA sequencing of libraries created from matched FFPE biosamples and RNA-stabilized fresh-frozen (FF) colorectal cancer tissues obtained from the same 29 human patients.

Materials and methods

Patient enrollment and sample collection

Primary colorectal cancer patients were enrolled in this study. All patients underwent surgical removal of their tumor tissue. For each patient, the tumor tissue was either immediately placed into RNAlater stabilizing solution (Ambion) and stored at −70°C, or fixed in formalin and subsequently embedded into a paraffin (FFPE) block. Since the duration of fixation can be a defining feature for identifying the fusion genes, formalin fixation time for all FFPE samples was 16 h according to the previous protocol (Cappello et al., 2022). Patient inclusion criteria included an age range of 18–75 years and histologically confirmed colorectal cancer.

RNAseq library preparation and sequencing

RNA was extracted from FFPE slices or RNA-stabilized solutions using the QIAGEN RNeasy Kit, adhering to the manufacturer's protocol. Library construction and ribosomal RNA depletion were

performed using the KAPA RNA Hyper with rRNA Erase (HMR only) kit. To multiplex samples in one sequencing run, different adaptors were utilized. Library concentrations were measured using the Qubit dsDNA HS Assay kit (Life Technologies), and quality was assessed with the Agilent Tapestation (Agilent). RNA sequencing was conducted on the Genolab M engine for paired-end sequencing with a read length of 75 bp.

RNAseq data processing

RNAseq FASTQ files were processed using the STAR aligner (Dobin et al., 2013) in "GeneCounts" mode, with the Ensembl human transcriptome annotation (Build version GRCh38, transcript annotation GRCh38.89) as a reference. Quantile normalization (Bolstad, 2017) was applied for gene expression clustering and PCA analyses. Cancer fusion transcripts were detected using the STAR-Fusion software (Haas et al., 2019). Identified putative fusion candidates were included in downstream analysis only if they passed specific thresholds, with either a JunctionReadCount greater than 1 or a SpanningFragCount greater than 1.

Statistics and data visualization

The results were visualized using the R packages ggplot2 and ggpubr. Principal component analysis (PCA) was performed using the prcomp function in R. The Student's T-test was employed to compare differences between the means, and Spearman's Rho was calculated for pairwise correlation analysis.

Results

Patient enrollment and tumor profiling

In this prospective study, we enrolled 29 patients with histologically confirmed primary colorectal cancer, comprising 17 male (age range 59–84 years, mean age 70 years) and 12 female (age range 62–85 years, mean age 72.5 years) patients. Post-operative tumor tissue specimens were either freshly frozen in RNAlater (FF) or available as formalin-fixed paraffin-embedded (FFPE) blocks. Both types of materials underwent paired-end RNA sequencing with a 75 bp read length. On average, each sample yielded 15 million raw sequencing reads. We employed the STAR-Fusion software to detect chimeric transcripts in the RNAseq profiles and used the ChimerDB database (Jang et al., 2020), the Mitelman Database (https://mitelmandatabase.isb-cgc.org), and PubMed searches with fusion-forming gene IDs to classify fusions as new or previously published. According to the criteria previously deduced for finding cancer gene fusions in FFPE reads (Rabushko et al., 2022), only chimeric transcripts supported by at least two non-duplicated paired reads were considered for further analysis. This data filtering setting, adapted from our previous research, allowed for the identification of novel and known chimeric transcripts in FFPE RNAseq data with nearly 100% specificity, as confirmed by reverse transcription PCR followed by Sanger sequencing of the resulting products (Rabushko et al., 2022).

Fusion transcript detection and analysis

In this study, only one patient's tumor exhibited the same fusion transcripts in both fresh frozen (FF) and formalin-fixed paraffin-embedded (FFPE) tissue samples; in the remaining cases, the outputs from FF and FFPE paired samples differed (Supplementary Table S1). In total, we identified 113 fusion transcripts, of which 69 included fragments of protein-coding genes and 44 involved fusions of non-coding RNAs (Supplementary Table S1). We detected at least one common fusion transcript in 17 out of 29 cases (59%) in the paired FF/FFPE samples. In 13 cases (45%), the number of detected fusions in FF samples was higher than in the FFPE tumor tissue blocks, while in 10 cases (34%), the number of FFPE fusions was higher. Overall, there was no statistically significant difference in the number of fusions between FFPE and paired FF materials (paired analysis p-value = 0.2, Figure 1A).

We also compared the number of uniquely mapped reads among the paired FF and FFPE sequenced libraries, a measure referred to as effective coverage for an RNA sequencing profile. On average, FFPE samples exhibited approximately twice the coverage of FF samples (p-value = 5.4 × 10^-8, Figure 1B). We did not observe a correlation between the number of fusion transcripts detected and the number of reads per library neither for FF, nor for FFPE samples (Figure 1C). Only fusions detected in at least two samples were included in this analysis.

Details on the numbers of uniquely mapped reads per sample and other mapping statistics are provided in Supplementary Table S2. Thus, the efficient detection of fusion transcripts in FFPE blocks, comparable to that in FF samples, may be at least partly due to the higher coverage by RNAseq reads. Interestingly, the median insert size was 20 bases shorter in FFPE than in FF samples, 186 vs. 206 bases, respectively (Supplementary Table S2, p-value = 3.9 × 10^-7), which could influence the fusion detection process due to the STAR-Fusion aligner properties.

Interestingly, perhaps due to the drastically different coverage, principal component analysis (PCA) revealed clearly separate clustering of the FF and FFPE gene expression profiles (Figure 1D). However, dendrogram analysis of pairwise distances primarily showed clustering that was specific to the sample IDs, rather than to the type of biomaterial, among the FF and FFPE biosamples (Supplementary Figure S1).

The most commonly identified fusion transcripts in this study were *KANSL1-ARL17A/B* read-through transcripts, found in 20 patients (69%), followed by the fusions *MACC1-AC005062.1*, *LEPROT-LEPR*, *SMG1-NPIPB13*, and *AL353138.1-PTCHD4*, found in 7 (24%), 5 (17%), 3 (10%), and 3 (10%) patients, respectively (Figure 2; Supplementary Table S1). Of these, only the *KANSL1-ARL17A/B* fusion was previously reported in the literature (Zhou et al., 2017) while the others are newly identified or newly reported. Interestingly, *KANSL1-ARL17A/B* fusions have been detected not only in various solid and hematological cancers but also in patient-matched normal control tissues. Specifically, the *KANSL1-ARL17A* fusion has been associated with unfavorable outcomes in high-grade serous ovarian cancer (Newtson et al., 2021). Both the *KANSL1* and *ARL17A* genes are located on the reverse strand of chromosome 17 at the q21.31

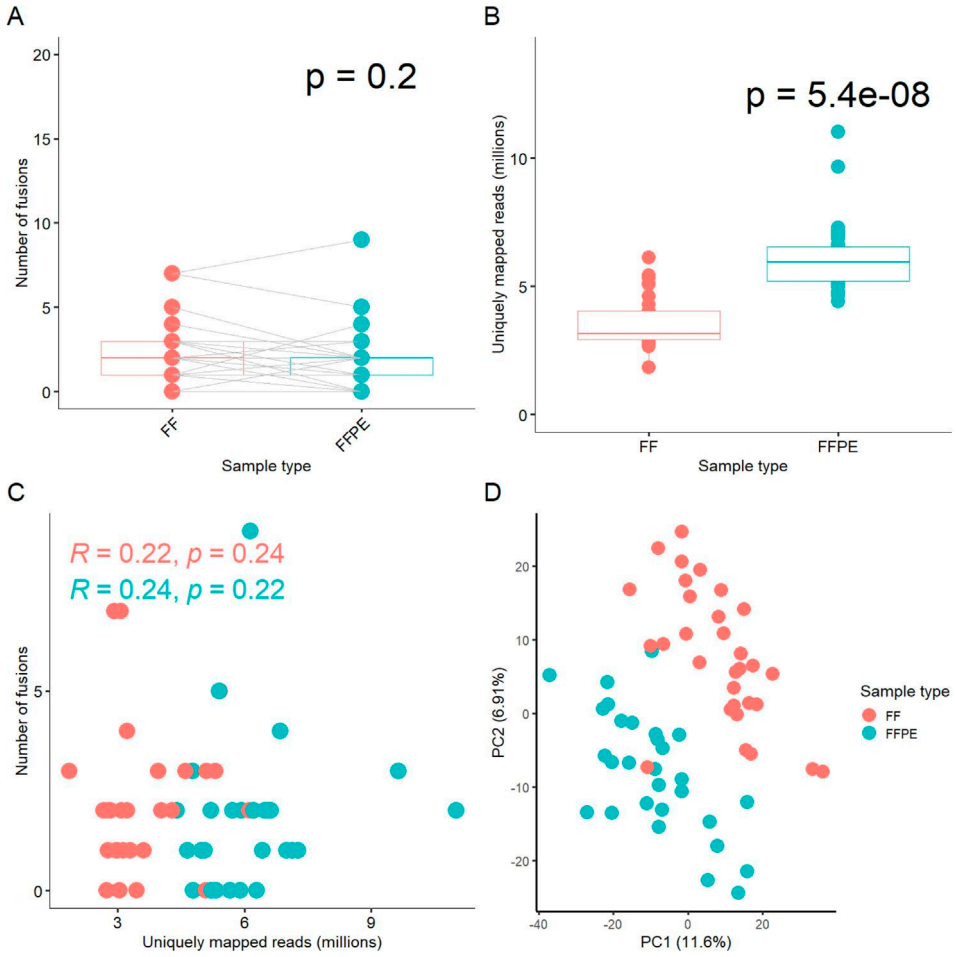

FIGURE 1
Comparison of experimental FF and FFPE paired gene expression profiles. **(A)** Box-plot for number of fusion transcripts detected in FF versus matched FFPE samples. **(B)** Box-plot for number of uniquely mapped reads in sequenced FF and FFPE libraries. **(C)** Scatterplot for relationship between the number of fusion transcripts detected and the number of uniquely mapped reads in the respective libraries. **(D)** Principal component analysis (PCA) of log-transformed gene expression levels (TPM) in FF and FFPE libraries.

locus. The frequent occurrence of *KANSL1-ARL17A/B* fusions may be attributed to two partial duplications of the *KANSL1* gene, which are prevalent at frequencies of 26% and 19%, respectively, in the European ancestry population (Boettger et al., 2012). This suggests that the mechanism of fusion generation could involve aberrant or alternative splicing of the two genes, rather than ongoing DNA rearrangement events (López-Nieva et al., 2019; Zhou et al., 2017).

The fusions that could be found in two patients were one known fusion *TFG-ADGRG7* and six new fusions *AC108865.1-AC110772.2*, *CCDC32-CBX3*, *CAST-AC104123.1*, *AC090517.5-ZNF280D*, *BOLA2B-SMG1P6*, and *UMAD1-GLCCI1* (Figure 2; Supplementary Table S1). Among these, the previously reported *TFG-ADGRG7* fusion could be also detected simultaneously in the normal and tumor samples (López-Nieva et al., 2019). Both fusion partners here are located on 3q12.2 genome locus.

Furthermore, except *CCDC32-CBX3* that most probably represented 15q15.1 – 7p15.2 translocation, all detected fusions occurring in at least two patient biosamples had fusion partners located in the same genomic region (Supplementary File S1). This strongly suggests read-through, duplication, or local deletion mechanisms for their generation. Many of them were presented by two or more alternative variants with different fusion sites (Supplementary File S1).

In total, of the 112 fusion transcripts detected in this study, 19 (17%) were previously documented in the ChimerSeq database of known fusions (Jang et al., 2020) or the Mitelman Database, while 93 (83%) were not previously reported in the literature or in the above repositories.

Detection of the novel ALK fusion

In the FF sample from patient P23, we detected an in-frame fusion transcript involving the *ALK* gene and *LRRFIP2*, which encodes the LRR-binding FLII-interacting protein 2. This fusion retains the entire tyrosine kinase domain spanning exons 20–29 of the *ALK* gene (Figure 3A, Supplementary File S1), suggesting the

FIGURE 2
Fusion transcripts experimentally detected in FF or FFPE materials in more than one patient. Fusion statistics is ordered by patient ID, grey label showing FF and red label–FFPE biosamples.

potential clinical efficacy of ALK inhibitors in this case. However, no supporting chimeric reads for this fusion were found in the FFPE sample of P23. We have previously demonstrated that an overall asymmetry in exon coverage by RNAseq reads of the 5′- and 3′-parts of a gene may indicate a gene fusion event (Rabushko et al., 2022). For patient P23, we observed a significant

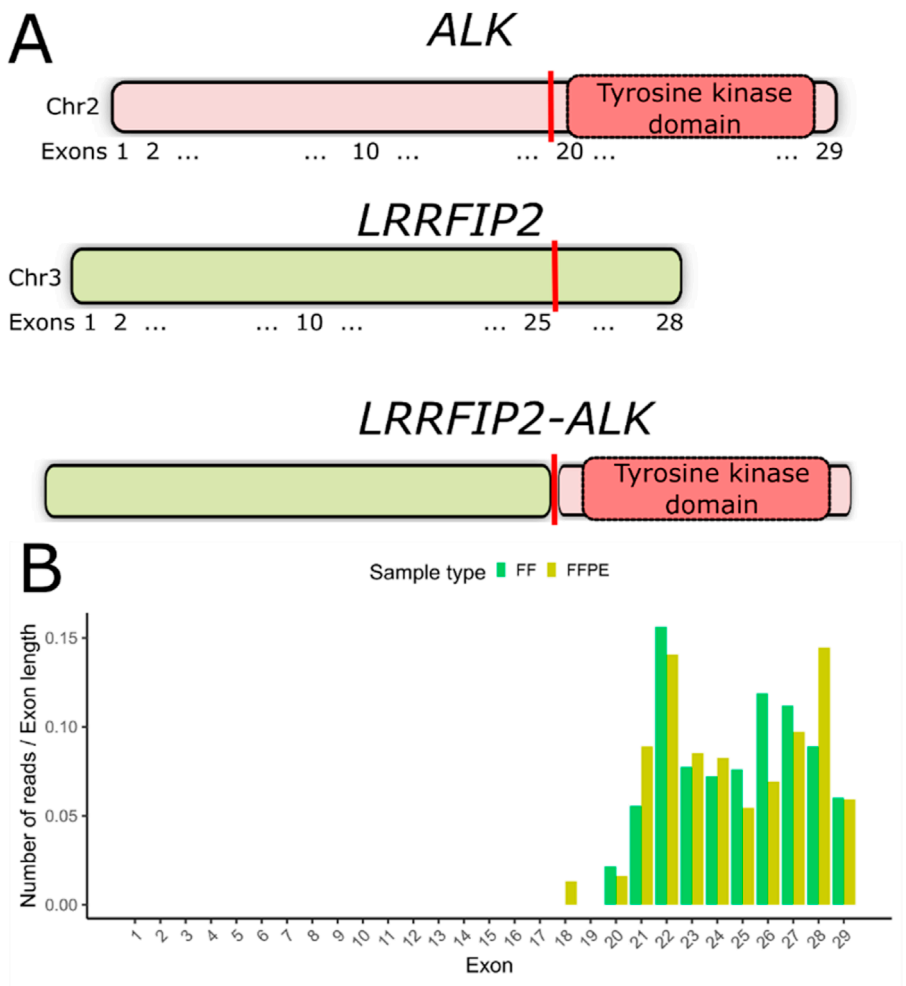

FIGURE 3
(A) Schematic representation of the *LRRFIP2-ALK* fusion transcript detected in patient P23. The vertical red line indicates the deduced fusion breakpoint. **(B)** Coverage of *ALK* gene exons by RNAseq reads in both FF and FFPE samples from patient #23. The number of counts mapped to exons has been normalized to exon lengths.

increase in *ALK* gene exon coverage beginning with exon 20 in both matched FF and FFPE RNAseq profiles (Figure 3B). We validated the presence of *LRRFIP2-ALK* fusion in both FF and FFPE samples using reverse transcription PCR followed by Sanger sequencing.

Discussion

Detecting fusion events can be particularly challenging in FFPE tumor tissue samples. Fluorescent *in situ* hybridization (FISH) is commonly used to detect fusions in FFPE tissues, but this method is typically restricted to identifying known fusion pairs (Wagener-Ryczek and Pappesch, 2021). Alternative approaches, such as targeted RNA sequencing and various reverse transcription PCR-based methods, also face similar limitations in that they can only detect previously identified fusions (Wagener-Ryczek and Pappesch, 2021). Therefore, total RNA sequencing and/or whole-genome sequencing remain the only viable options for discovering novel gene fusions in both FFPE and FF tumor tissue materials (Yang et al., 2023).

We previously demonstrated that RNA sequencing of FFPE human tumor samples provides accurate gene expression profiling, establishing reproducible transcriptional patterns (Samii et al., 2021) and reliable quantification of cancer biomarkers (Sorokin et al., 2020a). However, to our knowledge, no published studies have directly compared the efficiency of fusion detection between FFPE and FF biomaterials. In our current study, we found that using FFPE materials resulted in a comparable number of fusion transcripts detected from total RNAseq data as with FF materials, although approximately twice as many reads were required for the FFPE libraries compared to the FF samples. Notably, the number of fusion transcripts identified in both FF and FFPE samples did not significantly differ. Interestingly, fusions identified in FF and FFPE samples from the same patient showed little overlap, suggesting that the STAR-Fusion software might not detect all existing fusions in the biosamples. The non-overlapping sets of chimeric transcripts could also be

attributed to low expression levels of the transcripts and/or tumor heterogeneity.

Alternative RNA sequencing approaches that focus not only on detecting reads directly supporting a fusion event may significantly enhance the detection efficiency of chimeric cancer genes in FFPE samples. We have previously demonstrated that the pattern of exon coverage by RNAseq reads can be useful for identifying fusion genes, particularly when the major oncogenic partner (e.g., the gene moiety encoding the tyrosine kinase domain) is located on the 3′part of the chimera (Rabushko et al., 2022). In this study, we tested this approach and successfully identified a new, potentially clinically relevant *ALK* gene fusion in a matched FFPE sample as well.

ALK, a member of the insulin receptor superfamily of receptor tyrosine kinases, is composed of 29 exons, with exons 20–29 encoding the tyrosine kinase domain (Della Corte et al., 2018) *ALK* fusions are primarily found in lung cancer, where they occur with a prevalence of approximately 5% (Jazieh et al., 2021). The most frequent 5′fusion partner of *ALK* is *EML4*, which encodes the echinoderm microtubule-associated protein-like 4. Other common partners include *SQSTM1* (sequestosome), *DCTN1* (dynactin), *HIP1* (Huntington interacting protein 1), and *KIF5B* (kinesin family member 5B) (Shreenivas et al., 2023). Research indicates that the specific fusion partner may influence tumor sensitivity to ALK inhibitors (Childress et al., 2018). Although *ALK* fusions are less common in other tumor types, they have been occasionally detected in sarcomas, neuroblastoma, and esophageal, renal, breast, ovarian, thyroid, and colorectal cancers (Ross et al., 2017). In such cases, treatment with ALK-targeting drugs, such as crizotinib and alectinib, can lead to durable tumor responses (Childress et al., 2018).

In this study, we detected an *ALK* fusion with *LRRFIP2* as the 5′partner in a case of colorectal cancer. This same fusion was previously identified in one clinical case of epithelioid fibrous histiocytoma (Mansour et al., 2022). LRRFIP2, leucine-rich binding FLII interacting protein 2, is known to negatively regulate NLRP3 inflammasome activation in macrophages (Jin et al., 2013) and activate nuclear factor kappa B signaling by binding to the cytosolic tail of toll-like receptor 4 (Gunawardena et al., 2011). Notably, *LRRFIP2* has also been involved in fusions with *RAF1* in acral melanoma (LeBlanc et al., 2020) and with *MLH1* in hereditary non-polyposis colorectal cancer (Morak et al., 2011).

Using the bioinformatic tool STAR-Fusion (Haas et al., 2019), we identified the *LRRFIP2-ALK* fusion transcript in the FF sample but not in the FFPE sample of a patient. This discrepancy could be due to insufficient coverage, lower RNA integrity, tumor heterogeneity, or other factors. However, we detected a pattern of exon coverage by RNAseq reads that indicates the presence of this fusion in both FF and FFPE samples of this patient. Therefore, we conclude that inspecting exon coverage patterns for clinically relevant oncogenes can be valuable for characterizing FFPE-derived materials. This method can complement widely used software tools for detecting chimeric transcripts.

Since targeted therapies are available for less than a dozen oncogenic fusion types, such an inspection can even be performed manually when exon coverage is visualized. Additionally, an automated method for high-throughput exon coverage asymmetry analysis may be beneficial for batch detection of fusion gene candidates in FFPE RNAseq data. While this approach has limitations—it cannot identify the fusion partner or determine whether the open reading frame of a chimeric transcript is preserved—it can roughly identify the fusion breakpoint position and narrow the analysis to candidate cases requiring further in-depth investigation and molecular profiling.

Data availability statement

RNA sequencing profiles were deposited in NCBI Sequencing Read Archive (SRA) under accession ID PRJNA1208692.

Ethics statement

The study was approved by the ethical committee of the Russian Medical Academy of Continuous Professional Education of the Ministry of Healthcare, Moscow, Russian Federation (protocol ID #25, signed on 25 March 2022). The studies were conducted in accordance with the local legislation and institutional requirements. The participants provided their written informed consent to participate in this study.

Author contributions

MxS: Funding acquisition, Investigation, Writing–original draft. VL: Investigation, Supervision, Writing–review and editing. MrS: Investigation, Writing–review and editing. MG: Investigation, Writing–review and editing. AS: Investigation, Writing–review and editing. NP: Writing–review and editing. EG: Investigation, Software, Writing–review and editing. RH: Investigation, Writing–original draft. MZ: Funding acquisition, Investigation, Writing–review and editing. XZ: Investigation, Writing–review and editing. QY: Investigation, Writing–review and editing. YW: Funding acquisition, Investigation, Writing–original draft. EK: Investigation, Software, Writing–review and editing. AB: Conceptualization, Investigation, Supervision, Writing–original draft, Writing–review and editing.

Funding

The author(s) declare that financial support was received for the research, authorship, and/or publication of this article. The collection of tumor biosamples and RNA sequencing were supported by the Russian Science Foundation under grant 22-24-00682. PCR followed by Sanger sequencing and bioinformatic detection of chimeric reads were supported by the Russian Science Foundation under grant 22-74-10031. Anton Buzdin's contribution to the detection of unbalanced exon coverage in putative fusionforming genes by RNA sequencing reads was supported by the Ministry of Science and Higher Education of the Russian Federation. This support was part of state-sponsored efforts to create and develop World-Class Research Centers for 'Digital Biodesign and Personalized Healthcare,' under grant No. 075-15-2022-304. The contribution of Xiaowen Zhao, Qing Yan, and Ye Wang was supported by the National Natural Science Foundation of China grant 81800805.

Conflict of interest

Author MS was employed by OmicsWay Corp.

The remaining authors declare that the research was conducted in the absence of any commercial or financial relationships that could be construed as a potential conflict of interest.

Publisher's note

All claims expressed in this article are solely those of the authors and do not necessarily represent those of their affiliated organizations, or those of the publisher, the editors and the reviewers. Any product that may be evaluated in this article, or claim that may be made by its manufacturer, is not guaranteed or endorsed by the publisher.

Supplementary material

The Supplementary Material for this article can be found online at: https://www.frontiersin.org/articles/10.3389/fmolb.2024.1448792/full#supplementary-material

References

Boettger, L. M., Handsaker, R. E., Zody, M. C., and McCarroll, S. A. (2012). Structural haplotypes and recent evolution of the human 17q21.31 region. *Nat. Genet.* 44, 881–885. doi:10.1038/ng.2334

Bolstad, B. M. (2017). preprocessCore: a collection of pre-processing functions. Available at: https://github.com/bmbolstad/preprocessCore (Accessed May 21, 2017).

Buzdin, A., Sorokin, M., Garazha, A., Glusker, A., Aleshin, A., Poddubskaya, E., et al. (2020). RNA sequencing for research and diagnostics in clinical oncology. *Semin. Cancer Biol.* 60, 311–323. doi:10.1016/j.semcancer.2019.07.010

Cappello, F., Angerilli, V., Munari, G., Ceccon, C., Sabbadin, M., Pagni, F., et al. (2022). FFPE-based NGS approaches into clinical practice: the limits of glory from a pathologist viewpoint. *J. Pers. Med.* 12, 750. doi:10.3390/jpm12050750

Childress, M. A., Himmelberg, S. M., Chen, H., Deng, W., Davies, M. A., and Lovly, C. M. (2018). ALK fusion partners impact response to ALK inhibition: differential effects on sensitivity, cellular phenotypes, and biochemical properties. *Mol. Cancer Res.* 16, 1724–1736. doi:10.1158/1541-7786.MCR-18-0171

Della Corte, C. M., Viscardi, G., Di Liello, R., Fasano, M., Martinelli, E., Troiani, T., et al. (2018). Role and targeting of anaplastic lymphoma kinase in cancer. *Mol. Cancer* 17, 30. doi:10.1186/s12943-018-0776-2

Dobin, A., Davis, C. A., Schlesinger, F., Drenkow, J., Zaleski, C., Jha, S., et al. (2013). STAR: ultrafast universal RNA-seq aligner. *Bioinformatics* 29, 15–21. doi:10.1093/bioinformatics/bts635

Doebele, R. C., Drilon, A., Paz-Ares, L., Siena, S., Shaw, A. T., Farago, A. F., et al. (2020). Entrectinib in patients with advanced or metastatic NTRK fusion-positive solid tumours: integrated analysis of three phase 1–2 trials. *Lancet Oncol.* 21, 271–282. doi:10.1016/S1470-2045(19)30691-6

Dorney, R., Dhungel, B. P., Rasko, J. E. J., Hebbard, L., and Schmitz, U. (2023). Recent advances in cancer fusion transcript detection. *Brief. Bioinform.* 24, bbac519. doi:10.1093/bib/bbac519

Drilon, A., Laetsch, T. W., Kummar, S., DuBois, S. G., Lassen, U. N., Demetri, G. D., et al. (2018). Efficacy of larotrectinib in TRK fusion-positive cancers in adults and children. *N. Engl. J. Med.* 378, 731–739. doi:10.1056/NEJMoa1714448

Gunawardena, H. P., Huang, Y., Kenjale, R., Wang, H., Xie, L., and Chen, X. (2011). Unambiguous characterization of site-specific phosphorylation of leucine-rich repeat fli-I-interacting protein 2 (LRRFIP2) in toll-like receptor 4 (TLR4)-mediated signaling. *J. Biol. Chem.* 286, 10897–10910. doi:10.1074/jbc.M110.168179

Haas, B. J., Dobin, A., Li, B., Stransky, N., Pochet, N., and Regev, A. (2019). Accuracy assessment of fusion transcript detection via read-mapping and *de novo* fusion transcript assembly-based methods. *Genome Biol.* 20, 213. doi:10.1186/s13059-019-1842-9

Hafstad, V., Häkkinen, J., and Persson, H. (2023). Fast and sensitive validation of fusion transcripts in whole-genome sequencing data. *BMC Bioinforma.* 24, 359. doi:10.1186/s12859-023-05489-5

Haley, L., Parimi, V., Jiang, L., Pallavajjala, A., Hardy, M., Yonescu, R., et al. (2021). Diagnostic utility of gene fusion panel to detect gene fusions in fresh and formalin-fixed, paraffin-embedded cancer specimens. *J. Mol. Diagn.* 23, 1343–1358. doi:10.1016/j.jmoldx.2021.07.015

Huang, X., Li, G., Li, L., Wang, J., Shen, J., Chen, Y., et al. (2023). Establishing an RNA fusions panel in soft tissue sarcoma with clinical validation. *Sci. Rep.* 13, 4403. doi:10.1038/s41598-023-29511-1

Jang, Y. E., Jang, I., Kim, S., Cho, S., Kim, D., Kim, K., et al. (2020). ChimerDB 4.0: an updated and expanded database of fusion genes. *Nucleic Acids Res.* 48, D817–D824. doi:10.1093/nar/gkz1013

Javle, M., Roychowdhury, S., Kelley, R. K., Sadeghi, S., Macarulla, T., Weiss, K. H., et al. (2021). Infigratinib (BGJ398) in previously treated patients with advanced or metastatic cholangiocarcinoma with FGFR2 fusions or rearrangements: mature results from a multicentre, open-label, single-arm, phase 2 study. *Lancet Gastroenterol. Hepatol.* 6, 803–815. doi:10.1016/S2468-1253(21)00196-5

Jazieh, A. R., Gaafar, R., Errihani, H., Jaafar, H., Al Dayel, F., Bahnassy, A. A., et al. (2021). Real-world data on the prevalence of anaplastic lymphoma kinase–positive non–small-cell lung cancer in the Middle East and north africa. *JCO Glob. Oncol.* 7, 1556–1563. doi:10.1200/GO.21.00067

Jin, J., Yu, Q., Han, C., Hu, X., Xu, S., Wang, Q., et al. (2013). LRRFIP2 negatively regulates NLRP3 inflammasome activation in macrophages by promoting Flightless-I-mediated caspase-1 inhibition. *Nat. Commun.* 4, 2075. doi:10.1038/ncomms3075

Lazar, V., Zhang, B., Magidi, S., Le Tourneau, C., Raymond, E., Ducreux, M., et al. (2023). A transcriptomics approach to expand therapeutic options and optimize clinical trials in oncology. *Ther. Adv. Med. Oncol.* 15, 17588359231156382. doi:10.1177/17588359231156382

LeBlanc, R. E., Lefferts, J. A., Baker, M. L., and Linos, K. D. (2020). Novel LRRFIP2-RAF1 fusion identified in an acral melanoma: a review of the literature on melanocytic proliferations with RAF1 fusions and the potential therapeutic implications. *J. Cutan. Pathol.* 47, 1181–1186. doi:10.1111/cup.13817

Li, J., Lu, H., Ng, P. K.-S., Pantazi, A., Ip, C. K. M., Jeong, K. J., et al. (2023). A functional genomic approach to actionable gene fusions for precision oncology. *Sci. Adv.* 8, eabm2382. doi:10.1126/sciadv.abm2382

López-Nieva, P., Fernández-Navarro, P., Graña-Castro, O., Andrés-León, E., Santos, J., Villa-Morales, M., et al. (2019). Detection of novel fusion-transcripts by RNA-Seq in T-cell lymphoblastic lymphoma. *Sci. Rep.* 9, 5179. doi:10.1038/s41598-019-41675-3

Loriot, Y., Necchi, A., Park, S. H., Garcia-Donas, J., Huddart, R., Burgess, E., et al. (2019). Erdafitinib in locally advanced or metastatic urothelial carcinoma. *N. Engl. J. Med.* 381, 338–348. doi:10.1056/NEJMoa1817323

Mansour, B., Donati, M., Michalová, K., Michal, M., Ptáková, N., Hájková, V., et al. (2022). Epithelioid fibrous histiocytoma: three diagnostically challenging cases with novel ALK gene fusions, unusual storiform growth pattern, and a prominent spindled morphology. *Virchows Arch.* 481, 751–757. doi:10.1007/s00428-022-03418-0

Morak, M., Massdorf, T., Locher, M., and Holinski-Feder, E. (2011). Disease-causing gene-flanking genomic rearrangements in HNPCC patients. *Hered. Cancer Clin. Pract.* 9, P28. doi:10.1186/1897-4287-9-S1-P28

Newtson, A., Reyes, H., Devor, E. J., Goodheart, M. J., and Bosquet, J. G. (2021). Identification of novel fusion transcripts in high grade serous ovarian cancer. *Int. J. Mol. Sci.* 22, 4791. doi:10.3390/ijms22094791

Rabushko, E., Sorokin, M., Suntsova, M., Seryakov, A. P., Kuzmin, D. V., Poddubskaya, E., et al. (2022). Experimentally deduced criteria for detection of clinically relevant fusion 3′ oncogenes from FFPE bulk RNA sequencing data. *Biomedicines* 10, 1866. doi:10.3390/biomedicines10081866

Ross, J. S., Ali, S. M., Fasan, O., Block, J., Pal, S., Elvin, J. A., et al. (2017). ALK fusions in a wide variety of tumor types respond to anti-ALK targeted therapy. *Oncologist* 22, 1444–1450. doi:10.1634/theoncologist.2016-0488

Samii, A., Sorokin, M., Kar, S., Makovskaia, L., Garazha, A., Hartmann, C., et al. (2021). Case of multifocal glioblastoma with four fusion transcripts of ALK, FGFR2, NTRK2, and NTRK3 genes stresses the need for tumor tissue multisampling for transcriptomic analysis. *Cold Spring Harb. Mol. case Stud.* 7, a006100. doi:10.1101/MCS.A006100

Schubert, L., Elliott, A., Le, A. T., Estrada-Bernal, A., Doebele, R. C., Lou, E., et al. (2023). ERBB family fusions are recurrent and actionable oncogenic targets across cancer types. *Front. Oncol.* 13, 1115405. doi:10.3389/fonc.2023.1115405

Shaw, A. T., Ou, S.-H. I., Bang, Y.-J., Camidge, D. R., Solomon, B. J., Salgia, R., et al. (2014). Crizotinib in ROS1-rearranged non-small-cell lung cancer. *N. Engl. J. Med.* 371, 1963–1971. doi:10.1056/NEJMoa1406766

Shreenivas, A., Janku, F., Gouda, M. A., Chen, H.-Z., George, B., Kato, S., et al. (2023). ALK fusions in the pan-cancer setting: another tumor-agnostic target? *Precis. Oncol.* 7, 101. doi:10.1038/s41698-023-00449-x

Sorokin, M., Gorelyshev, A., Efimov, V., Zotova, E., Zolotovskaia, M., Rabushko, E., et al. (2021). RNA sequencing data for FFPE tumor blocks can Be used for robust estimation of tumor mutation burden in individual biosamples. *Front. Oncol.* 11, 732644. doi:10.3389/fonc.2021.732644

Sorokin, M., Ignatev, K., Poddubskaya, E., Vladimirova, U., Gaifullin, N., Lantsov, D., et al. (2020a). RNA sequencing in comparison to immunohistochemistry for measuring cancer biomarkers in breast cancer and lung cancer specimens. *Biomedicines* 8, 114. doi:10.3390/BIOMEDICINES8050114

Sorokin, M., Poddubskaya, E., Baranova, M., Glusker, A., Kogoniya, L., Markarova, E., et al. (2020b). RNA sequencing profiles and diagnostic signatures linked with response to ramucirumab in gastric cancer. *Mol. Case Stud.* 6, a004945. mcs.a004945. doi:10.1101/mcs.a004945

Sorokin, M., Rabushko, E., Rozenberg, J. M., Mohammad, T., Seryakov, A., Sekacheva, M., et al. (2022). Clinically relevant fusion oncogenes: detection and practical implications. *Ther. Adv. Med. Oncol.* 14, 17588359221144108. doi:10.1177/17588359221144108

Subbiah, V., Cassier, P. A., Siena, S., Garralda, E., Paz-Ares, L., Garrido, P., et al. (2022a). Pan-cancer efficacy of pralsetinib in patients with RET fusion–positive solid tumors from the phase 1/2 ARROW trial. *Nat. Med.* 28, 1640–1645. doi:10.1038/s41591-022-01931-y

Subbiah, V., Wolf, J., Konda, B., Kang, H., Spira, A., Weiss, J., et al. (2022b). Tumour-agnostic efficacy and safety of selpercatinib in patients with RET fusion-positive solid tumours other than lung or thyroid tumours (LIBRETTO-001): a phase 1/2, open-label, basket trial. *Lancet Oncol.* 23, 1261–1273. doi:10.1016/S1470-2045(22)00541-1

Suntsova, M., Gaifullin, N., Allina, D., Reshetun, A., Li, X., Mendeleeva, L., et al. (2019). Atlas of RNA sequencing profiles for normal human tissues. *Sci. data* 6, 36. doi:10.1038/s41597-019-0043-4

Wagener-Ryczek, S., and Pappesch, R. (2021). Targeted RNA-sequencing for the evaluation of gene fusions in lung tumors: current status and future prospects. *Expert Rev. Mol. diagn.* 21, 531–534. doi:10.1080/14737159.2021.1920399

Walden, D., Eslinger, C., and Bekaii-Saab, T. (2022). Pemigatinib for adults with previously treated, locally advanced or metastatic cholangiocarcinoma with FGFR2 fusions/rearrangements. *Ther. Adv. Gastroenterol.* 15, 17562848221115317. doi:10.1177/17562848221115317

Wu, J., Savooji, J., and Liu, D. (2016). Second- and third-generation ALK inhibitors for non-small cell lung cancer. *J. Hematol. Oncol.* 9, 19. doi:10.1186/s13045-016-0251-8

Yang, Y., Shu, Y., Tang, Y., Zhao, S., Jia, Y., Ji, J., et al. (2023). RNA sequencing of myeloid sarcoma, shed light on myeloid sarcoma stratification. *Cancer Med.* 12, 9156–9166. doi:10.1002/cam4.5654

Zhou, J. X., Yang, X., Ning, S., Wang, L., Wang, K., Zhang, Y., et al. (2017). Identification of KANSARL as the first cancer predisposition fusion gene specific to the population of European ancestry origin. *Oncotarget* 8 (31), 50594–50607. doi:10.18632/oncotarget.16385

Zhu, G., Benayed, R., Ho, C., Mullaney, K., Sukhadia, P., Rios, K., et al. (2019). Diagnosis of known sarcoma fusions and novel fusion partners by targeted RNA sequencing with identification of a recurrent ACTB-FOSB fusion in pseudomyogenic hemangioendothelioma. *Mod. Pathol.* 32, 609–620. doi:10.1038/s41379-018-0175-7

Frontiers in
Molecular Biosciences

Explores biological processes in living organisms on a molecular scale

Focuses on the molecular mechanisms underpinning and regulating biological processes in organisms across all branches of life.

Discover the latest Research Topics

See more →

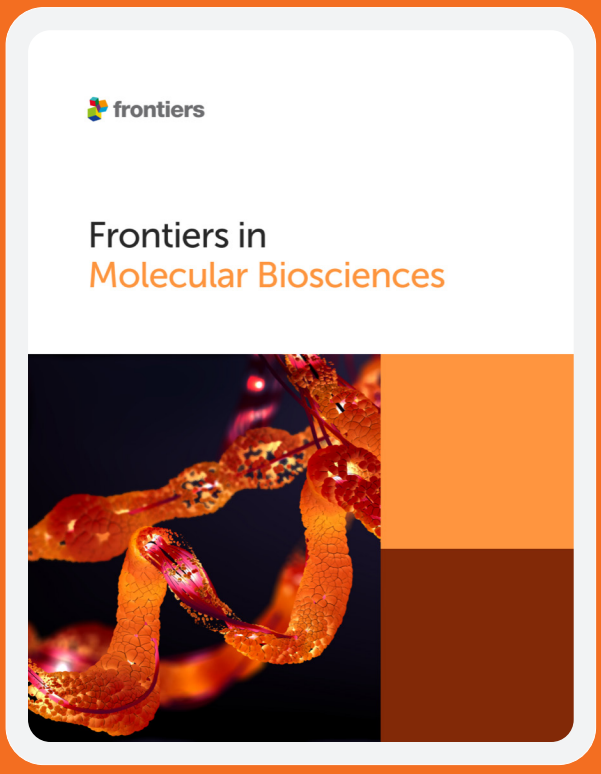

Frontiers

Avenue du Tribunal-Fédéral 34
1005 Lausanne, Switzerland
frontiersin.org

Contact us

+41 (0)21 510 17 00
frontiersin.org/about/contact